Filipe Gonçalo Jacinto Gomes

Exfoliation in Bags Using Sonication for Nanomaterials Synthesis

Dissertation submitted in partial fulfillment
of the requirements for the degree of

Master of Science in
Chemical and Biochemical Engineering

Advisor: David Fernández Rivas, Assistant Professor, University of Twente

Co-advisor: Pedro Simões, Assistant Professor, Faculdade de Ciências e Tecnologia da Universidade Nova de Lisboa

Examination Committee

Chairperson: Ana Aguiar Ricardo, Full Professor, FCT-UNL
Members: Isabel Ferreira, Associate Professor, FCT-UNL
Pedro Simões, Assistant Professor, FCT-UNL

FACULDADE DE CIÊNCIAS E TECNOLOGIA
UNIVERSIDADE NOVA DE LISBOA

September, 2016

Exfoliation in Bags
Using Sonication for
Nanomaterials Synthesis

This document was created using the (pdf)LaTeX processor, based in the "unlthesis" template[1], developed at the Dep. Informática of FCT-NOVA [2].
[1] https://github.com/joaomlourenco/unlthesis [2] http://www.di.fct.unl.pt

To everyone who has helped me
become the person I am today.

Acknowledgements

Firstly I would like to thank Professor David Fernández Rivas for his never ending and always present support, for his teachings, his kindness and help in completing this thesis. I would also like thank Bram Verhaagen, as well as Professor David, for the opportunity to closely collaborate with their start-up *BuBclean*.
To all the people at the UT who made this work possible through their help on the various scientific methods used. Thank you Dr. Tibor Kudernac, Richard Egberink, Marcel de Bruine, Mark Smithers, Rico Keim, Gerard Kip, Aufried Lenferink, Cees Otto, Sonia Blanco, Frans Segerink, Robert Wijn, Mark Hempenius and the POF research group for making their lab and equipment accessible for me.
A special appreciation to Stefan Schlautman for making it easier to pass the afternoons at the office and for allowing me to share his and Prof. David's office during my stay at the University of Twente. To Prof. Gardeniers, Peter, Henk-Willem, Pieter, Ilse, Julie, Yuyan, Sebastiaan, Thijs, Hoon, Jöel all the remaining MCS research group, for the friendly welcome, availability in helping with any doubts, the amazing pop-quizz night at the Molly Malone, the kart race and the farewell dinner.
I am also thankful to the Science and Technology Faculty of the University of Twente for their openness to international students. To the various organisations which were critical for an easy integration, ESN, Kick-in, Buddy Program... And to the people I met at the UT who created a friendly atmosphere away from home, which surely eased the stress of writing a thesis.
A special thanks to Professor Carlos Lodeiro Espiño, for allowing this agreement between both Universities and so giving me this opportunity.
To all my family who besides all the distance were surely wishing for my greatest success and worrying for my safe return. To all my friends who I missed a lot during these six months. A special word of appreciation for Vasco for traveling all the way to Amsterdam when I needed his friendly presence and wise words like never before.
Lastly, I must thank João Paulo for his advice, which never left my mind through out these five years of studies.

"Do I dare
Disturb the universe?"
-T.S. Elliot

Abstract

With the discovery of the amazing properties of graphene a wide range of applications were devised for this material. Due to the foreseeable great demand for graphene, new materials with similar properties, cheaper and of wider availability had to be studied. Molybdenum Disulfide, MoS_2, is one of the members of the transition metal dichalcogenides. When this material is in a single-layer disposition it presents very interesting properties for optical and electronic applications. Many of those applications complement areas where graphene is not useful. However, to obtain the MoS_2 mono-layers it is necessary to exfoliate this material. Currently the available exfoliation procedures lack the simplicity and the desired scalability for industrial porpuses.

With this project is attempted to use the *BuBclean* Cavitation Intensifying Bags or CIBs to exfoliate MoS_2. The applicability of plain bags and bags with pits will be tested, as well as to which ultrasonic equipment better suits for this new setup. Understanding what cavitation effects cause the material exfoliation is another objective of this project. For that, the mechanical and chemical effects from cavitation will be isolated and the different results compared. In an important analysis will be studied if the *BuBclean* CIBs are prepared to sustain the intense effects from cavitation.

It was verified that the bags with pits generate very intense cavitation slightly damaging the obtained layers of MoS_2. The plain bags showed better yields as well as less damaged flakes. The mechanical effects from cavitation proved to be the main factor in the exfoliation process, but lead to the formation of damaged flakes in the long run. The chemical effects on their own, manage to produce some exfoliated MoS_2. The *BuBclean* CIBs showed proper resistance to cavitation but also leaked when the temperature in the bath increased with time. Further studies must be done to understand if this is viable upgrade to the exfoliation process.

Keywords: Exfoliation - Molybdenum Disulfide - Cavitation - *BuBclean* CIB

Resumo

Com a descoberta das propriedades inigualáveis do grafeno surgiram um enorme número de aplicações para este material. Devido à expectável procura por este material, novos materiais de propriedades semelhantes e com maior disponibilidade tiveram de ser estudados. O Dissulfato de Molibedénio, MoS_2, é um dos membros da família dos metais de transição dicalcogenídeos. Quando este material é utilizado como uma mono-camada apresenta propriedades muito interessantes para ser aplicado nos campos da óptica e eletrónica. No entanto, para obter mono-camadas de MoS_2 é necessário exfoliar o MoS_2 bruto até atingir a sua forma bi-dimensional. Actualmente, os processos de exfoliação existentes pecam na sua complexidade e incapacidade de serem aplicados industrialmente.

Com este projecto é pretendido utilizar os sacos *BuBclean* para exfoliar o MoS_2. A aplicabilidade dos dois tipos de sacos existentes será testada assim como qual o equipamento ultrassónico que melhor se ajusta a este novo método. Compreender que efeitos provenientes da cavitação geram a exfoliação é outro objectivo deste projecto. Para isso, os efeitos mecânicos e químicos da cavitação serão isolados a fim de comparar o efeito de cada. Numa última análise, será estudada a resistência dos sacos da *BuBclean* aos efeitos da cavitação.

Foi verificado que os sacos com cavidades geram cavitação muito intensa que danifica as mono-camadas de MoS_2 obtidas. Os sacos não alterados apresentaram melhores rendimentos em mono-camadas que também se apresentavam menos danificadas. Os efeitos mecânicos da cavitação provaram ser mais influentes no processo de exfoliação, mas por outro lado mostraram danificar as camadas. Os efeitos químicos por si só, conseguem produzir MoS_2 exfoliado. Os sacos da *BuBclean* mostraram resistir aos efeitos da cavitação mas permitiram o derrame de solução com o aquecimento do banho ultrassónico ao fim de algum tempo de sonificação. Mais estudos devem ser feitos para explorar se esta aplicação é viável enquanto método de exfoliação.

Palavras-chave: Exfoliação - Dissulfato de Molibedénio - Cavitação - *BuBclean* CIB

Contents

List of Figures

List of Tables

CHAPTER 1

INTRODUCTION

1.1 Sonochemistry

Acoustic cavitation is the formation and collapse of vapour cavities on a liquid volume from an external negative pressure [1] induced by a high-intensity ultrasound to a system. This ultrasound has various effects on the system, from chemical to physical. The chemical effects it can induce in a system can fall in three categories: homogeneous sonochemistry of liquids, heterogeneous sonochemistry of liquid-liquid or liquid-solid and sonocatalysis [2]. The physical effects involve enhanced mass transport, emulsification, bulk thermal heating and many other effects on solids such as exfoliation [3].

Despite being called sonochemistry, the effects from inducing a high-intensity ultrasound between 20 kHz and 10 MHz [4] to a system are not a direct consequence from the ultrasound's acoustic waves, since their dimension is much larger than the molecules' dimensions [5]. Instead these effects arise from the cavitation generated from the ultrasound. It is possible to distinguish two types of cavitation, stable and transient. The first happens when the conditions allow for the bubbles to remain for extended periods of time without collapsing while sonication is applied. These bubbles oscillate radially around an equilibrium size persisting for many acoustic cycles. Whereas in transient cavitation the bubbles will persist only for one or two acoustic cycles. They grow to a size two or three times their original size during the negative acoustic pressures, when there is a rarefaction of the pressure on the solution, and collapse violently after a single compression half-cycle [6]. This later type of cavitation can be divided in three stages: nucleation, growth and collapse. Nucleation happens for the formation of the bubble. The sinusoidal wave that forms a sound is a mean through which energy is transported and it can be characterised by pitch, intensity and frequency, with the intensity, I, being given by equation 1.1, where P_A is the maximum amplitude of the acoustic pressure, ρ_o the average density of the medium and V the sound

velocity [7].

$$I{=}P_A^2/2\rho_o V \tag{1.1}$$

The intensity differences in the sinusoidal wave create zones of rarefaction and compression in the pressure verified on the medium through which it propagates [8]. The differences in pressure from the acoustic longitudinal wave can be described as the movement of a spring and the differences it generates in the pressure of a liquid throughout space and time can be described by equation 1.2 [6], where $P(t)$ is the total external pressure, P_0 is the static pressure and ω is the angular frequency of the acoustic wave.

$$P(t){=}P_0{+}P_A\sin(\omega t) \tag{1.2}$$

This compression and expansion leads the liquid medium to a condition where its normal average pressure is exceeded and as a result, the distance between the molecules exceeds the critical molecular distance to hold the liquid intact and inevitably the liquid ruptures and generates bubbles of various sizes [7]. For distilled water at 22°C the difference in pressure needed to generate cavitation can vary from -0,1 MPa to -20 MPa if is saturated with air or degassed respectively [9]. In transient cavitation the bubbles must grow in size before collapsing. Just like a spring, the bubble gas-liquid interface will oscillate with the differences in pressure and the bubble will grow before collapsing. On the other hand, in stable cavitation, the bubble will shrink during the compressional phase of the sinusoidal wave and diffuse gas out into the medium. During the rarefaction cycle, it will expand due to the gas diffusions that happen, this time into the bubble. This process, shown in Figure 1.1, is called rectified diffusion and allows for the longer lifespan of the bubble when compared to transient cavitation [6]. Eventually, after some time, collapse occurs due to the pressure inside the bubble no longer being in equilibrium with the pressure verified in the medium. During their collapse are generated conditions with temperatures as high as 5000°C, heating and cooling rates of 10^{10} K/s, and pressures close to 1000 atmospheres [10]. When assuming an adiabatic collapse it has been demonstrated by Riesz [6] with equation 1.3, that the temperatures reached upon the collapse of a bubble are related to the bubble's size, reaching temperatures proportional to the cube of the fractional change in the radius of the bubble.

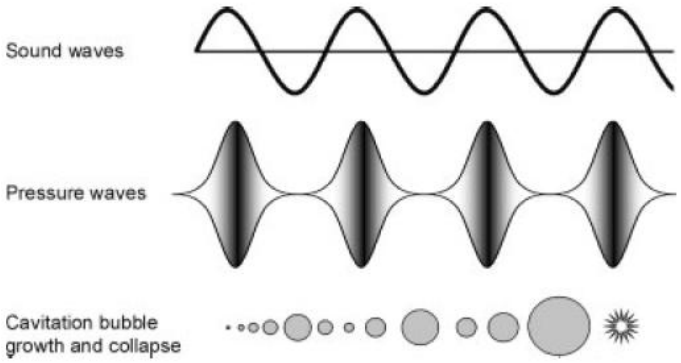

Figure 1.1: Schematic representation for the growth and collapse of stable cavitation bubbles during the rectified diffusion process [11].

$$T_f = T_0 (R_m / R_f)^{3(\gamma - 1)} \tag{1.3}$$

Being T_f the final temperature of the gas within the bubble, T_0 the liquid temperature, R_m the maximum bubble radius, R_f the final bubble radius and γ the ratio of specific heat for the liquid. Thus, the diffuse energy from sonication is concentrated in the bubbles and later released through these high temperatures and pressures [3]. The places where these conditions are verified are called hot spots. Here, the chemical and mechanical consequences of sonication are verified with the formation of radical species that interact with the species of the medium, sonochemiluminescence, from the recombination of the radical species [6], the occurrence of shock waves and other shear forces, which contribute to the mixing and particle fragmentation of the solids present in the medium [12], and sonoluminescence, when there is light emission from the bubble collapse [13].

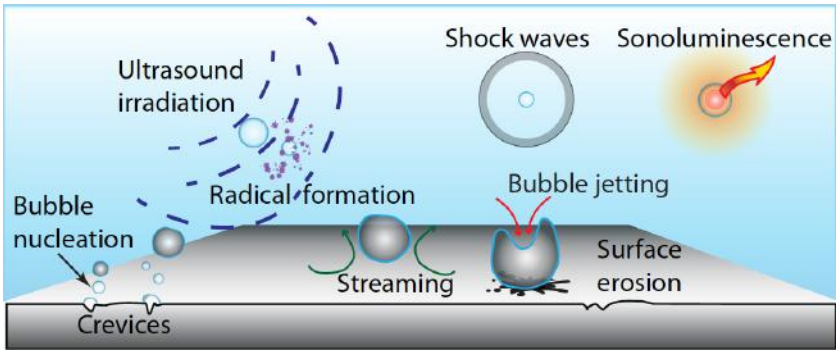

Figure 1.2: Schematic representation of the various chemical and physical effects from cavitation [2].

Three regions of sonochemistry have been identified for analysis of the behaviour of the bubble: bubble interior, bubble gas-liquid interface and liquid bulk [12]. The chemical effects derived from cavitation such as radical and excited species formation from molecular sonolysis, polymer rupture and changes in ligand-metal coordination mainly occur in the bubble interior or at the bubble interface. Later, these new species diffuse to the liquid bulk. The mechanical effects, on the other hand, are a result from the shockwaves, liquid jets and shear forces generated by the bubble collapse and therefore occur on the bulk liquid. When these effects act within the hot spot domain it is called primary sonochemistry and secondary sonochemistry when they act outside as depicted in Figure 1.3 [7].

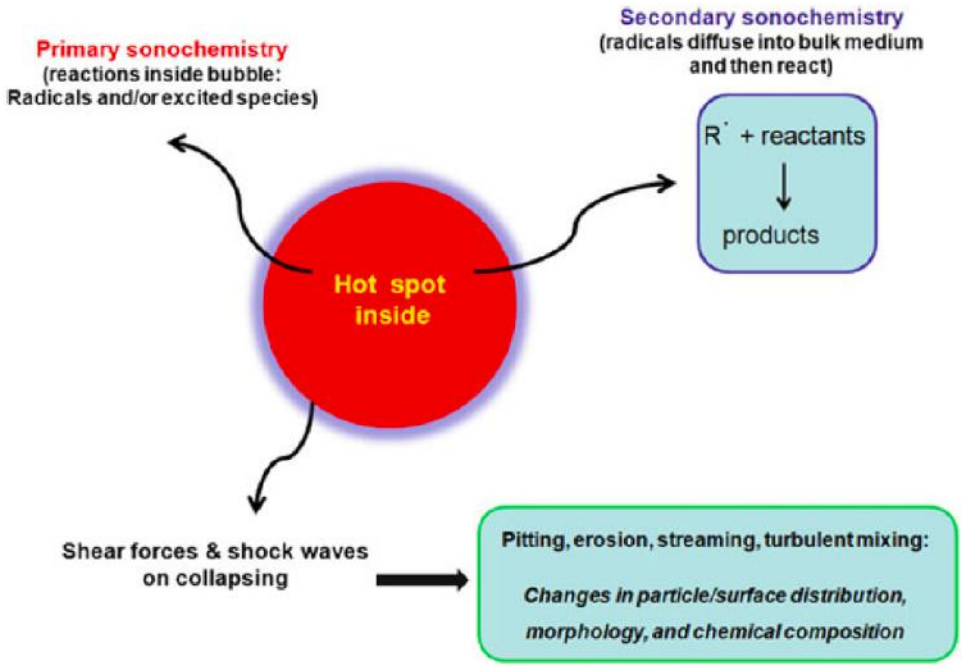

Figure 1.3: Schematic representation of primary and secondary effects of cavitation [7].

When it comes to radical generation the species generated in an aqueous solution are well known to be $H^{\bullet}$ and $OH^{\bullet}$ radicals [5, 14]. The generation of radicals is highly dependable on the conditions verified on the medium upon cavitation. These radicals besides interacting with the materials in solution, will recombine between themselves generating new species and sonochemiluminescence, from emitting light when interacting with other species in the solution outside the bubble [6, 13]. For the aqueous solutions it is known that cavitation generates H_2 and H_2O_2 [5].

The physical effects from sonication generate other phenomena unrelated to cavitation. The shockwaves from cavitation drive smaller particles into collision with other particles or elements of the apparatus and consequently they crash at very high speeds leading to intense localised heating, plastic deformation, spot-welding and melting of relatively low-melting point metals [15].

Cavitation has different effects when it occurs close to a solid surface instead of inside a pure liquid. In liquid-solid sonication, the crevices of the solid play an important role in increasing the effects of sonication. These small crevices store air, and the interface between the air and the liquid that covers the surface of the solid, oscillates with the ultrasound to a point where it may break and generate more bubbles, maximising the sonication effects by increasing the number of bubbles in the medium. Also, near a solid surface the bubble collapse is non-spherical, like in Figure 1.4, creating a shockwave that damages the surface and may break up brittle materials through a high-speed liquid microjet, which can reach velocities as high as hundreds of meters per second [10]. These distortions on the bubble collapse are dependable on the surface size which must be several times larger than the resonance bubble size. Thus, for ultrasonic frequencies of approximately 20 kHz, there is no damage from microjet formation on solid particles smaller than 200 μm. Ultrasonic cleaning is possible thanks to the erosion caused by these interactions between the bubbles and other solids in solution [3].

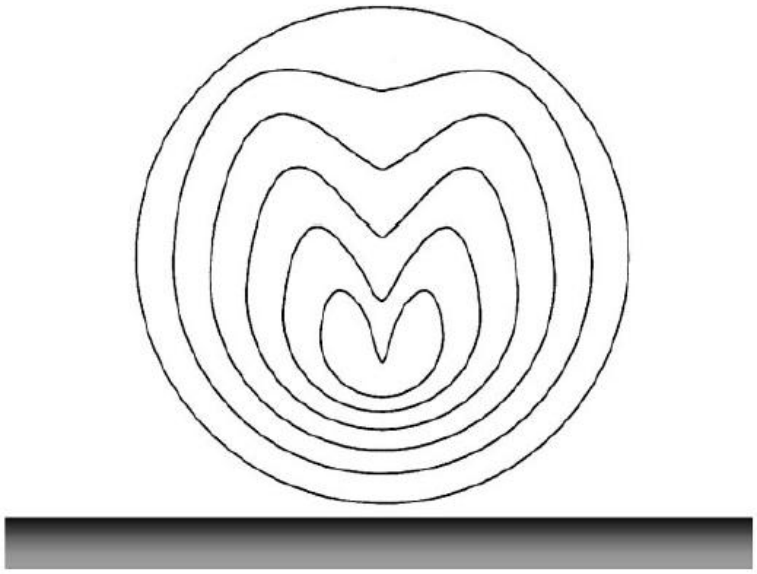

Figure 1.4: Formation of a liquid microjet near an extended surface [3].

Currently there is a wide variety of sonochemical apparatus being the most common ultrasonic cleaning baths, direct ultrasonic immersion horns and flow reactors. Cleaning baths are very useful for liquid-solid reactions despite having low intensities [10]. These apparatus have various transducers placed horizontally beneath the bath which induce the ultrasound on a liquid medium where the sample is placed. The ultrasonic horn, usually induces a higher intensity ultrasound on the solution through a titanium horn driven by a piezoelectric transducer into the sample, usually stored in a glass flask. These equipments operate at frequencies around the 40 kHz with the ultrasonic horns reaching the 20 kHz. Nonetheless, there are apparatus available for many other intensities [5].

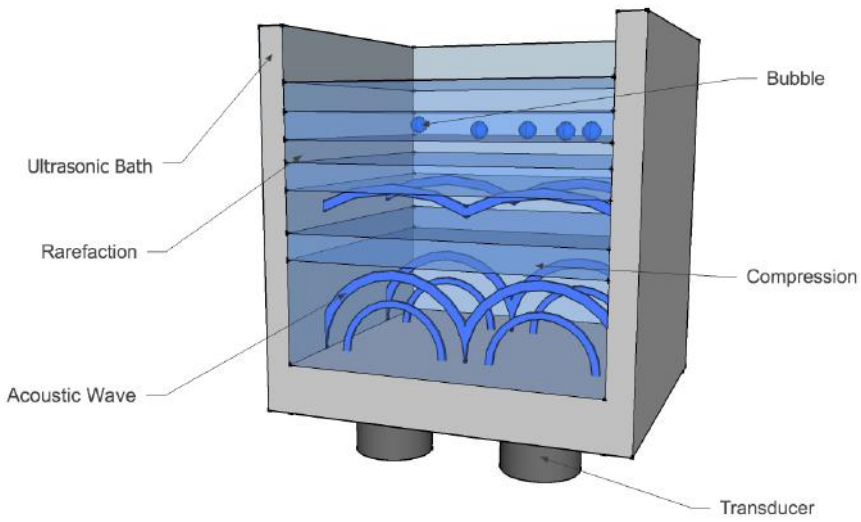

(a)

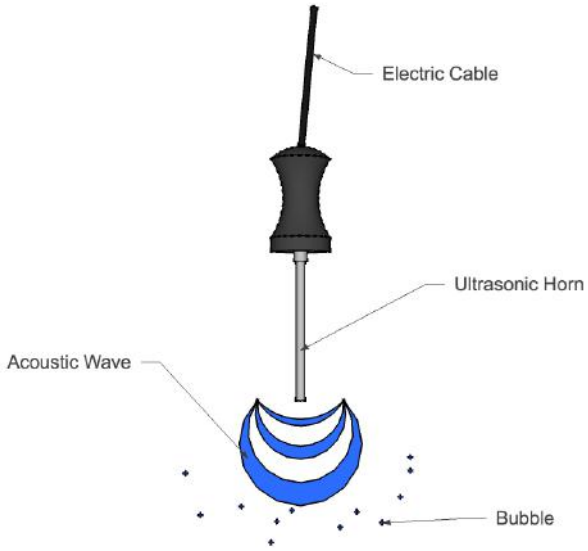

(b)

Figure 1.5: Schematic Representation of the Ultrasonic Bath from Figure 2.4 (a) and Horn from Figure 2.5 (b), both applying ultrasound and generating bubbles.

Any work done to study sonochemistry is subject to influences from so many effects that its reproducibility is always very limited [16]. In order to make proper observations while studying sonochemistry and generate reproducible results, the observer must control as many conditions affecting the following categories as possible: the exposure field, the conditions of the liquid and the method of observation. For the first category, is necessary to

control the frequency, intensity, pulse conditions, type of exposure field and total exposure time. As frequency increases, R_m will decrease resulting in less time for nucleation and growth. Higher intensities result in bubbles of bigger dimensions and consequently higher temperatures. When it comes to the conditions of the liquid it is important to know all the properties of the liquid and if it is in the proper conditions for use in the experiment, since it will highly influence the radical generation. Finally, like in any other experiment the method of observation must be similar in every experiment. All these parameters must be carefully controlled since cavitation is a very difficult phenomena to quantify [6].

1.2 MoS_2 Exfoliation

Due to the mechanical and chemical phenomena sonication generates, it can be used for a very particular and interesting process in nano-materials synthesis: exfoliation.
Currently, the research made on graphene, a two-dimensional network of sp^2 carbon atoms, has placed it as the flagship material for future technology [7]. It is still being researched to this day a process adaptable to large-scale synthesis of few-layer graphene and other materials called transition metal dichalcogenides, TMDCs. These materials have very interesting properties when used in a single-layer disposition for various applications like energy storage, catalysis, solar cells, sensing and electronic devices. These substances are a very large family of layered materials with crystal structures covalently bonded in X-M-X layers that interact through van der Walls forces, being the M a metal atom such as Mo, W, Ti, Zr, Hf, Ta, Re, Co, Ni, Ir, Pt, V, Nb, Tc, Rh or Pd, and X a chalcogen like S, Se or Te, and therefore due to these various combinations, these materials can either be semiconductors, metallic or superconducting [17]. Each single-layer of a TMDC is a layer of a metal sandwiched between two layers of chalcogens. One of the most promising TMDCs is MoS_2. Unlike graphite, molybdenum is a very common element and as a single-layer, MoS_2, is a p-type semiconductor, or a metal depending on its metallic phase [18], that transits from the indirect bandgap it has in the bulk state of 1,2 eV to a a direct bandgap of 1,8 eV [19]. This property is very interesting since it largely compensates the weakness of gapless graphene, making it very useful for the next generation in switching and opto-electronics devices. A MoS_2 mono-layer has a thickness of approximately 0.65nm [20]. In addition to the many applications of MoS_2 as a three-dimensional material, its mono-layers can also be used for memory devices, photodetectors, photovoltaic devices, field effect transistors [17] and as an hydrogen evolution catalyst [21].

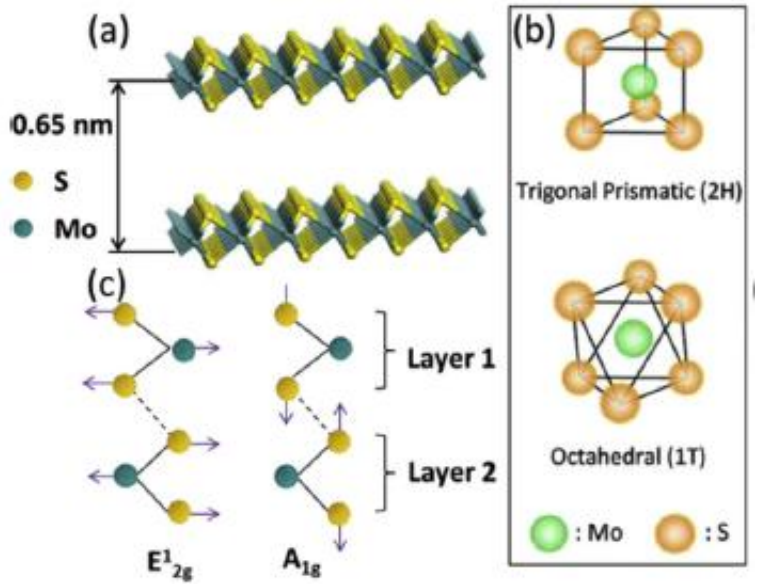

Figure 1.6: Chemical structure of two mono-layers of MoS_2 (a), the two metallic phases from MoS_2 as a mono-layer (b) and the two typical Raman active phonon nodes from this material [17].

In order to explore the interesting properties of these materials exfoliation is a mandatory step on their transition from a three-dimensional material to a two-dimensional one. To do so, many methods similarly used for the exfoliation of graphite into graphene may be implemented. These methods are either chemical, micromechanical, surfactant assisted liquid phase exfoliation or growth via chemical vapour deposition [22]. They can have a bottom-up approach or a top-down one [21]. Micromechanical cleavage techniques, such as the scotch tape method, rely on shear forces to overcome the weak forces that connect the various mono-layers and produce single-layered MoS_2 with very high structural quality but lacks the scalability for practical applications. The more common chemical cleavage relies on lithium intercalation between the single-layers of the TMDC overcoming the weak van der Walls forces [23, 24] as in Figure 1.7. However, despite being a scalable process the chemical cleavage of MoS_2 leads to a phase transition of the material to a metallic 1T-MoS_2 from the original semiconducting 2H-MoS_2 phase, needing further thermal treatments in order for the MoS_2 to regain its original phase. Currently, research is being made on new methods to fully recover the original metallic phase of the material [21]. The thermal treatments used for that purpose have not yet fully recovered the original semiconducting phase of the studied samples. This leads to the presence of residual metallic phase on the final product, which has detrimental effects on its applications. Despite these recent improvements, research is being made to develop new exfoliation methods since exfoliation of TMDCs through intercalating species still uses many solvents, some of them toxic and hazardous [25], very specific conditions and lengthy steps. MoS_2 growth from chemical vapour deposition has some disadvantages since it requires high processing temperatures and further treatments to retrieve the growth substrate [22]. More recently, the usage of

supercritical CO_2 for the exfoliation of MoS_2 mono-layers has been studied [26]. Thanks to the wide range of applications and properties of these material, new exfoliation methods are constantly being designed and tested but the lack of a simple and properly effective technique to exfoliate high-quality and defect free MoS_2 has hampered important studies and practical applications of this material [21].

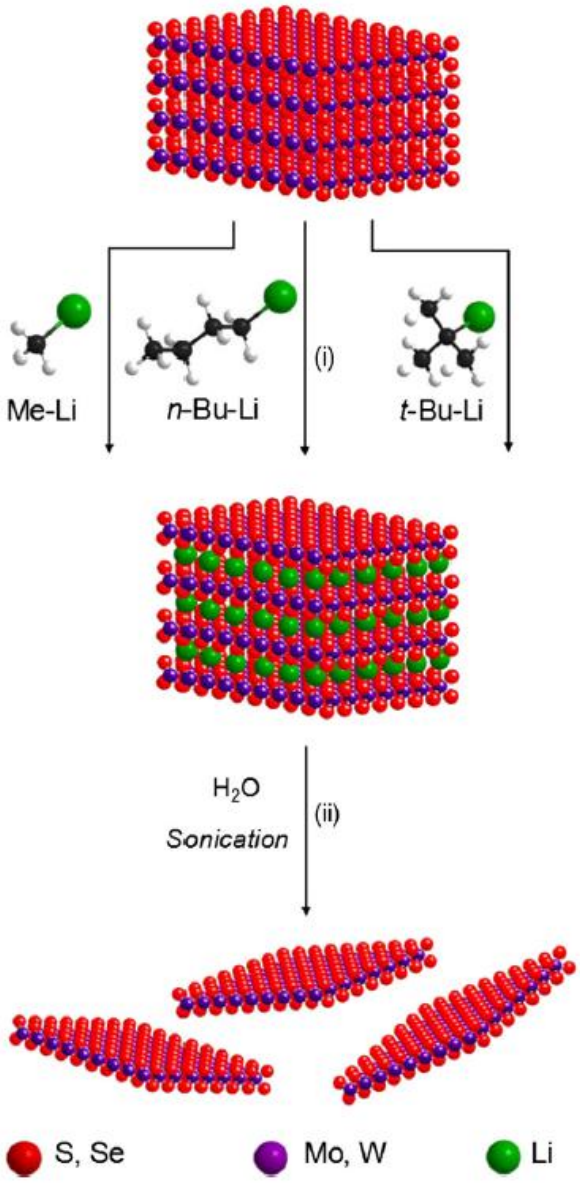

Figure 1.7: Representation of Li ions intercalation to later exfoliate MoS_2 through water sonication [23].

1.3 Novel exfoliation process

With the enormous difficulties in finding a straightforward and simple technique to exfoliate and synthethise nanomaterials, it is worth attempting to explore the capabilities of the *BuBclean* Cavitation Intensifying Bags, CIBs or *BuBble Bag* - Figure 1.8.

(a) (b)

Figure 1.8: *BuBclean* Cavitation Intensifying Bag [27] (a) and a schematic representation of the same bag showing the pits as a mean to intensify bubble nucleation [28] (b).

BuBclean is a start-up from the Netherlands focused on ultrasonic cleaning applications. It has developed small poly-propylene containers for ultrasonic cleaning of different objects such as 3D printed parts or dental equipment, but can also be used as reactors or emulsifiers. Recently, the company patented a small development on the bag by adding pits to its inner surface [29]. These small crevices were added to increase the efficiency from the generated cavitation and give better cleaning results without the need for adding more solvents. The addition of these pits makes these bags very useful as a sonochemical microreactor [16]. The small pits on the bags work as artificial nucleation sites by retaining small quantities of air after filling the bag with a solvent. Upon sonication, the interface between the gas bubble on the pit and the liquid poured inside the CIB vibrates thanks to the differences in pressure caused by the ultrasound. When the equilibrium between the pressures inside and outside of the bubble is broken, the bubble generates many more microbubbles than the bag without pits would generate. Unlike other glassware used for sonochemistry that

rely on small fractures and crevices on its surface to store small bubbles of air to generate cavitation, this setup already possesses the much needed crevices as the pits. The existence of pits not only enhances the intensity of the generated cavitation but also increases the reproducibility of the work done with the bags [16], a critical factor when working with sonochemistry.

Chapter 2

Techniques and Materials

2.1 Materials

This section describes the materials used in the experimental work made throughout this work, from reactants, solvents and other substances used.

2.1.1 Molybdenum(IV) Disulfide

In this work Molybdenum(IV) Disulfide, MoS_2, - from *Aldrich Chemical* - was the compound chosen to prove the exfoliation capabilities of the *BuBclean* bags. This compound is a very thin dark powder with a molecular weight of 160.07 g.mol^{-1} and a density of 5.06 g.mL^{-1} at 20°C. It is sold in the form of powder under the CAS number 1317-33-5.

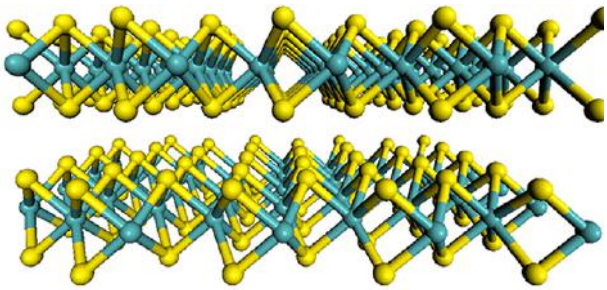

Figure 2.1: MoS_2 chemical structure.

2.1.2 Isopropanol

Isopropanol (C_3H_8O) was used as the main solvent in this experiment. Acquired from *Atlas Assink Chemie*, it has a molecular weight of 60,10 g.mol^{-1}, a density of 0,786 g.mL^{-1}

at 20°C and is a colourless liquid. It must remain away from fire due to its inflammable nature. It is identified under the CAS number 67-63-0.

2.1.3 Buffer Reactants

For this work a few reactants were used to adapt samples for certain observations. These reactants were used as radical trappers and to prepare a buffer solution. These were:

- Terephthalic Acid

  Terephthalic Acid was used on this work as a radical scavenger. It has a molecular weight of 166.13 g.mol^{-1}, has a density of 1,522 g.mL^{-1} at 20°C and resembles a white powder. It was supplied by *Aldrich Chemical* and is sold under the CAS number 100-21-0.

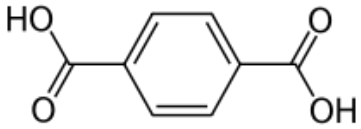

Figure 2.2: Terephthalic Acid chemical structure.

- Sodium Hydroxide

  Sodium Hydroxide (NaOH), was one of the compounds used in the preparation of the solution for the radical trapping. This compound is a strong base and was supplied from *Aldrich Chemical*. It has a molecular weight of 39,9971 g.mol^{-1}, a density of 2,13 g.mL^{-1} at 20°C and has the appearance of small white crystals. It is identified by the CAS number 1310-73-2.

- Monopotassium Phosphate

  Supplied by *Riedel-de Häen*, Monopotassium Phosphate (KH_2PO_4) or Potassium Dihydrogen Phosphate was one of the two compounds used in the preparation of a buffer solution. It has a molecular weight of 136,086 g.mol $^{-1}$, has a density of 2,338 g.mL^{-1} at 20°C and is a thin deliquescent white powder. It is identified by the CAS number 7778-77-0.

- Disodium Phosphate

  Disodium Phosphate (Na_2HPO_4) or Sodium Hydrogen Phosphate was acquired to *Riedel-de Häen*. It is a white powder, with a molecular weight of 141,96 g.mol^{-1} and a density of 1,7 g.mL^{-1} at 20°C. It is identified by the CAS number 7558-79-4.

Some precautions must be taken with the reactants described above due to their acid or basic nature.

2.1.4 Azobisisobutyronitrile

Azobisisobutyronitrile (AIBN) is a compound commonly used in polymer science as an initiator to generate radicals which will begin the polymerisation process. It was used in order to generate radicals without resorting to cavitation and this way avoid any mechanical effects from it.

The used AIBN was from *Aldrich Chemical*. It has a molecular weight of 164,21 g.mol^{-1}, a density of 1,1 g.mL^{-1} at 20°C and is identified under the CAS number 78-67-1. It must be stored on a fridge at a temperature between 2-8°C, otherwise it will start to decay.

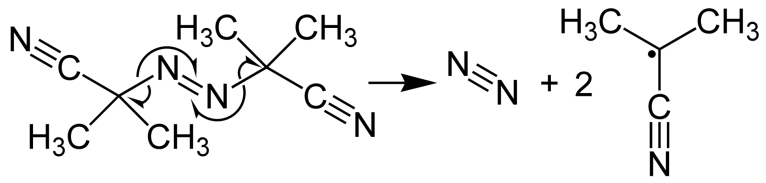

Figure 2.3: Formation of radicals from AIBN [30].

2.1.5 Cavitation Intensifying Bags

The Cavitation Intensifying Bags used were produced by the company *BuBclean*. The bags used were made of polyethylene or polypropylene, with a wall thickness of 5 μm and dimensions of 100x150 mm. These bags are made industrially through the pressing of a cast with pins on the inside side of the bag before it being folded. It was both used bags with pits and without pits.

2.2 Techniques

2.2.1 Solution Preparation

2.2.1.1 MoS_2 Exfoliation

This study followed an adaptation of the procedure used by Mandal [31] for the functionalization of MoS_2 flakes and by Coleman [32].

MoS_2 Exfoliation with the *BuBclean* bags in two different setups

For the experimental setup of this experiment were prepared the samples describe on table 2.1 in order to analyse the differences in the product obtained when comparing different ultrasonic sources and different bags. The solution inside the bag is a mixture of IPA and MoS_2 with a concentration of 20 $mg.ml^{-1}$. This mixture is called Basic because it does not contain radical scavengers nor an initiator to produce radicals like in other two solutions prepared to understand the exfoliation process as described later.

Sample	**Solution**	**Ultrasonic Equipment**	**Type of Bag**	**Time of Sonication**
BBP	Basic	Ultrasonic Bath	Bag with Pits	4,5 hours
BBNP	Basic	Ultrasonic Bath	Bag without Pits	4,5 hours
BHP	Basic	Ultrasonic Horn	Bag with Pits	4,5 hours
BHNP	Basic	Ultrasonic Horn	Bag without Pits	4,5 hours
BBNP 20 mins	Basic	Ultrasonic Bath	Bag without Pits	20 mins
BBP 20 mins	Basic	Ultrasonic Bath	Bag with Pits	20 mins

Table 2.1: Samples Description.

Inside the bags used for the Ultrasonic Bath (VWR USC200TH), were placed 50 ml of IPA whereas for the bags placed inside the Ultrasonic Horn (Bandelin Sonoplus mini20) were only placed 25 ml. This is because the bags for the horn were modified into a slightly smaller size due to the fact that the biggest probe (MS 2.5) available for the horn is used for 25 ml samples. Most samples were exposed to ultrasound for 4,5 h [31]. Later, two samples were exposed to ultrasound solely for 20 mins to observe how the difference in time and energy would affect the final result.
The Ultrasonic Bath has a frequency of 45 kHz and the Horn has a frequency of 50/60 Hz. The way both apply the ultrasound is also different. A sample inside the bath is equally exposed to the sound waves that propagate horizontally through the water contained in the bath. These horizontal planes represent the positive and negative amplitudes of the sound wave. The horn works differently and applies the ultrasound with increased intensity at its tip. This exposes the sample on that position to a more intense sound wave than the parts of the sample that stand further from the tip, which has effects on the cavitation intensity. It is important to have some precautions during sonication by not placing any fingers or

hands in the liquid exposed to ultrasound since it may generate air bubbles in the blood stream.

Figure 2.4: VWR USC200TH Ultrasonic Bath with a capacity of 1,8 L and a frequency of 45 kHz. This equipment is 17,5 cm wide, 16,5 cm deep and 22,5 cm height.

Figure 2.5: Bandelin Sonoplus mini20 Ultrasonic Horn with the MS 2.5 probe applies a frequency of 50/60 Hz and has 0,5 cm in diameter at the tip and 16 cm in height.

After sonication these samples were taken for centrifugation for 1 h at 1500 rpm at a Heraeus Labofuge 400 like the one shown in Figure 2.6. This way the heavier parts of the solution

would deposit at the bottom of the flask. Later, on top of this residue is a dispersion of IPA and the lighter parts of MoS_2. A third of this dispersion was retrieved and taken for analysis with the UV-Spectrophotometer. The dispersion left from the absorption measurements was then vacuum filtrated to retrieve the MoS_2 that stands on the dispersion. For this a PVDF membrane with 0,1 μm pore size from *Merk Millipore* was used. By measuring the volume before the filtration and the mass that is deposited on the membrane is possible to compare the various results. The volume is measured before the filtration because IPA easily evaporates through the hose that induces the vacuum. For the rest of the tests done, small pieces of the membrane were cut and used for each method after 24 h in the oven at 80°C to evaporate any remaining solvent. A diaphragm vacuum pump from *vacuubrand* type MZ 2C with a pump flow of 1,7 m^3/h was used.

Figure 2.6: Heraeus Labofuge 400 centrifuge [33].

Exfoliation as a result of Chemical or Physical effects

To observe if the exfoliation process occurs due to chemical or mechanical effects from cavitation a setup was devised where each of these effects would be removed from the experiment.

To remove any chemical effects, the solution MBP was prepared by adding to the solution of IPA and MoS_2, 5 mL of a solution [14] that acts as a radical scavenger. This way as radicals are generated, they are trapped by the scavenger solution and any interactions that may happen between the MoS_2 and the radicals is minimized. The scavenger solution used was prepared by mixing 0.0834 g (2 mmol.L^{-1}) of terephthalic acid, 0.0529 g of NaOH (5 mmol.L^{-1}), and phosphate buffer with a pH of 7.4, prepared from 0.1480 g of KH_2PO_4 (4.4 mmol.L^{-1}) and 0.2453 g of Na_2HPO_4 (7 mmol.L^{-1}). The solution was then placed inside a bag with pits, to maximise the mechanical effects, and on the ultrasonic bath.

On another experiment, the mechanical or physical effects were removed by not applying ultrasound to the solution. Instead, approximately 1 mg of AIBN was introduced to a basic solution of MoS_2 and IPA, which was heated to a temperature of 60°C. A temperature high enough for AIBN to generate radical species but still too low for IPA to boil. This solution was prepared inside a beaker and had a mixer at low speeds to avoid much turbulence, which would otherwise cause itself physical effects on the MoS_2 particles. The beaker was covered with Parafilm M® to avoid losing sample from evaporation. This sample was called C_NP.

The following diagrams in Figures 2.7, 2.8, 2.9 and 2.10 show the procedure used for all the samples and all the analysis done to each:

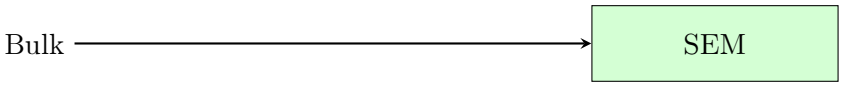

Figure 2.7: Experimental procedure used for the analysis of the Bulk sample.

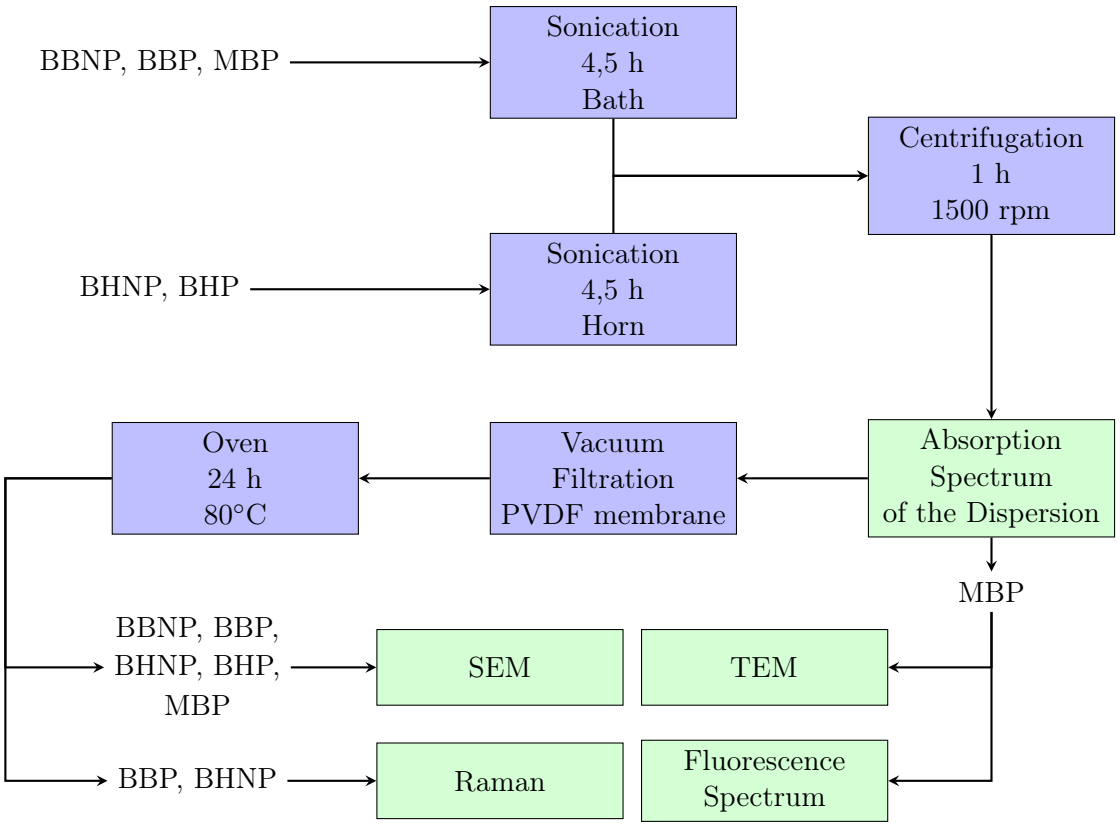

Figure 2.8: Experimental procedure used for the analysis of the BBNP, BBP, BHNP, BHP and MBP samples.

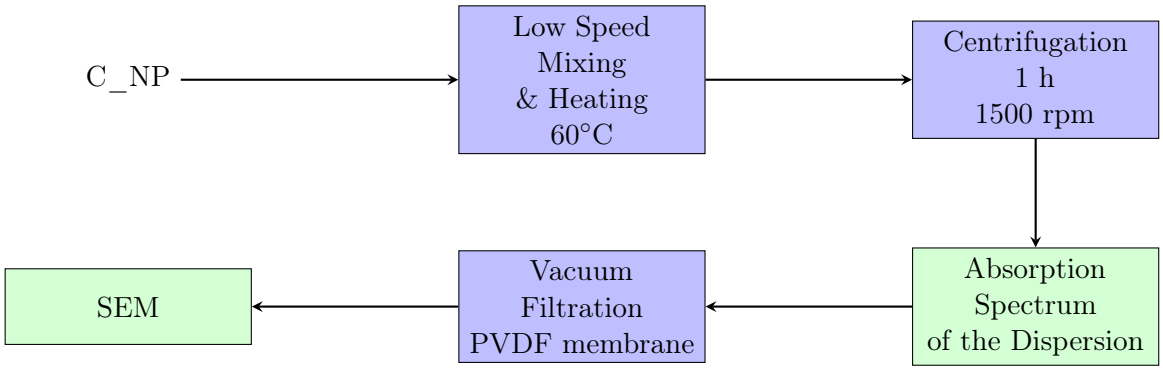

Figure 2.9: Experimental procedure used for the analysis of the C_NP sample.

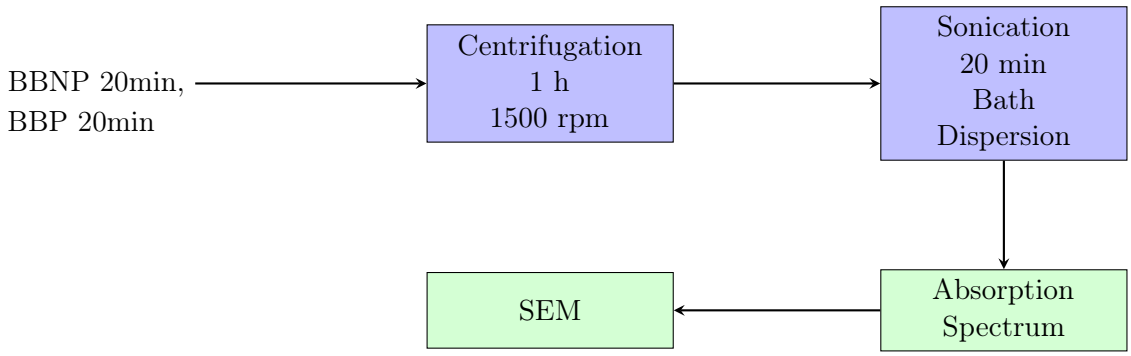

Figure 2.10: Experimental procedure used for the analysis of the BBNP 20min and BBP 20min samples.

2.2.1.2 Resistance of the *BuBclean* bags to Cavitation

On this experiment are evaluated the effects from cavitation on the bags. As known, cavitation generates very intense phenomena that can have effects on the physical and chemical stability of the polypropylene of which the bags are made.
A small piece of a *BuBclean* bag with approximately the size of a cover slip was cut from the top side of the bag, where there are no pits. This bag sample was then attached to a cover slip with the help of two smaller pieces of another cover slip and scotch tape, as shown in Figure 2.11.

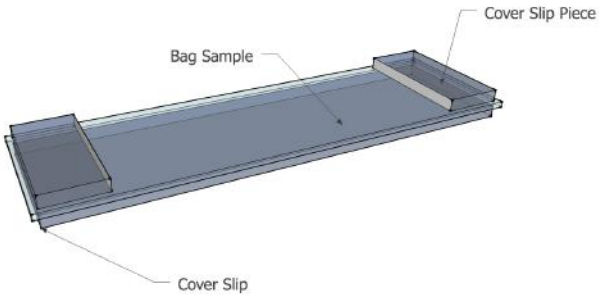

Figure 2.11: Sample preparation.

The sample was placed inside a small glass reservoir with 200 mL of *Mili-Q* water and an ultrasonic horn, being held by a grip, was placed 5 mm above the sample and turned on for 2, 5 and 10 minutes. The sample was divided in three parts to allow three measurements with just one sample. These samples are then observed through the SEM to analyse any erosion that may take place.

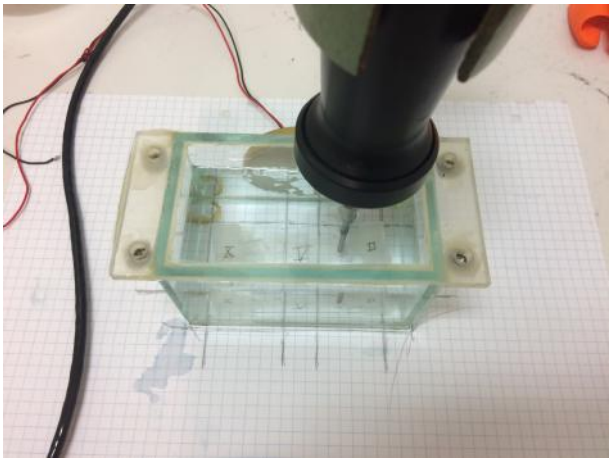

Figure 2.12: Experimental setup to evaluate the bag's resistance to cavitation.

In another attempt to observe changes on the bag after sonication, the bag was placed on the same glass reservoir as before and in the same conditions, but was exposed to ultrasound and then observed through the optical microscope until there were signs of erosion on its surface. Polarised lenses were used to help identifying small signs of erosion. The ultrasonic horn was placed 5 mm above the sample.
This experiment is a continuation of the ongoing resarch by Rivas on the erosion from acoustic cavitation on silicon surfaces [1].

2.2.2 Characterisation Methods

2.2.2.1 Spectrometry

Absorption Spectra

This method was used to qualitatively and quantitatively observe if the compounds on the dispersion are the ones which are intended to be produced and compare between samples their respective yield. This equipment uses a light beam of an identified wavelength to analyse what wavelengths are absorbed by the sample. An initial blank measurement is made to establish a zero absorption spectrum. Afterwards, a light beam is directed towards the sample and then captured through a detector. This detector measures the difference in the intensity of the light beam after passing the sample. This intensity is then subtracted to the intensity from the blank solution generating the absorption spectrum. During every measurement two cuvettes stand inside the spectrophotometer. One just with solvent and the other with the sample from the solution. This way the absorption from the solvent is not taken into account by the detector.

The Beer-Lambert Law makes it possible to relate the absorption from a sample with its concentration through equation 2.1.

$$A=\varepsilon\times l\times c \tag{2.1}$$

Being A the absorption intensity, l the cuvette's length, c the sample's concentration and ε the extinction coefficient. Since the sample's concentration is unknown it is necessary to determine the extinction coefficient value. For that, a series of five dilutions are made and the respective spectra peak are measured. After measuring the solution volume and the mass obtained through the filtration it is finally possible to determine the concentration from each of the five dilutions and relate it with the respective absorption bands. This relation returns a linear equation whose slope is the extinction coefficient.

It is known from literature [32] that MoS_2 mono-layers have two bands between the 600 nm and the 700 nm. Therefore, the picked wavelengths to run the sample were between 300 nm and 900 nm. This wider spectra allowed to see if certain behaviours of the MoS_2 mono-layers spectra were being noted, like the small peak at the 500 nm or the intense decrease in the absorption intensity that exists before the 400 nm. A Perkin Elmer Lambda 850 spectrophotometer like the one shown in Figure 2.13 was used for these measurements. This equipment was not equipped with a mirror to redirect any reflected light beams from the sample and therefore the obtained results have some error associated to them since there were solid particles in the measured samples.

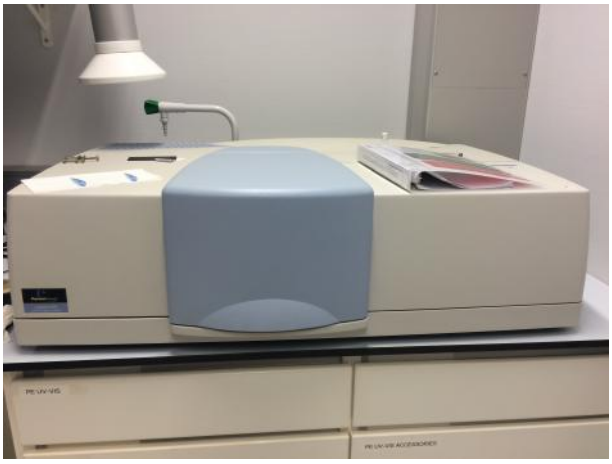

Figure 2.13: Perkin Elmer Lambda 850 UV-Spectrophotometer.

Raman Spectroscopy

Raman Spectroscopy is a method used to identify species through their vibrational, rotational and low-frequency modes. The monochromatic light from a laser is used to excite the rotational modes of the species present in the sample. Leading the phonons on the laser to shift in energy, which allows for the identification of the species present in the sample. Usually the laser is either on the visible spectra, close to the infrared, or in the infrared wavelength. The resulting data from this test is a simulated image from the area of the sample where the laser ran. This image indicates the Raman intensity for every point of that area and can be transformed into a graphic that indicates the average Raman intensity for the sample. From the generated graphic is possible to analyse the sample both quantitatively by analysing the peak intensity, and qualitatively by observing the obtained Raman shifts for each peak.

Ideally the samples for observation on this equipment are placed on top of a calcium fluoride holder to reduce the fluorescence and for the sample to have a flat surface. A silicon wafer can also be used as a holder. On this experiment the holder where the sample was placed was the membrane where it had been filtrated. The membrane is far from an ideal holder due to its high fluorescence and rugosity. Intense fluorescence results in high Raman intensities and the variable rugosity of a sample makes impossible for an even measurement since the laser propagates for a small distance into the surface of the sample and in these conditions sometimes the measurements may contain some air due to a lower thickness of the sample.

For this work was used the Raman apparatus from the Medical Cell BioPhysics research group from the University of Twente seen in Figure 2.14. It applied a laser beam with a power output of 350 μW, a frequency of 50 kHz for 50 ms over a surface with 50x50 μm.

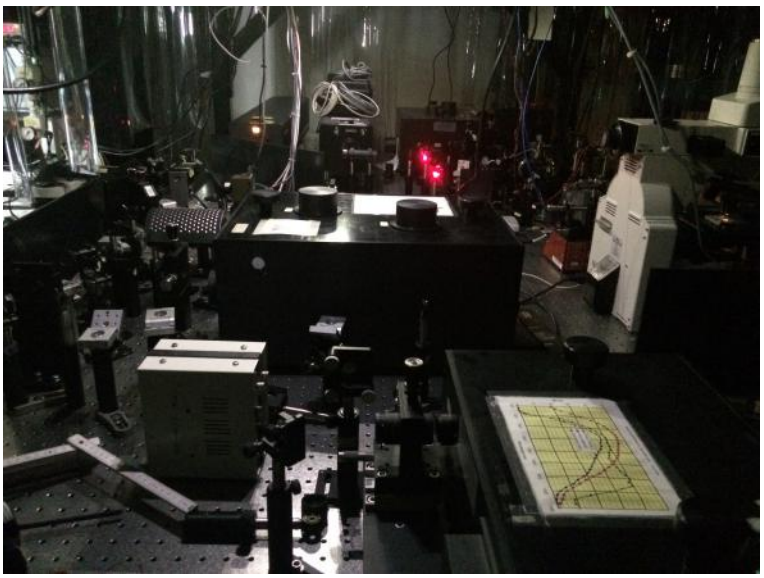

Figure 2.14: Raman Spectrophotometer at the Medical Cell BioPhysics research group.

Fluorescence

To measure the amount of radicals captured by the radical scavenger in the analysis made to either it is the mechanical effects or the physical effects that generate the exfoliation process, it was necessary to evaluate the concentration of the therephthalic acid present in the solution.

On this method, a light beam of know wavelength is directed to the sample. On the case of the therephthalic acid it is know that when a wavelength of 315 nm is used, its electrons reach an excited singlet state and when they return to their electronic ground state, emit photons with a wavelength of 425 nm. The fluorescence spectrophotometer then detects this emission and generates a graphic where is possible to observe the emission intensity of the photons emitted by the sample. Expectably, in the picked wavelength interval there should only be a peak at the previously known emission wavelength. It is also possible to make the opposite analysis by analysing the excitation of the sample instead of the emission.

For this work a Perkin Elmer fluorescence spectrophotometer was used - Figure 2.15. The sample is a small volume of the obtained dissolution which is placed in a cuvette. Fluorescence measurements, unlike absorption, are made in a 90 ° angle. This means that the wavelength detected is measured in a plane that is 90° to the face of the cuvette where the original light beam strikes the sample. After defining the interval where the emission detection is to be made, which must stand away from the excitation wavelength for the emission detection and away from the emission wavelength for the excitation detection, is defined the wavelength of the light beam to hit the sample. It is important to keep the slits as closed as possible in the first measurements to avoid too much light from hitting the sample and the detector, and then to perfect the results slightly open them until the

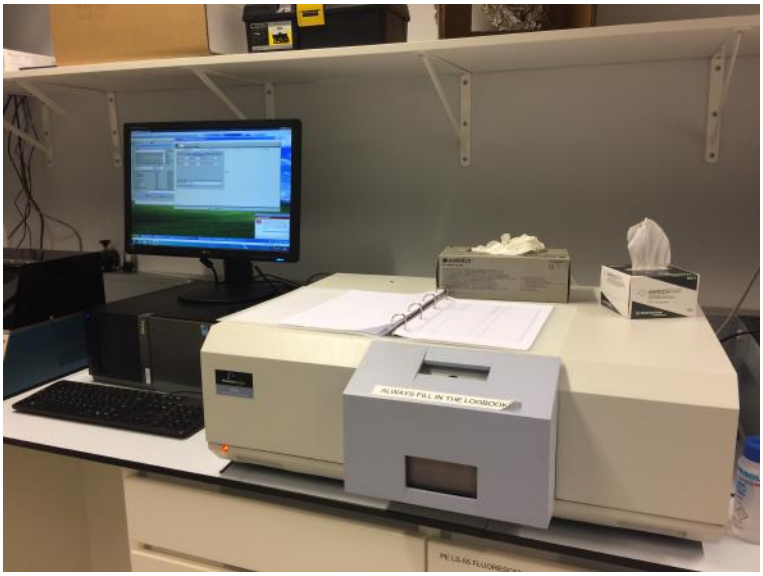

Figure 2.15: Perkin Elmer fluorescence spectrophotometer.

fluorescence intensity detected is satisfactory. It is important to avoid exposing the sample to too much light because this may compromise the results obtained through this method. To determine the concentration of terephthalic acid on solution and then calculate the amount of radicals that were generated and trapped by the scavenger the same procedure used for absorption with the Beer-Lambert Law is used.

2.2.2.2 Microscopy

Scanning Electron Microscopy

The scanning electron microscope (SEM) is used for the observation of a samples' topography and can also be used to determine its surface composition. This microscope is different from the more common microscopes since it relies on an electron beam and the particles emitted by the sample upon being hit by it to generate a two dimensional image and to determine which compounds are present on the surface. This procedure allows for resolutions as high as 25 Å, much higher than the resolutions obtained through common microscopes.

For this procedure a Zeiss Merlin SEM as seen in Figure 2.16 was used. This equipment, as any other SEM, is composed of two main parts: the electron column and the control console. The electron column is where the electron beam is generated and directed towards the sample which is also stored on this part of the SEM. This segment of the equipment is in vacuum during the observation and also contains electromagnetic deflectors to direct the beam towards the sample. To produce the electron beam a tungsten filament is heated to very high temperatures to generate free electrons. These electrons are accelerated through the column by a potential difference and pass through lenses which converge the beam through the focal point. For the samples observed in this work various potential differences

Figure 2.16: Zeiss Merlin Scanning Electron Microscope [34].

were used. When the beam reaches the sample chamber and hits the surface of the sample various particles are released due to the kinetic energy of the electrons. This kinetic energy leads to two different types of scattering interactions with the sample which translates into two different types of particles: secondary electrons, when there are inelastic scattering interactions, and backscattered electrons, for when the scattering interactions are elastic. Both are detected by a detector in the sample chamber and used to generate the SEM image, being the first important in analysing the topography and morphology of the sample and the latter in showing contrast between areas of different chemical composition. X-rays are occasionally emitted when an inner shell electron is removed from the sample and can be used to determine the sample's chemical composition.
For this method a small piece of the membrane used for the filtration with sample was cut and placed on a metal holder for observation. For a second batch of samples, a drop of their dispersion was placed on top of a carbon grid for better images. To observe the effects from cavitation on the bag, the entire sample was placed inside the equipment as it was.

Transmission Electron Microscopy

Transmission Electron Microscopy (TEM) is a method used to generate images from a sample at the atomic level. It not only allows to observe the surface's morphology of a sample but can also be used for a thorough analysis of its structural order. Just like SEM, this method relies on an electron beam to produce two dimensional images of the sample. But unlike SEM, which relies on scattered electrons, TEM relies on the transmitted ones.

A transmission electron microscope is also made up of an electron column and a control panel. A Phillips CM300ST-FEG transmission electron microscope - Figure 2.17 - was used.
For this method, a part of the dilution obtained of the sample to be observed was not filtrated. Instead a small drop of it was placed on a carbon grid. This grid serves as a holder which is then placed in the electron column for the observations.

Figure 2.17: Philips CM300ST-FEG Transmission Electron Microscope 300 kV [35].

Optical Microscope

For the observation of the erosion effects from cavitation on the bags was used the Motic microscope seen in Figure 2.18. This microscope had a camera (Moticam 1SP with 1.3 MP) that transmitted the captured image to a computer from where the obtained images were captured. To capture the images were used the programs Motic Live Imaging Module and Motic Images Plus 2.0 ML.
The polarised lenses from ThorLabs Inc. shown in Figure 2.19 were used to detect any initial signs of erosion before being observable through normal lenses. The lenses and sample were placed together with the microscope as can be seen from Figure 2.18. By placing these lenses in a cross planar angle as in Figure 2.20 is possible to observe the sample through a light that has only one orientation.

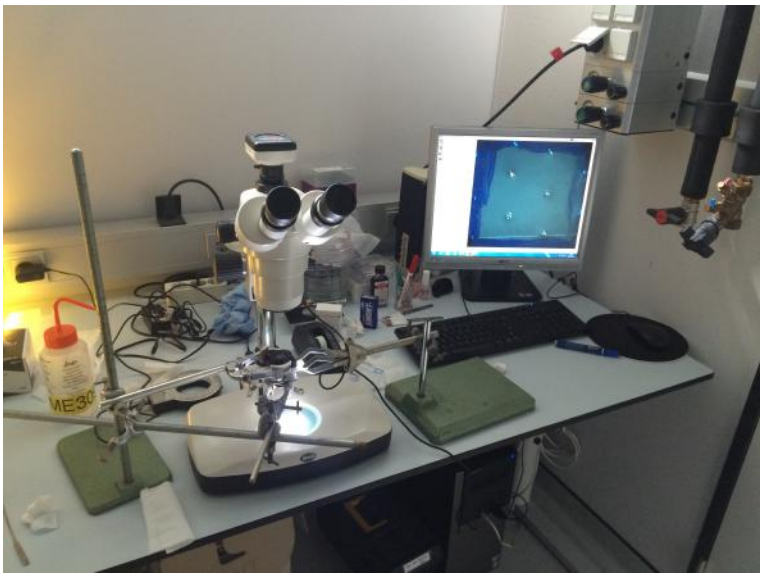

Figure 2.18: Motic microscope and the used setup for the observations.

Figure 2.19: Polarised lenses used for observations.

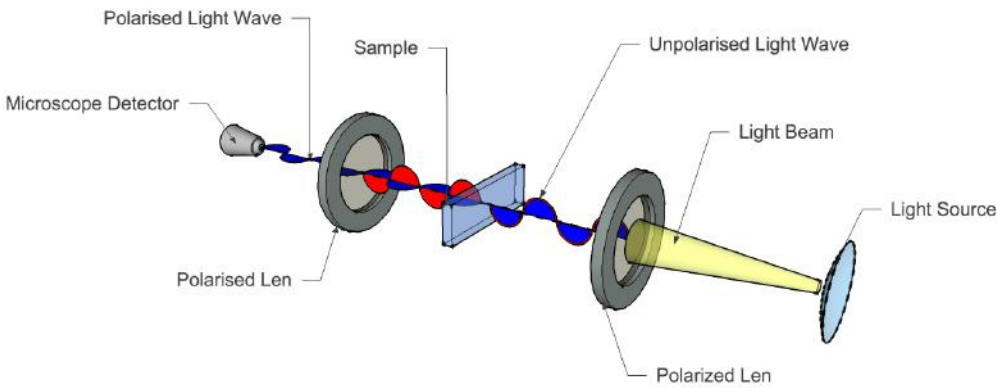

Figure 2.20: The polarisers only allow for the observation of the light oriented in one direction.

Chapter 3

Experimental Results

In this chapter will be presented and analysed the results from this work.
On this work was attempted the applicability of the CIBs for the exfoliation of MoS_2 using two different types of sonication equipment. It was also studied on whether it is the physical or chemical effects from cavitation that induce the exfoliation of the bulk material by inhibiting interactions between the formed radicals and the MoS_2 and not generating mechanical effects.
On another experiment, it was studied if the CIBs suffered significant damage from the cavitation effects on its surface.
All the images and other data obtained for the following samples can be viewed on the Appendix A.1. On this chapter is presented a selection of the more interesting data.

3.1 MoS_2 Liquid-Phase Exfoliation in Cavitation Intensifying Bags

For this experiment, were firstly measured the absorption spectra of the obtained MoS_2 dispersions. With this first step was intended to determine if there were MoS_2 monolayers present in the solution. Afterwards were made the SEM and TEM observations. Later the qualitative analysis made with the absorption spectra were verified with another measurement, this time with the Raman Spectra.
Due to timing and technical factors not every sample went through all the measurements.

3.1.1 Bulk

SEM

As a reference for other SEM observations, a sample solely with bulk MoS_2 was observed. This sample was not exposed to ultrasonic conditions - Figure 2.7. Instead, it was observed as it was received from the manufacturer.

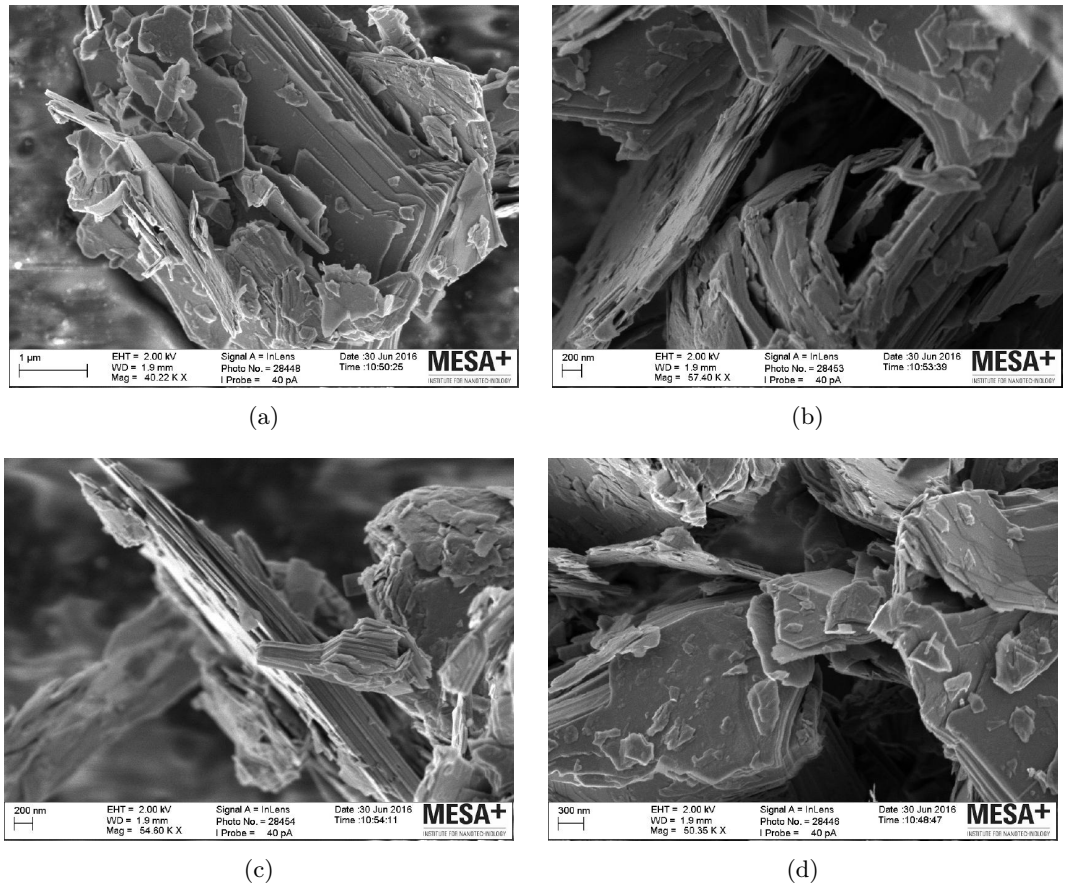

Figure 3.1: SEM images of Bulk MoS_2 flakes.

The images from Figure 3.1 already show some defects on the flakes and also the presence of smaller particles on top of thicker flakes.

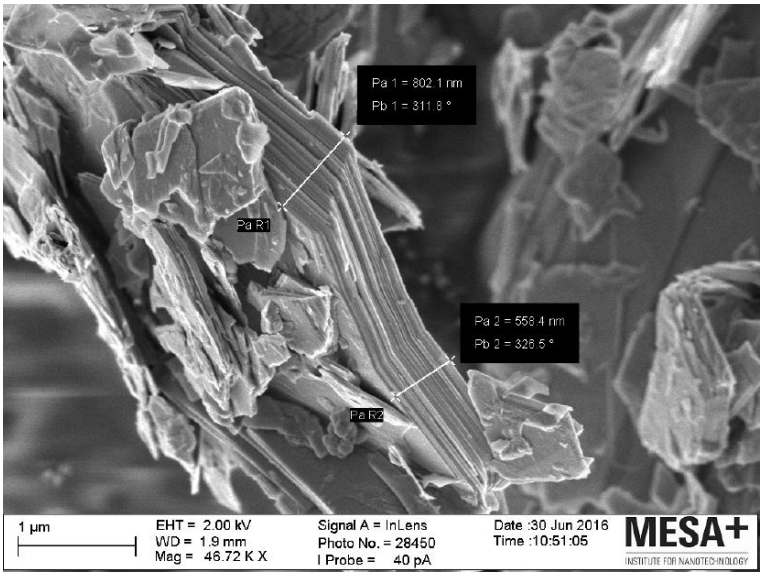

Figure 3.2: Thickness measurement through SEM to a Bulk MoS_2 flake.

As seen from Figure 3.2 measuring flake thickness from SEM is not an accurate procedure. It can be used for reference but is dependent of the spacial orientation of the flake, as can be seen from the significant difference in thickness measured for the same flake in Figure 3.2, where two thicknesses of 802,1 nm and 558,4 nm were measured.

3.1.2 BBNP - Basic, Ultrasonic Bath, No Pits

Sample prepared with a concentration of 20 mg.ml^{-1} MoS_2 in 50 mL of IPA. It was sonicated in the ultrasonic bath for 4,5 h with tap water, inside a bag without pits - Figure 2.8. The dispersion obtained after centrifugation showed there were some particles dispersed in the solvent indicating there were particles in solution light enough to not settle at the bottom of the centrifugation flask. The differences in the sample concentration can be observed in Figure 3.3 by the difference in colour before centrifugation and the obtained dispersion.

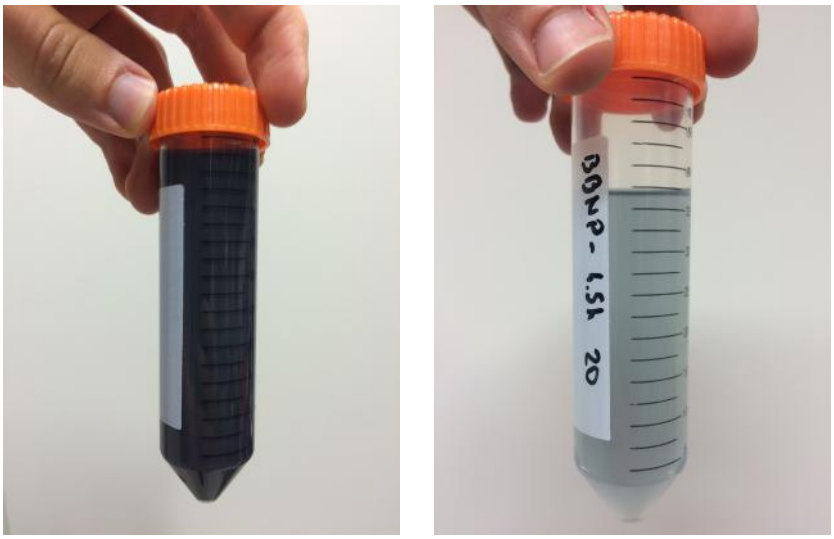

(a) (b)

Figure 3.3: BBNP sample before centrifugation (a) and its dispersion after centrifugation (b) where is possible to see many flakes were too big to be mono-layers and therefore settled at the bottom after centrifugation.

Absorption Spectra

The absorption spectra from the BBNP sample showed the distinct bands of MoS_2 mono-layers at the wavelengths of 650 nm and 690 nm - Figure 3.4. However, these bands appeared fused together instead of showing approximately 50 nm between their respective wavelengths as would have been expected. From these results was proven the existence of MoS_2 mono-layers in the solution [32, 36].

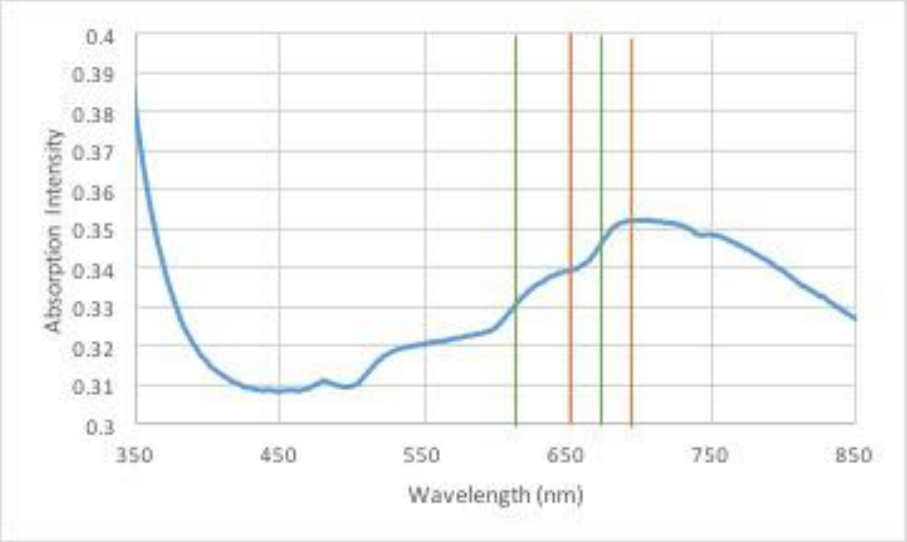

Figure 3.4: BBNP sample absorption spectrum with the orange lines showing the obtained bands and the green ones showing the wavelengths at which they were expected.

SEM

Images at different resolutions are shown in Figure 3.5 from the morphology studies of this sample of MoS_2.

This study showed that there were still very thick layers of MoS_2 in this sample. Compared to the images of bulk MoS_2 flakes, these flakes appear more eroded and regular on the edges. From the SEM observations was possible to determine that one of the flakes from this sample measured about 673 nm in thickness as seen in Figure 3.6.

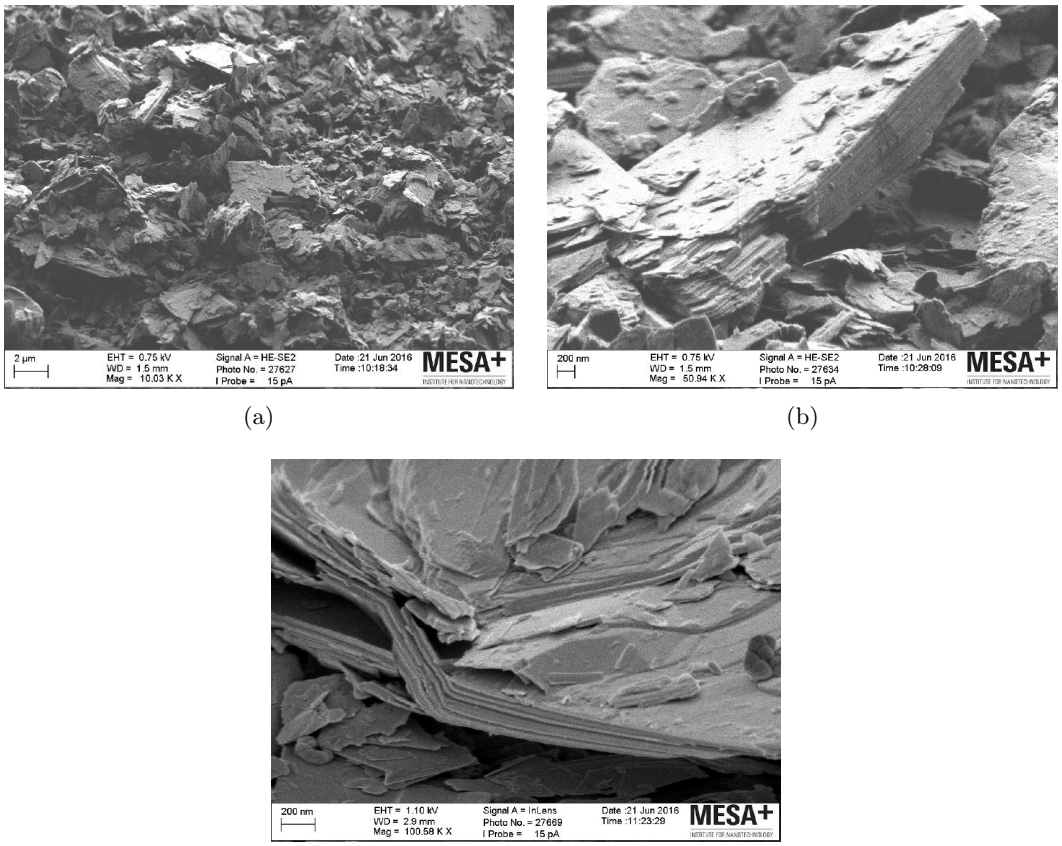

(a) (b)

(c)

Figure 3.5: SEM images for the BBNP sample with (a) an overview of the sample, (b) an image of one of the bigger flakes and (c) shows signs of deformation on the flakes.

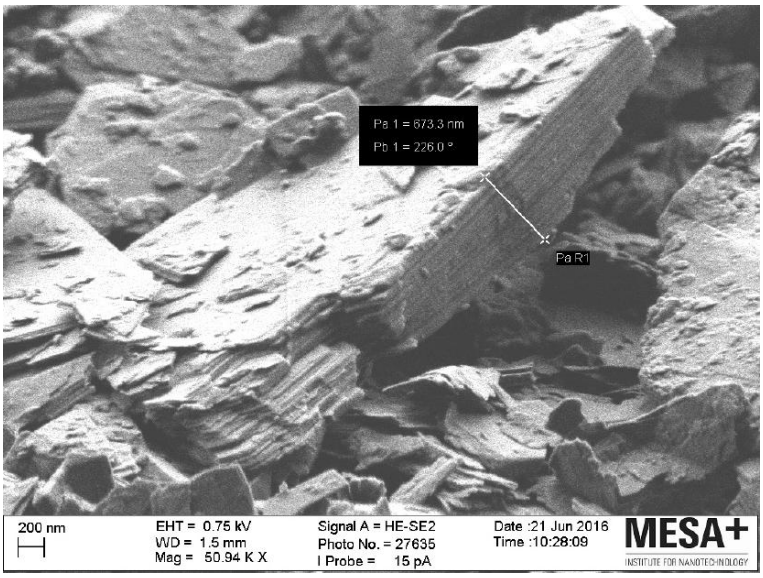

Figure 3.6: BBNP thickness measurement through SEM showing a thickness of 673 nm for this flake.

3.1.3 BBP - Basic, Ultrasonic Bath, Pits

Sample prepared with a concentration of 20 $mg.ml^{-1}$ MoS_2 in 50 mL of IPA. It was sonicated in the ultrasonic bath for 4,5 h with tap water, inside a bag with pits - Figure 2.8. The dispersion obtained after centrifugation showed there were some particles dispersed in the solvent. The visual differences in the sample concentration can be observed in Figure 3.7 by the difference in colour before centrifugation and the obtained dispersion.

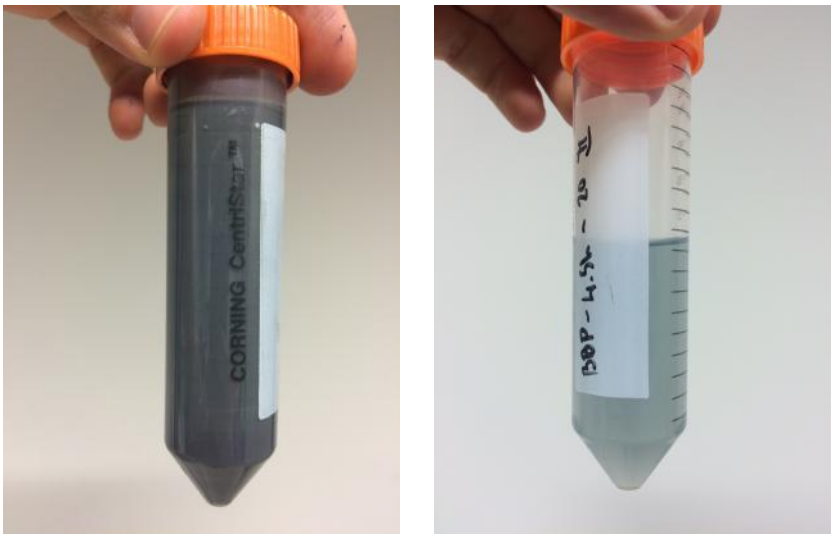

(a) (b)

Figure 3.7: BBP sample before centrifugation (a) and its dispersion after centrifugation (b) showing a substantial decrease in the concentration of the dispersion after centrifugation.

Absorption Spectra

The absorption spectra from the BBP sample showed the distinct bands of MoS_2 mono-layers. However these bands appeared fused. The bands were considered at 655nm and 691nm - Figure 3.8. From these results was proven the existence of MoS_2 mono-layers in the solution [32, 36].

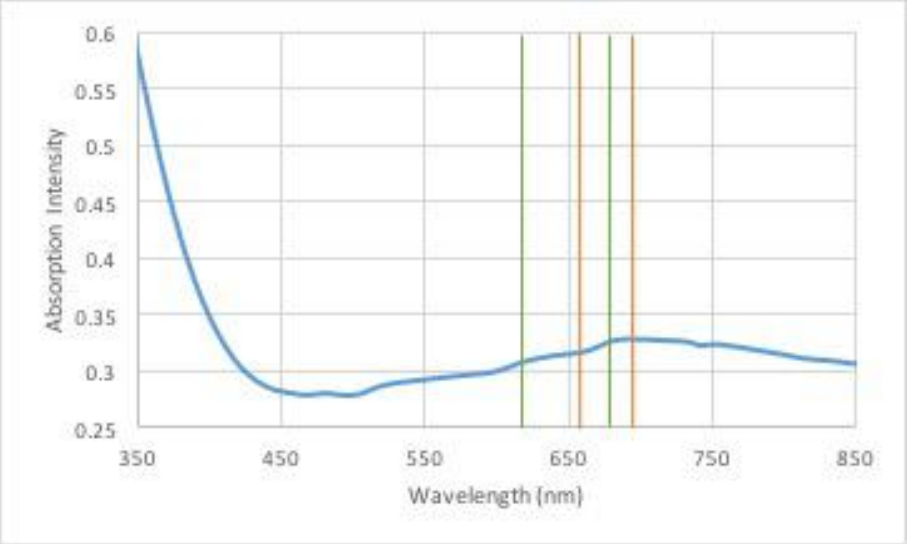

Figure 3.8: BBP sample absorption spectrum with the expected wavelengths in green and the obtained ones in orange.

SEM

In Figure 3.9 are shown three images at different resolutions from the morphology studies of this sample of MoS_2.

This study showed that there were still very thick layers of MoS_2 in this sample. It also showed a very large amount of broken particles from the flakes dispersed on top and around bigger flakes. From the SEM was possible to determine that one of the flakes from this sample measured about 224 nm in thickness as seen in Figure 3.10. From the same figure is also showed that the edges of the flakes are more rounded when compared to the Bulk sample.

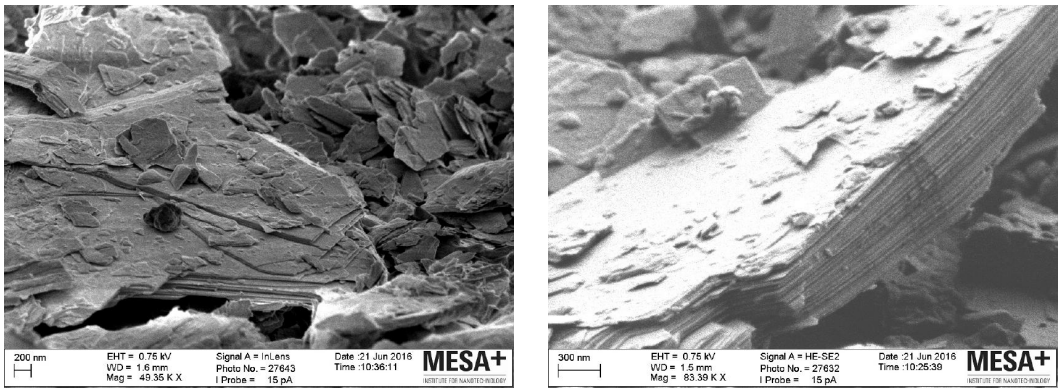

(a) (b)

Figure 3.9: SEM images for the BBP sample with (a) an overview of the sample and (b) an image of a single flake.

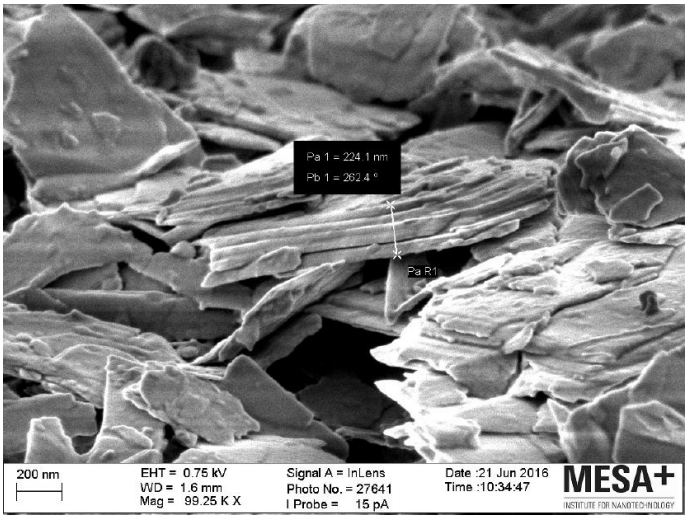

Figure 3.10: BBP thickness measurement through SEM showing a thickness of 224 nm for this flake.

TEM

A drop of the dispersion from this sample was used to generate the images in Figure 3.11, which show that flakes on the dispersion are very thin since it is possible to observe layers beneath the top layer. It is also possible to observe Moiré lines meaning the layers are not aligned on top of each other. Observations on the crystalline structure of the layers confirmed that the observed crystalline structure on the obtained flakes matches the original 2H-MoS_2 semiconducting phase of bulk MoS_2.

Raman Spectra

The Raman Spectra measurements for this sample were done with a power of 350 μW for 50 ms, with a frequency of 50 kHz and through an area of 50x50 μm, which generated an

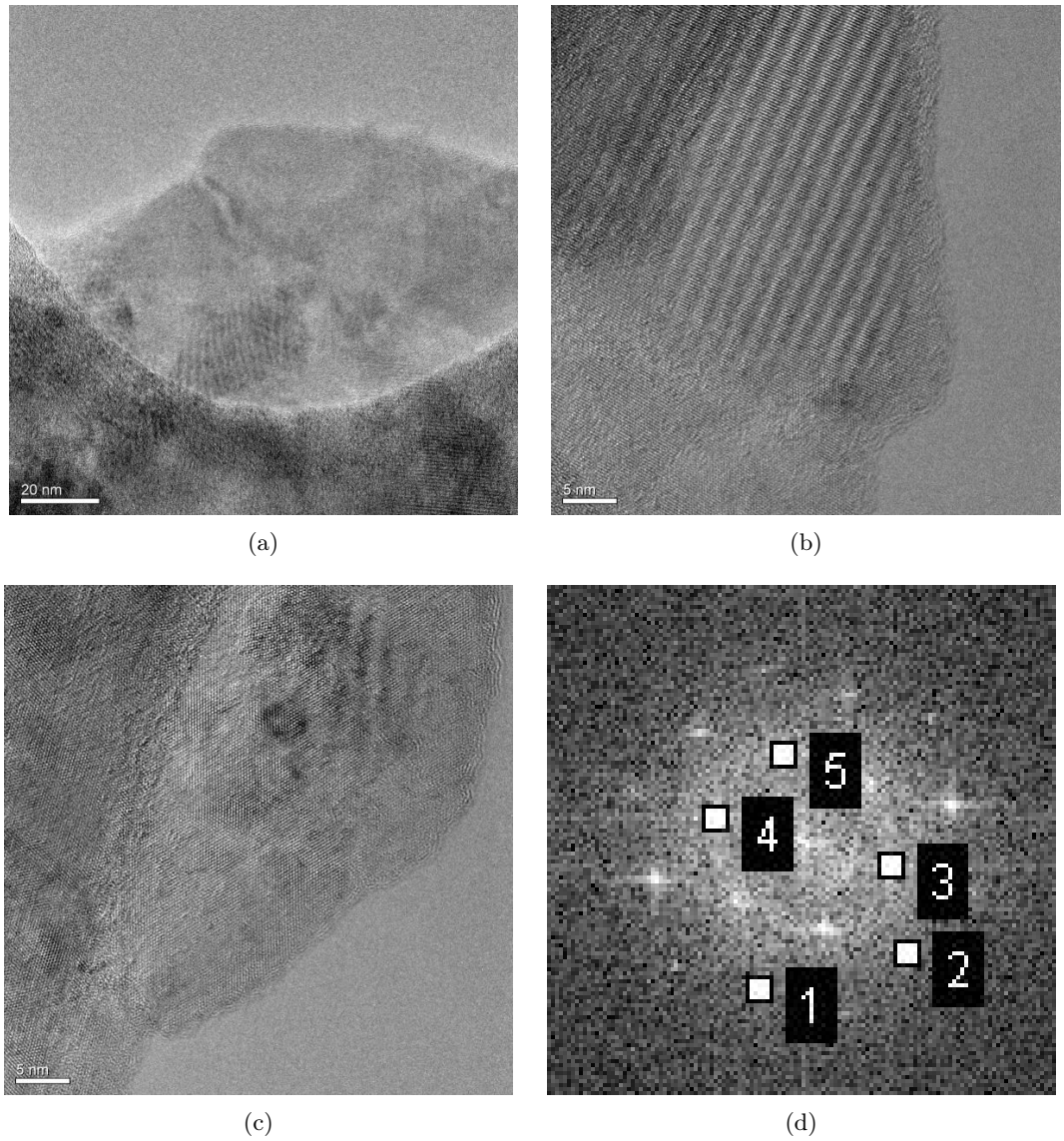

(a) (b)

(c) (d)

Figure 3.11: TEM images for the BBP sample with (a) an overview of two layers on top of each other, (b) observed Moiré lines, (c) image showing a flake with various thicknesses and (d) an observation of the x-ray diffraction pattern showing the crystalline structure of the sample.

image with 100x100 pixels.

From Figure 3.12 is possible to confirm the presence of MoS_2 in the sample. From the slight downshift of the second peak, A_{1g}, from 408 cm^{-1} to 403 cm^{-1} is possible to say that there are micromechanically cleaved single layers of MoS_2 present in the sample. The generated images in Figure 3.13 confirm this by showing that there are less areas with Raman intensity in the interval of 407 and 410 cm^{-1} than to 402 and 405 cm^{-1}. These images indicate with the clear dots the areas of the sample where the Raman intensity observed is more intense.

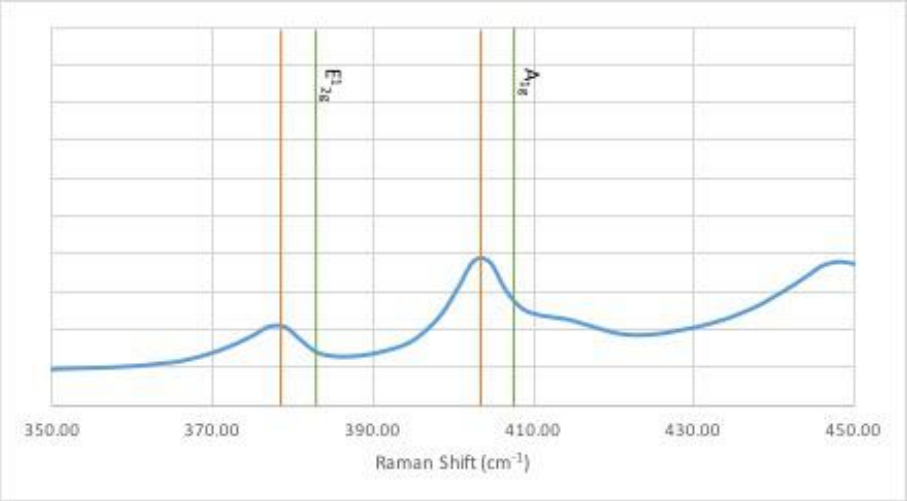

Figure 3.12: Average Raman Intensity for BBP with the lines in orange and green showing the obtained shifts and the expected ones respectively.

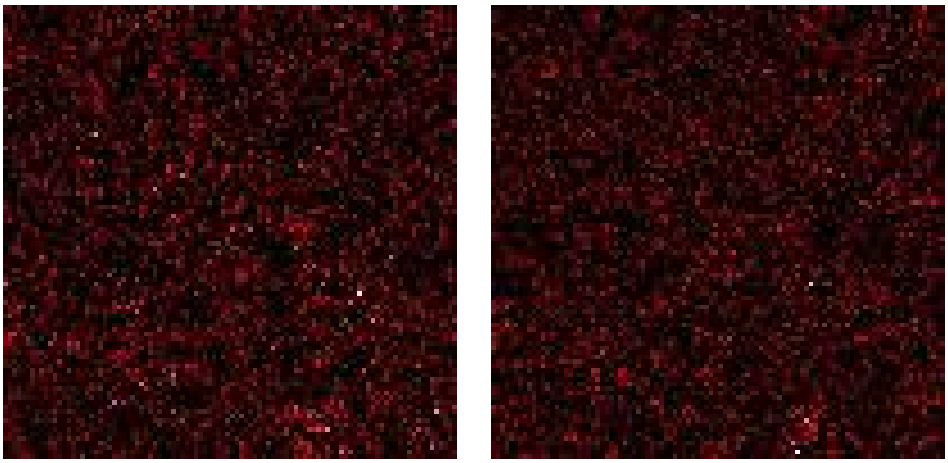

(a) (b)

Figure 3.13: Raman intensities for BBP between 402 and 405 cm^{-1} (a) and between 407 and 410 cm^{-1} (b) showing that the areas with the Raman intensity for cleaved layers, 403 cm^{-1}, is more predominant than the areas with the Raman intensity associated to 408 cm^{-1}.

3.1.4 BHNP - Basic, Ultrasonic Horn, No Pits

Sample prepared with a concentration of 20 mg.ml^{-1} MoS_2 in 25 mL of IPA. It was sonicated in the ultrasonic horn for 4,5h inside a bag without pits - Figure 2.8.
The dispersion obtained after centrifugation showed there were some particles dispersed in the solvent proving there were particles in solution light enough to not settle at the bottom of the centrifugation flask.

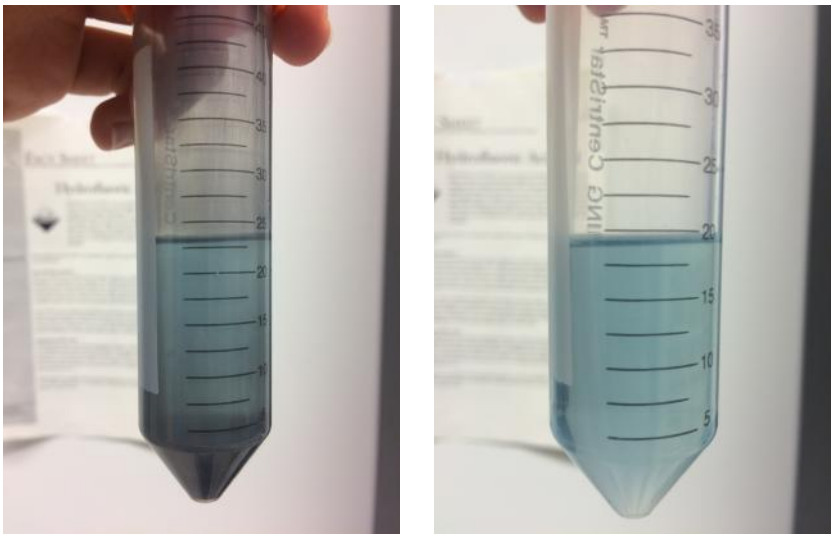

(a) (b)

Figure 3.14: BHNP sample after centrifugation (a) and its dispersion (b) showing a slight decrease in the concentration after removing the heavier flakes through centrifugation.

Absorption Spectra

The absorption spectra from the BHNP sample presented a very wide peak with a slight plateau at the wavelength of 650nm - Figure 3.15. This plateau was considered as the first peak and the following peak at around 685 nm as the second peak. From these results is possible to say that there are MoS_2 mono-layers in the solution [32, 36].

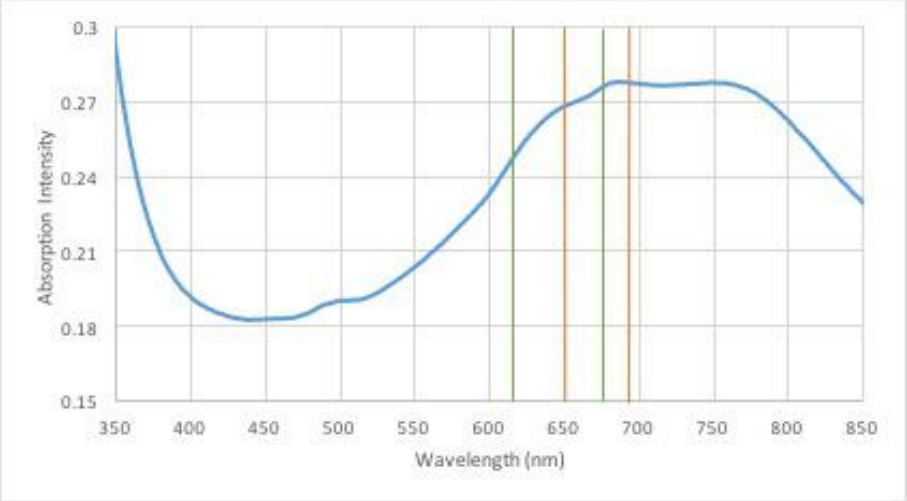

Figure 3.15: BHNP sample absorption spectrum with the expected wavelengths and the obtained ones in green and orange respectively.

SEM

In Figure 3.16 are shown three images at different resolutions from the morphology studies of this sample of MoS_2. From these pictures is observable that the obtained flakes are very different in sizes among them. There are large flakes dispersed on the surface as well as flakes of much smaller size. This can be explained due to the higher intensity of the ultrasonic horn on areas close to it and its weaker intensity on areas further away from it. This way the different intensities experienced by the bulk flakes on the various areas of the solution translates in flakes of various sizes.

This study also showed that there were still very thick layers of MoS_2 in this sample. Through the SEM was possible to determine that one of the flakes from this sample measured about 351 nm in thickness as seen in Figure 3.17.

Raman Spectra

The Raman Spectra measurements for this sample were done with a power of 350 μW for 50 ms, with a frequency of 50 kHz and through an area of 50x50 μm, which generated an image with 100x100 pixels.

Qualitatively was possible to confirm the presence of MoS_2 on the surface of the PVDF membrane as seen in Figure 3.18. Due to the slight downshift of the second peak, A_{1g}, from 408 cm^{-1} to 403 cm^{-1} is possible to say that there are micromechanically cleaved layers of MoS_2 present in the sample. The generated images in Figure 3.19 confirm this by showing that there are less areas with Raman intensity in the interval of 407 and 410 cm^{-1} than to 402 and 405 cm^{-1}.

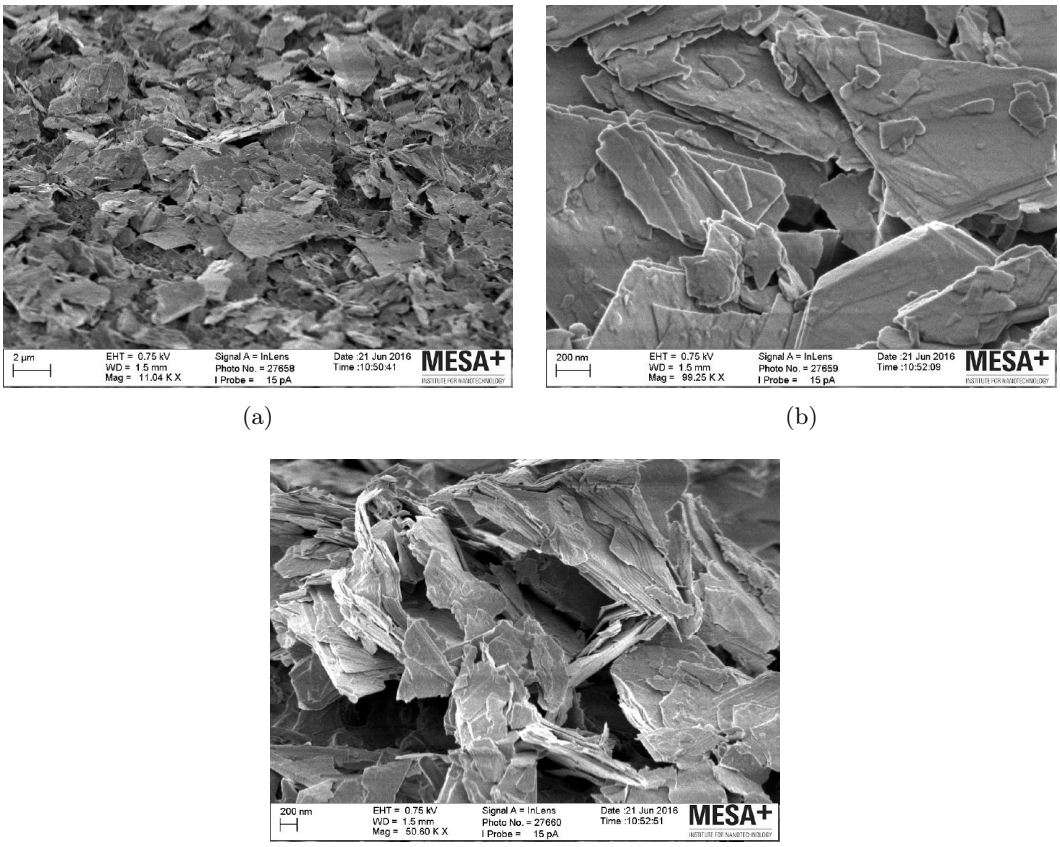

(a) (b)

(c)

Figure 3.16: SEM images for the BHNP sample with (a) an overview of the sample and (b) and (c) images of the obtained flakes.

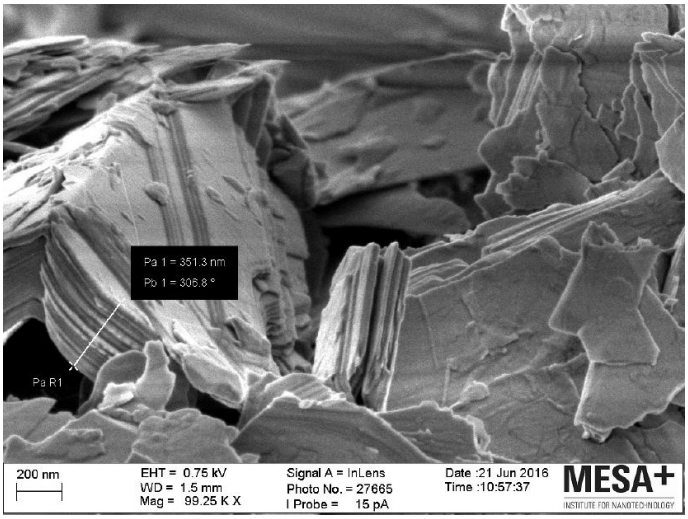

Figure 3.17: BHNP thickness measurement through SEM showing a thickness of 351 nm for this particular flake.

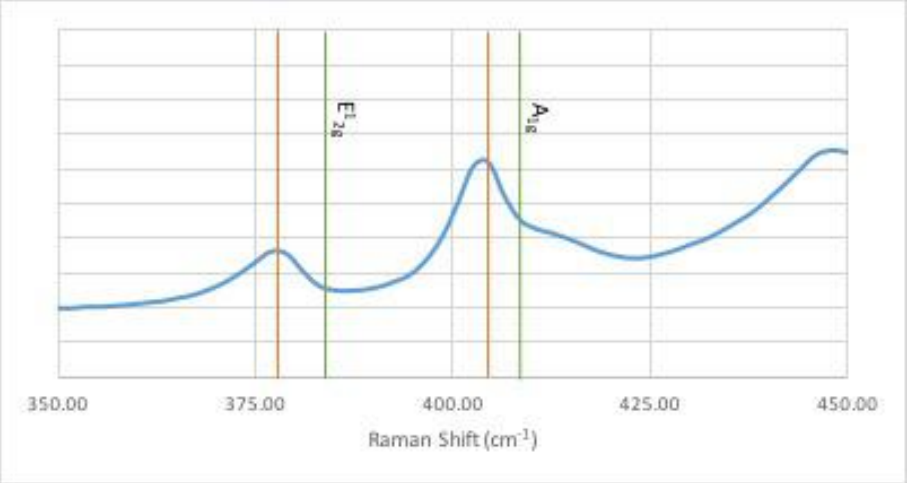

Figure 3.18: Average Raman Intensity for BHNP with the lines in orange and green showing the obtained shifts and the expected ones respectively.

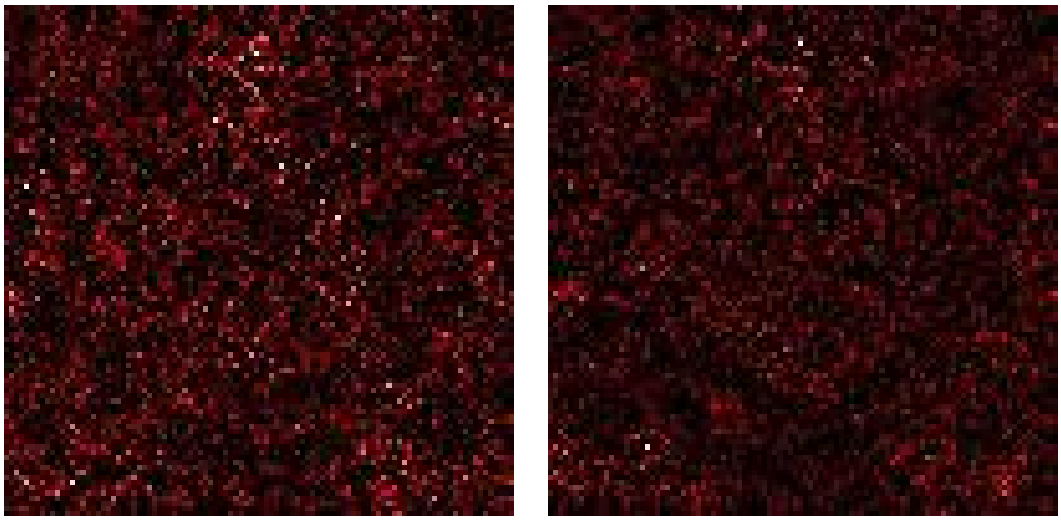

(a) (b)

Figure 3.19: Raman intensities for BHNP between 402 and 405 cm^{-1} (a) and between 407 and 410 cm^{-1} (b), with (a) showing a higher predominance of the Raman Shift respective to the cleaved layers.

3.1.5 BHP - Basic, Ultrasonic Horn, Pits

Sample prepared with a concentration of 20 mg.ml^{-1} MoS_2 in 25 mL of IPA. It was sonicated in the ultrasonic horn for 4,5 h inside a bag with pits - Figure 2.8.
The dispersion obtained after centrifugation showed a very clear colour proving there were few particles in the solution. This could mean the particles generated were not small enough to avoid being stored at the bottom of the flask during centrifugation. The visual differences in the sample concentration can be observed in Figure 3.20 by the difference in colour before centrifugation and the obtained dispersion.

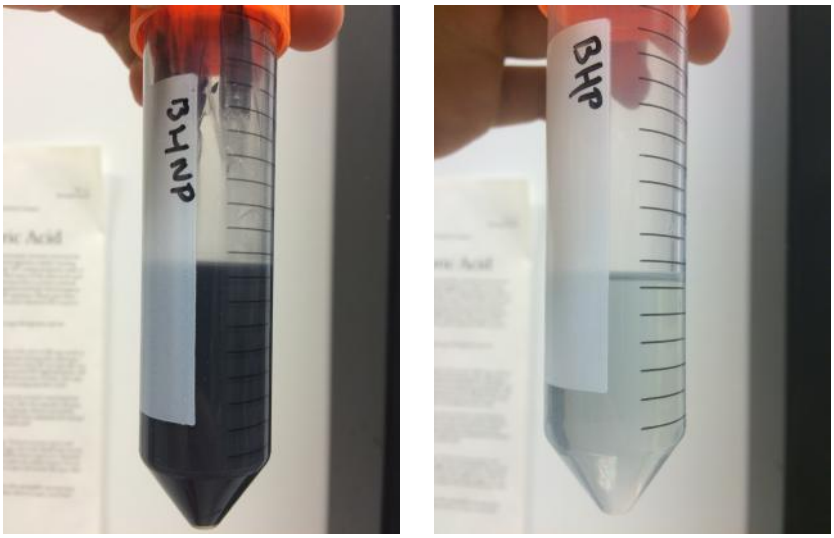

(a) (b)

Figure 3.20: BHP sample before centrifugation (a) and its dispersion after centrifugation (b), showing that most obtained particles were very large to remain in the dispersion after centrifugation.

Absorption Spectra

The absorption spectra from the BHP sample showed the distinct bands of MoS_2 mono-layers, with the first one rather a plateau than an actual peak - Figure 3.21. Once more, these bands appeared fused together instead of showing wavelengths without absorption between them as would have been expected. Still, from these results was proven the existence of MoS_2 mono-layers in the solution [32, 36].

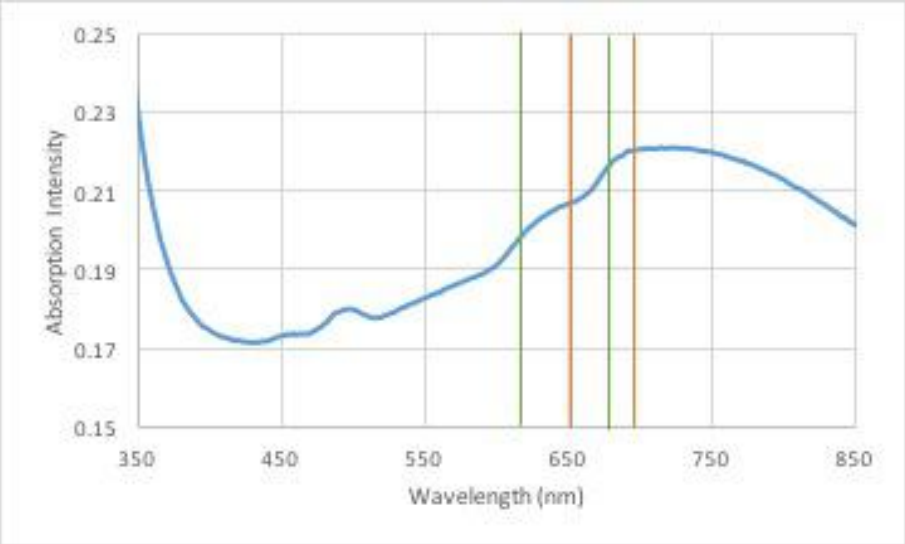

Figure 3.21: BHP sample absorption spectrum with the expected wavelengths for MoS_2 mono-layers in green and the obtained ones in orange.

SEM

In Figure 3.22 are shown three images at different resolutions from the morphology studies of this sample of MoS_2. From these pictures is observable that through this method were obtained some big flakes with many smaller particles on top and around them. The existence of very small debris and big particles is a result of the differences in the ultrasound and cavitation intensity around the sample. Some interesting deformities on the morphology of the flakes is also observable on these images. Due to the low concentration of this dispersion is possible to see on these images the PVDF membrane below the MoS_2 flakes.
This study showed that there were still very thick layers of MoS_2 in this sample. Through the SEM was possible to determine that one of the flakes from this sample measured more than 300 nm in thickness as seen in Figure 3.23.

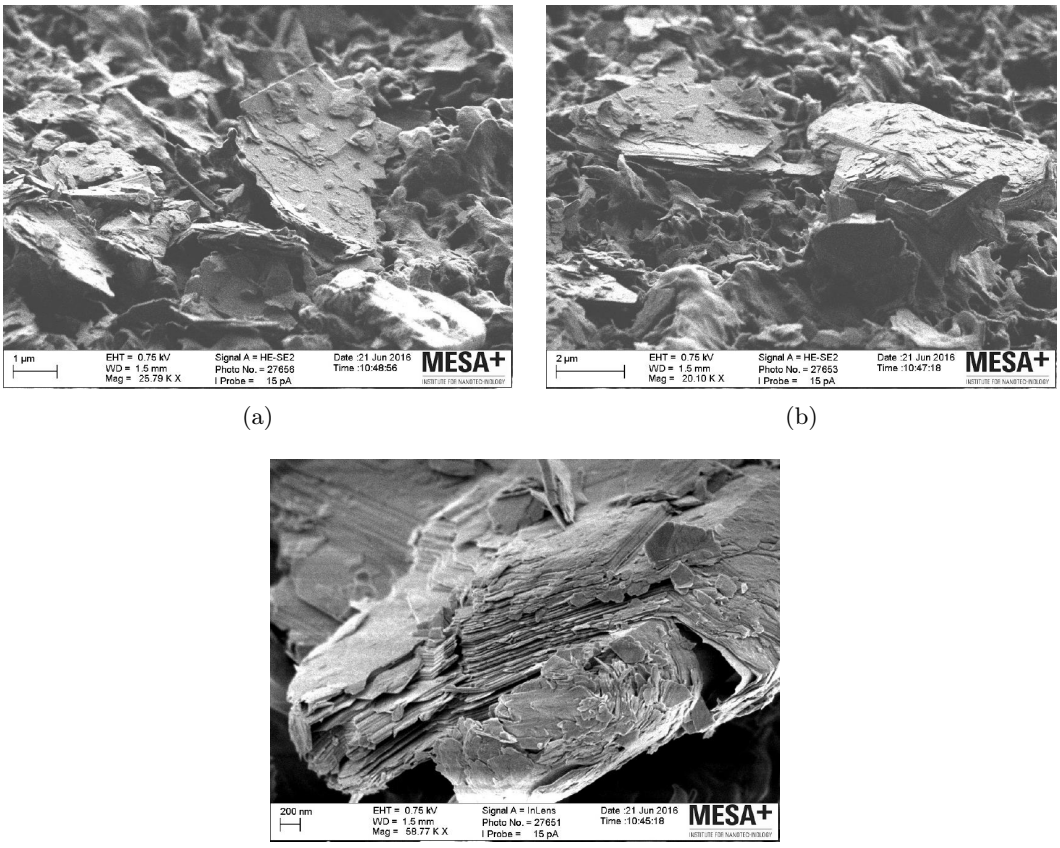

(a) (b)

(c)

Figure 3.22: SEM images for the BHP sample with (a) and (b) overviews of the obtained sample with some visible surface from the PVDF membrane and (c) showing a large defect on the observed flake.

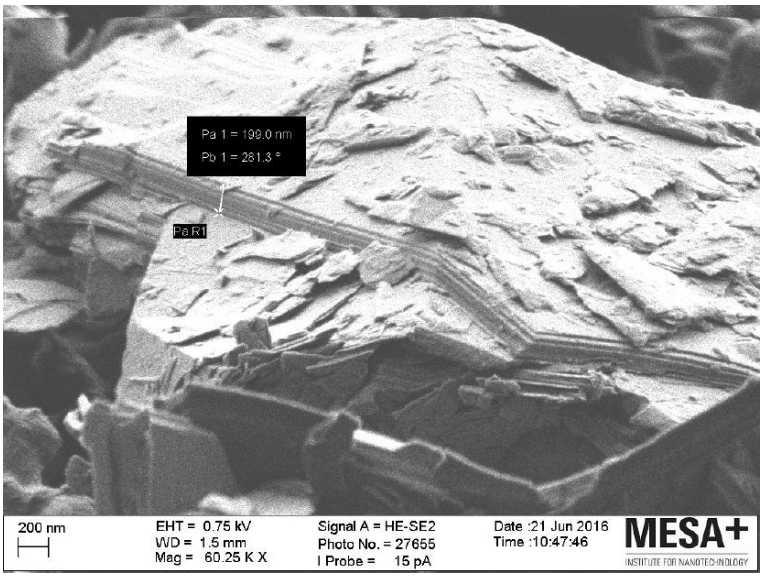

Figure 3.23: BHP thickness measurement through SEM with 300 nm in thickness for this particular flake.

3.1.6 C_NP - Chemical, No Pits

Sample prepared with a concentration of 20 $mg.ml^{-1}$ MoS_2 in 50 mL of IPA. It was placed inside a glass and no ultrasound was applied to this sample. To this solution was added a small mass of AIBN of about 0,0012 g. The solution was then heated to 60ºC for 4,5 h to generate radicals from breaking the chains from the molecules of AIBN, but at the same time avoid IPA from boiling - Figure 2.9.
The dispersion obtained after centrifugation showed a very clear colour proving there were few particles in the solution. The differences in the sample concentration can be observed in Figure 3.24 by the difference in colour before centrifugation and the obtained dispersion.

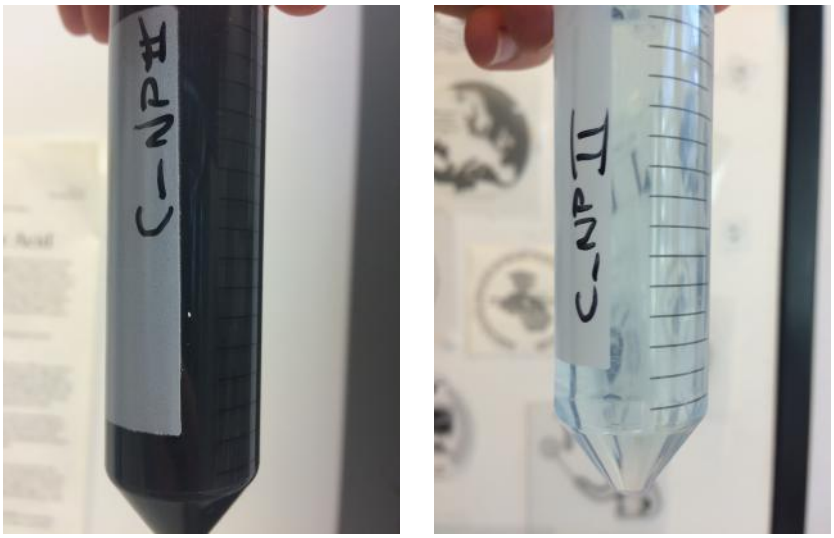

(a) (b)

Figure 3.24: C_NP sample before centrifugation (a) and its dispersion after centrifugation (b) with a very clear colour.

Absorption Spectra

The absorption spectra from the C_NP sample barely showed the first peak for MoS_2 mono-layers - Figure 3.25. Instead there is only a single peak at 680 nm and a continuity of the absorption line for higher wavelengths which suggests the obtained layers are still very thick. Nonetheless, it was attempted to identify the second peak from the slope obtained having been calculated that as the previous samples the slope is less intense at a wavelength of 650 nm. From this result, the existence of MoS_2 mono-sheets in the solution is unclear.

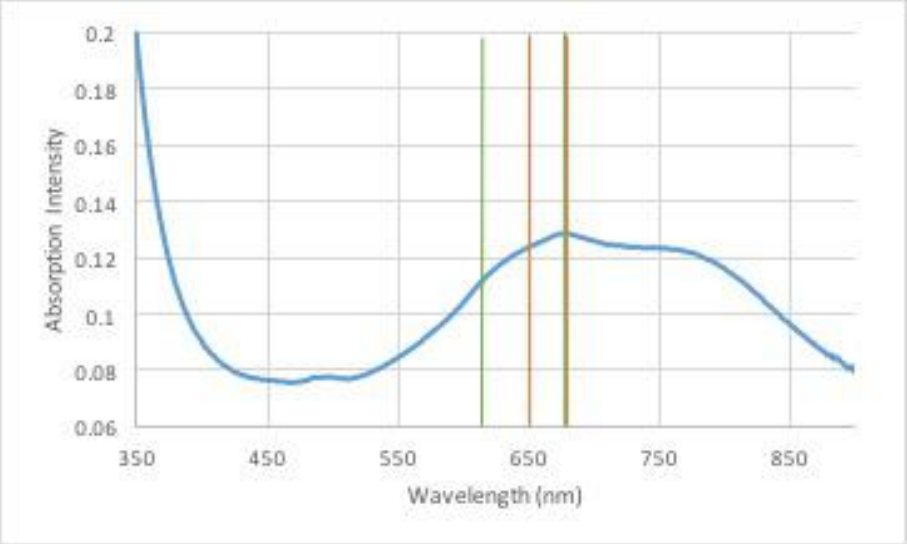

Figure 3.25: C_NP sample absorption spectrum with the obtained wavelengths overlapped by the orange line and the expected ones by the green one.

SEM

Figure 3.26 shows three images at different resolutions of areas of the same sample from the morphology studies of this sample of MoS_2.

From the pictures in Figure 3.26 is observable that through this method were obtained big flakes with a few smaller particles on top of them. There were no apparent deformities on the flakes from the observations made. There are no signs of erosion on the edges of the flakes as well.

Due to the low concentration of this dispersion is possible to see on these images the PVDF membrane below the MoS_2 flakes in a darker colour.

This study showed that there were still very thick layers of MoS_2 in this sample. Through the SEM was possible to determine that one of the flakes from this sample measured almost 600 nm in thickness as seen in Figure 3.27. Still another observation of another flake from the same sample showed there were present flakes of smaller thickness as well, as can be seen in Figure A.89 where a flake with 270 nm in thickness was observed.

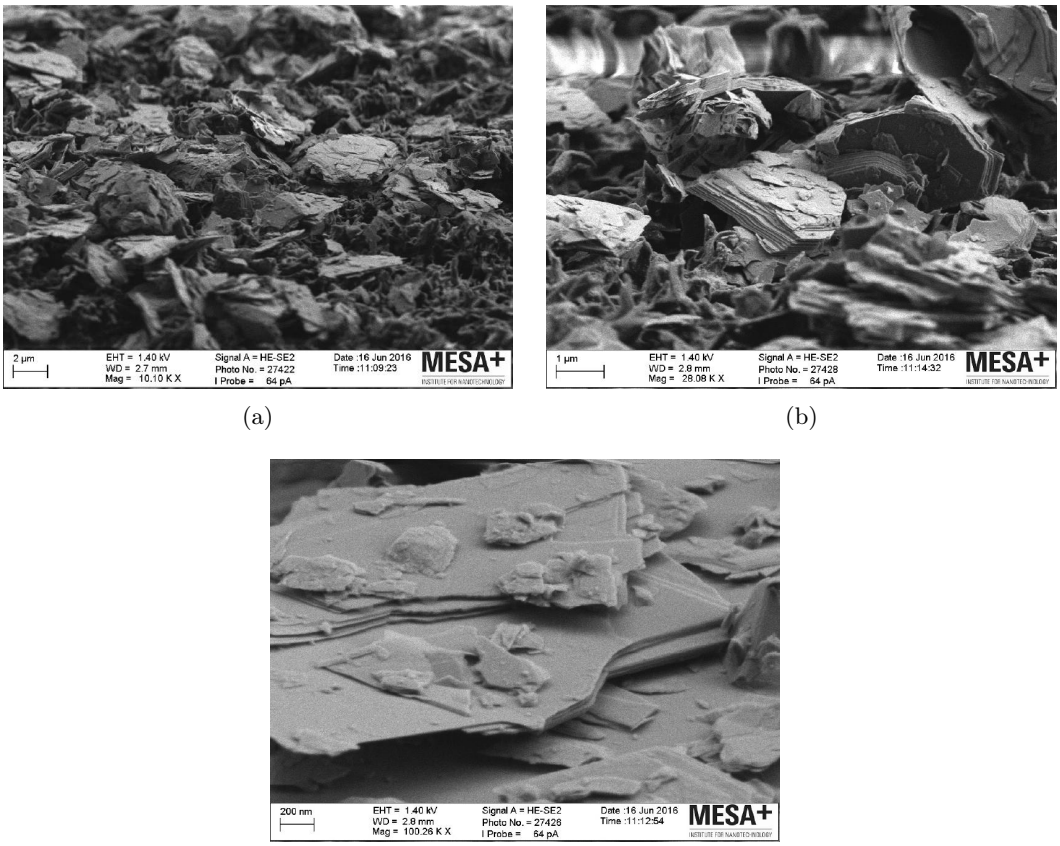

(a) (b)

(c)

Figure 3.26: SEM images for the C_NP sample with (a) and (b) overviews of the sample and (c) a detailed image from the surface of one flake.

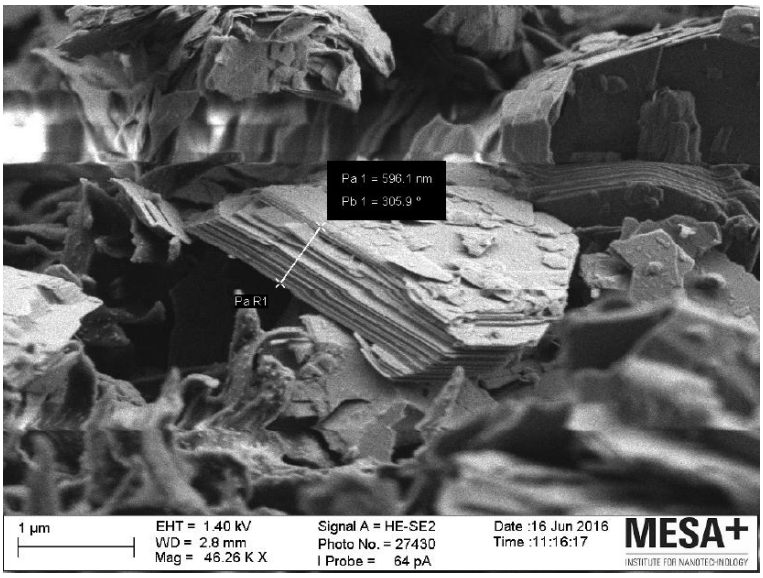

Figure 3.27: C_NP thickness measurement through SEM indicating a thickness of almost 600 nm for this flake.

3.1.7 MBP - Mechanical, Ultrasonic Bath, Pits

Sample prepared with a concentration of 20 mg.ml^{-1} MoS_2 in 45 mL of IPA and 5 mL of the solution prepared as described in Table 3.1 [2]. It was placed inside a bag with pits, to maximise cavitation, and the ultrasonic bath, so that the ultrasound would not act differently throughout the sample. The time of exposition to the ultrasound was 4,5 h - Figure 2.8.
The initial volume of the buffer solution was 250 mL. This solution besides serving as a radical scavenger can be identified through the fluorescence spectrophotometer since it can emit light at a wavelength close to 429 nm when excited by a wavelength of 310 nm.

Substance	**Mass of reactant (g)**
Terephthalic Acid	0,0834
Sodium Hydroxide	0,0529
Phospate Buffer	
Monopotassium Phospate	0,1480
Disodium Phosphate	0,2453

Table 3.1: Buffer solution preparation.

The dispersion obtained after centrifugation showed a clear colour proving there were few particles in the solution. The differences in the sample concentration can be observed in Figure 3.28 by the difference in colour before centrifugation and the obtained dispersion.

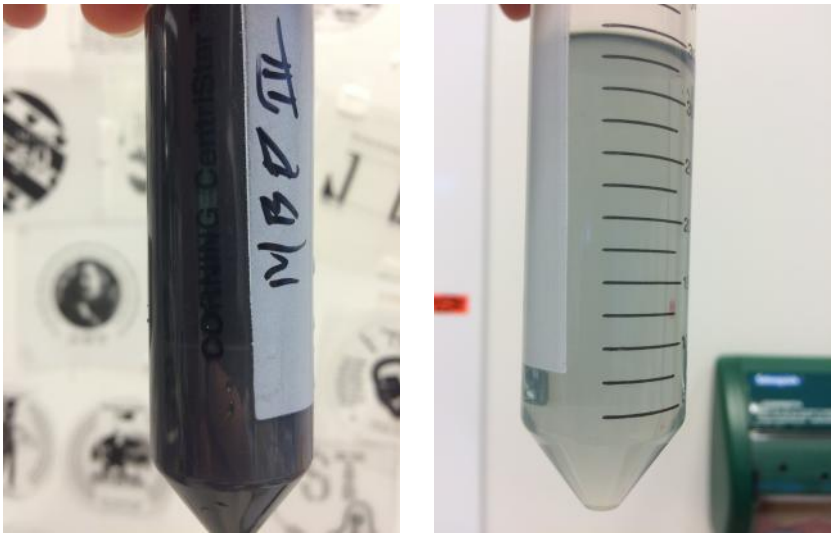

(a) (b)

Figure 3.28: MBP sample before centrifugation (a) and its almost clear dispersion after centrifugation (b).

Absorption Spectra

The absorption spectra from the MBP sample showed the first peak for MoS_2 mono-layers as a plateau due to the wider second peak - Figure 3.29. For the second peak the absorption line continues at a higher intensity than expected proving the obtained flakes are too thick to be mono-layers.

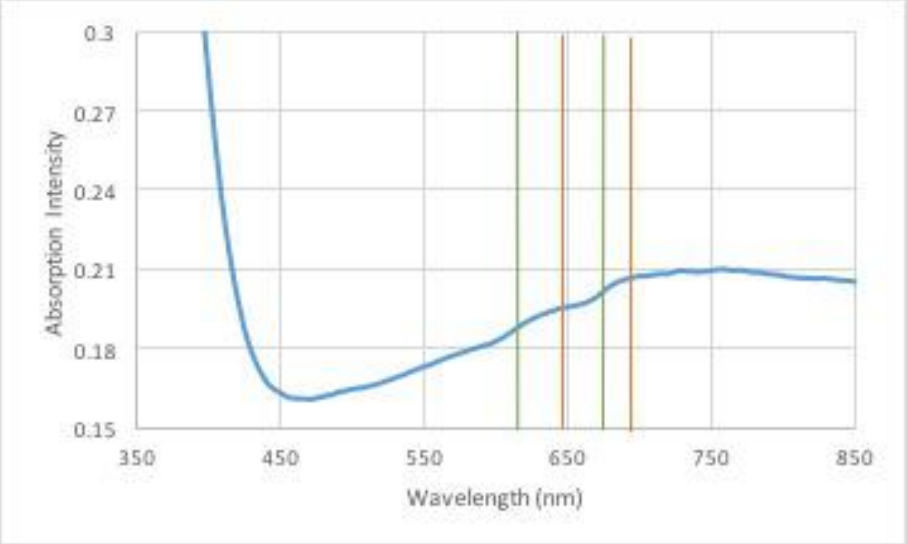

Figure 3.29: MBP sample absorption spectrum with the expected wavelengths in green and the obtained ones in orange.

SEM

In Figure 3.30 are shown three images at different resolutions and areas of the same sample from the morphology studies of this sample of MoS_2.

From the pictures in Figure 3.30 is observable that through this method were obtained big flakes with many smaller particles on top of them. It is possible to observe some deformities on the flakes like the one in Figure 3.30 (c) where the flake folded on top of one of the teeth that form the membrane. No signs of erosion on the edges of the flakes can be seen on the obtained pictures.

This study showed that there were still very thick layers of MoS_2 in this sample. For this sample were not made any measurements from the thickness of the obtained flakes.

Fluorescence Spectrophotometry

After measuring the concentration of HTA in the solution from the obtained peak, was concluded that the volume of buffer solution added to the sample was not enough to fully minimise the chemical effect from the radical formation. Therefore, any effects caused by the radicals on the solute have been minimised but not fully avoided.

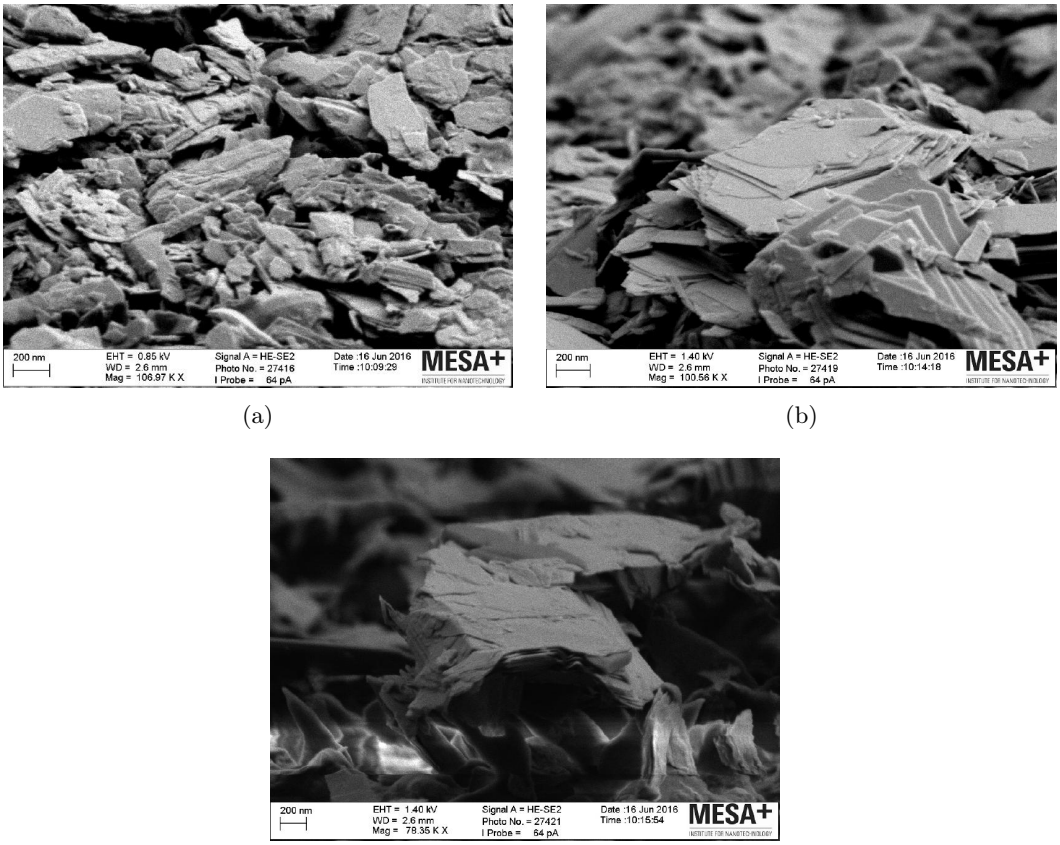

(a) (b)

(c)

Figure 3.30: SEM images for the MBP sample with an overview of the sample (a), (b) an image of a flake from this sample and (c) shows a flake folded on top of one of the peaks from the surface of the PVDF membrane.

3.1.8 BBNP 20min - Basic, Ultrasonic Bath, No Pits, 20 min

Sample prepared with a concentration of 20 $mg.ml^{-1}$ MoS_2 in 50 mL of IPA. Before applying ultrasound to the sample, it was centrifuged for one hour to separate heavier flakes from lighter ones. Afterwards, 40 ml of the obtained dispersion were retrieved and placed inside a bag without pits, and for 20 min was exposed to ultrasound in an ultrasonic bath filled with tap water - Figure 2.10.
The dispersion obtained after centrifugation showed a very clear colour proving there were little particles in the solution. From Figure 3.31 is possible to observe how dilute the sample was.

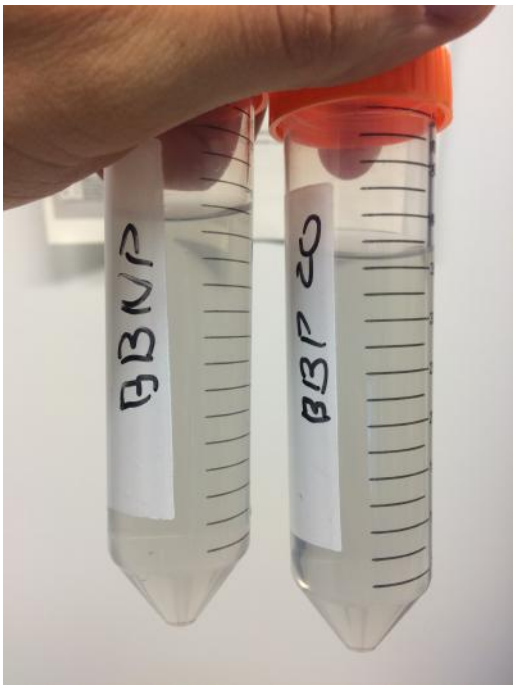

Figure 3.31: Dispersions used for both the BBNP 20min and BBP 20min.

Absorption Spectra

The absorption spectra from the BBNP 20min sample barely showed any peak for MoS_2 mono-layers - Figure 3.32. Two very slight slopes could be observed around the 640 nm and 685 nm but are both inconclusive due to their low intensity.

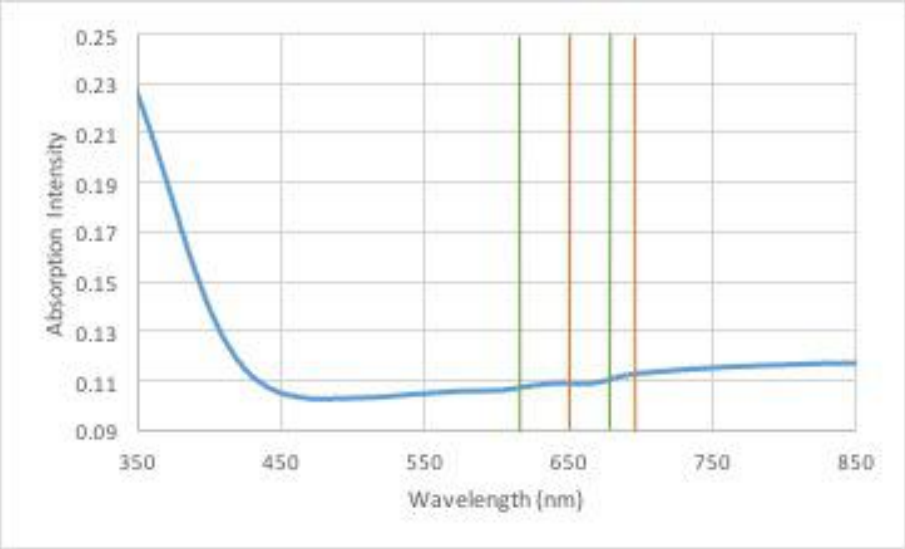

Figure 3.32: BBNP 20min sample absorption spectra with the expected and obtained wavelengths in green and orange respectively.

SEM

In Figure 3.33 are shown three images at different resolutions and areas of the same sample from the morphology studies of this sample of MoS_2. For this sample a drop from the solution was placed on a carbon grid for observation instead of observing the flakes on top of a PVDF membrane.

From observing the pictures in Figure 3.33 is understood that were obtained few particles. In Figure 3.33 (c) it is possible to observe a deformity on top of the right flake that cannot be understood. No signs of erosion on the edges of the flakes can be seen on the obtained pictures.

For the only SEM measurement made to the side of one flake was observed that it would have a thickness larger than 100 nm. However this result has a lot of errors associated to it since there were no flakes in a position that would allow for a correct side observation of the flake.

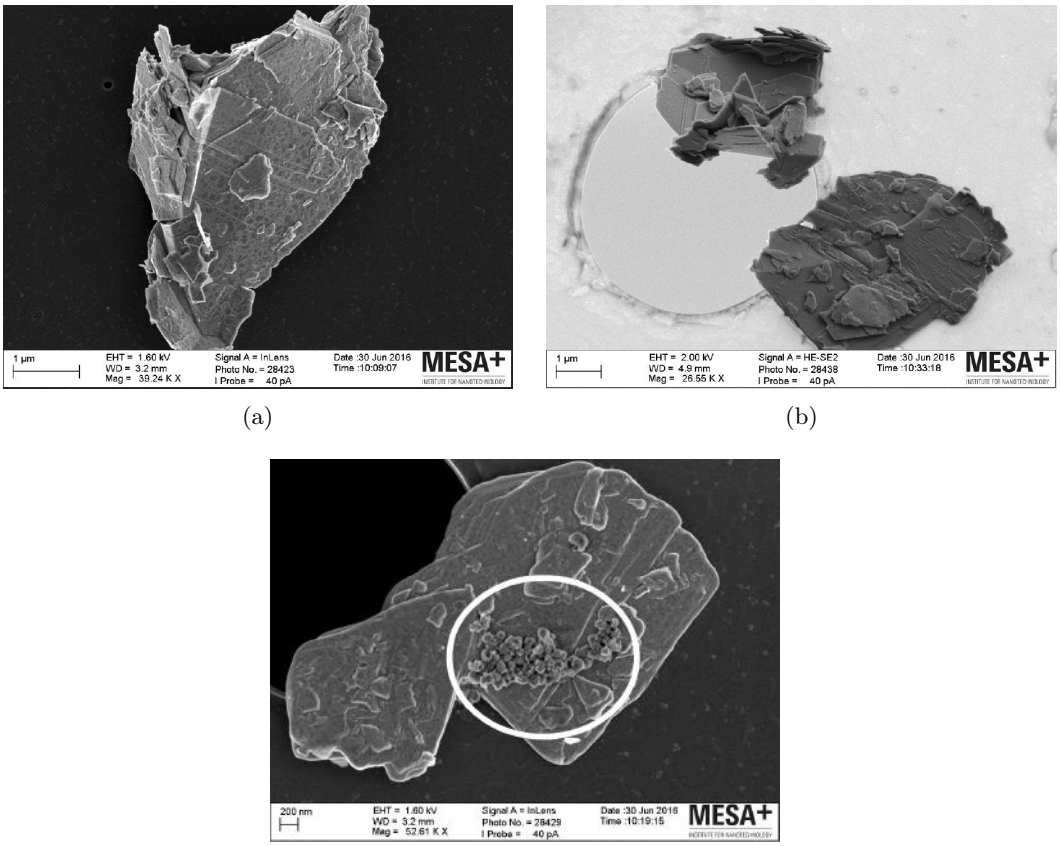

(a) (b)

(c)

Figure 3.33: Overview of three MoS_2 flakes from the BBNP 20min sample obtained through the SEM, with (b) showing the flakes on the border of a hole on the carbon grid and (c) an unknown deformity.

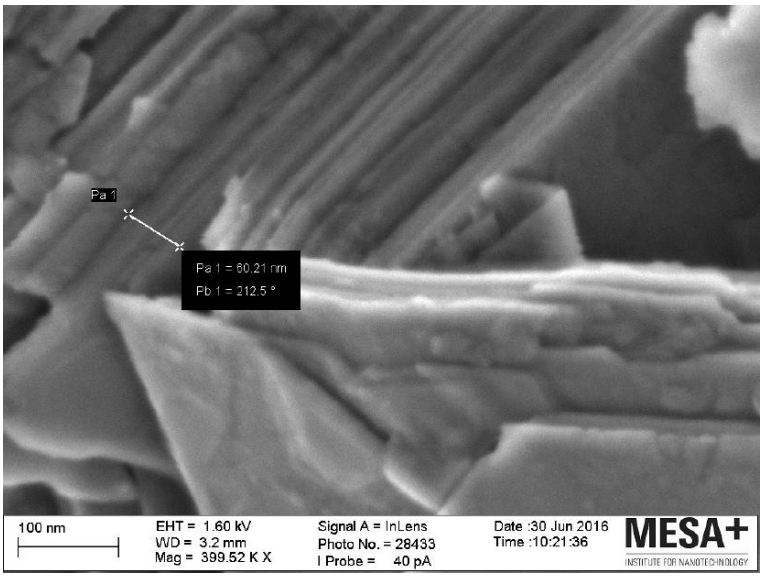

Figure 3.34: BBNP 20min thickness measurement through SEM.

3.1.9 BBP 20min - Basic, Ultrasonic Bath, Pits, 20 min

Sample prepared with a concentration of 20 mg.ml^{-1} MoS_2 in 50 mL of IPA. Just as for sample BBNP 20min, this sample was centrifuged for one hour to separate heavier flakes from lighter ones. Afterwards, 40 ml of the obtained dispersion were retrieved and placed inside a bag with pits, and exposed to ultrasound in an ultrasonic bath filled with tap water for 20 min.
The dispersion obtained after centrifugation showed a very clear colour proving there were little particles in the solution just as sample BBNP 20min. From Figure 3.31 is possible to observe how dilute the sample was.

Absorption Spectra

The absorption spectra from the BBP 20min sample barely showed any peak for MoS_2 mono-layers. Two very low bands can be observed in Figure 3.35 at around 640 nm and 685 nm but are both inconclusive due to their low absorption intensity.

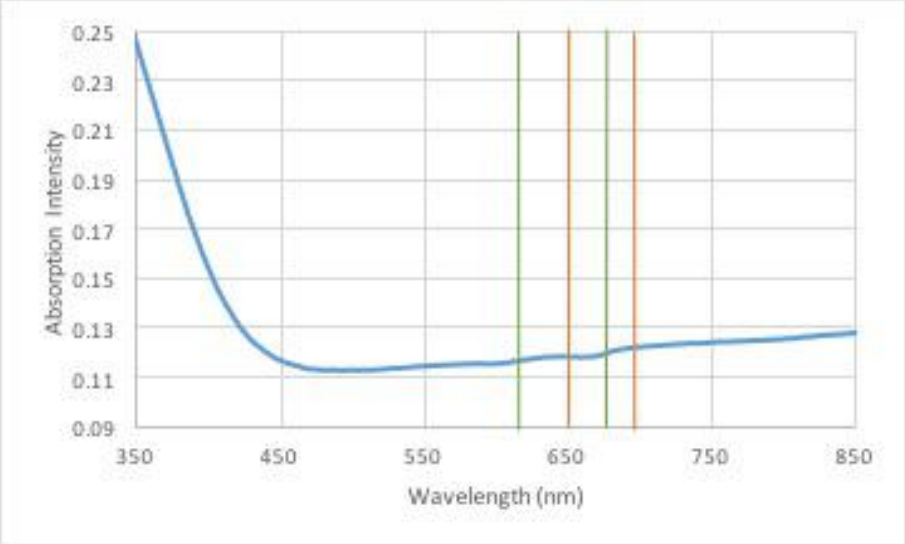

Figure 3.35: BBP 20min sample absorption spectra with the green line indicating the expected wavelengths and the orange line the obtained ones.

SEM

Figure 3.36 shows three images at different resolutions and areas of the same sample from the morphology studies of this sample of MoS_2. For this sample a drop from the solution was placed on a carbon grid for observation instead of observing the flakes on top of a PVDF membrane.
From the pictures in Figure 3.36 is observable that were obtained few particles and that some debris were present on top of the obtained particles. In Figure 3.36 (c) it is possible to observe foldadge of the MoS_2 layers. No signs of erosion on the edges of the flakes can be seen on the obtained pictures.

From this sample was possible to measure the thickness of one flake at approximately 342 nm.

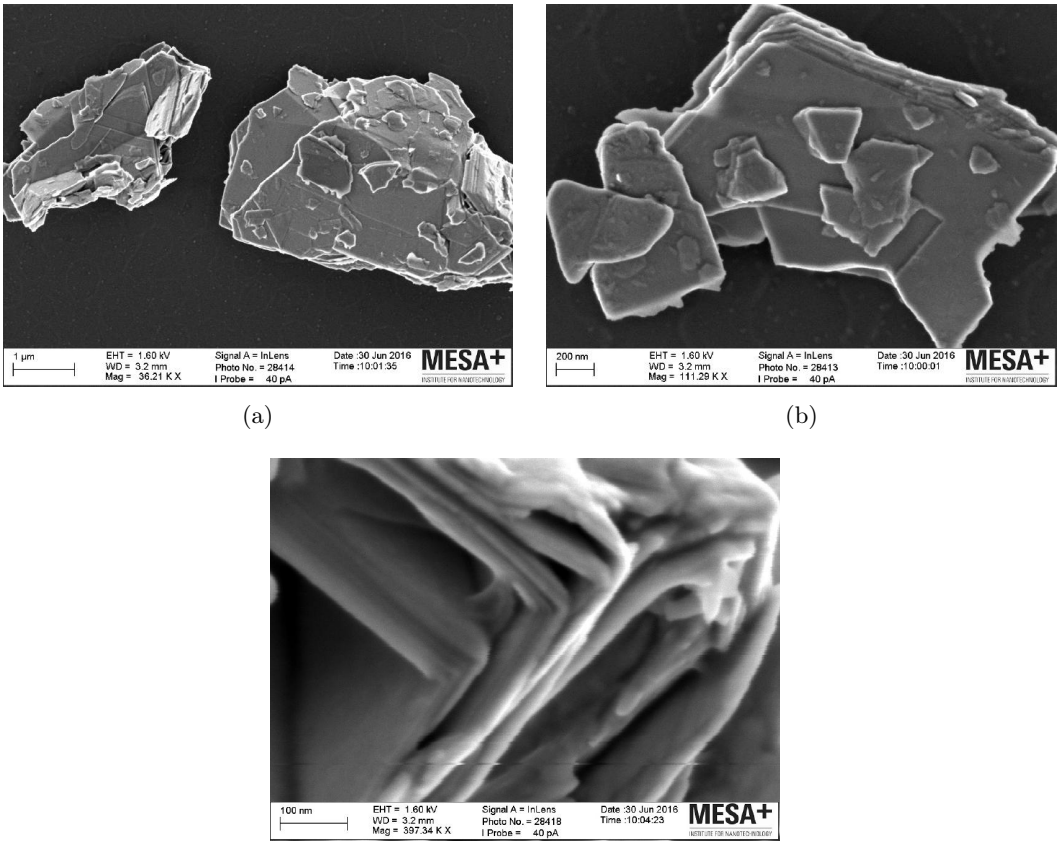

(a) (b)

(c)

Figure 3.36: SEM images for the BBP 20min sample with two flakes on (a) and (b) and a folded flake on (c).

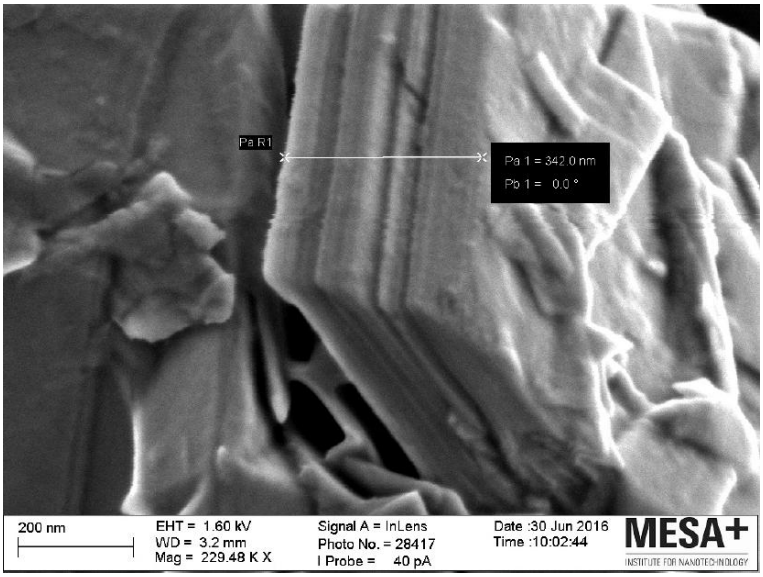

Figure 3.37: BBP 20min thickness measurement through SEM showing a thickness of 342 nm for the observed flake.

3.2 Cavitation Effects on the Cavitation Intensifying Bags

From the SEM observations done to the bag with three different exposition times was not possible to identify any signs of erosion. The bag had been exposed to intense cavitation for 2, 5 and 10 min.
On another attempt, where the times of exposition were extended, was still not possible to identify any signs of erosion as can be seen from Figure 3.38 and Figure 3.39. For the observations to the bag without pits the use of polarised lenses was discarded since the cavitation effects would be inferior than to the bag with pits and therefore no effects should occur for the same time of exposition as was later observable. After 30 min of exposition the experiment was ended since there were still no signs of erosion.
During these experiments, on one attempt the ultrasonic horn got in contact with the surface of the bag and as can be seen from Figure 3.40 there were significant erosion effects on the bag.

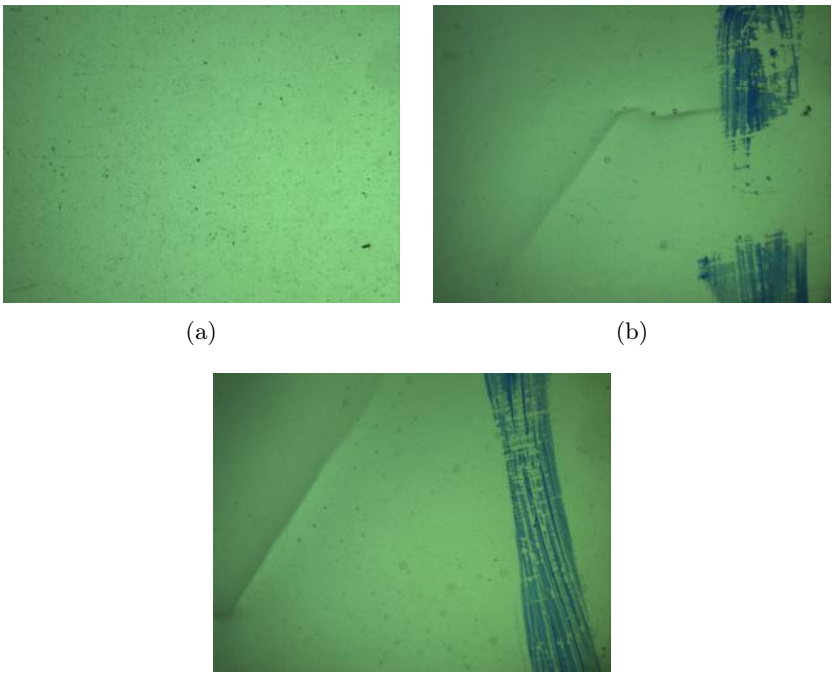

(a) (b)

(c)

Figure 3.38: Optical Microscope images at normal light from a bag without pits after exposition to intense cavitation for 0min (a), 20min (b) and 30min (c) showing no signs of damage from cavitation.

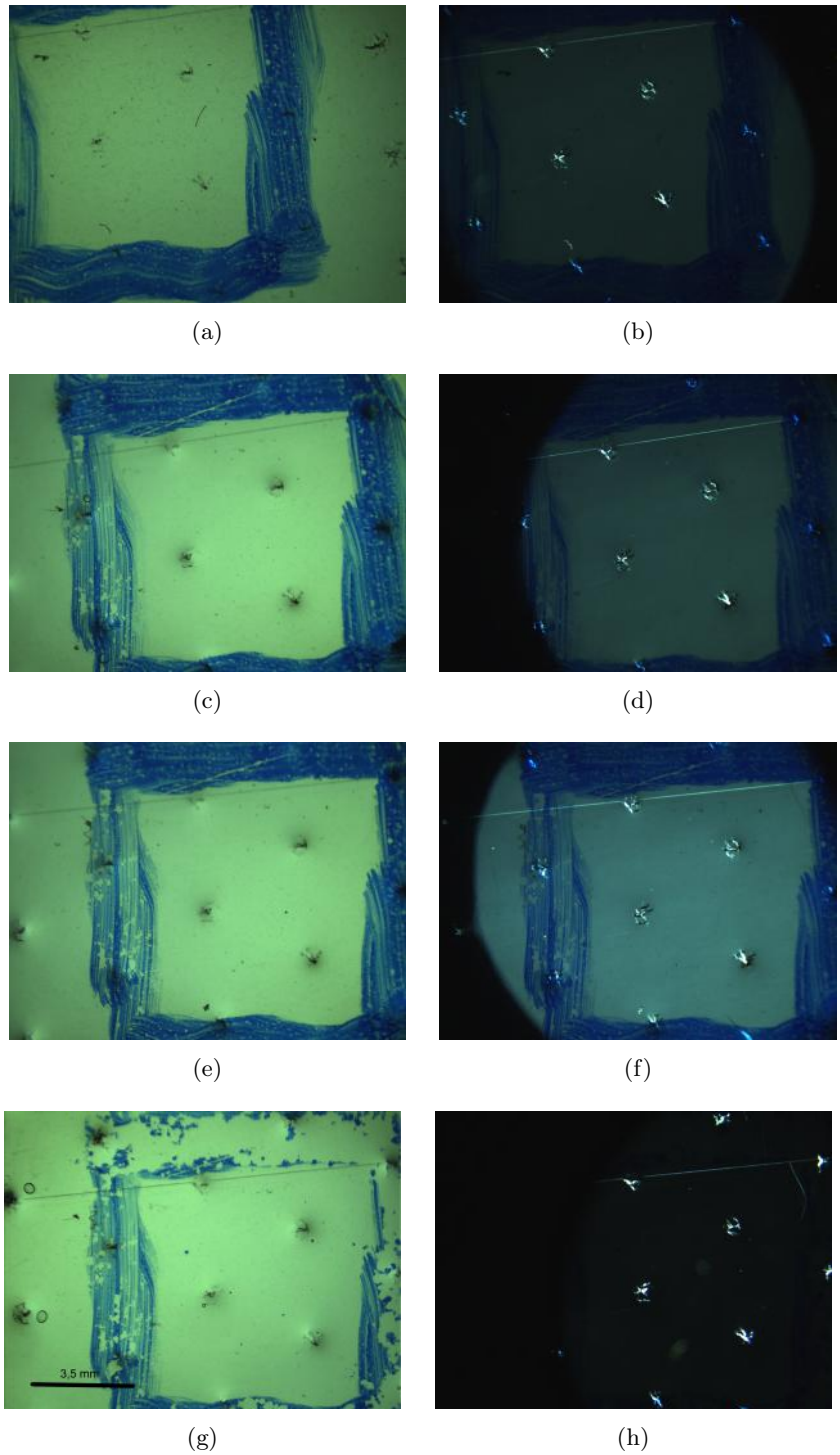

(a) (b) (c) (d) (e) (f) (g) (h)

Figure 3.39: Optical Microscope images at normal light (left) and polarised light (right) from a bag with pits after exposition to intense cavitation for 0min (a) and (b), 2min (c) and (d), 10min (e) and (f) and 30min (g) and (h) showing no signs of damage caused by cavitation.

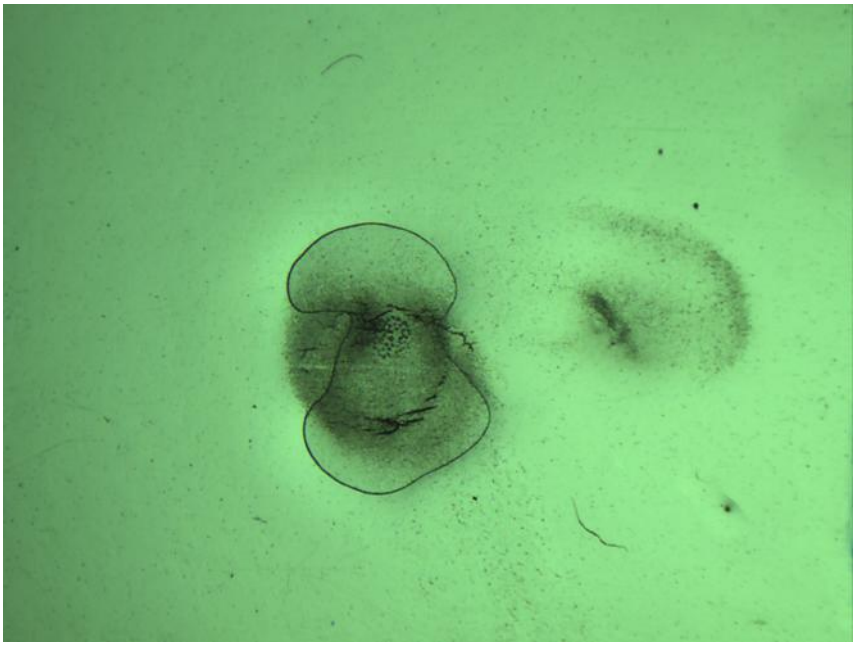

Figure 3.40: Optical Microscope images at normal light from a bag without pits after exposition to intense cavitation for 5min from an ultrasonic horn placed in contact with it.

Chapter 4

Discussion and Conclusions

MoS_2 Liquid-Phase Exfoliation in Cavitation Intensifying Bags

From the absorption spectra of the samples is firstly observable the fact that the two bands that should be seen separated [32, 36] are fused in a single one. This can be explained from the high concentrations of thick flakes that are still present on the samples. Instead of having samples solely containing MoS_2 mono-layers, the obtained samples contain MoS_2 with various thicknesses and as a result the obtained spectra is more similar to a flat line of high absorption intensity as can be seen in Figure 4.1. This conclusion is supported by fact that the absorption line after the second peak remains with a high absorption instead of decreasing to zero as would happen if there were solely mono-layers on the sample. In a sample with thick layers of MoS_2 is expectable to have an absorption line that does not decrease to an absorption intensity of zero before the first peak and after the second peak [37].

Figure 4.1 also shows that centrifuging the 20 min samples before exposing them to cavitation, removed too many particles to have a higher concentration on the final dispersion. Another possible explanation for those samples, is that the 20 min of cavitation were not enough to exfoliate the existent flakes to a thickness where the two excitonic bands between 600 nm and 700 nm would be distinguishable from the rest of the absorption line.

Surprisingly the bags without pits showed higher concentrations of MoS_2 than the bags with pits. It would be expectable that increased cavitation from the existence of pits, would help on the exfoliation of MoS_2 resulting in smaller flakes that manage to remain in the dispersion after centrifugation. On the equipment used to induce sonication, the ultrasonic bath showed better concentrations of MoS_2 on its dispersions than the ones from the ultrasonic horn. This can be explained from the more uniform way in which the ultrasound

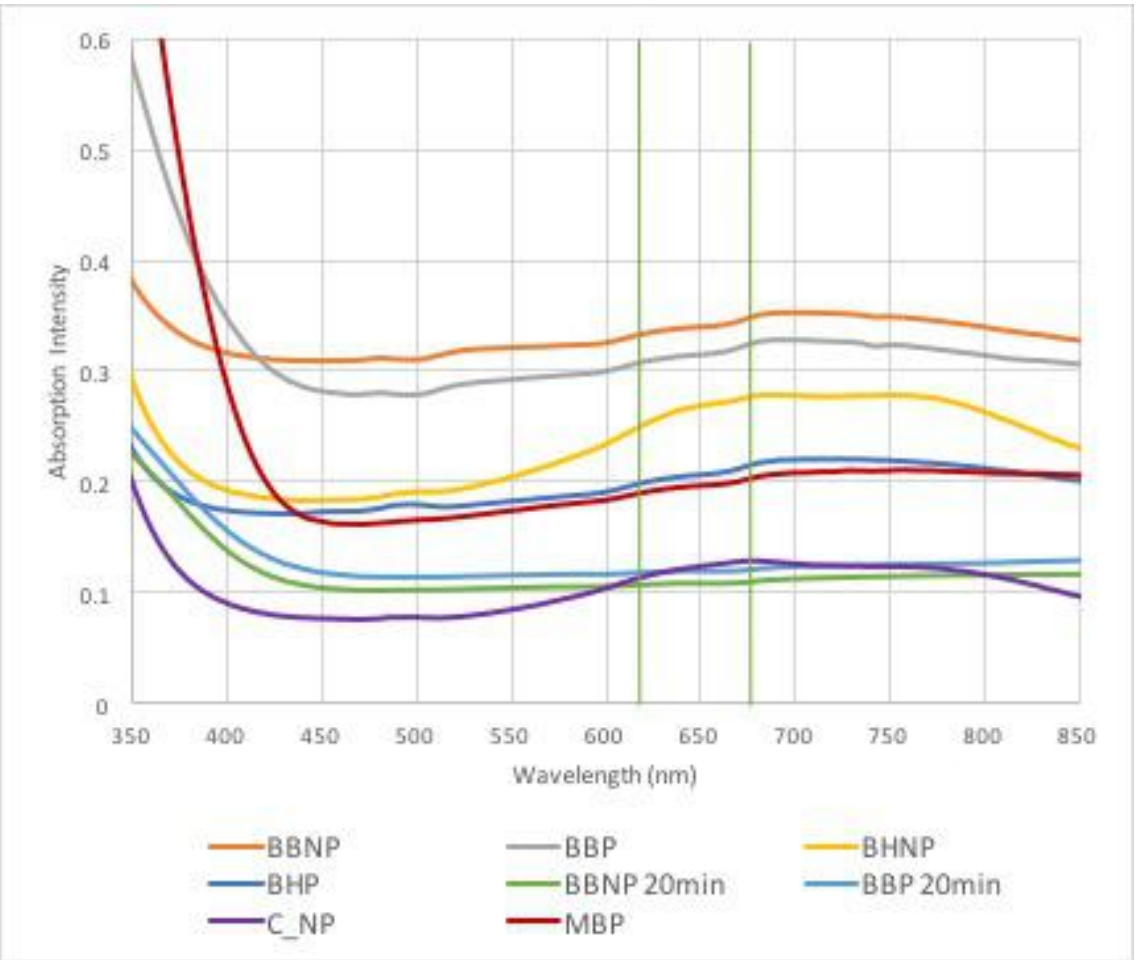

Figure 4.1: Compilation of the UV-vis Absorption spectrum from all samples with the green lines pointing the wavelengths for the MoS_2 mono-layers bands.

propagates through the sample in the ultrasonic bath comparing to the ultrasonic horn, as stated in subsection 2.2.1.1. The ultrasonic horn cannot manage to cleave the flakes further away from its tip and therefore it produces less thinner and lighter flakes than the bath. As previously stated in subsection 2.2.2.1, the obtained results from the UV-spectrophotometer have some errors associated to them as a result of the equipment not having a tool which would redirect into the detector any light scattered from solid particles dispersed on the sample.

Below, in Table 4.1, are the various masses of MoS_2 obtained after vacuum filtration. It was not possible to precisely determine the concentration of each sample since during vacuum filtration an undetermined volume of solvent would evaporate and before there was still solid dispersed on the sample increasing the actual solvent volume.

Sample	Mass of MoS_2 (mg)
BBNP	0,8
BBP	0,6
BHNP	0,2
BHP	0,7
C_NP	0,4
MBP	0,5

Table 4.1: MoS_2 masses obtained after vacuum filtration through the PVDF membranes.

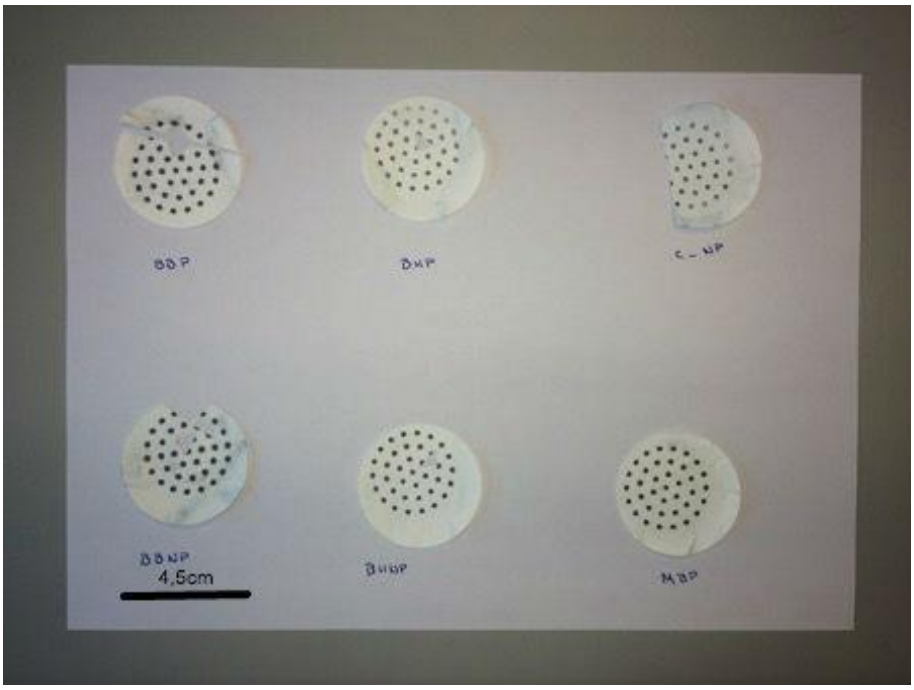

Figure 4.2: PVDF membranes with the obtained MoS_2.

The presence of MoS_2 mono-layers in some samples is further confirmed by the Raman analysis. The two characteristic nodes from MoS_2, firstly the E^1_{2g} as the in-plane vibrational node and secondly A_{1g} as the out-plane, are visible in the obtained Raman spectra and for both samples there is a correlation between the Raman intensities around the expected values of 383 cm^{-1} and 408 cm^{-1}. The downshift which indicates the presence of micromechanically cleaved single layers of MoS_2 at the second node is visible for both samples by occurring at the 403 cm^{-1} instead of the regular 408 cm^{-1} [32], as happens for bulk MoS_2. Other literature suggests that a downshift on the second node is not enough proof for the existence of MoS_2 mono-layers. Instead, both nodes must come closer to each other [17]. For these sample both the nodes downshifted instead of coming closer to each other, suggesting from this other analysis that it was inconclusive if there were mono-layers in the observed samples.

Considering only the downshift on the second node as proof of MoS_2 mono-layers in the sample, the Raman study allows to conclude that the pits increase the number of smaller

particles with more intense cavitation but do not help on the exfoliation process. As can be seen from the Raman study, the sample from the bag with no pits (BHNP) has more cleaved layers than the sample from a bag with pits (BBP). However, when these results are compared to the results from the absorption spectra, its possible to observe that there is a higher absorption intensity for sample BBP - Figures 3.8 and A.29 - than for BHNP - Figure 3.15 and A.57 -, but at the same time BHNP presents a clear increase in absorption intensity for the wavelengths expected to have bands for the mono-layers. This shows how the bags with pits generate samples with smaller particles and higher concentrations and how the lack of pits helps in generating samples with thinner layers and less particles that would otherwise increase the concentration of the sample. Nonetheless, this comparison could only be done to two different samples and better conclusions could be drawn if this comparison were possible for the remaining samples.

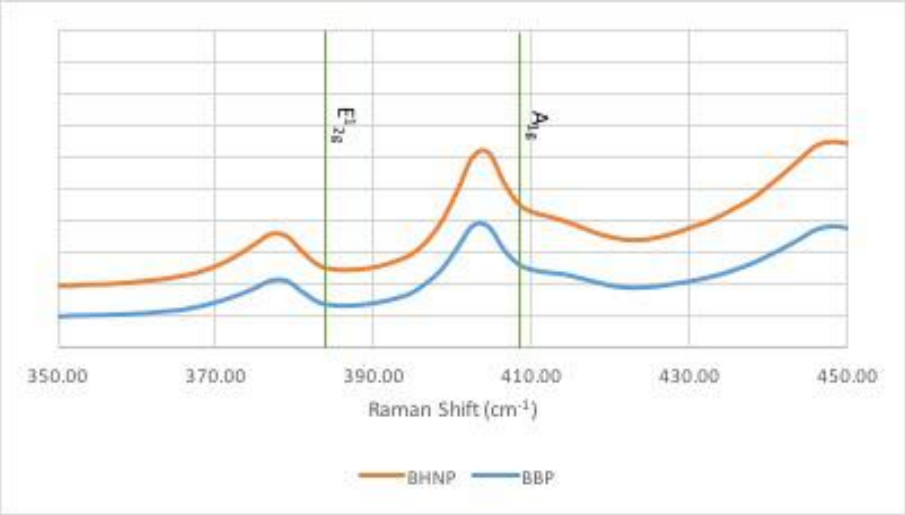

Figure 4.3: Average Raman Intensity for samples BHNP and BBP with the green lines indicating the Raman Shift for bulk MoS_2, clearly showing the downshift in intensity for the obtained samples due to the presence of mono-sheats.

Using the PVDF membrane as a holder for the material analysed by the Raman, proved to be a challenge in obtaining clear results. Its fluorescence was too intense considerably disturbing the signal obtained from the actual MoS_2 measurements, which added some errors to the obtained results.

The study done with the SEM showed that the higher cavitation intensity from the bags with pits resulted in obtaining flakes with more rounded edges. Not showing significant effects on the exfoliation process. It also confirmed that doing an AFM analysis to the surfaces would be redundant since the surface of the samples showed a too chaotic disposition of the flakes for proper AFM analysis.
Despite the measurements made with the SEM to the layer thickness, they cannot be used

as an actual value of their thickness since it is highly dependable of the layers' spacial orientation and to the fact that the measurements were only made to a single MoS_2 flake in every sample instead of to a few, which would give a better idea of their actual thickness. Had the AFM been done and this procedure could have taken place. But since the measurements to the thickness of the layers were being performed by the SEM it would have been counterproductive to do this analysis since they have plenty of errors. Also mono-layers cannot be observed through the SEM due to their small size. Nonetheless, to the flakes to which the measurement was made, was possible to determine that they had thicknesses between 224 nm and 675 nm, or between 345 and 1038 mono-layers. Which means that there are still very thick layers on these samples by the end of this exfoliation process. It is possible that these thick layers are the result of re-stacking of thinner layers during the vacuum filtration. And therefore the results from SEM show far thicker layers than the TEM results.
The images obtained from the 20 min samples are considerably better and show that not doing vacuum filtration to the obtained dilutions results in better observations because the flakes are not packed together on top of the membrane and its surface will not place the flakes in random positions.

The TEM study besides confirming the hexagonal crystalline structure of MoS_2 (2H-MoS_2), delivered images which show very thin layers. Since this method is done from the top of a sample that is placed horizontally, it was not possible to measure the thickness of these layers. However, from some images is possible to see a layer through the layer on top of it, suggesting the top layer is very thin. A surprising observation were the Moiré patterns showing that on the observed sample there were very thin, separated layers on top of each other. These patterns are the result of the rotation of one of those layers. Nonetheless, it can only be concluded that these layers are vey thin, but it is not possible to state that they are mono-layers.
Further conclusions from the TEM cannot be made since only a sample was observed through this method.

Through these methods is possible to say that MoS_2 mono-layers were present on these samples in a significant amount. Still for future works an AFM analysis must be performed to confirm the thickness of the obtained mono-layers in a more precise manner. It will also be interesting in understanding how the CIBs will perform when exfoliating MoS_2 with a solvent with better results than IPA when it comes to exfoliation through sonication, like NVP - N-vinyl-pyrrolidinone [32]. Two different times were tested in this work, but it is not enough to state an ideal time of exposure to exfoliate MoS_2 by this setup. Further times of sonication must be performed in order to conclude if the CIBs can reduce the long sonication periods that many times must be performed in order to exfoliate materials, since the tested sonication periods are still below many of the used in similar experiments [37]. A study based on the work from Mason [38] can be done to understand how these bags may increase

the energy efficiency of this process when compared to other exfoliation methods. Measuring the increase in temperature of the solvent used inside the bag and through calorimetry studies is possible to determine the actual intensity inputed through the equipment on the system. These results can then be compared between different exfoliation methods that produced flakes of similar dimensions. Finally, a study should be made combining this new exfoliation setup with already established intercalation processes [36, 39] in an attempt to intensify the formation of more mono-layers while further reducing the sonication time to decrease the dependance from the mechanical effects that slightly damage the obtained flakes.

On the work done to understand if either are the mechanical or chemical effects from cavitation that exfoliate the material, was possible to conclude from the absorption studies that the mechanical effects were critical in producing a more concentrated sample by forming lighter and smaller MoS_2 layers, as can be observed from the higher absorption intensities of the MBP sample. However, as is proven from sample C_NP, the radicals play an important role in weakening the van der Walls forces that connect the sheets and consequently separating the layers from one another instead of breaking apart the flakes. This conclusion comes from the fact that the absorption line from this second sample instead of increasing in intensity, as would be expected from having smaller particles, only increases at the wavelengths relevant to the bands of the MoS_2 mono-layers. Showing a predominance of very thin layers of MoS_2. This goes in accordance to what recent studies have shown where charged particles can be used to intercalate between layers and induce exfoliation [39] or where small concentrations of water are used in the solution to induce the formation of radicals from cavitation and induce cleavage on the layers [36].
The SEM study to samples MBP and C_NP showed similar results to the ones obtained from the other samples. But also proved the mechanical effects are the reason for the erosion on the edges of the layers since there were no signs of erosion on the SEM images from the C_NP sample.

Cavitation Effects on the Cavitation Intensifying Bags

This study to the cavitation effects on the CIBs showed that there were no significant effects on the bag's surface after 30 min of exposition to intense cavitation induced from an ultrasonic horn placed 5 mm above the sample. Still, direct contact between the bags and the equipment which induces the ultrasound must be avoided as was shown on this work. For experiments on the ultrasonic bath this work showed that for times of exposition that are continuous and last more than an hour, the water inside the bath should be cooled. Otherwise, a dilation of the bag due to the increase in temperature of the water in the bath may occur releasing sample into the bath as can be seen in Figure 4.4. It is unknown if this happens on the glued side of the bags or if it happens on other more sensitive areas of the bag like the pits.

Figure 4.4: Example of MoS_2 spill from the bag into the bath.

Chapter 5

Final Remarks

In the present work were described attempts to exfoliate MoS_2 with the aid of the *BuBclean* CIBs and normal bags. Various samples with a concentration of 20 $mg.ml^{-1}$ of MoS_2 in IPA were prepared to obtain MoS_2 mono-layers. An ultrasonic horn and bath were used to generate cavitation from ultrasound. The samples were exposed to ultrasound for 4,5 h and 20 min.
The chemical and mechanical role from cavitation on the exfoliation process were also analysed.
On a final study, the effects of cavitation on the two types of *BuBclean* bags was studied.

The existence of pits on the *BuBclean* CIB proved to be damaging to the MoS_2 flakes in solution. Instead of promoting solely the exfoliation, it damages and breaks apart the existing flakes. It is therefore concluded that there must be a limit to the cavitation intensity which can be applied to the system in order to obtain undamaged flakes or mono-layers. As for the equipment used to promote cavitation the ultrasonic bath is a better solution in promoting a uniform exfoliation due to the way in which it propagates the ultrasonic waves in the solution. For the two times of sonication period of 4,5 h and 20 min, was concluded that despite attempting to separate smaller flakes from the bulk material through centrifugation to reduce the cavitation time, the 20 min samples did not produce many MoS_2 mono-layers.

In the exfoliation process the mechanical effects are the main factor in promoting smaller and thinner flakes, but just as the *BuBclean* CIBs, it promotes the breaking and erosion of the flakes instead of their exfoliation. The radicals generated from cavitation, on the other hand, act as exfoliating agent, intercalating between the layers of the material and separating these layers by overcoming the van der Waals forces that connect them.

The *BuBclean* CIBs proved to be resistant enough to sustain cavitation for at least 30 min. However, as the solution or the bath where they are inserted heats up, they tend to let some material spill. This can be a result of the bags dilation from the higher temperatures. It is unknown if it happens on the glued side of the bag or the pits. A way to lock the top of the bags must also be used for long experiments, especially when working with volatile solvents since the increase in temperature from sonication will promote evaporation of the solution as well.

References

[1] David Fernandez Rivas, Joris Betjes, Bram Verhaagen, Wilco Bouwhuis, Ton C. Bor Detlef Lohse, and Han J. G. E. Gardeniers. "Erosion evolution in mono-crystalline silicon surfaces caused by acoustic cavitation bubbles". In: *Journal of Applied Physics* 113 (2013), pp. 1–13.

[2] David Fernández Rivas. "Taming Acoustic Cavitation". PhD thesis. Enschede, Netherlands: University of Twente, 2012.

[3] Kenneth S. Suslick and Gareth J. Price. *Applications of Ultrasound to Materials Chemistry.* Vol. 29. Annual Reviews Materials Science, 1999, pp. 295–326.

[4] Aharon Gedanken. "Using sonochemistry for the fabrication of nanomaterials". In: *Ultrasonics Sonochemistry* 11 (2004), pp. 47–55.

[5] Jin Ho Bang and Kenneth S. Suslick. "Applications of Ultrasound to the Synthesis of Nanostructured Materials". In: *Advanced Materials* 22 (2010), pp. 1039–1059.

[6] P. Riesz, D. BerdahI, and C. L. Christman. "Free Radical Generation by Ultrasound in Aqueous and Nonaqueous Solutions". In: *Environmental Health Perspectives* 64 (1985), pp. 233–252.

[7] Pedro Cintas, Giancarlo Cravotto, Alessandro Barge, and Katia Martina. *Interplay Between Mechanochemistry and Sonochemistry.* Vol. 369. Switzerland: Springer International Publishing, 2015.

[8] Yan Wang, Yiming He, Qinghua Lai, and Maohong Fan. "Review of the Progress in Preparing Nano TiO2: An Important Environmental Engineering Material". In: *Journal of Environmental Sciences* 26 (2014), pp. 2139–2177.

[9] Frédéric Caupin and Eric Herbert. "Cavitation in water: a review". In: *C. R. Physique* 7 (2006), pp. 1000–1017.

[10] K. S. Suslick, M. M. Fang, T. Hyeon, and M. M. Mdleleni. *Applications of Sonochemistry to Materials Synthesis.* Ed. by L. A. Crum, T. J. Mason, J. Reisse, and K. S. Suslick. Dordrecht, Netherlands: Kluwer Publishers, 1999, pp. 291–320.

[11] Jos M. J. Paulusse and Rint P. Sijbesma. "Ultrasound in Polymer Chemistry: Revival of an Established Technique". In: *Journal of Polymer Science* 44 (2006), pp. 5445–5453.

[12] David Fernandez Rivas, Pedro Cintas, and Han J. G. E. Gardeniers. "Merging Microfluidics and Sonochemistry: Towards Greener and More Efficient Micro-sonoreactors". In: *Chemm. Commun.* 48 (2012), pp. 10935–10947.

[13] David Fernandez Rivas, Muthupandian Ashokkumar, Thomas Leong, Kyuichi Yasui, Toru Tuziuti, Sandra Kentish, Detlef Lohse, and Han J.G.E. Gardeniers. "Sonoluminescence and sonochemiluminescence from a microreactor". In: *Ultrasonics Sonochemistry* 19 (2012), pp. 1252–1259.

[14] Y. Iida, K. Yasui, T. Tuziuti, and M. Sivakumar. "Sonochemistry and its Dosimetry". In: *Microchemical Journal* 80 (2005), pp. 159–164.

[15] John R.G. Sander, Brad W. Zeiger, and Kenneth S. Suslick. "Sonocrystallization and sonofragmentation". In: *Ultrasonics Sonochemistry* 21 (2014), pp. 1908–1915.

[16] Bram Verhaagen, Youlin Liu, Andrés Galdames Pérez, Elena Castro-Hernandez, and David Fernandez Rivas. "Scaled-up sonochemical microreactor with increased efficiency and reproducibility". In: *Chemistry Select* 2 (2016), pp. 136–139.

[17] Xiao Li and Hongwei Zhu. "Two-dimensional MoS2: Properties, preparation, and applications". In: *Journal of Materiomics* 1 (2015), pp. 33–44.

[18] C. N. R. Rao, Urmimala Maitra, and Umesh V. Waghmare. "Extraordinary attributes of 2-dimensional MoS2 nanosheets". In: *Chemical Physical Letters* 609 (2014), pp. 172–183.

[19] Gyeong Sook Bang, Kwan Woo Nam, Jong Yun Kim, Jongwoo Shin, Jang Wook Choi, and Sung-Yool Choi. "Effective Liquid-Phase Exfoliation and Sodium Ion Battery Application of MoS2 Nanosheets". In: *Applied Materials and Interfaces* 6 (2014), pp. 7084–7089.

[20] Hee Sung Lee, Sun-Wook Min, Youn-Gyung Chang, Min Kyu Park, Taewook Nam, Hyungjun Kim, Jae Hoon Kim, Sunmin Ryu, and Seongil Im. "MoS2 Nanosheet Phototransistors with Thickness-Modulated Optical Energy Gap". In: *Nano Letters* 12 (2012), pp. 3695–3700.

[21] Xiaobin Fan, Pengtao Xu, Dekai Zhou, Yifan Sun, Yuguang C. Li, Minh An T. Nguyen, Mauricio Terrones, and Thomas E. Mallou. "Fast and Efficient Preparation of Exfoliated 2H MoS2 Nanosheets by Sonication-Assisted Lithium Intercalation and Infrared Laser-Induced 1T to 2H Phase Reversion". In: *Nano Letters* 15 (2015), pp. 5956–5960.

[22] Joohoon Kang, Jung-Woo T. Seo, Diego Alducin, Arturo Ponce, Miguel Jose Yacaman, and Mark C. Hersam. "Thickness sorting of two-dimensional transition metal dichalcogenides via copolymer-assisted density gradient ultracentrifugation". In: *Nature Communications* (2014), pp. 1–7.

[23] Carmen C. Mayorga-Martinez, Adriano Ambrosi, Alex Yong Sheng Eng, Zdeněk Sofer, and Martin Pumera. "Transition metal dichalcogenides (MoS2, MoSe2, WS2 andWSe2) exfoliation technique has strong influence upon their capacitance". In: *Electrochemistry Communications* 56 (2015), pp. 24–28.

[24] Stanley S. Chou, Mrinmoy De, Jaemyung Kim, Segi Byun, Conner Dykstra, Jin Yu, Jiaxing Huang, and Vinayak P. Dravid. "Ligand Conjugation of Chemically Exfoliated MoS2". In: *Journal of the American Chemical Society* 135 (2013), pp. 4584–4587.

[25] Artur Ciesielski and Paolo Samorı. "Graphene via sonication assisted liquid-phase exfoliation". In: *The Royal Society of Chemistry* 43 (2014), pp. 381–398.

[26] Yuhang Qi, Nan Wang, Qun Xu, Hongxiang Li, Pengshang Zhou, Xin Lub, and Guoqiang Zhao. "A green route to fabricate MoS2 nanosheets in water–ethanol–CO2". In: *Royal Society of Chemistry* 51 (2015), pp. 6726–6729.

[27] Visited: 30-08-2016. URL: http://www.bubclean.nl/bubble-bags-2/.

[28] Visited: 14-09-2016. URL: http://www.cmmmagazine.com/cmm-articles/high-precision-cleaning-from-twente\%E2\%80\%99s-spin-off-bubclean/.

[29] D Fernandez Rivas, B Verhaagen, Andres Galdamez Perez, Elena Castro-Hernandez, Ralph van Zwieten, and Karin Schroen. "A novel ultrasonic cavitation enhancer". In: *Journal of Physics: Conference Series* 656 (2015).

[30] Visited: 30-08-2016. URL: https://en.wikipedia.org/wiki/Azobisisobutyronitrile.

[31] Amal Kumar Mandal, Sidharam P. Pujari, Han Zuilhof, Jurriaan Huskens, and Tibor Kudernac. "Enhancing the Optical Emission of Liquid-Exfoliated Two-Dimensional 2H-MoS2 through Functionalization". 2016.

[32] Jonathan N. Coleman et al. "Two-Dimensional Nanosheets Produced by Liquid Exfoliation of Layered Materials". In: *Science* 331 (2011), pp. 568–571.

[33] Visited: 30-08-2016. URL: https://www.thermofisher.com/order/catalog/product/75008371.

[34] Visited: 16-06-2016. URL: https://www.utwente.nl/mesaplus/nanolab/analyselab/Analysis_Facilities/SEM/.

[35] Visited: 16-06-2016. URL: https://www.utwente.nl/mesaplus/nanolab/analyselab/Analysis_Facilities/TEM/.

[36] Ali Jawaid, Dhriti Nepal, Kyoungweon Park, Michael Jespersen, Anthony Qualley, Peter Mirau, Lawrence F. Drummy, and Richard A. Vaia. "Mechanism for Liquid Phase Exfoliation of MoS2". In: *Chemistry of Materials* 28 (2015), pp. 337–348.

[37] Jian Peng and Jian Weng. "One-pot solution-phase preparation of a MoS2/graphene oxide hybrid". In: *Carbon* 94 (2015), pp. 568–576.

[38] T. J. Mason, J. P. Lorimer, and D. M. Bates. "Quantifying sonochemistry: casting some light on a "black art"". In: *Ultrasonics* 30.1 (1992), pp. 40–42.

[39] Gabin Yoon, Dong-Hwa Seo, Kyojin Ku, Jungmo Kim, Seokwoo Jeon, and Kisuk Kang. “Factors Affecting the Exfoliation of Graphite Intercalation Compounds for Graphene Synthesis”. In: *Chemistry of Materials* 27 (2015), pp. 2067–2073.

Appendix A

Appendix

A.1 Experimental Results

A.1.1 Bulk

SEM

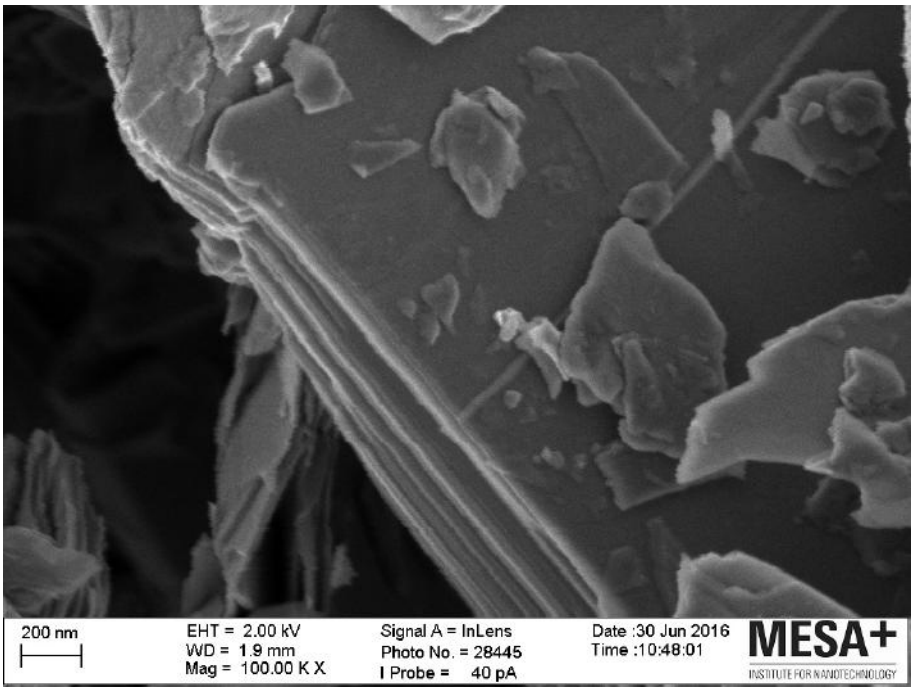

Figure A.1

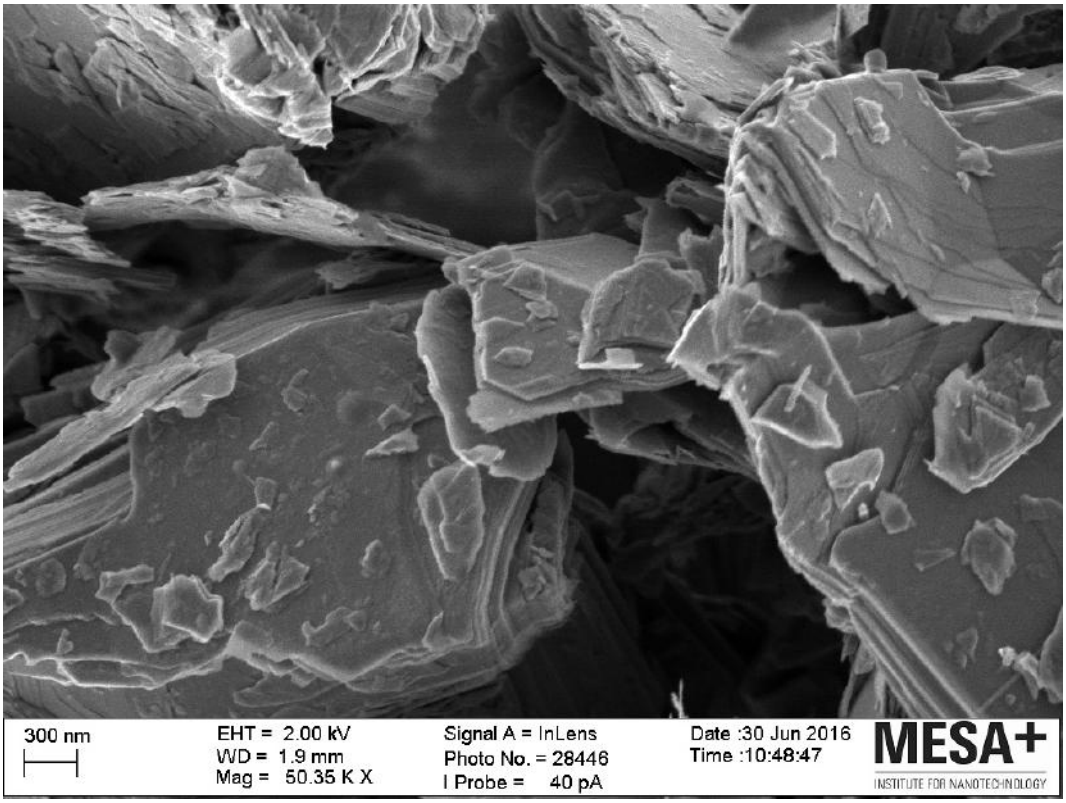

Figure A.2

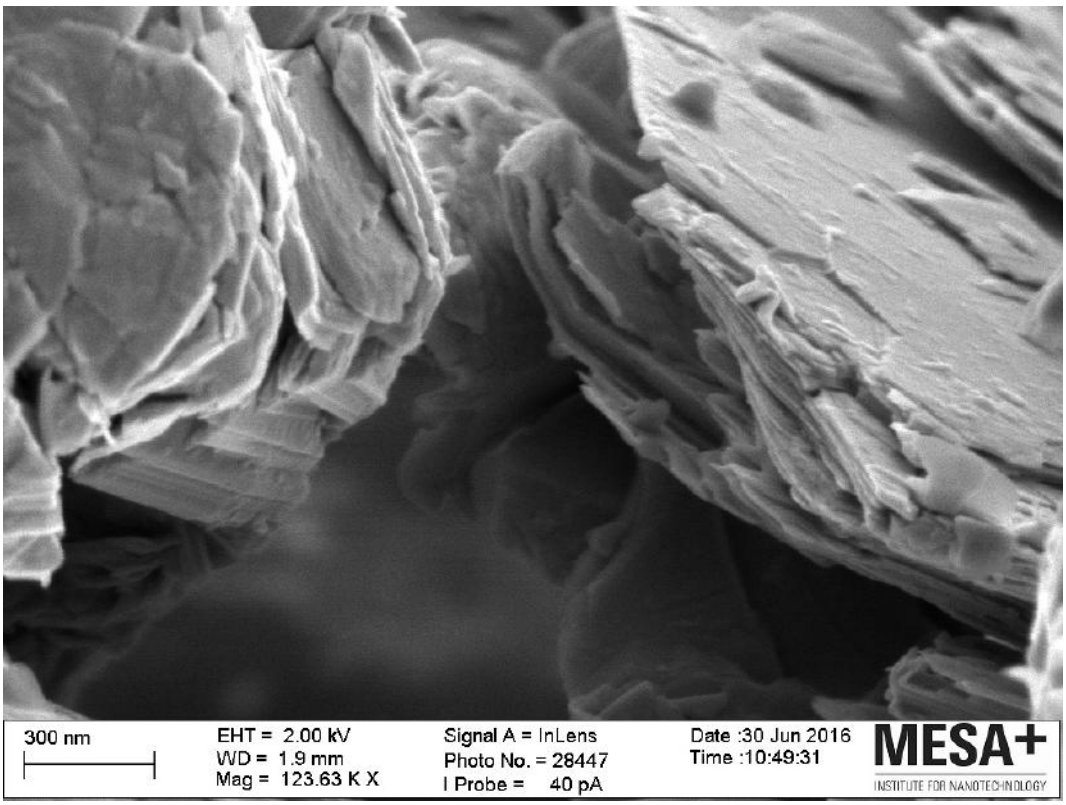

Figure A.3

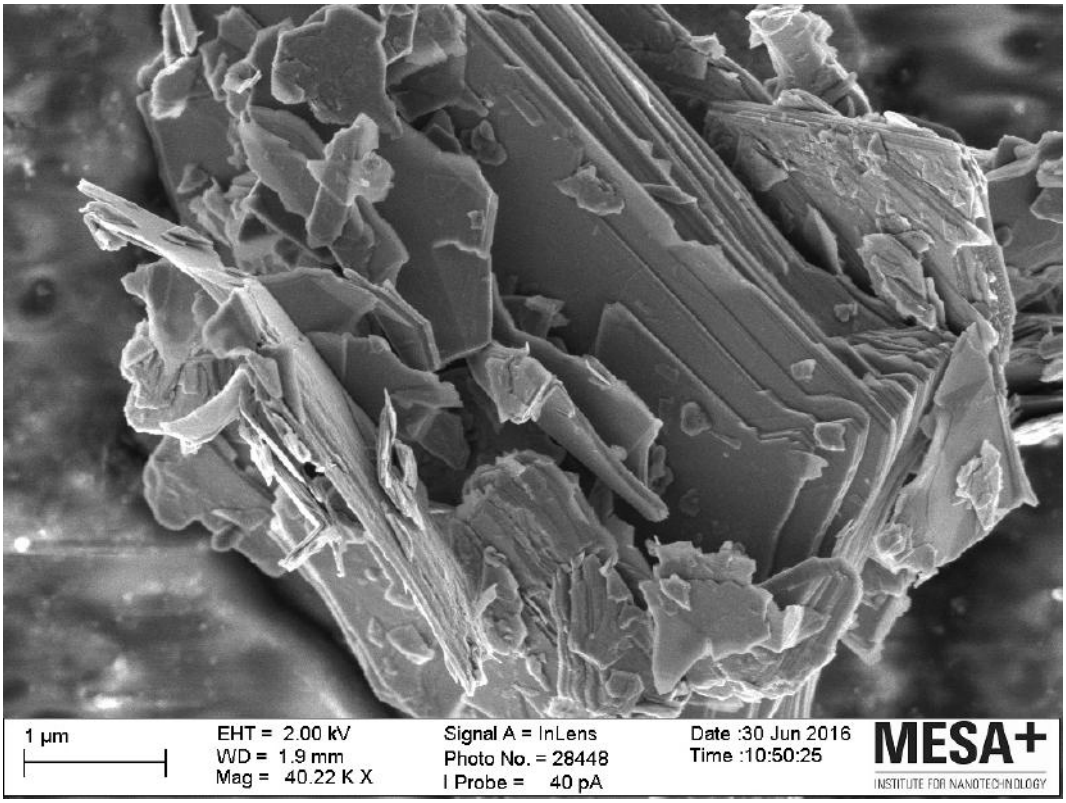

Figure A.4

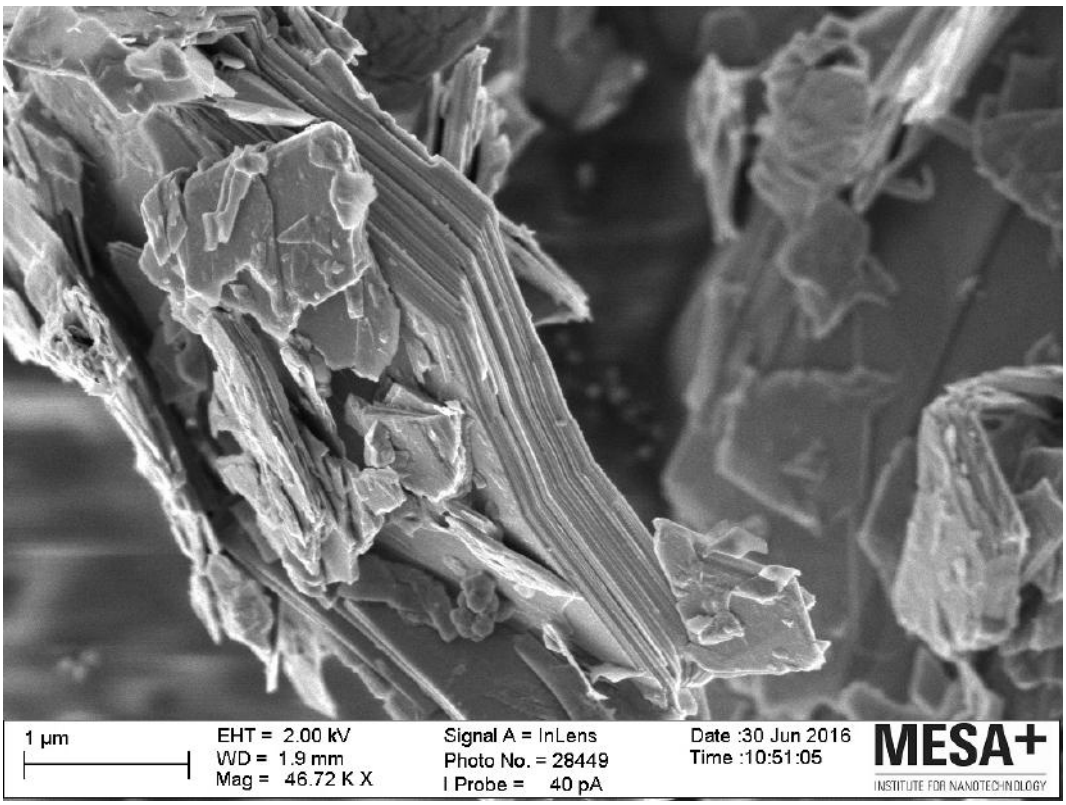

Figure A.5

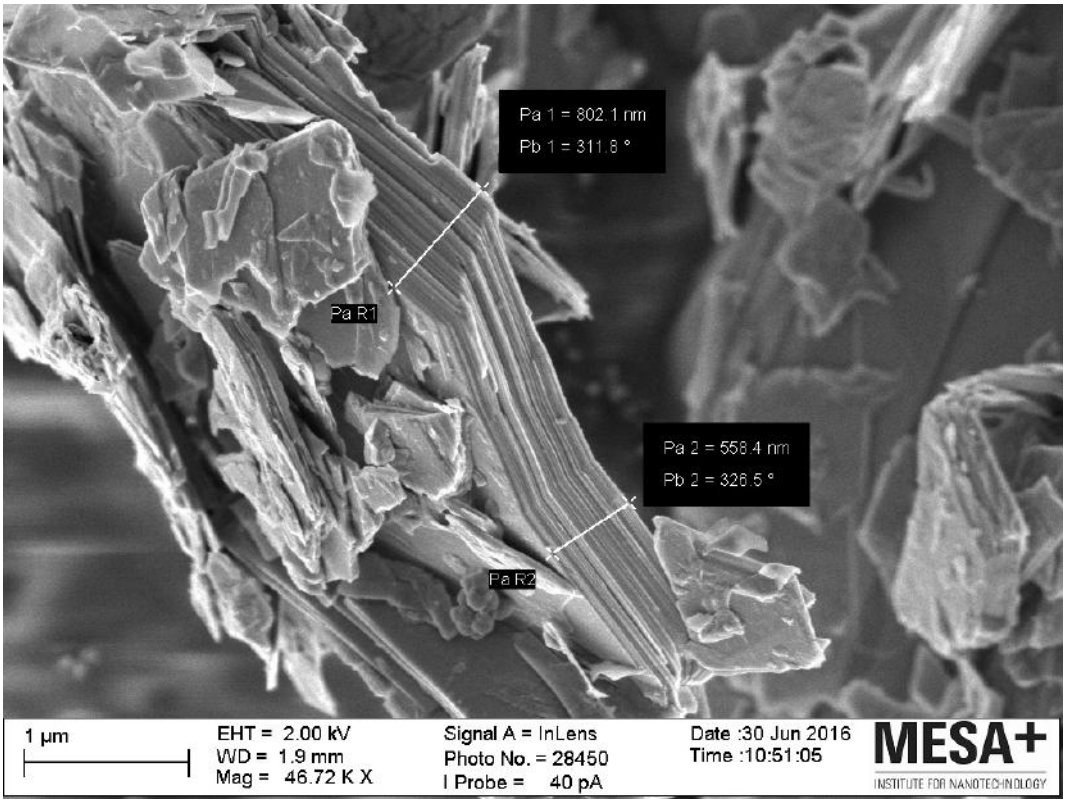

Figure A.6

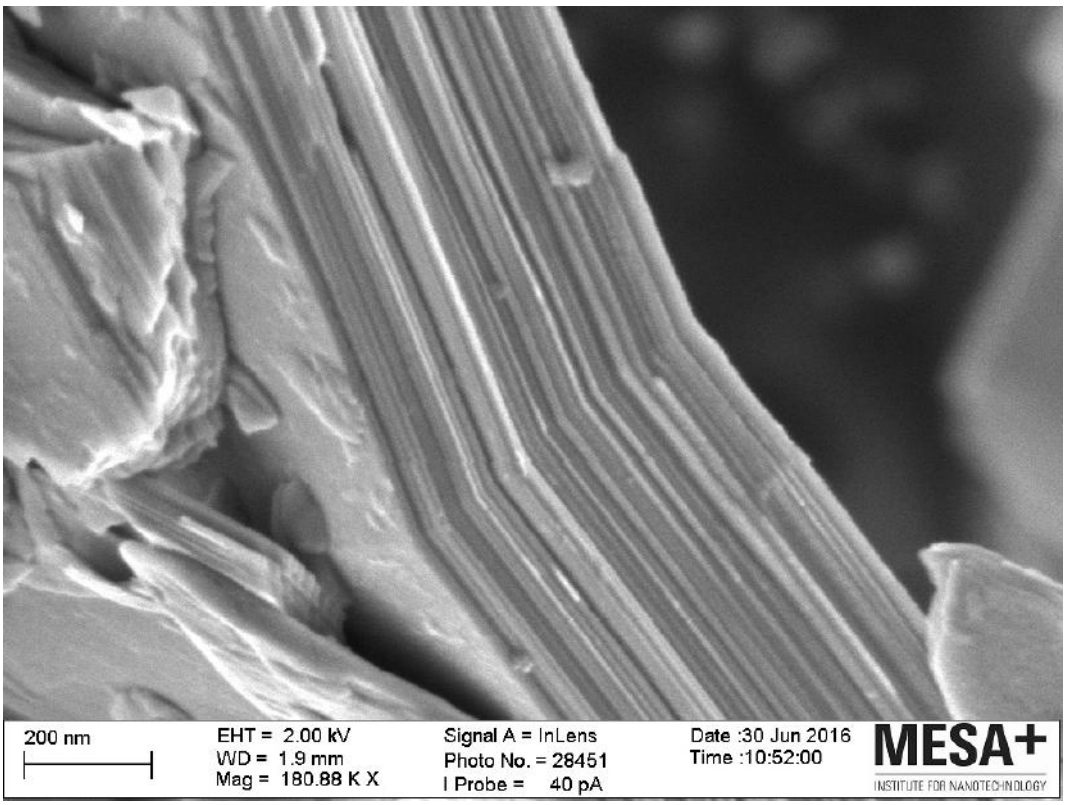

Figure A.7

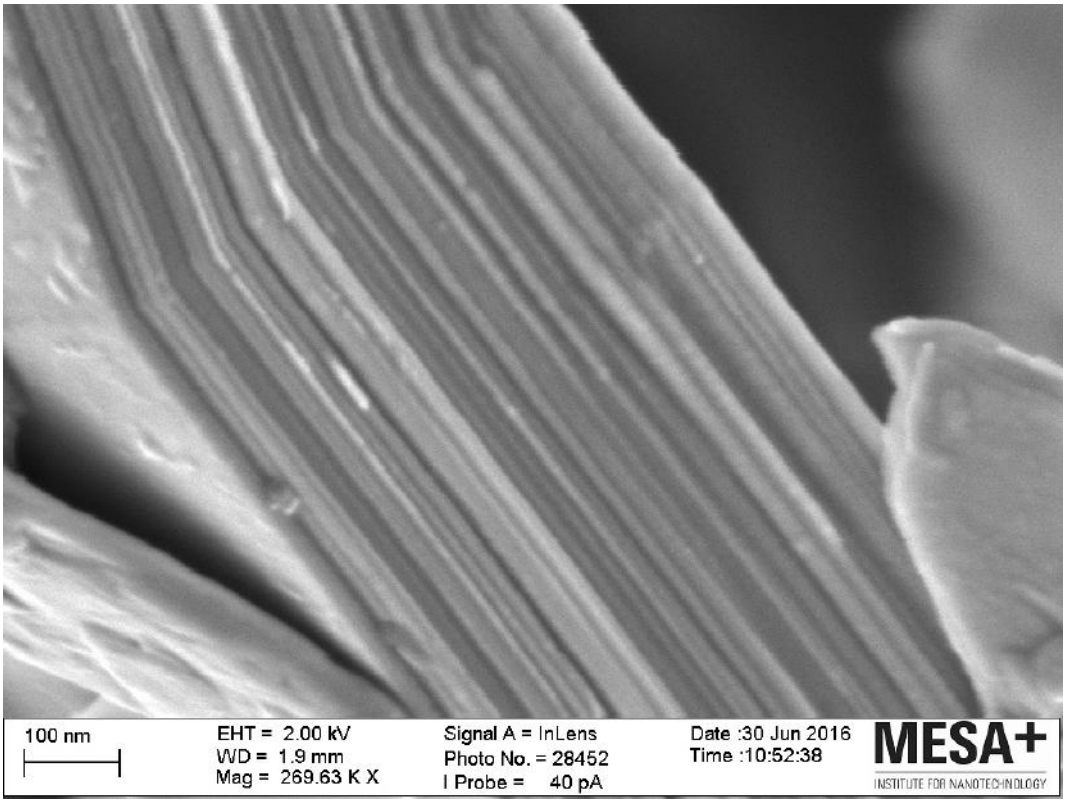

Figure A.8

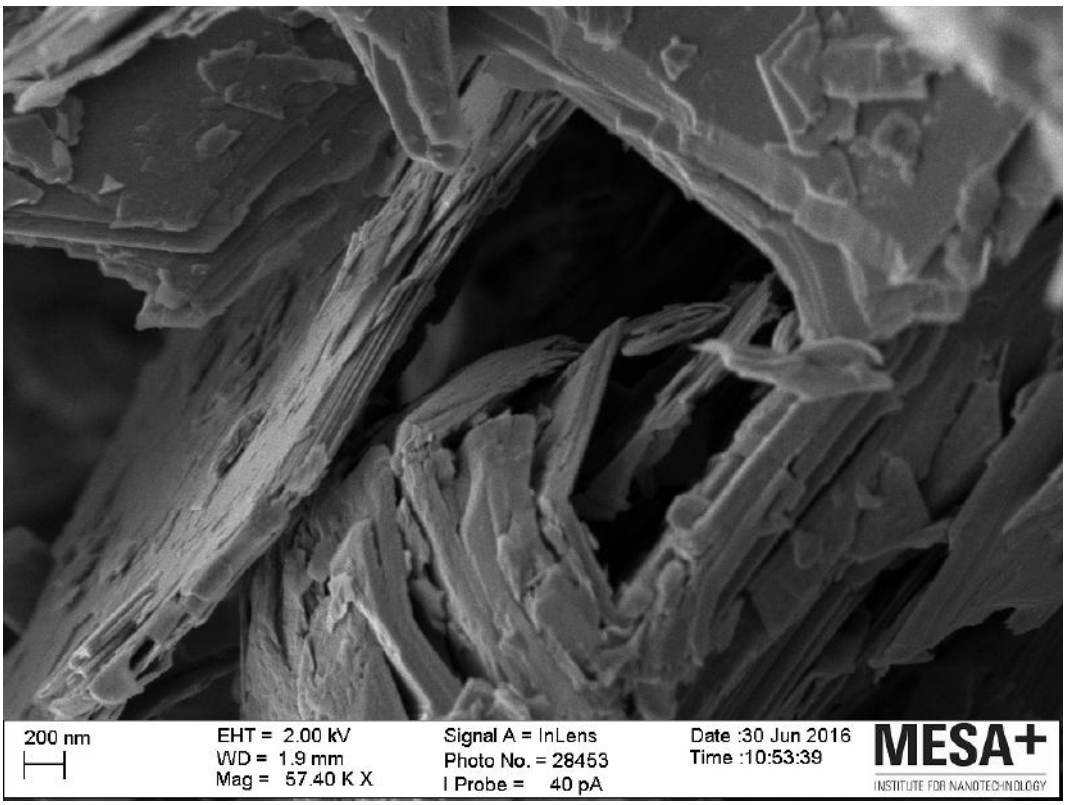

Figure A.9

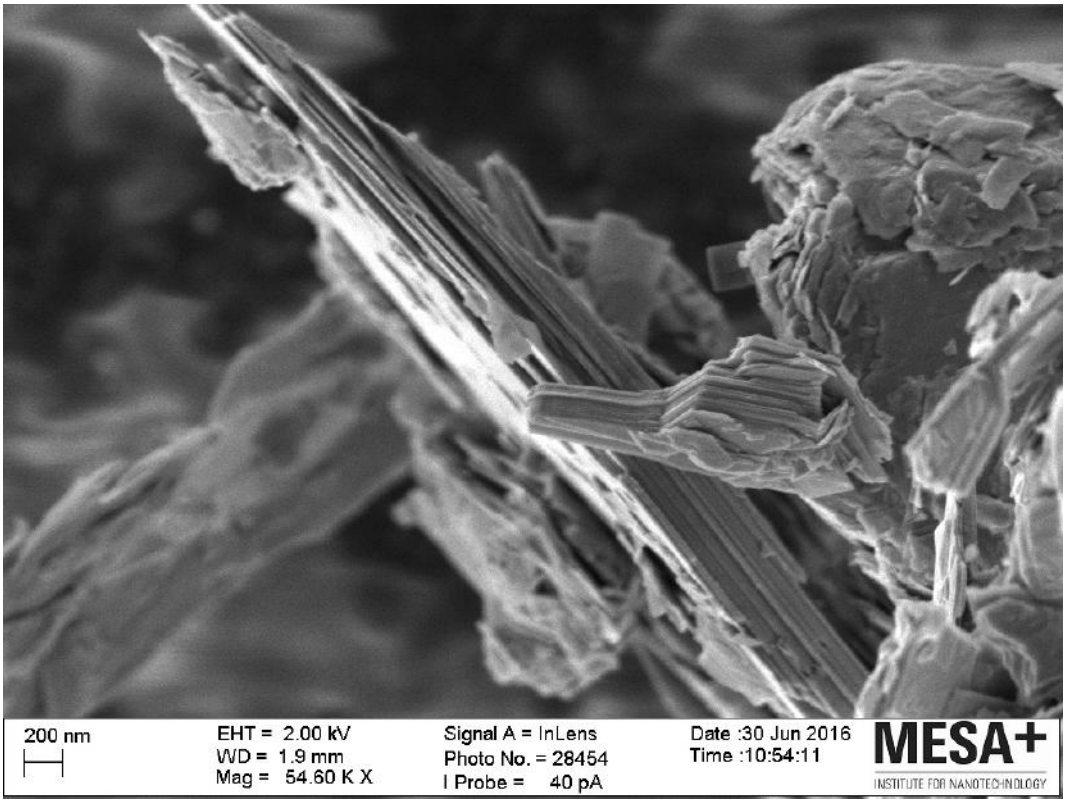

Figure A.10

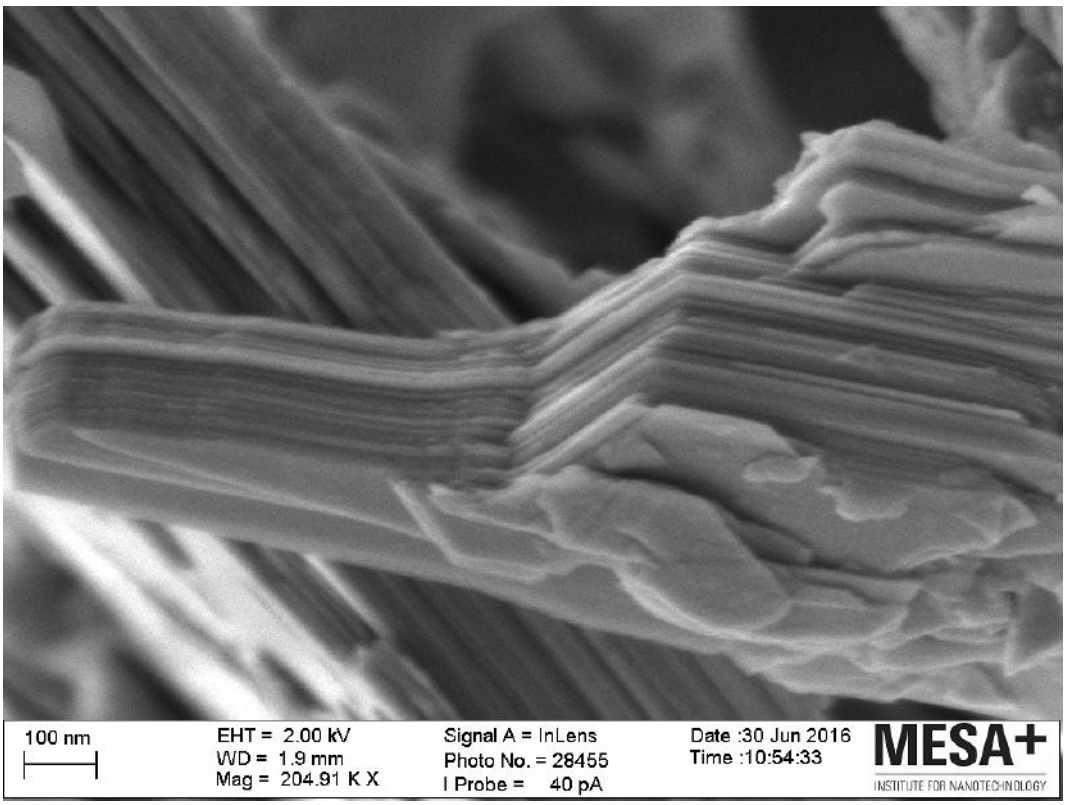

Figure A.11

A.1.2 BBNP

Absorption Spectra

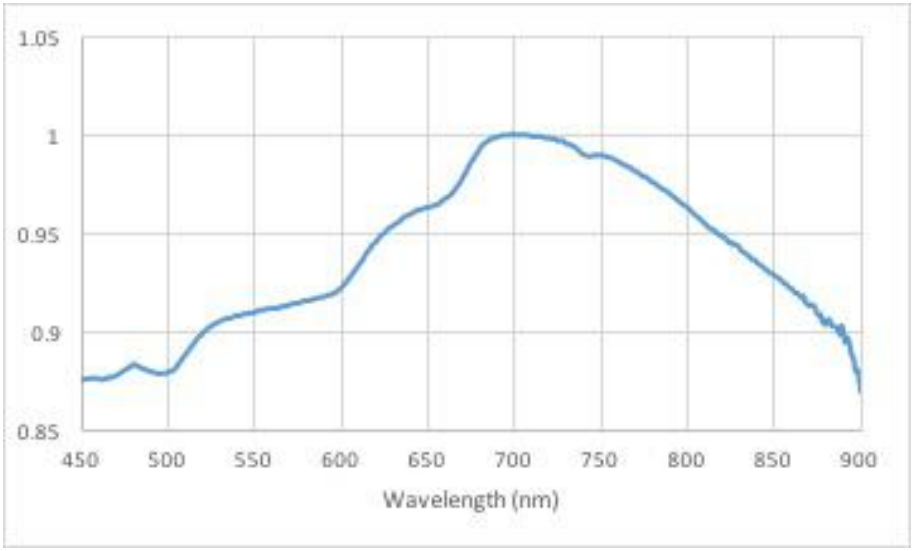

Figure A.12: Normalised absorption spectra for a maximum absorption intensity of 0,352 at the wavelength of 699 nm.

SEM

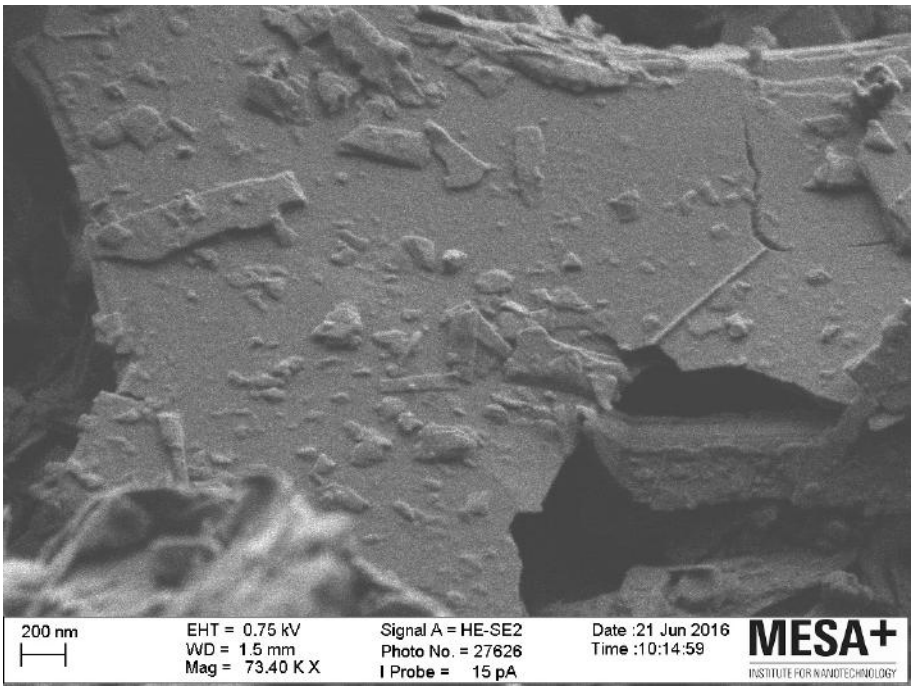

Figure A.13

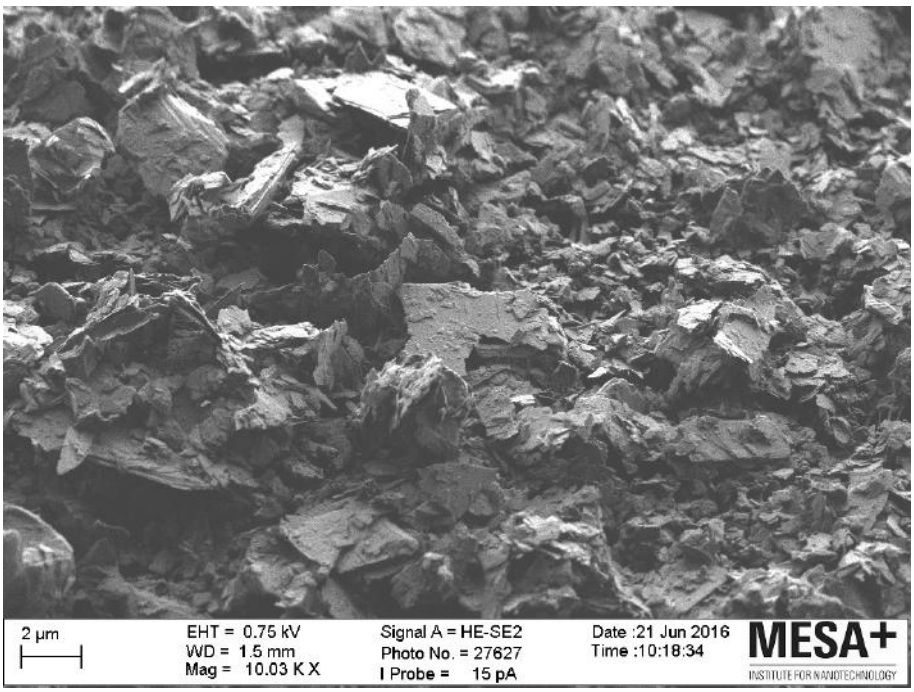

Figure A.14

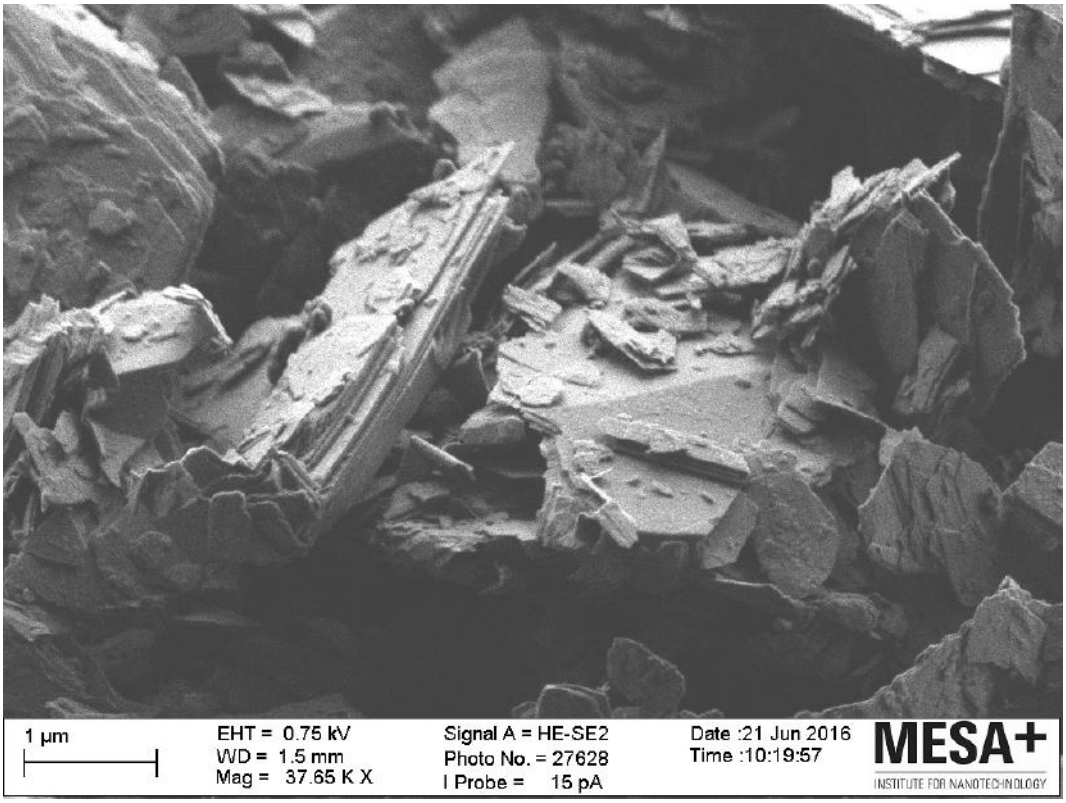

Figure A.15

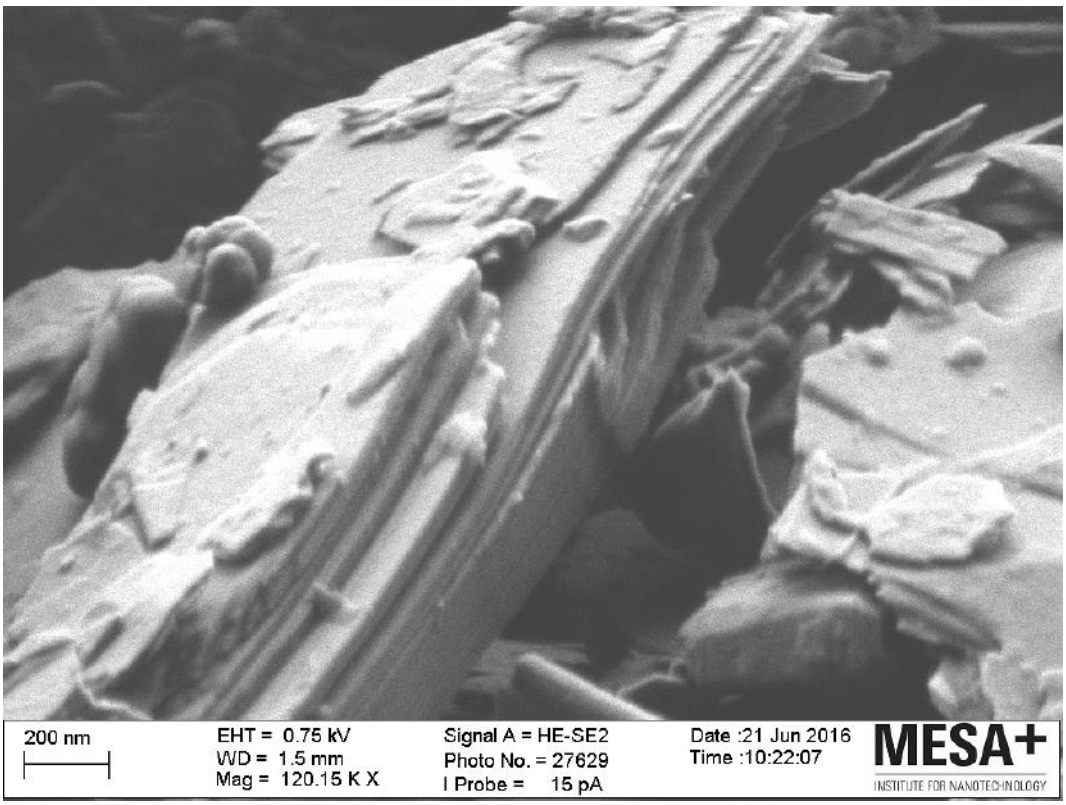

Figure A.16

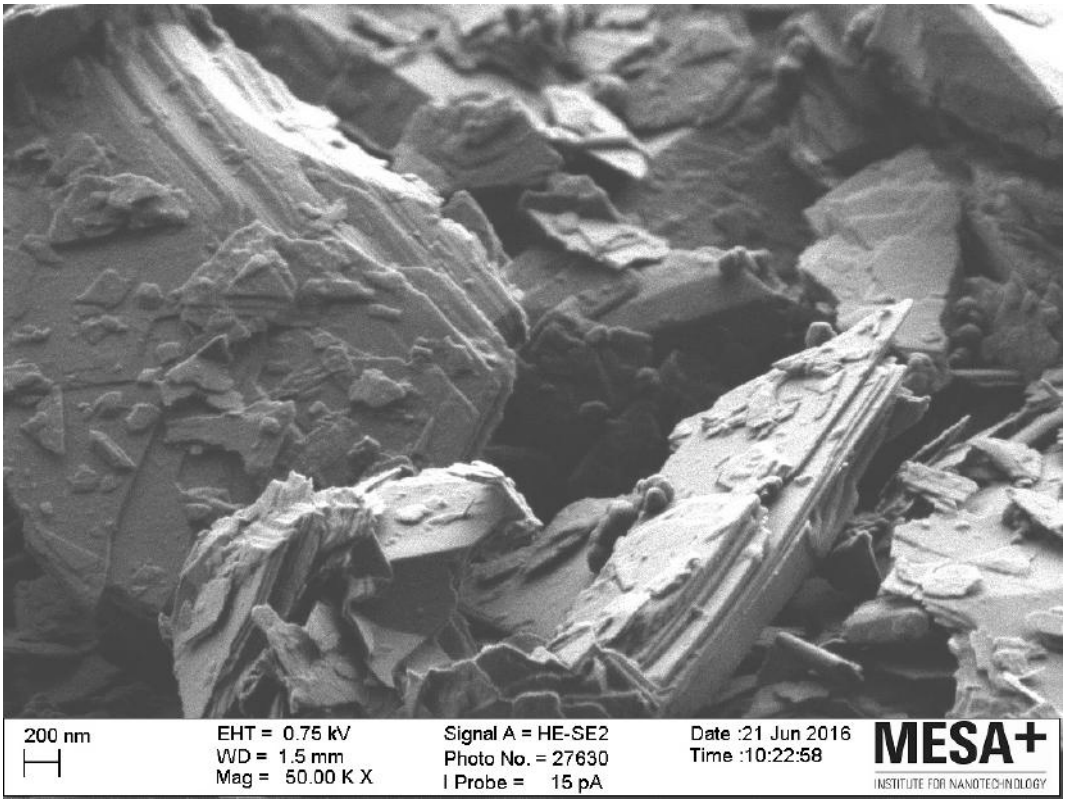

Figure A.17

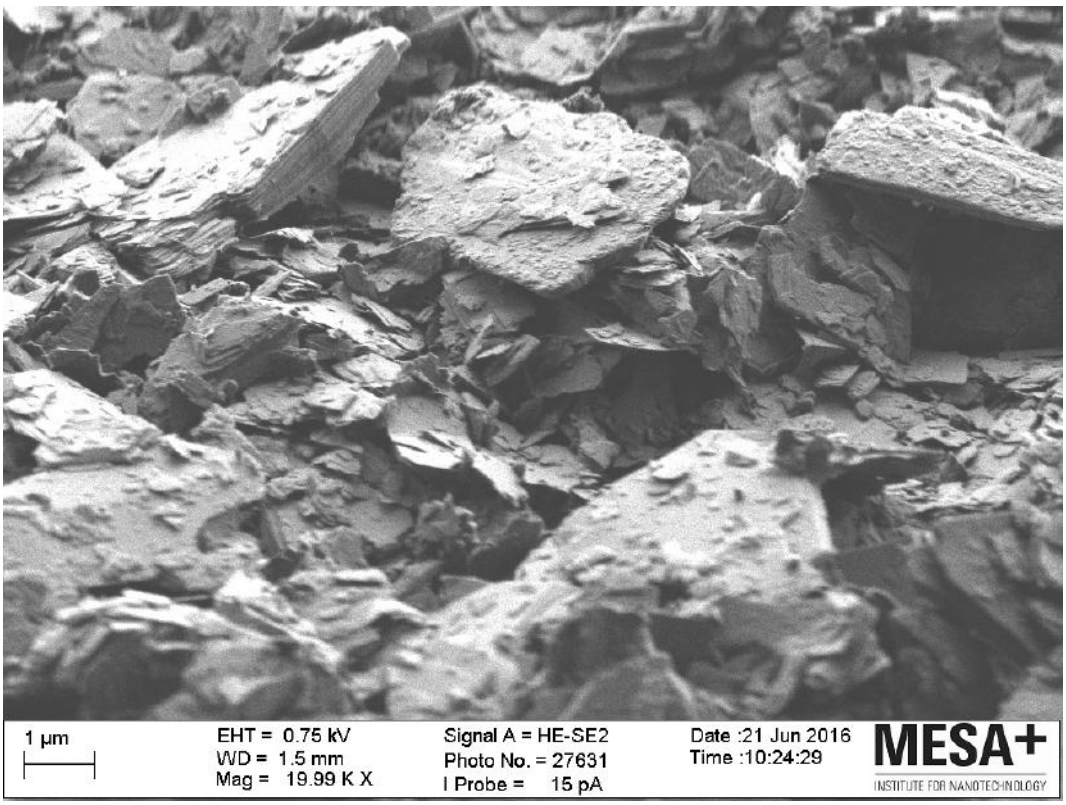

Figure A.18

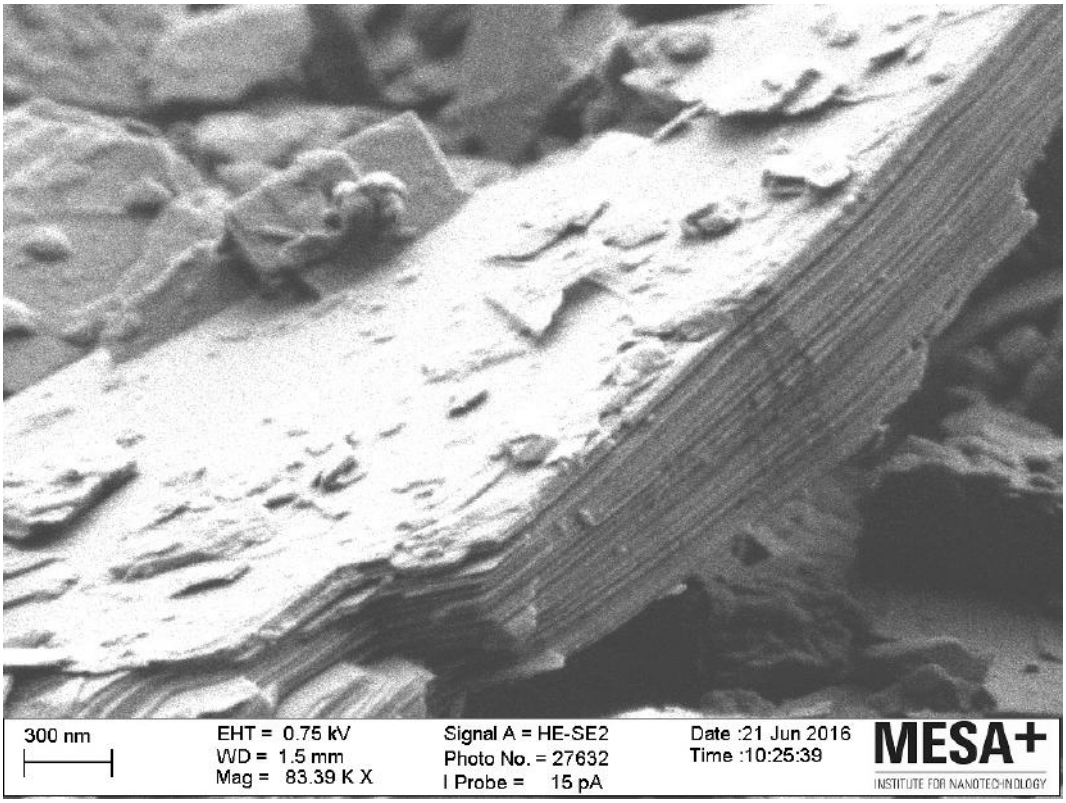

Figure A.19

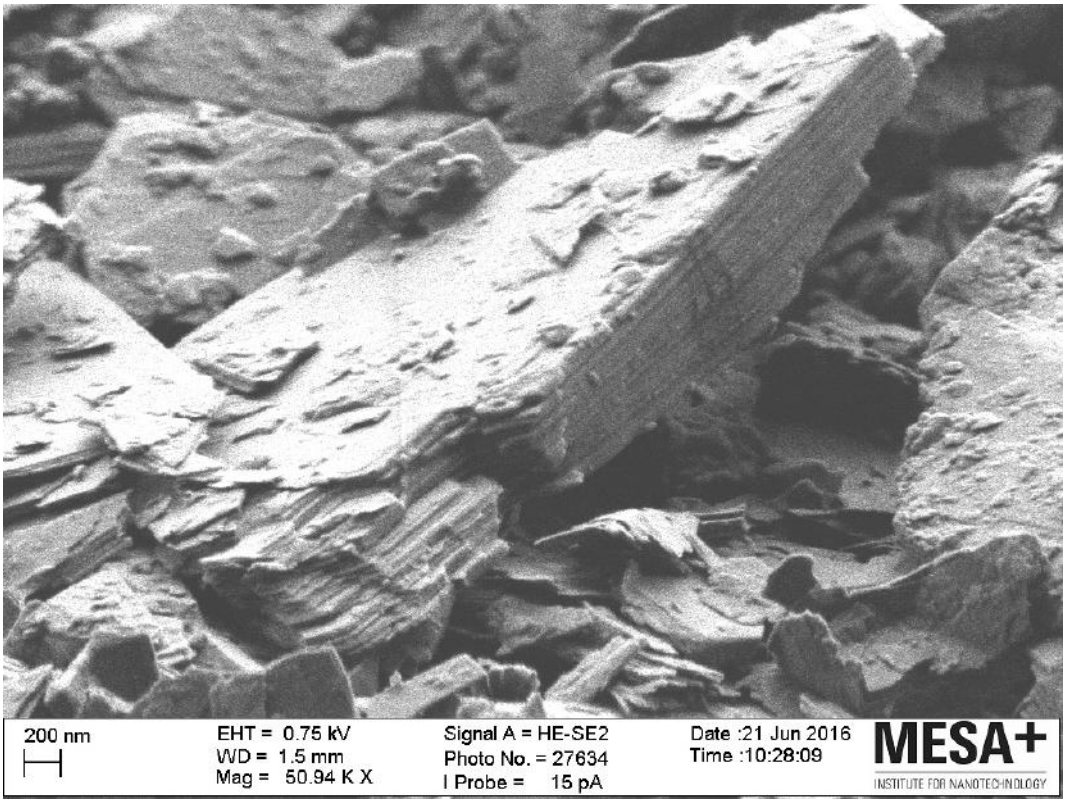

Figure A.20

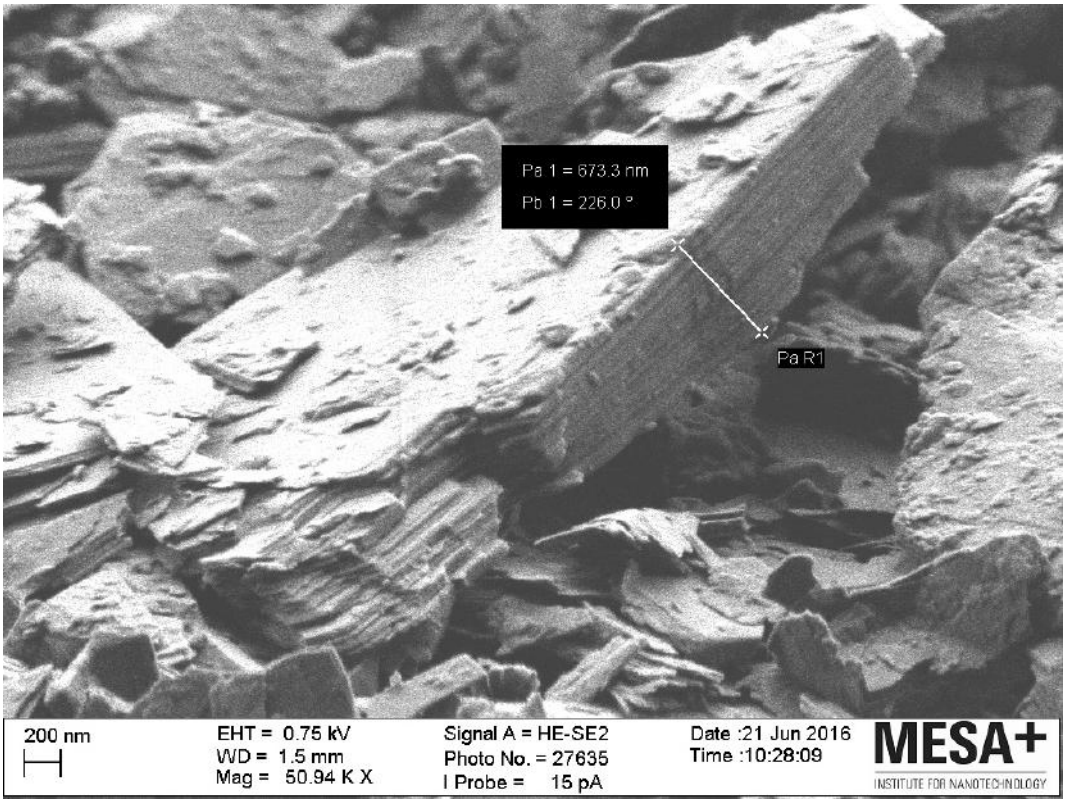

Figure A.21

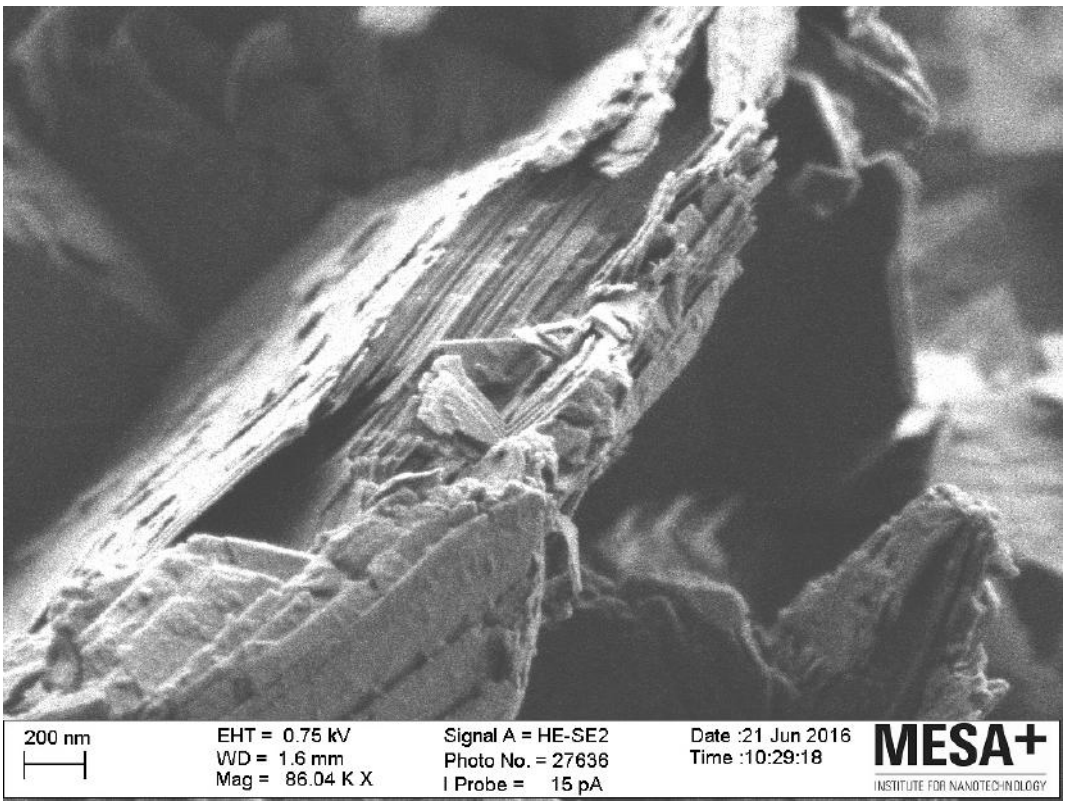

Figure A.22

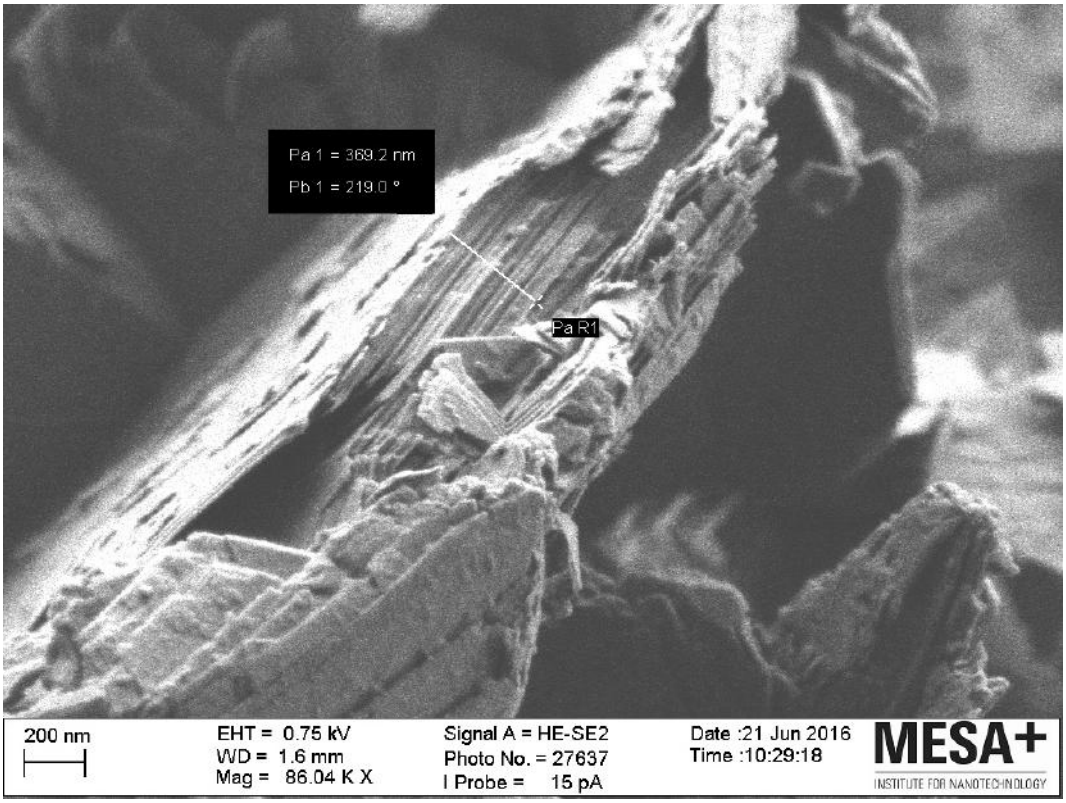

Figure A.23

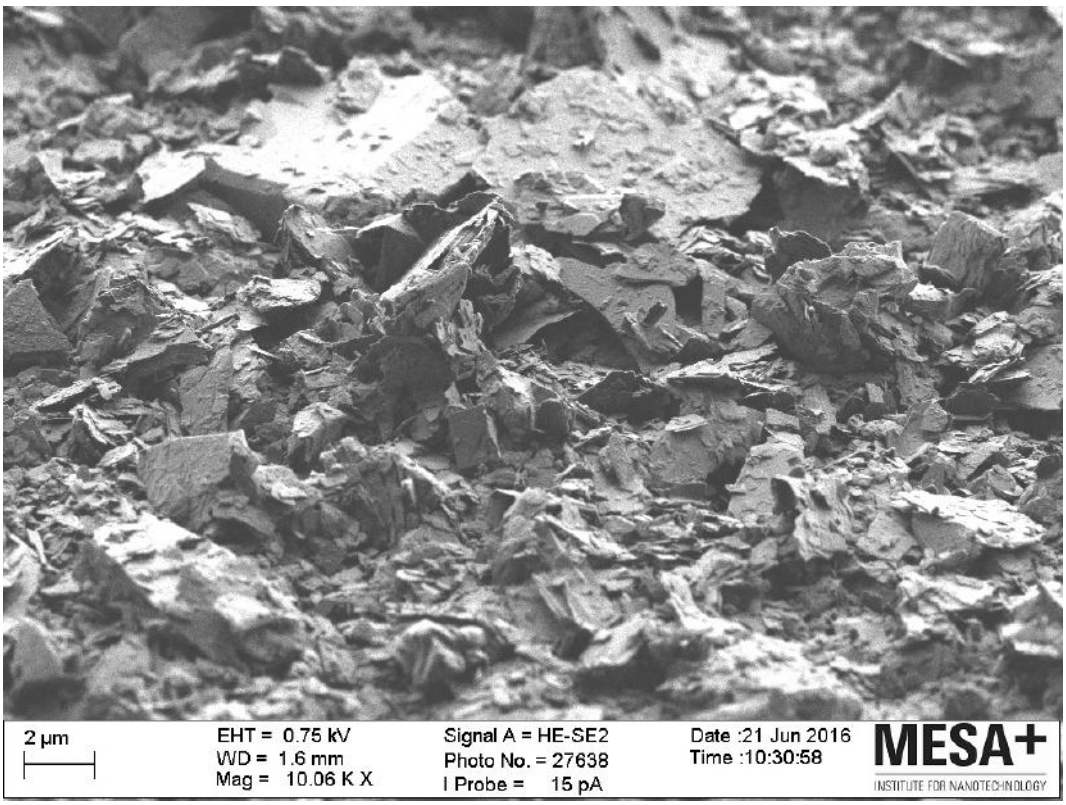

Figure A.24

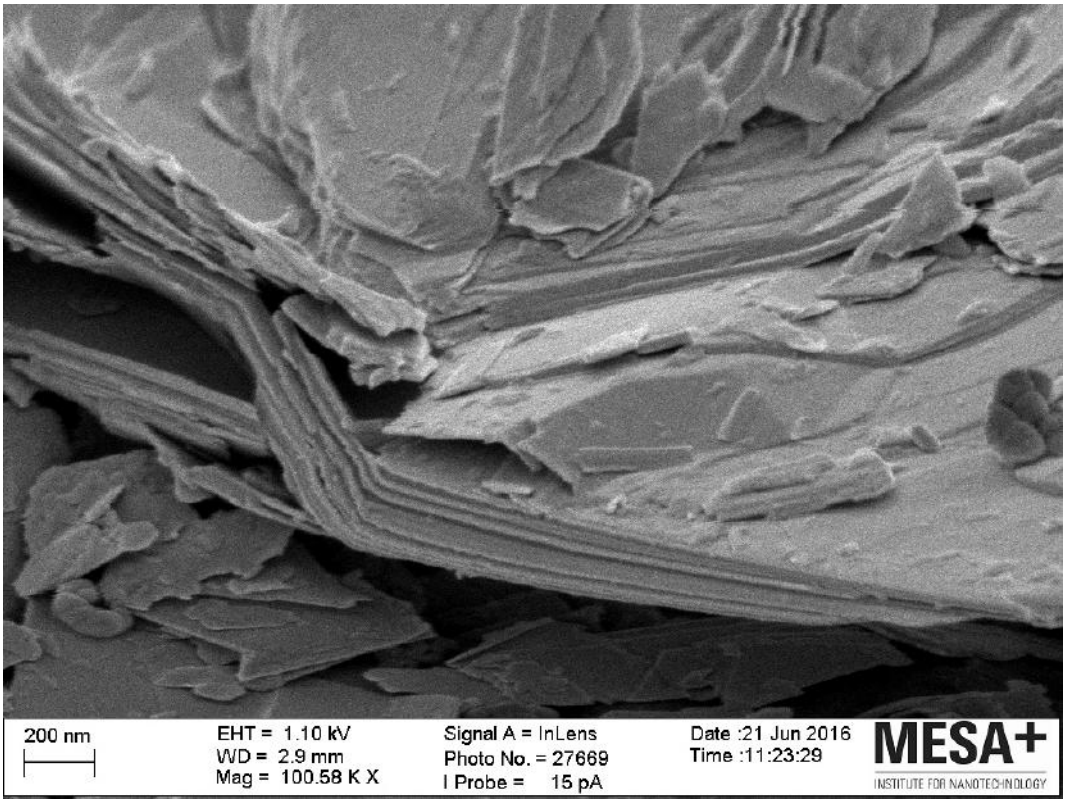

Figure A.25

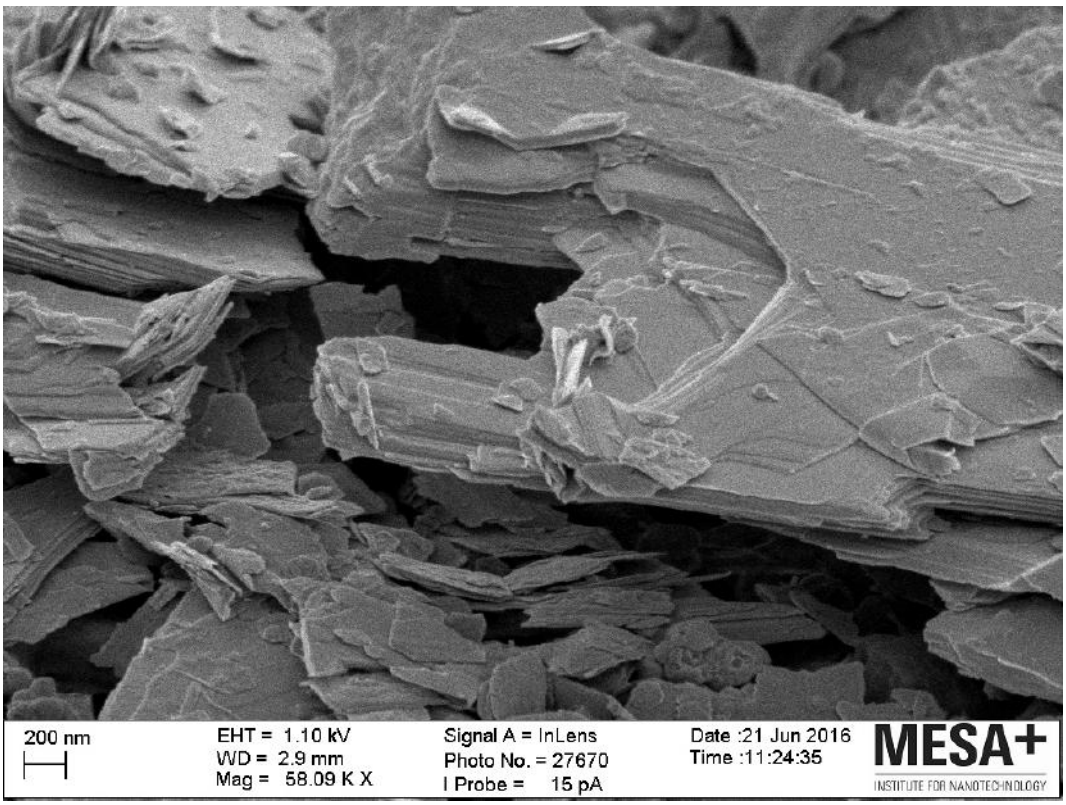

Figure A.26

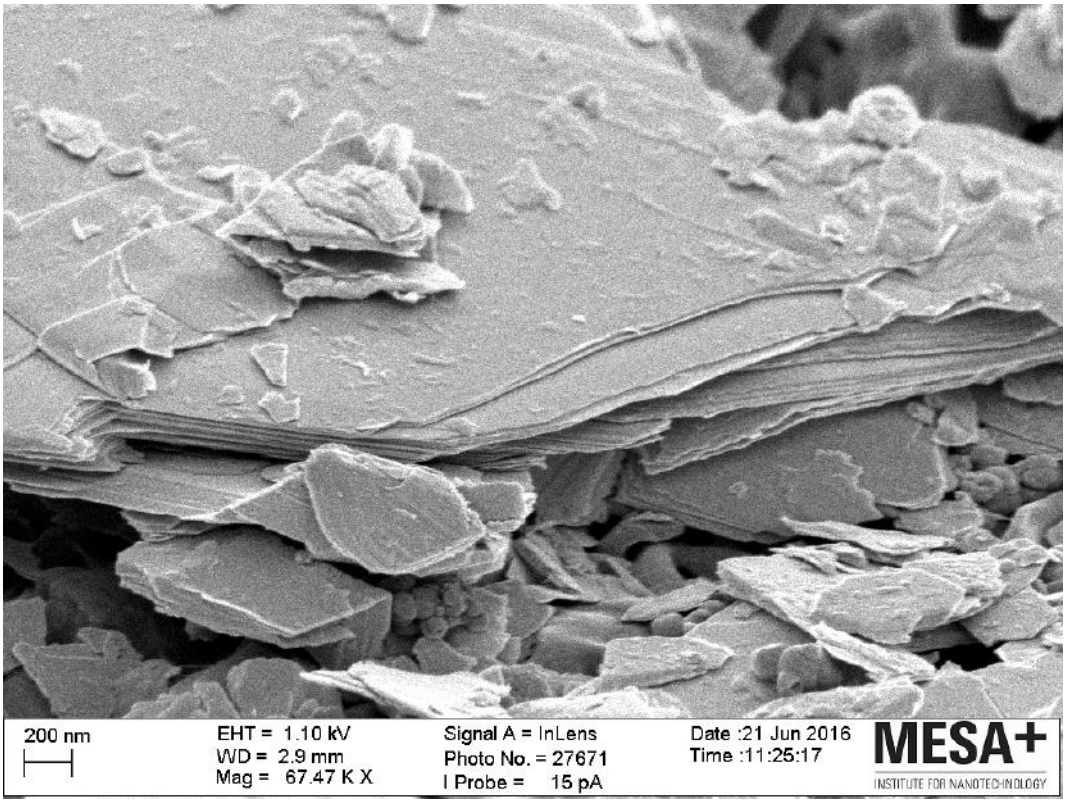

Figure A.27

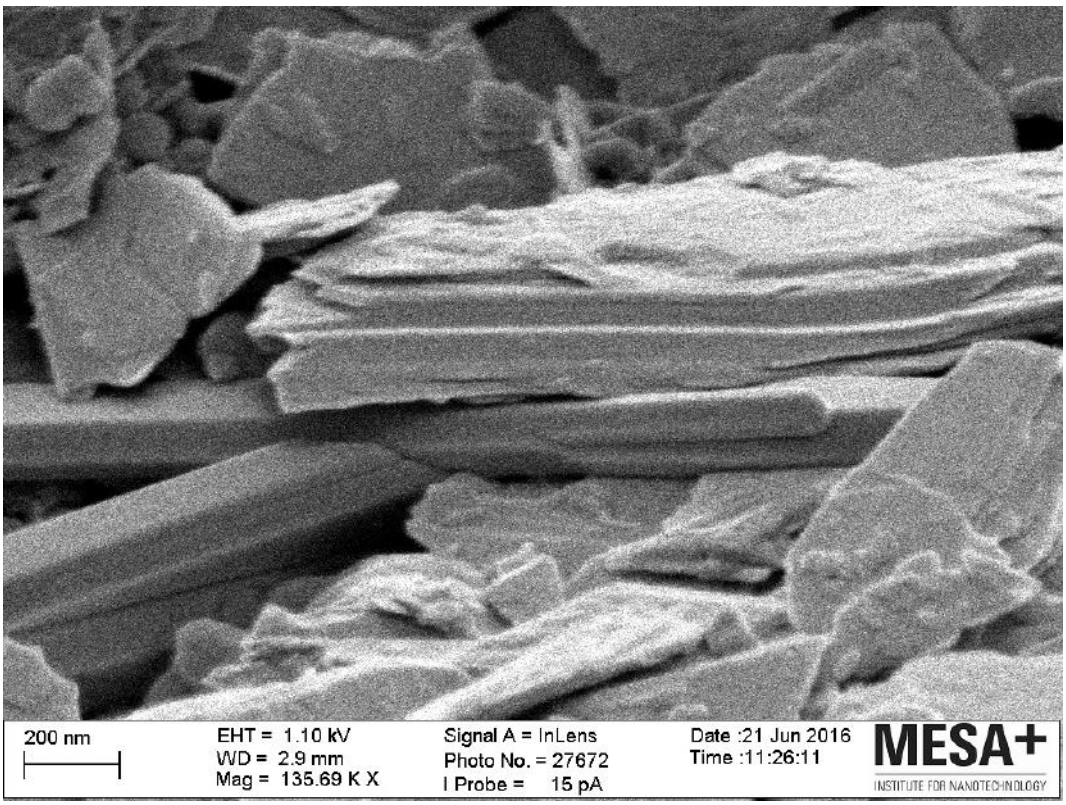

Figure A.28

A.1.3 BBP

Absorption Spectra

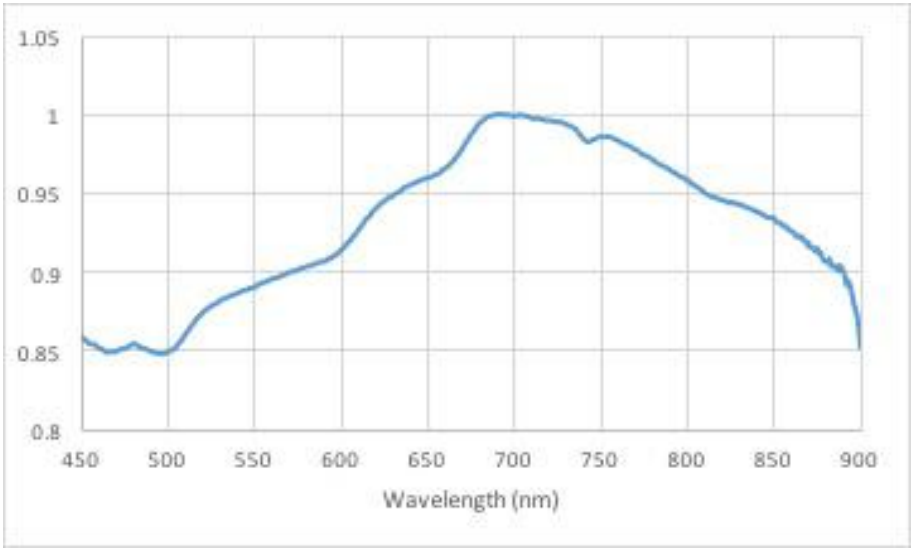

Figure A.29: Normalised absorption spectra for a maximum absorption intensity of 0,969 at the wavelength of 758 nm.

SEM

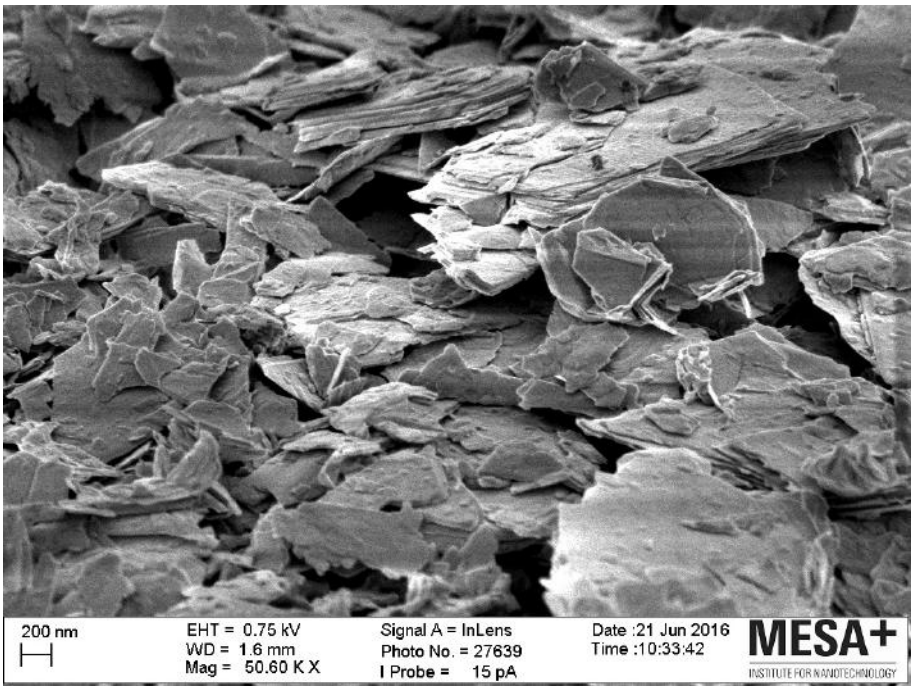

Figure A.30

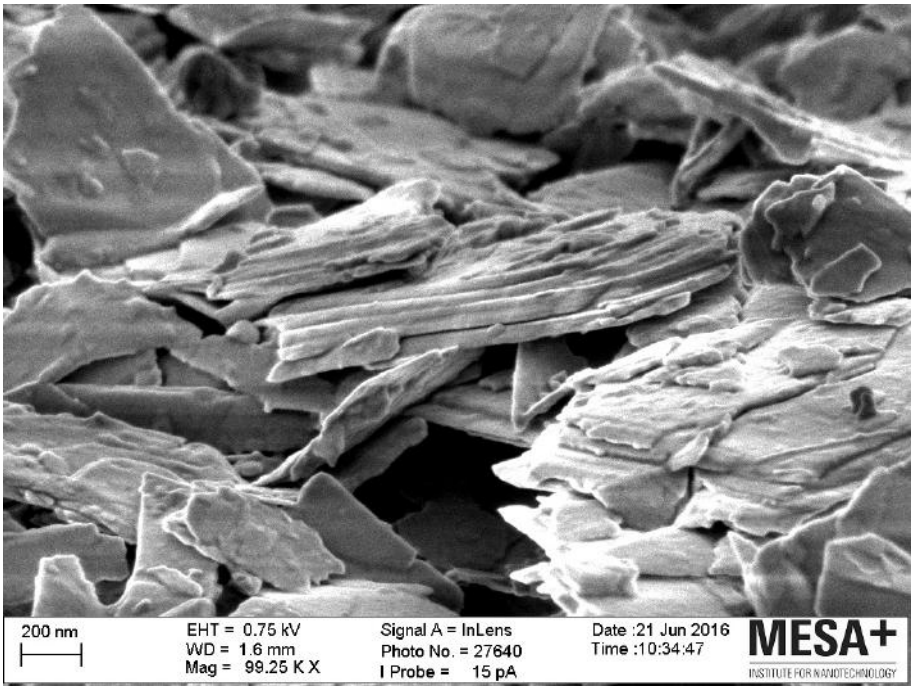

Figure A.31

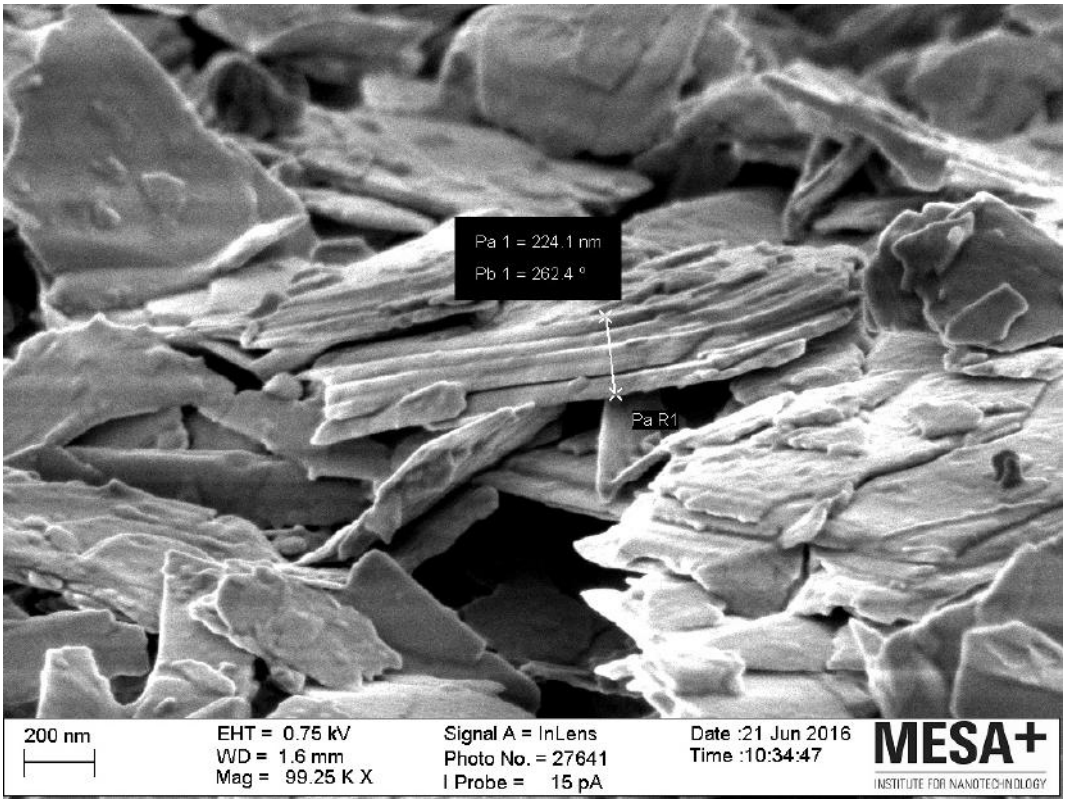

Figure A.32

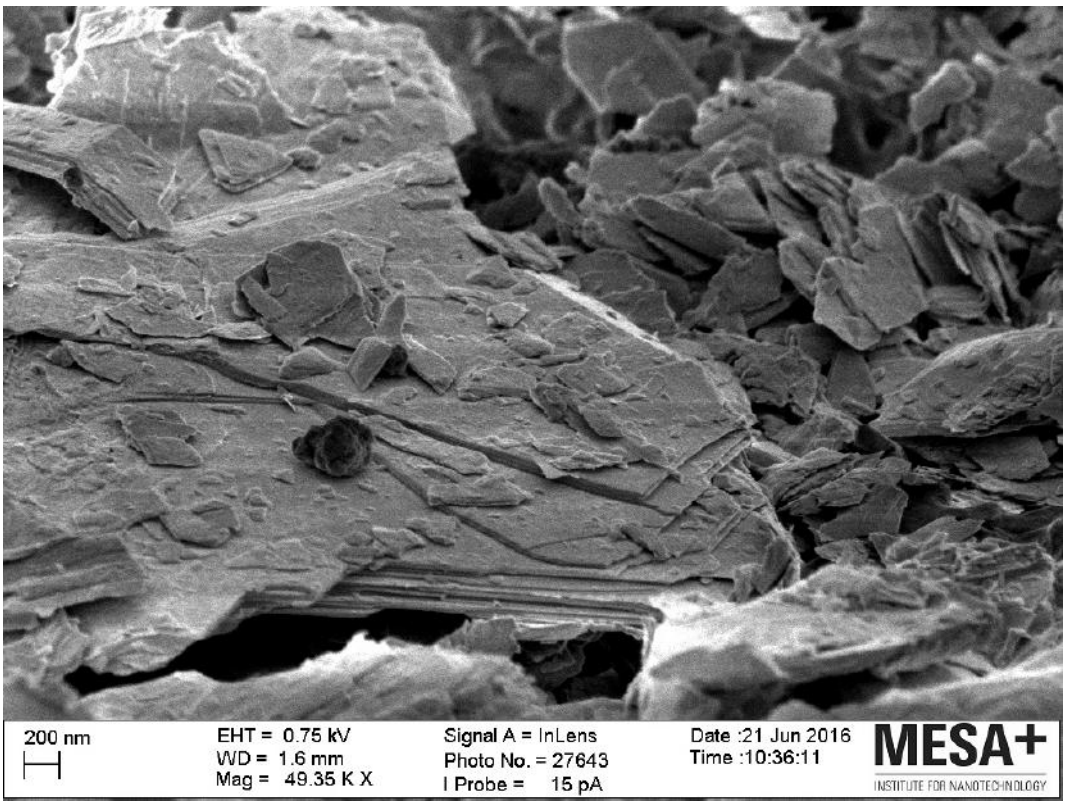

Figure A.33

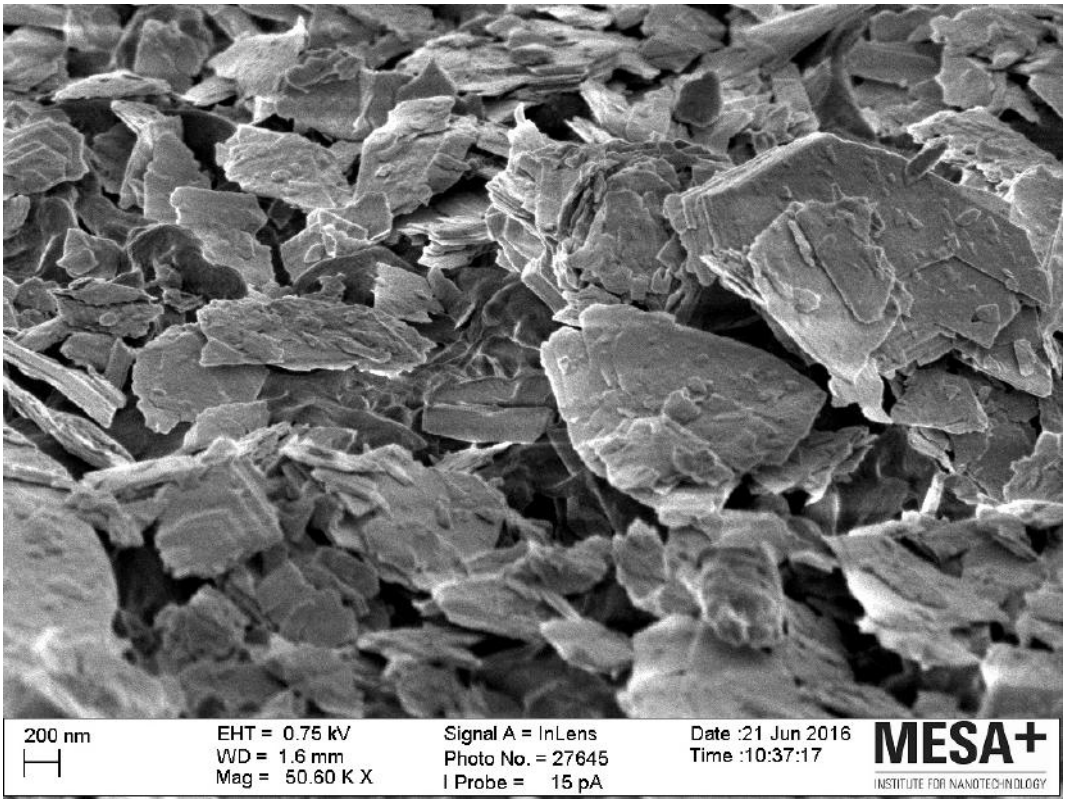

Figure A.34

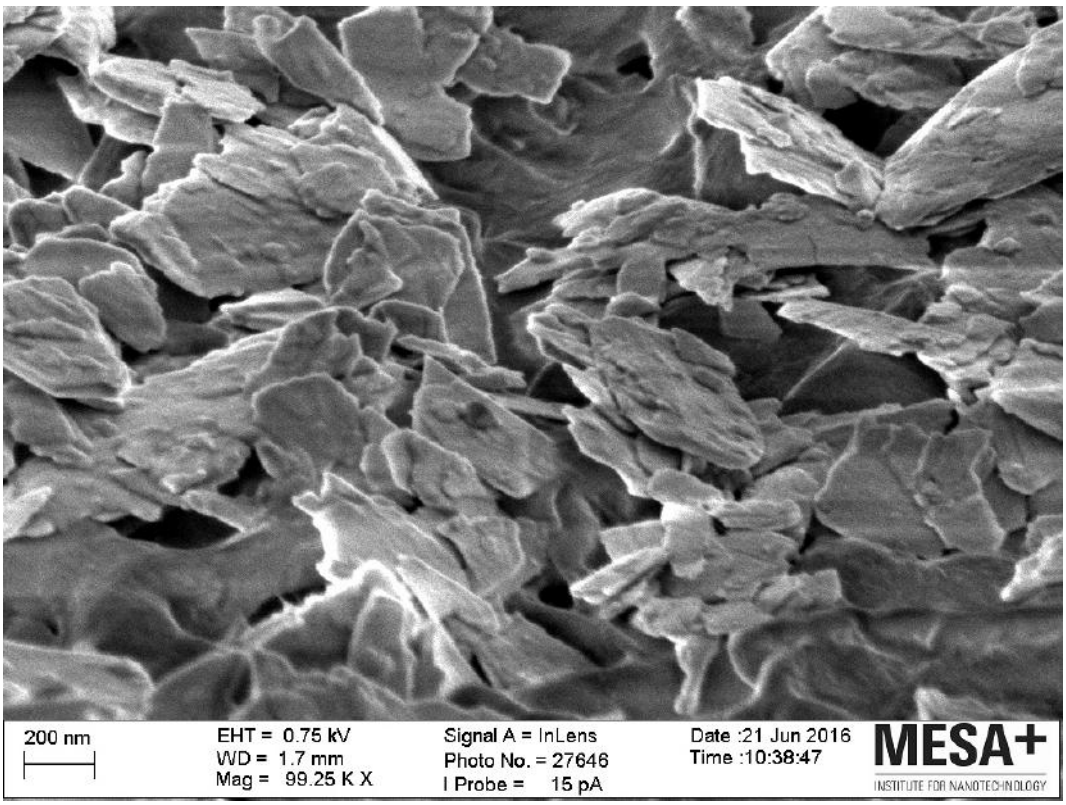

Figure A.35

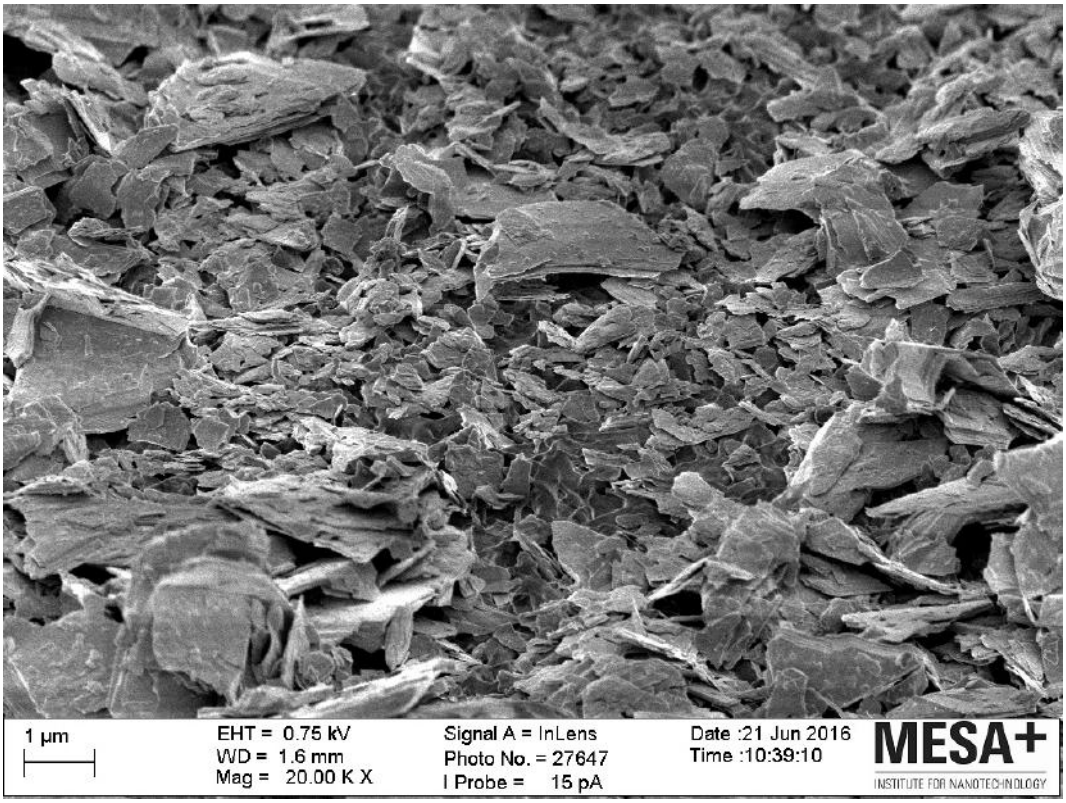

Figure A.36

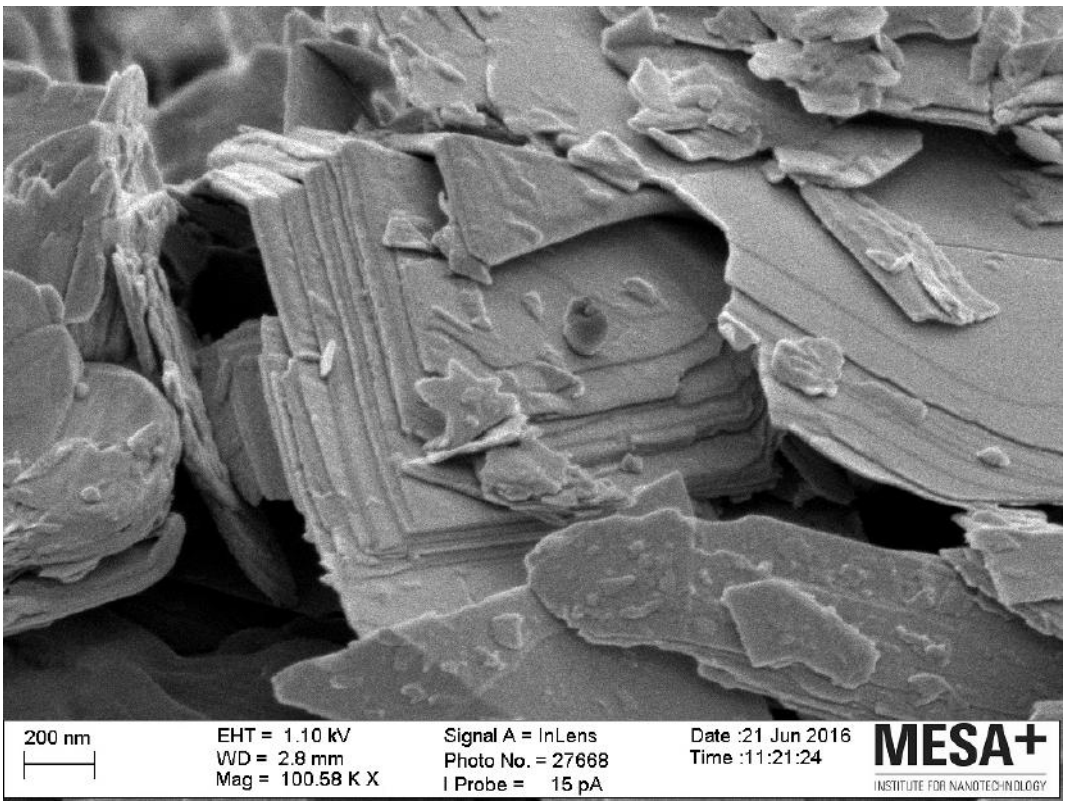

Figure A.37

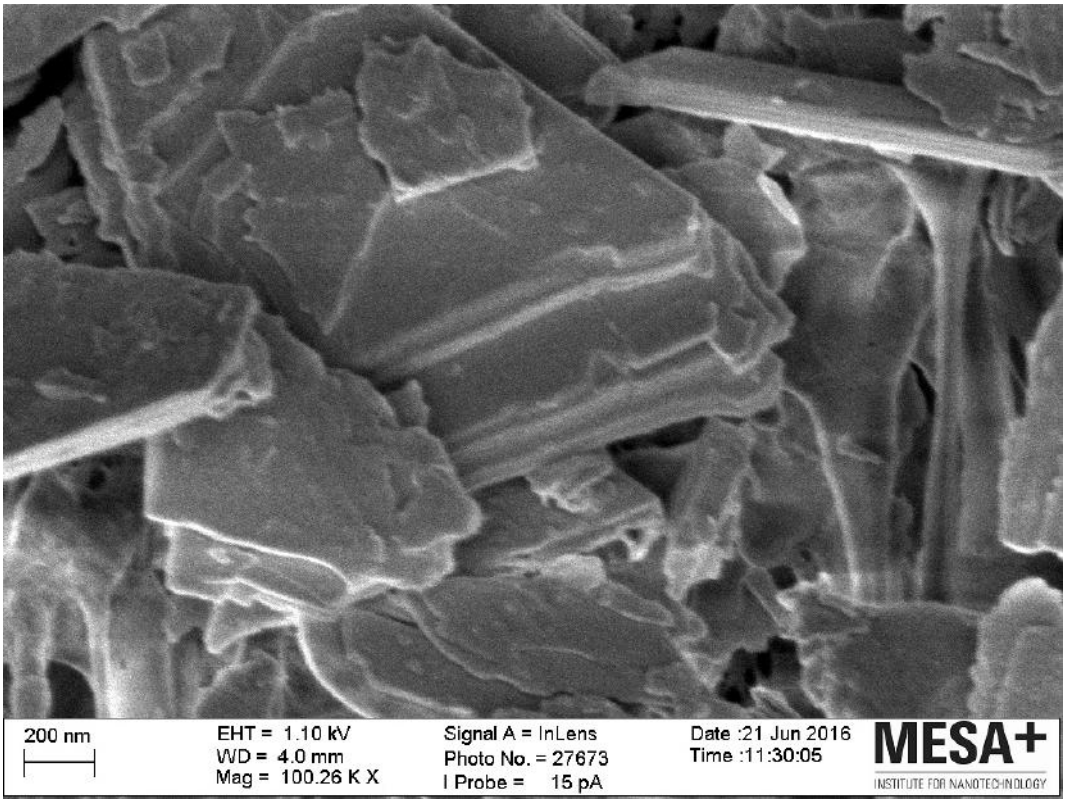

Figure A.38

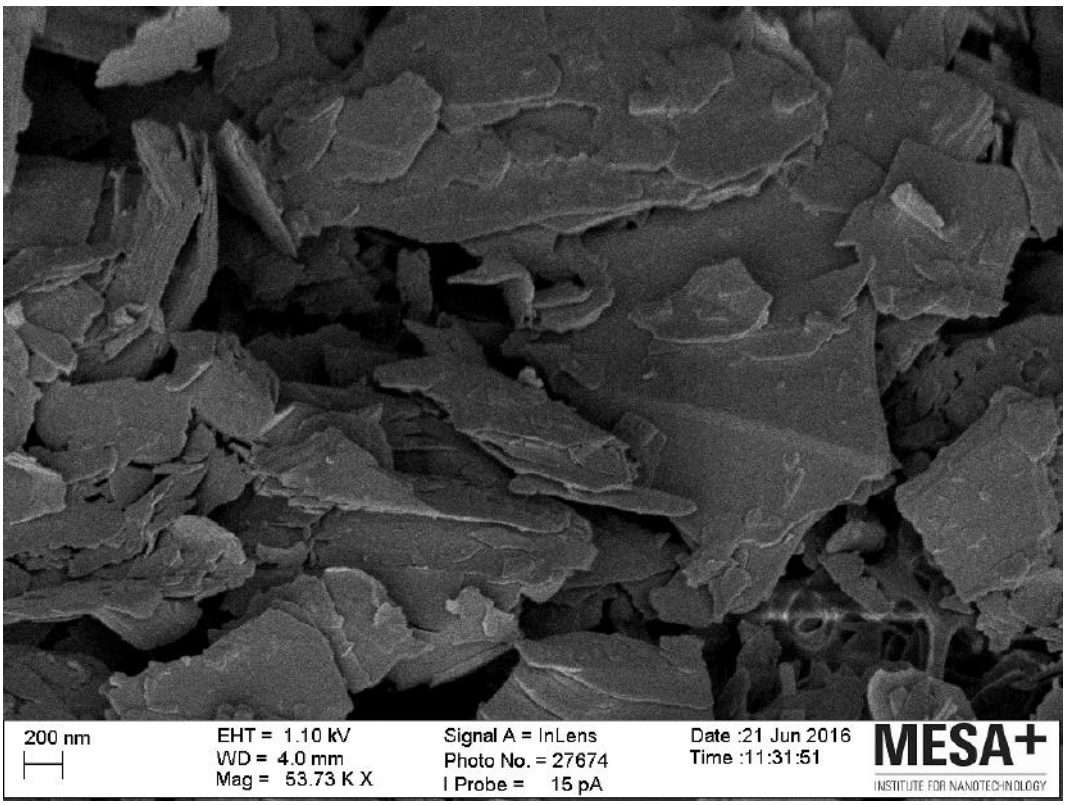

Figure A.39

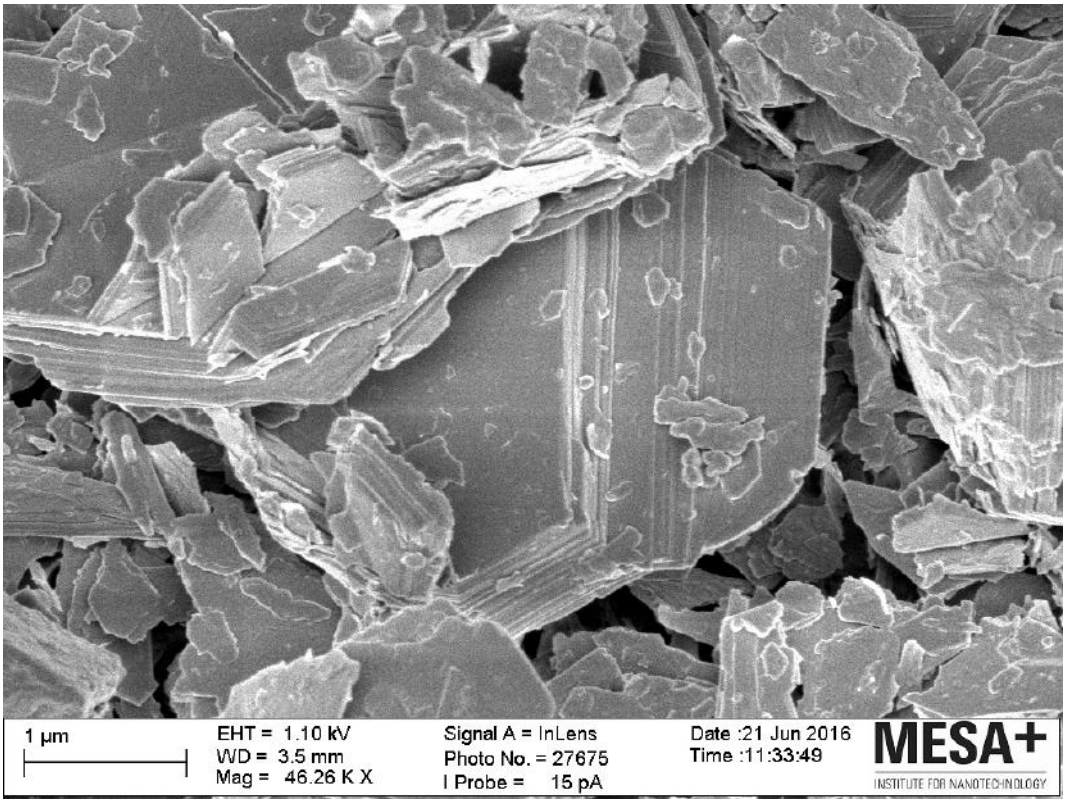

Figure A.40

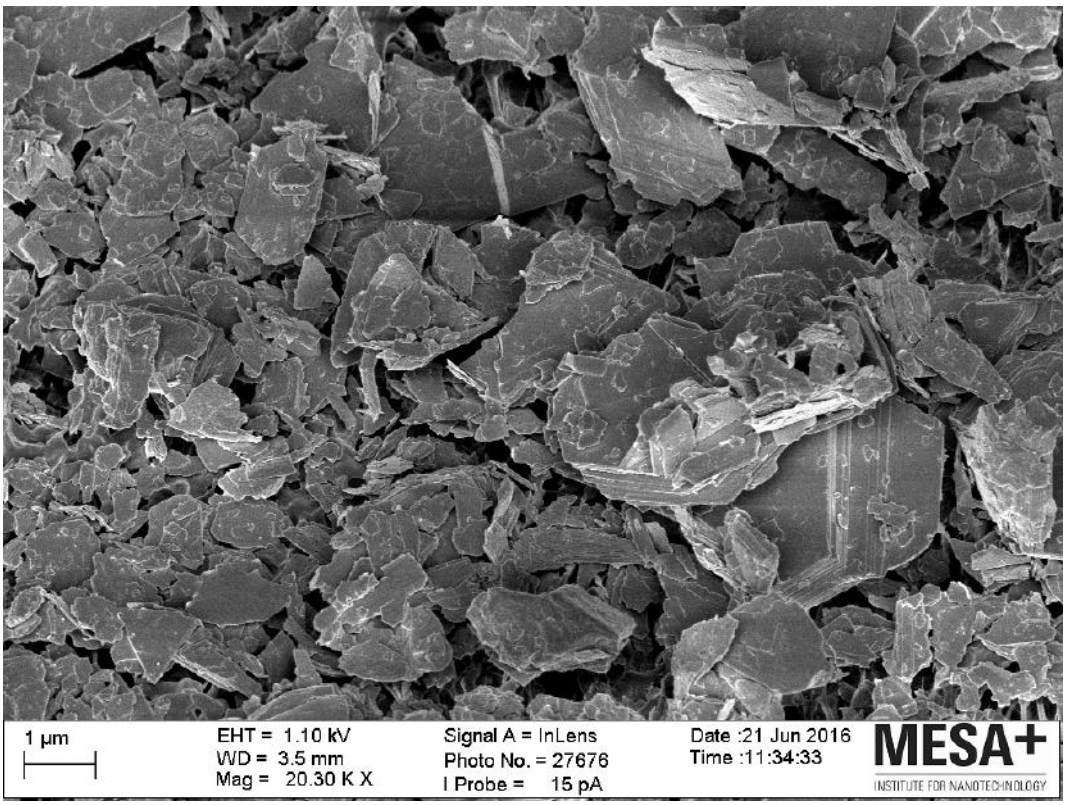

Figure A.41

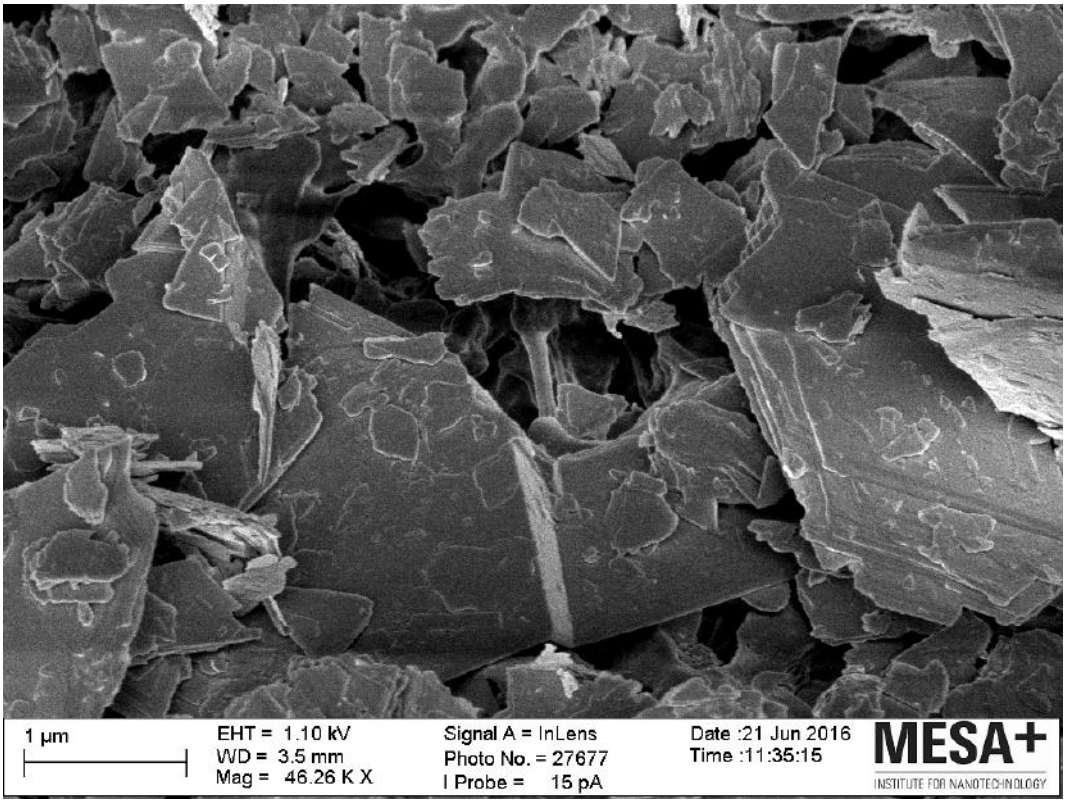

Figure A.42

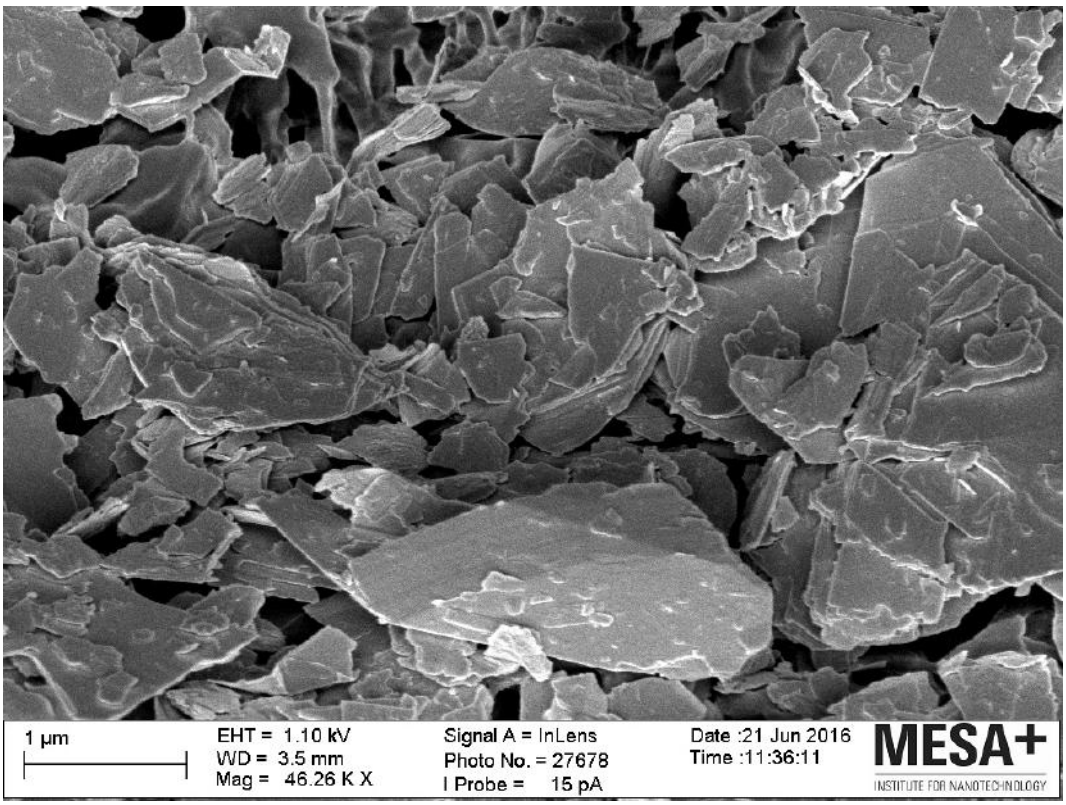

Figure A.43

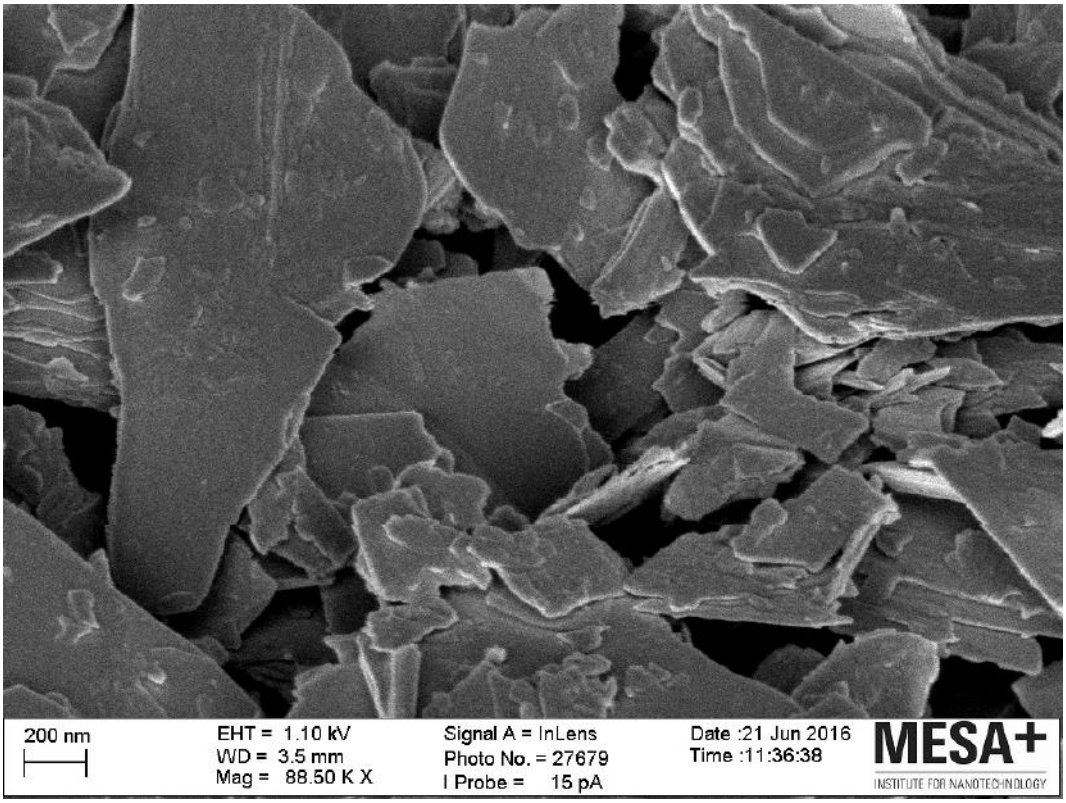

Figure A.44

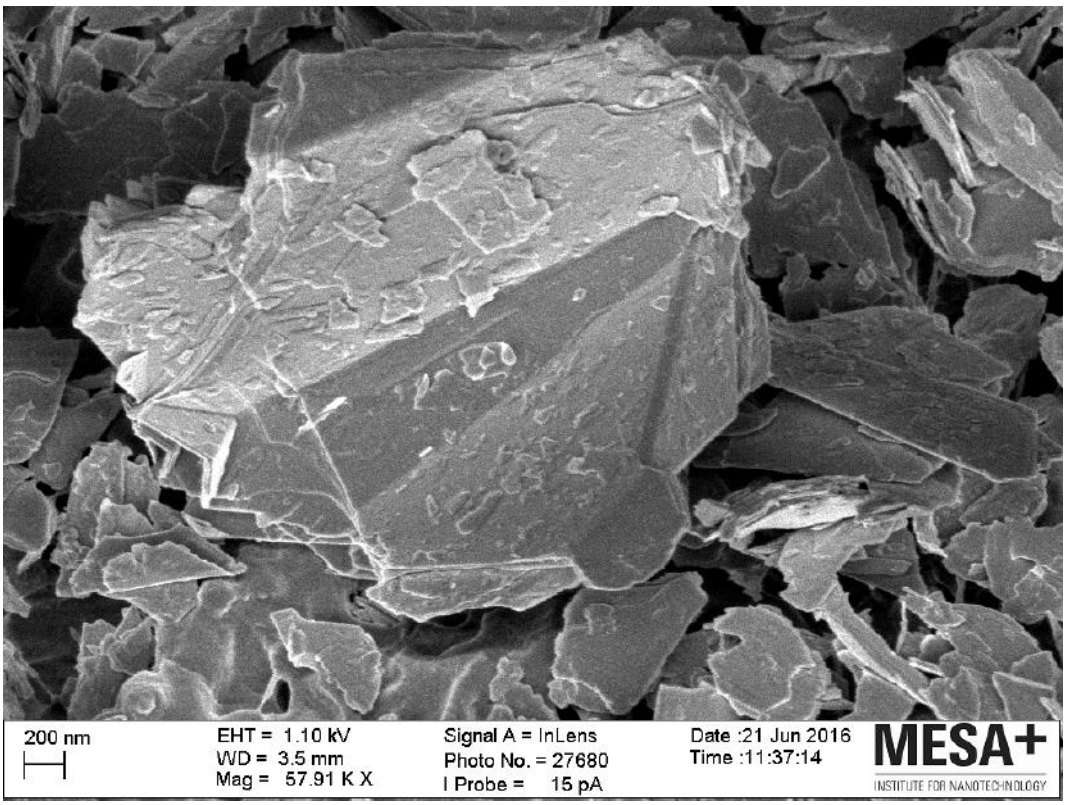

Figure A.45

TEM

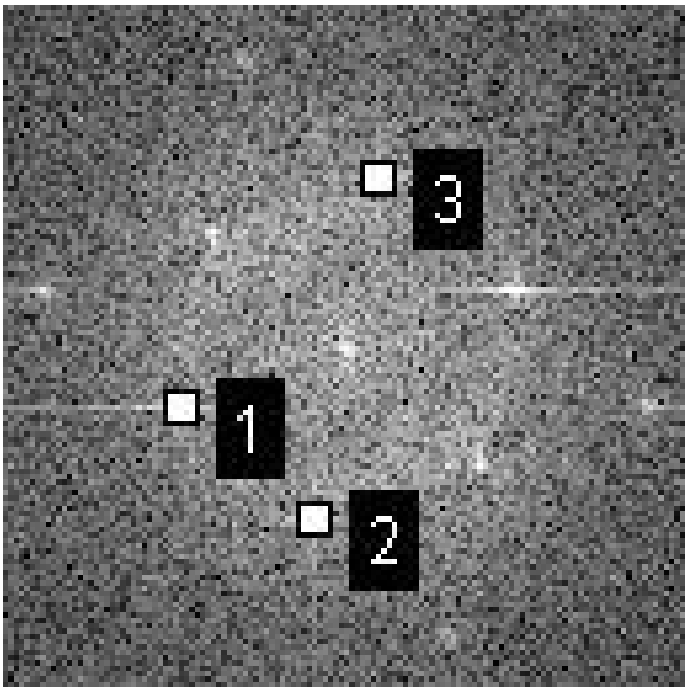

Figure A.46

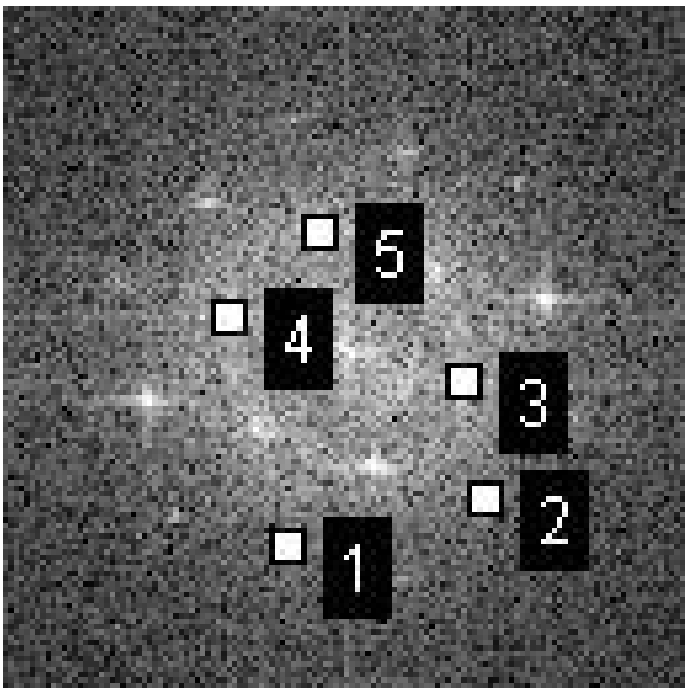

Figure A.47

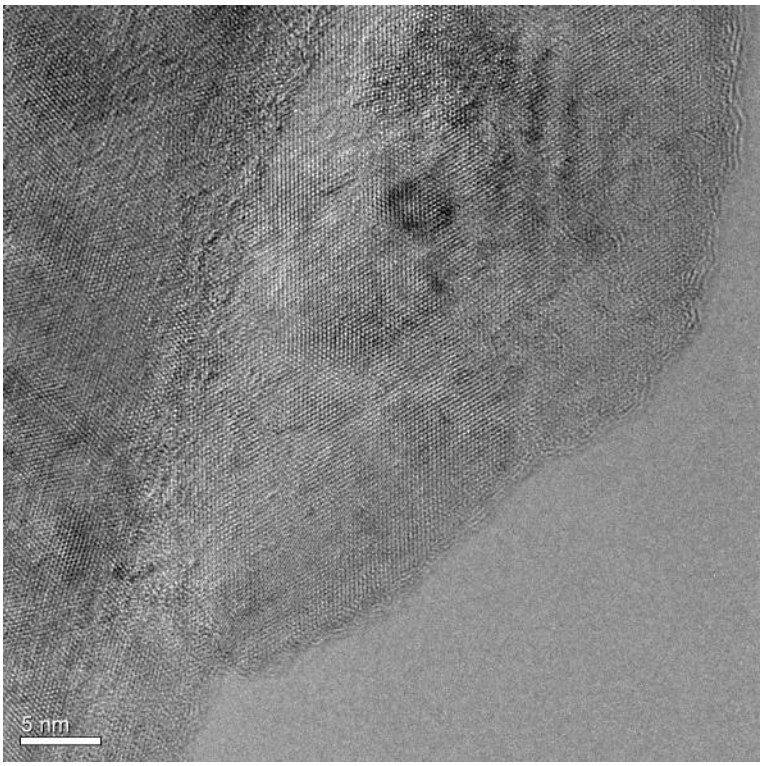

Figure A.48

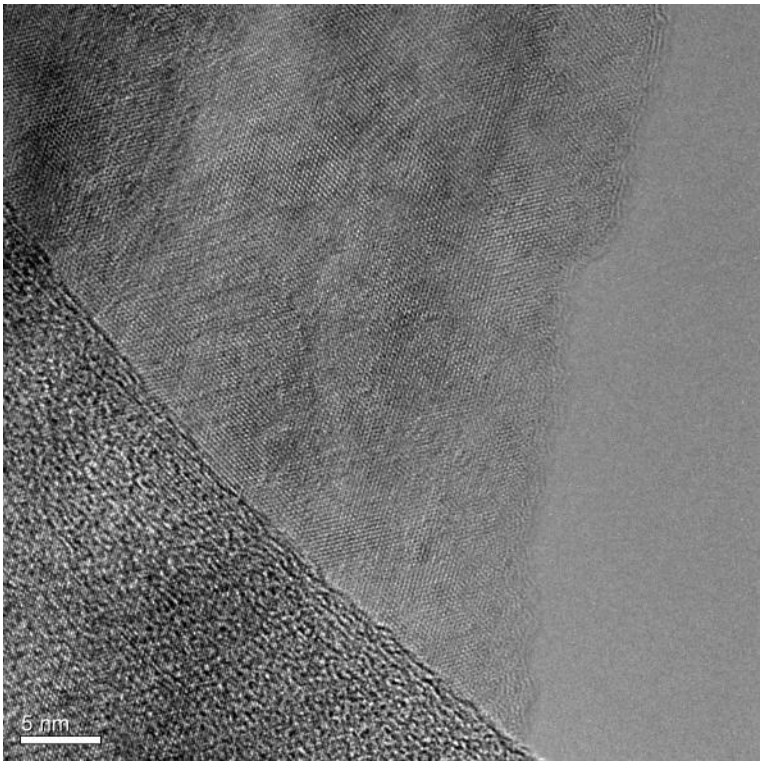

Figure A.49

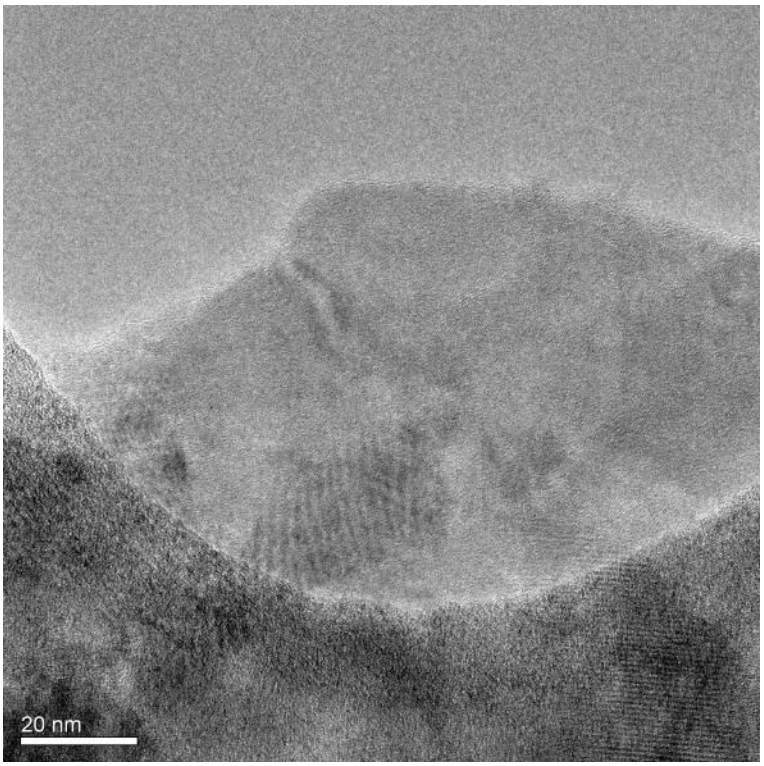

Figure A.50

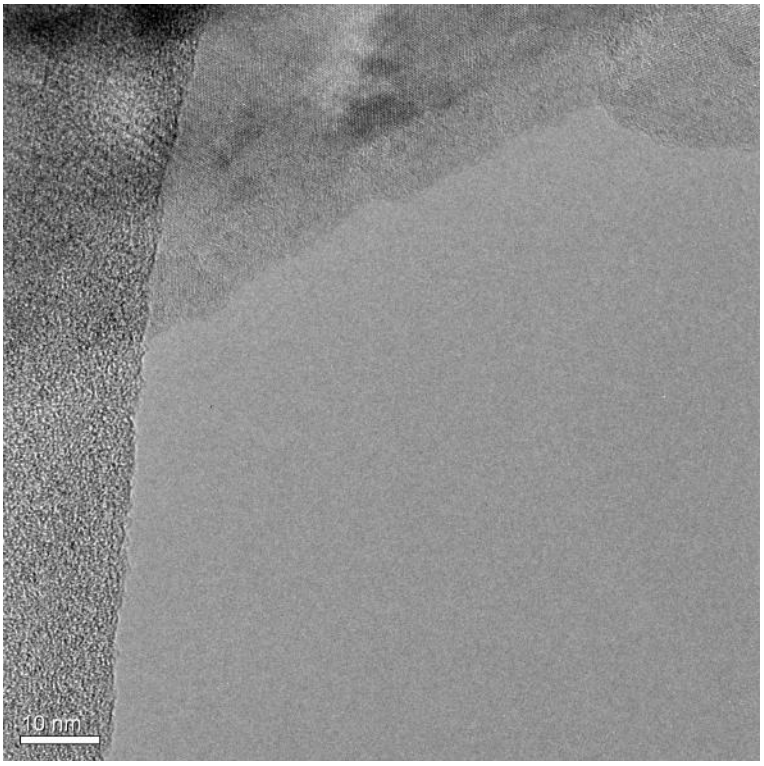

Figure A.51

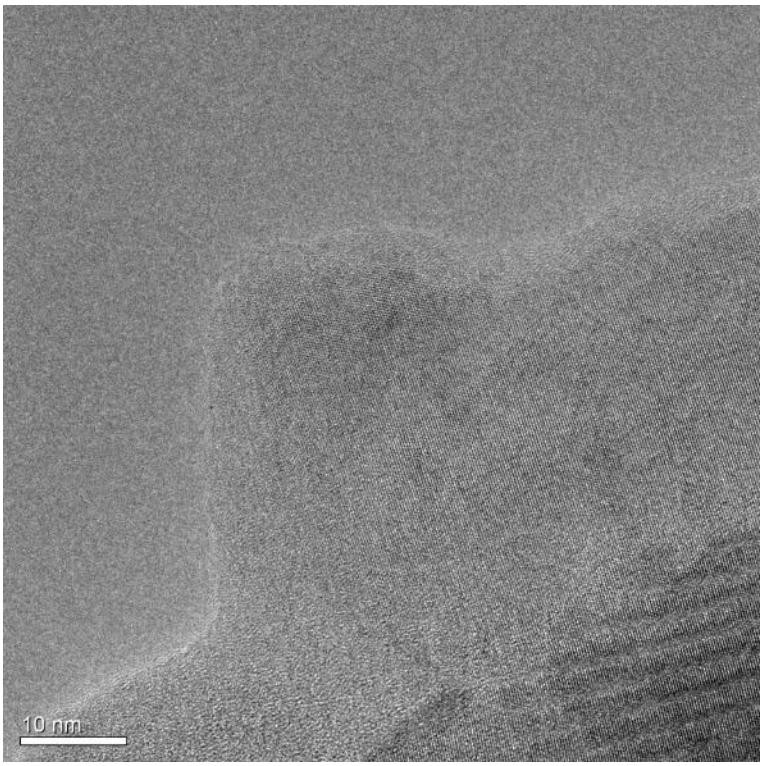

Figure A.52

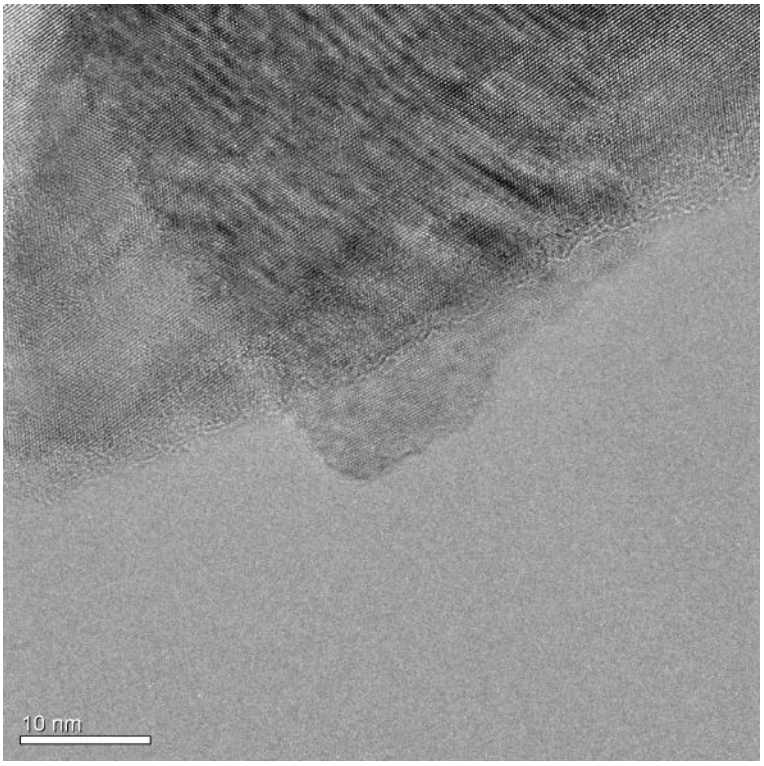

Figure A.53

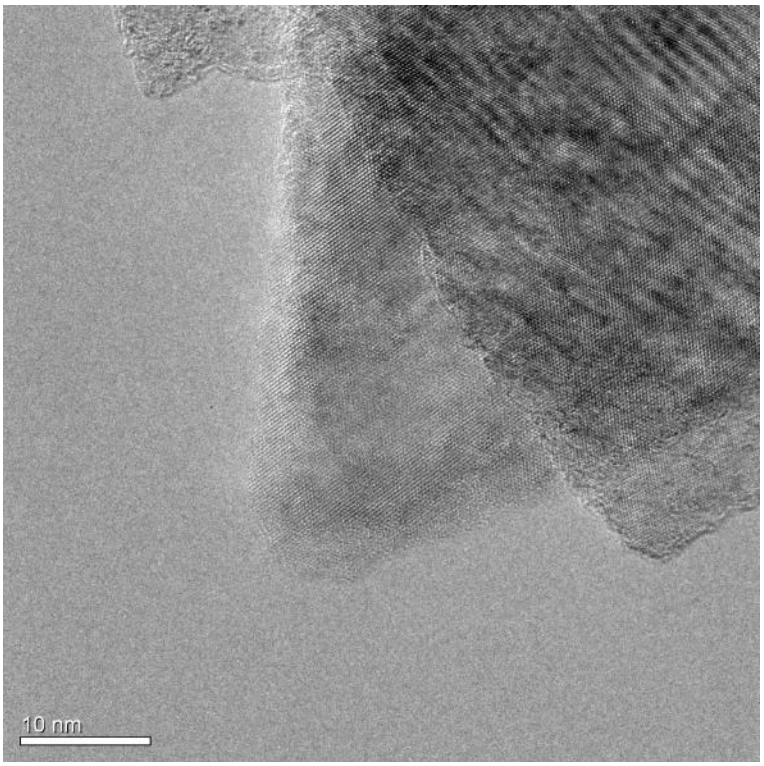

Figure A.54

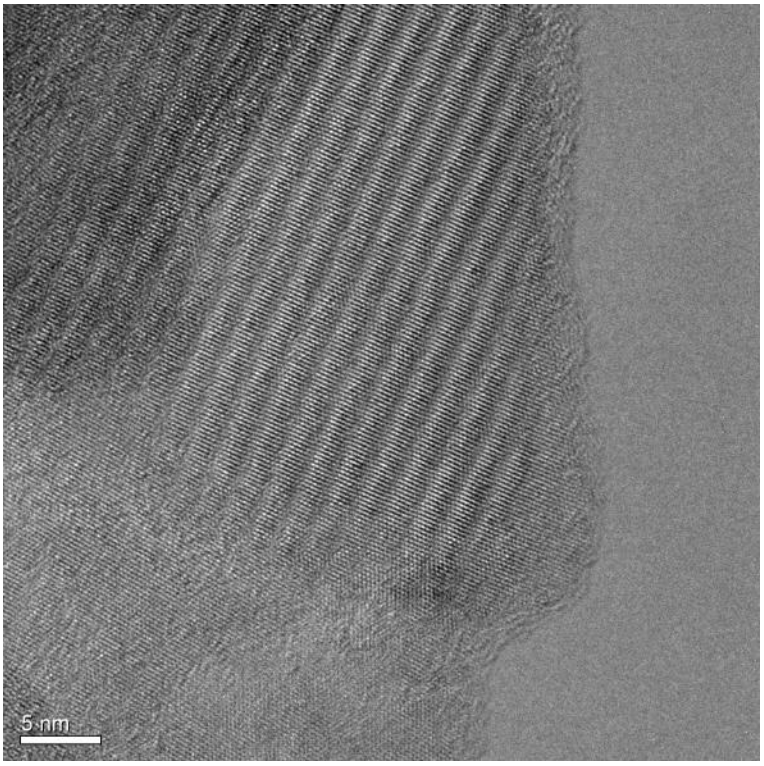

Figure A.55

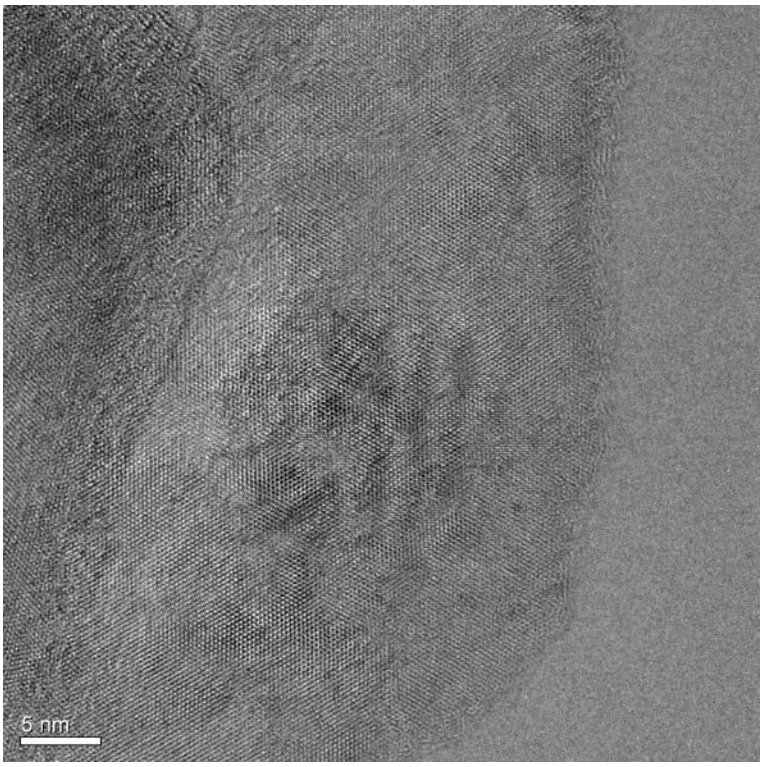

Figure A.56

A.1.4 BHNP

Absorption Spectra

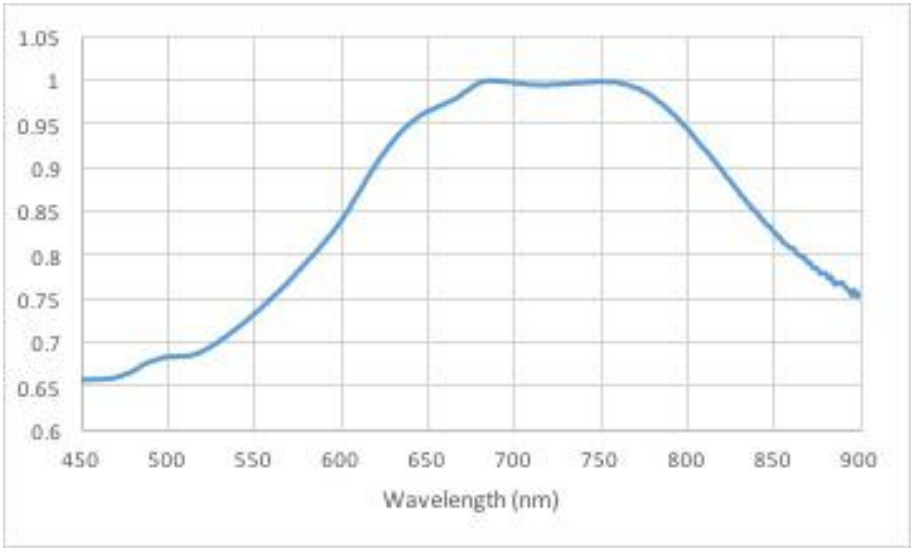

Figure A.57: Normalised absorption spectra for a maximum absorption intensity of 0,278 at the wavelength of 686 nm.

SEM

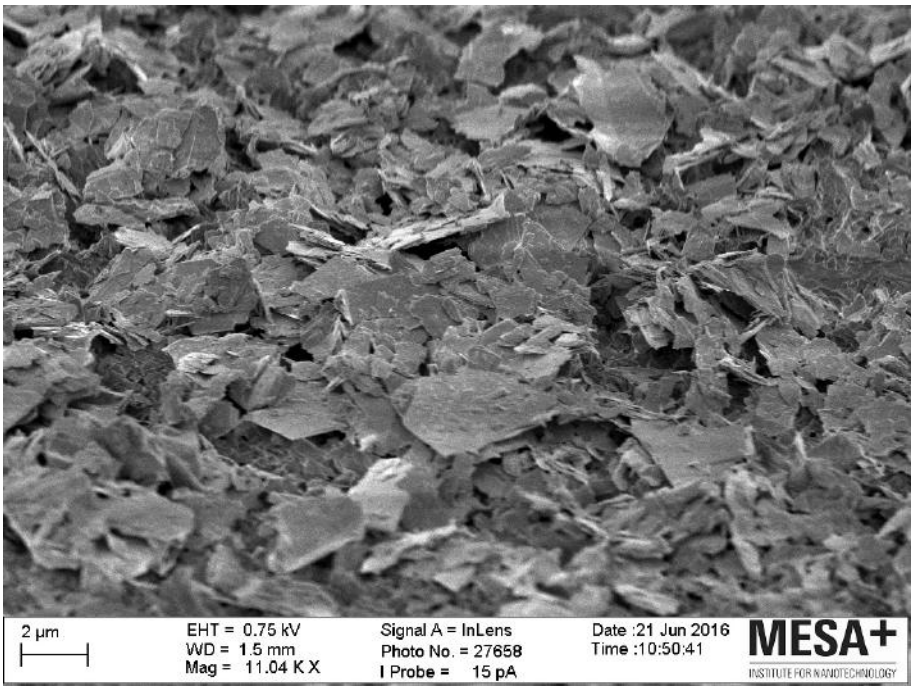

Figure A.58

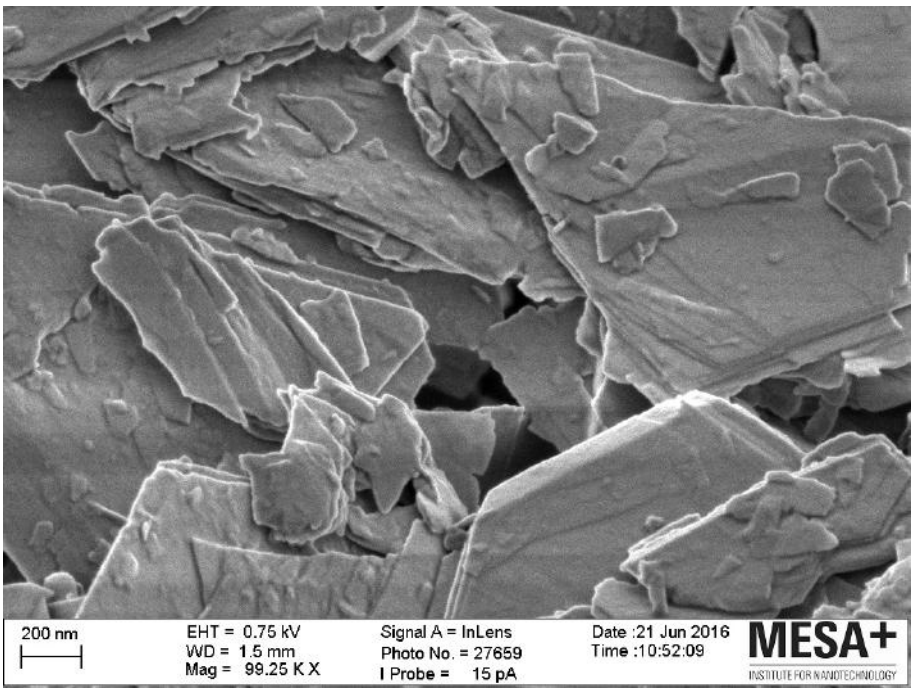

Figure A.59

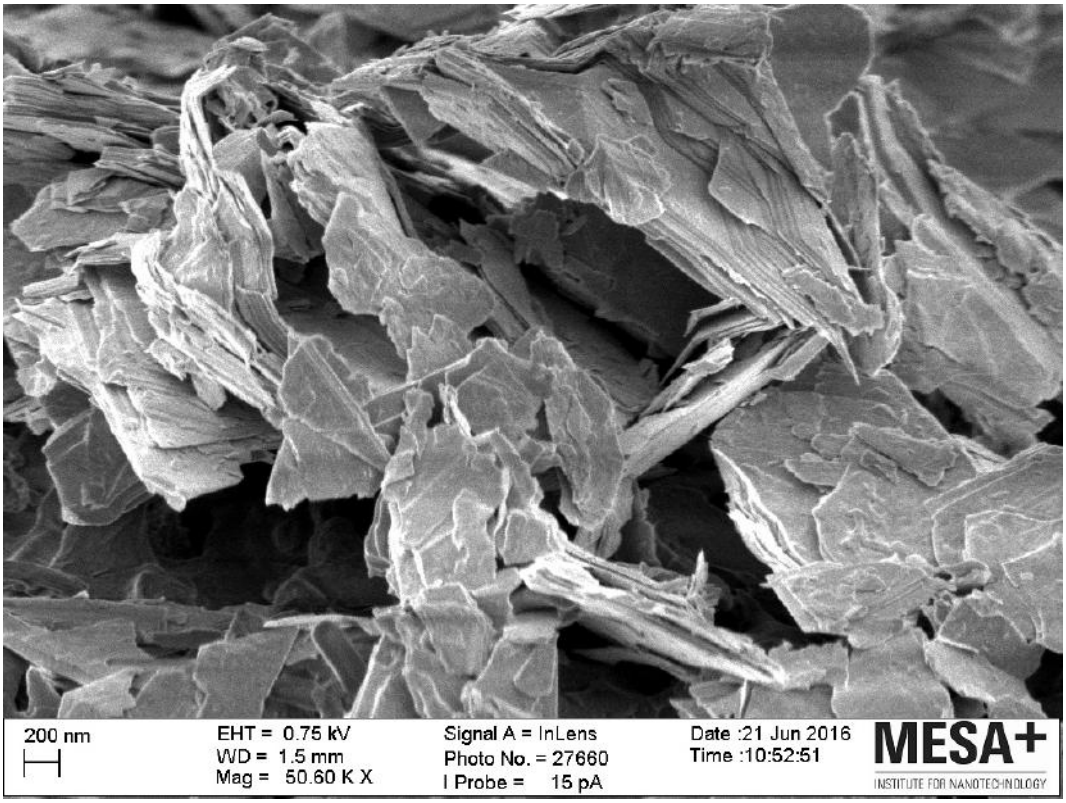

Figure A.60

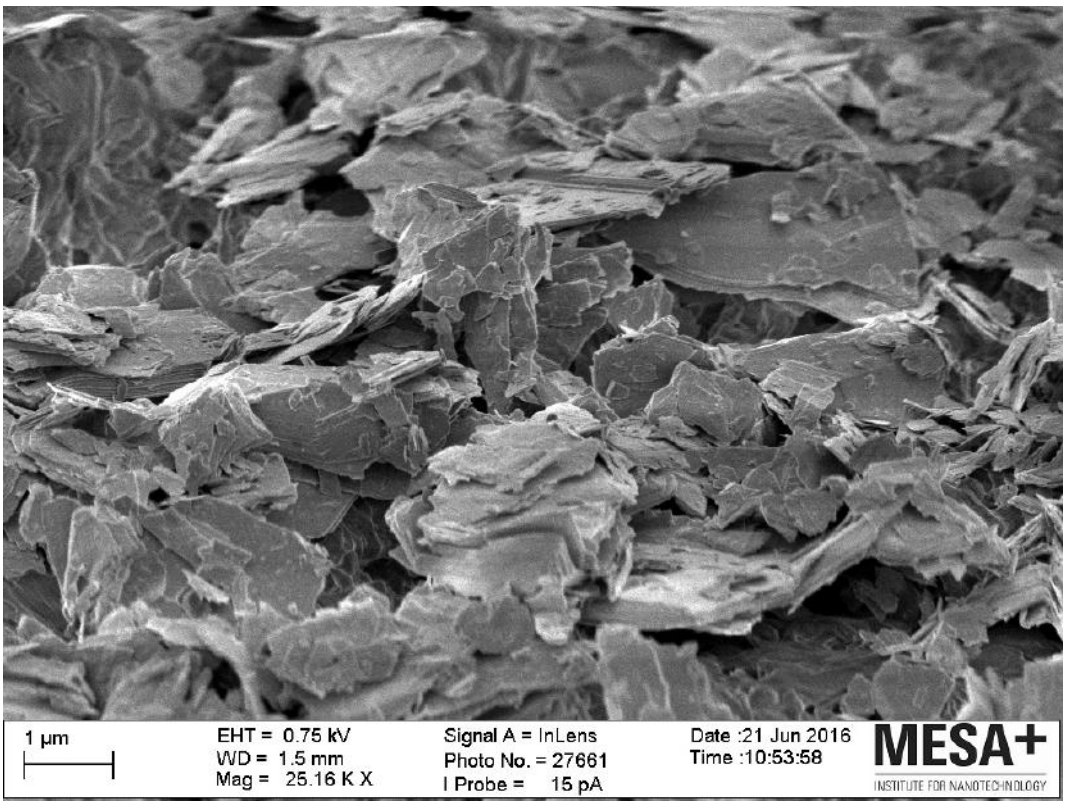

Figure A.61

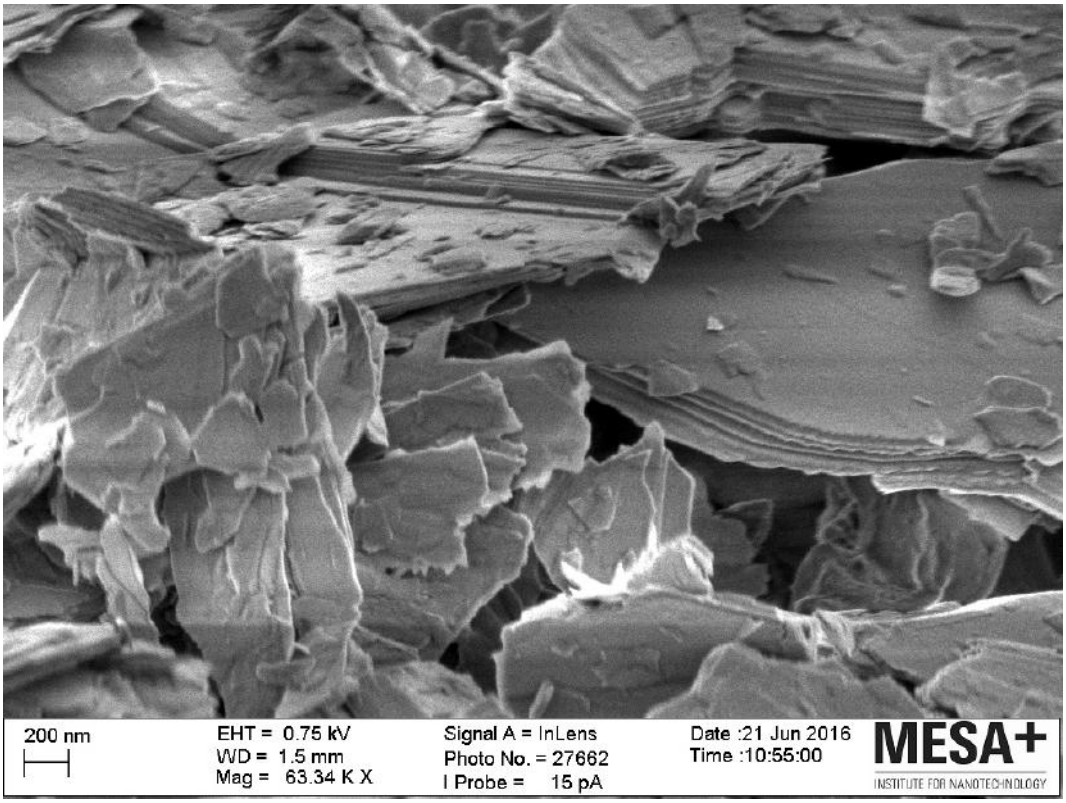

Figure A.62

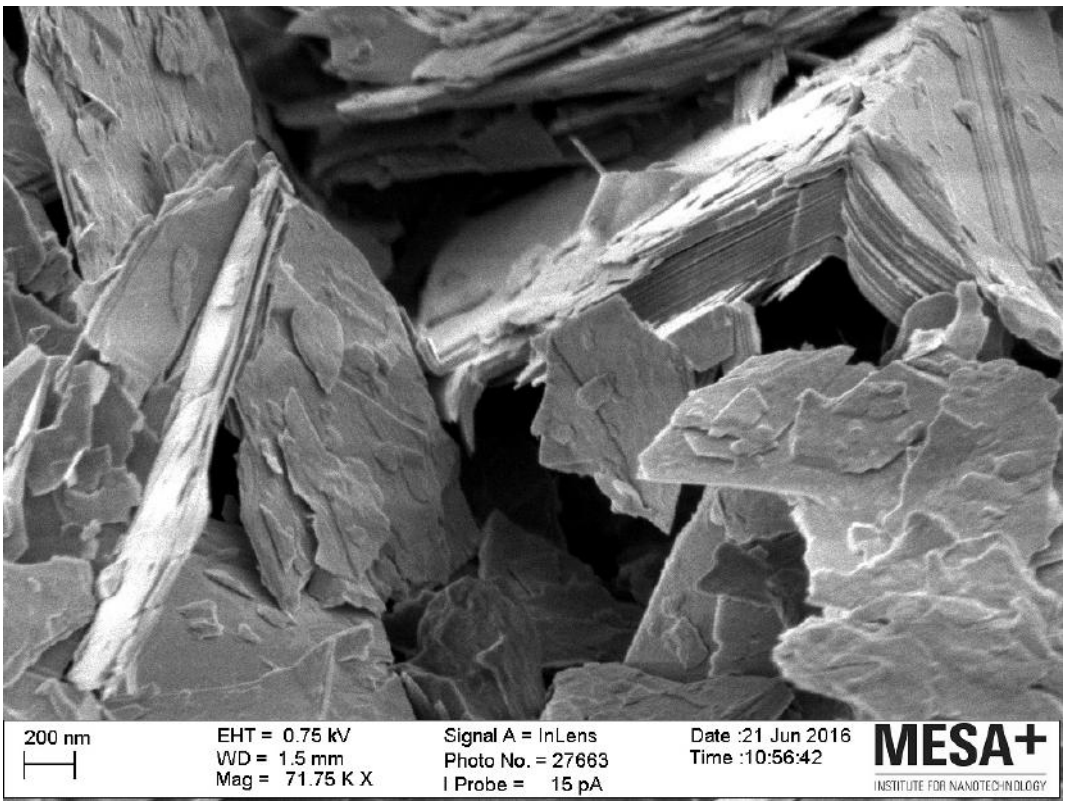

Figure A.63

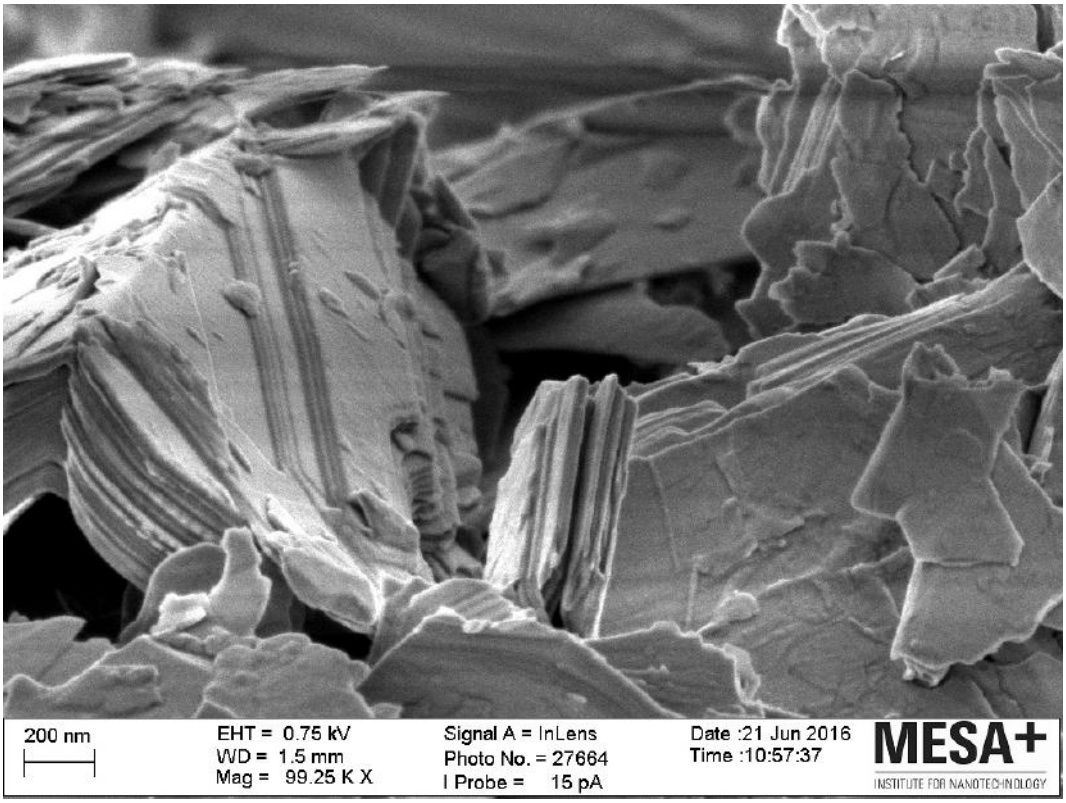

Figure A.64

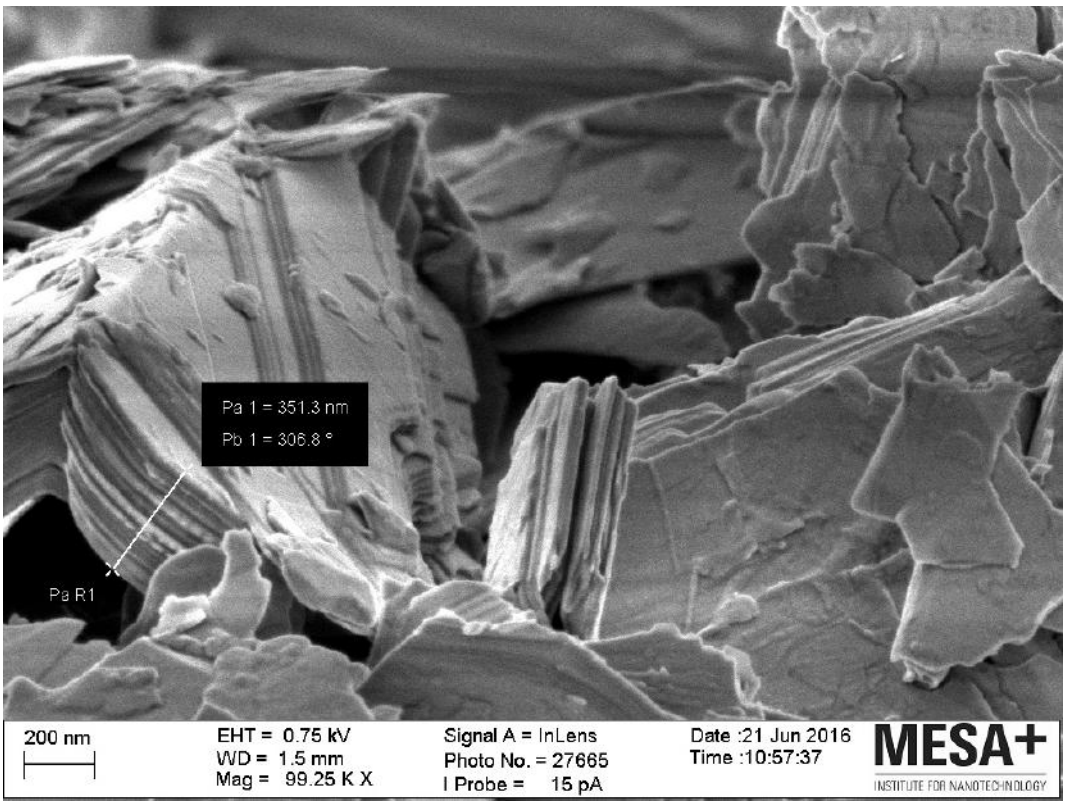

Figure A.65

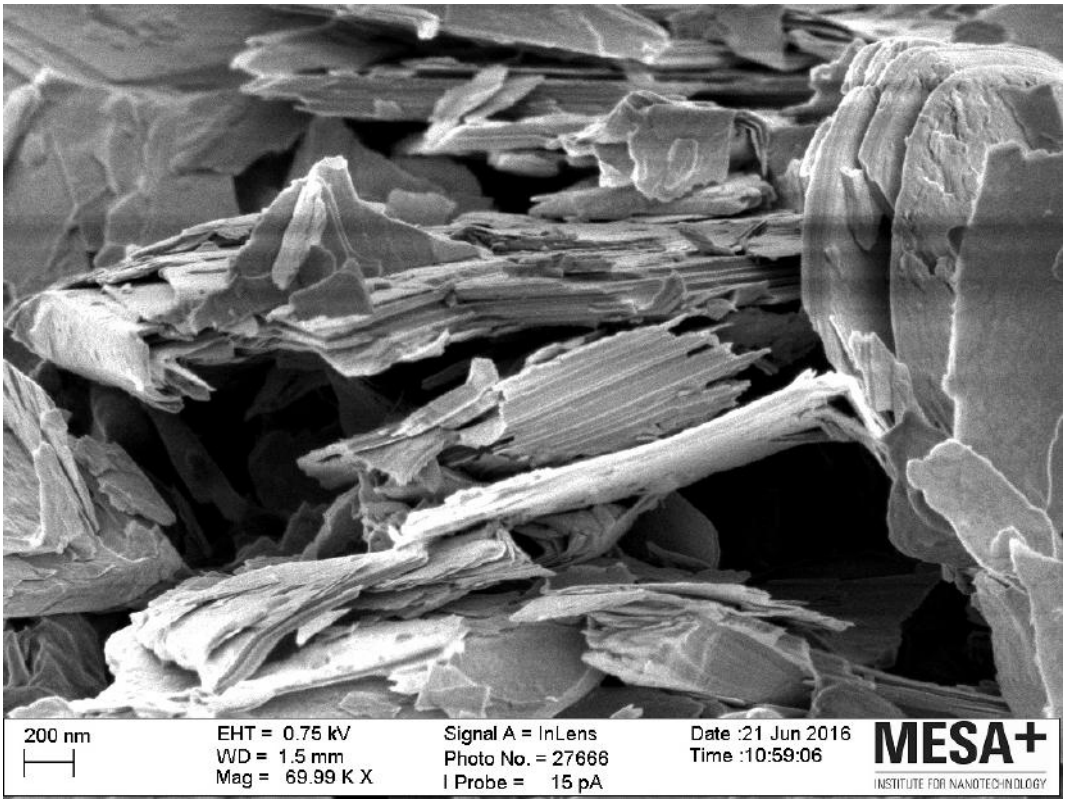

Figure A.66

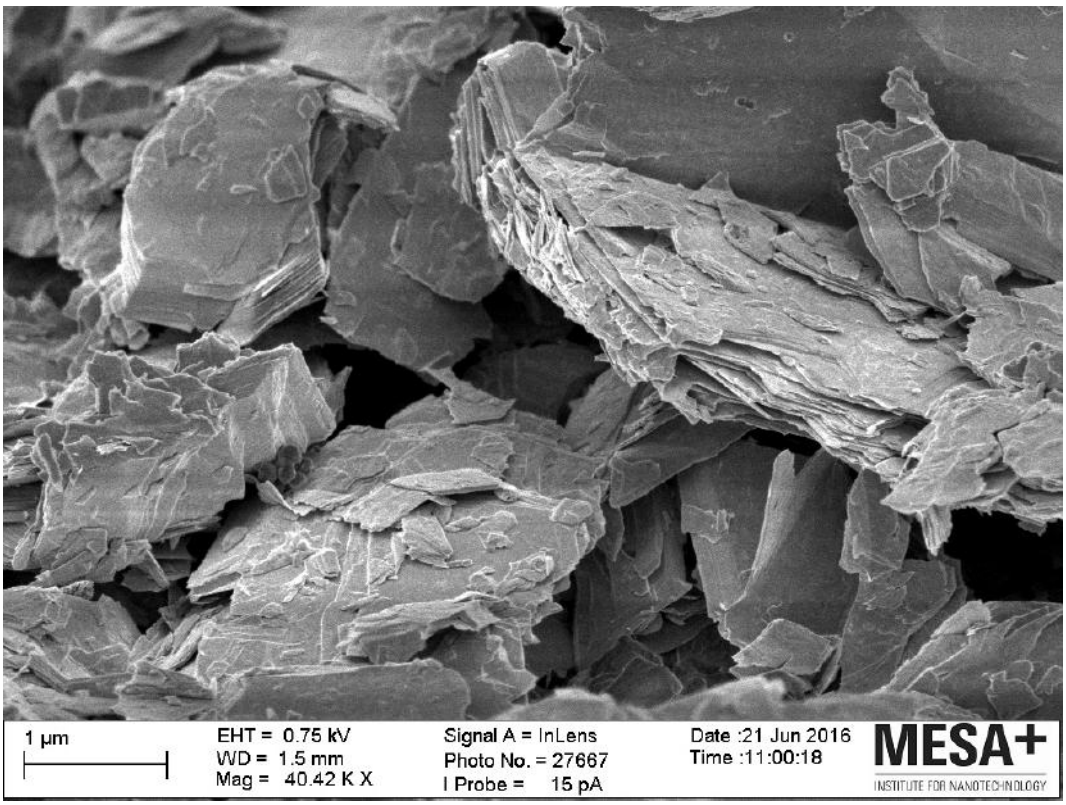

Figure A.67

A.1.5 BHP

Absorption Spectra

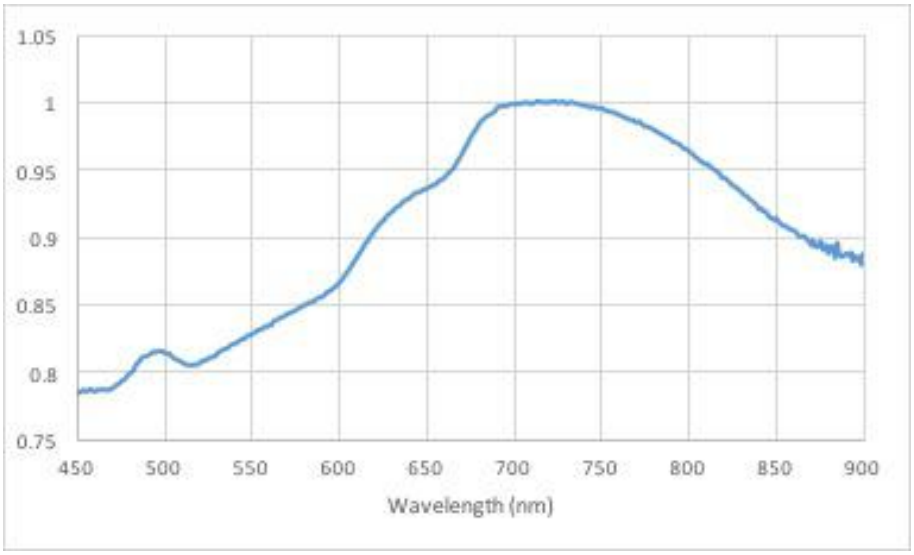

Figure A.68: Normalised absorption spectra for a maximum absorption intensity of 0,221 at various wavelengths between 714 nm and 724 nm.

SEM

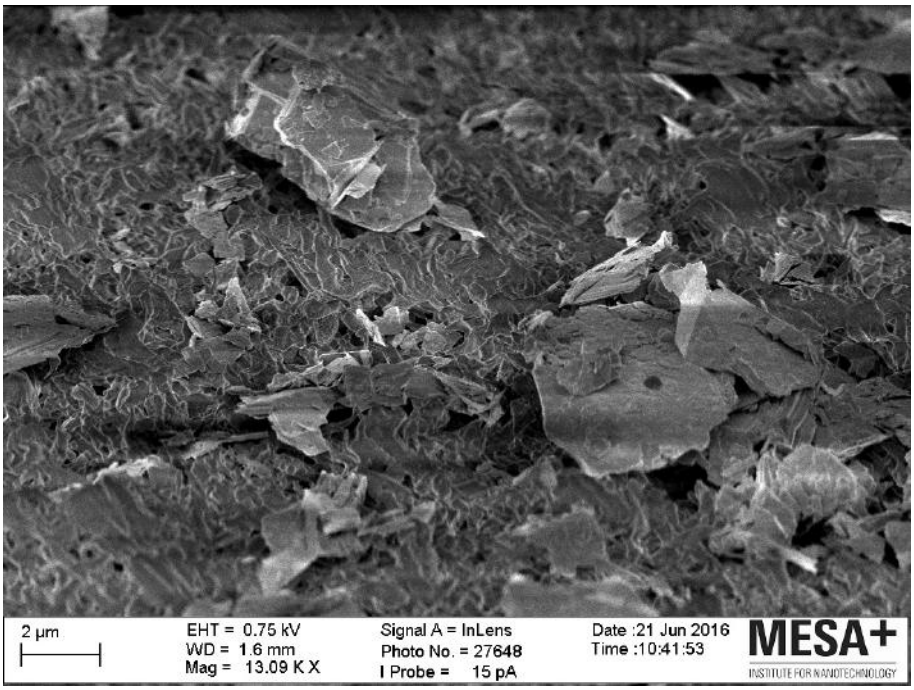

Figure A.69

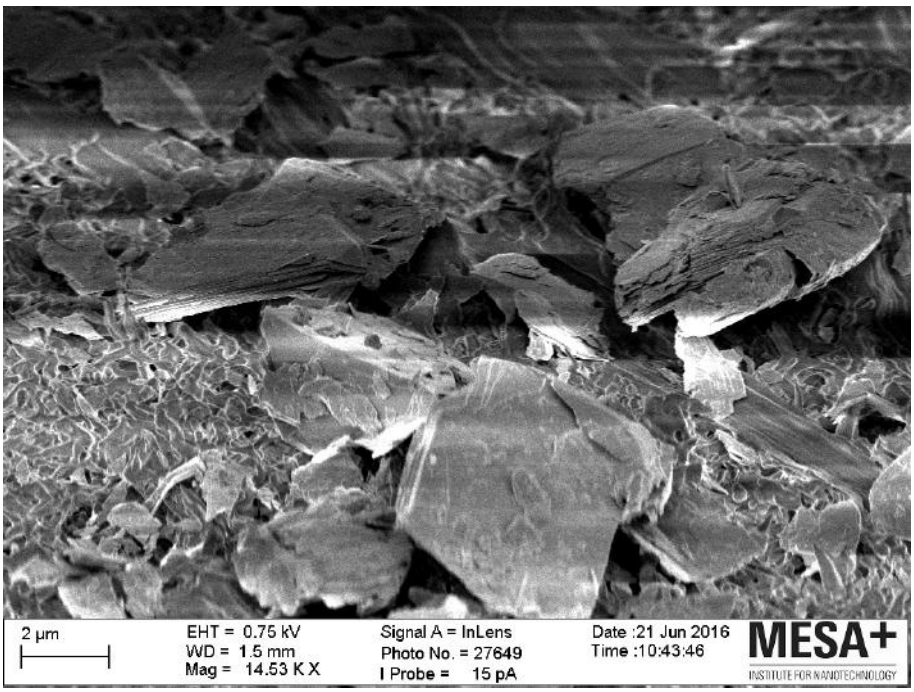

Figure A.70

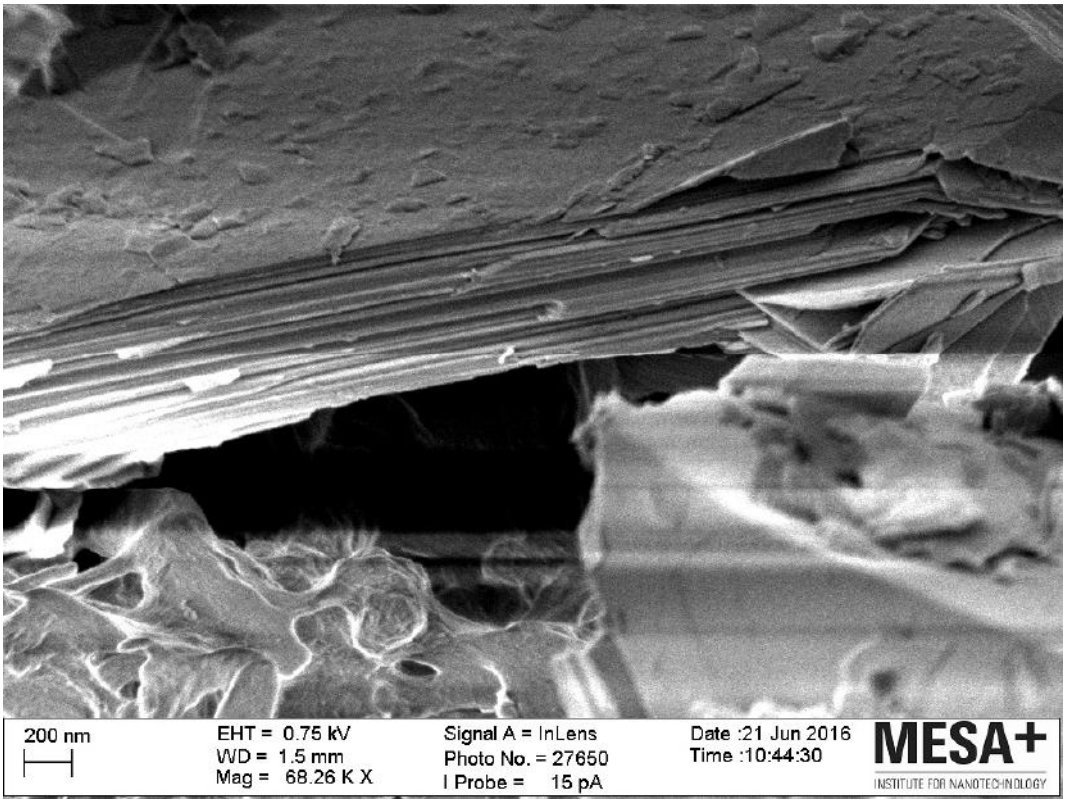

Figure A.71

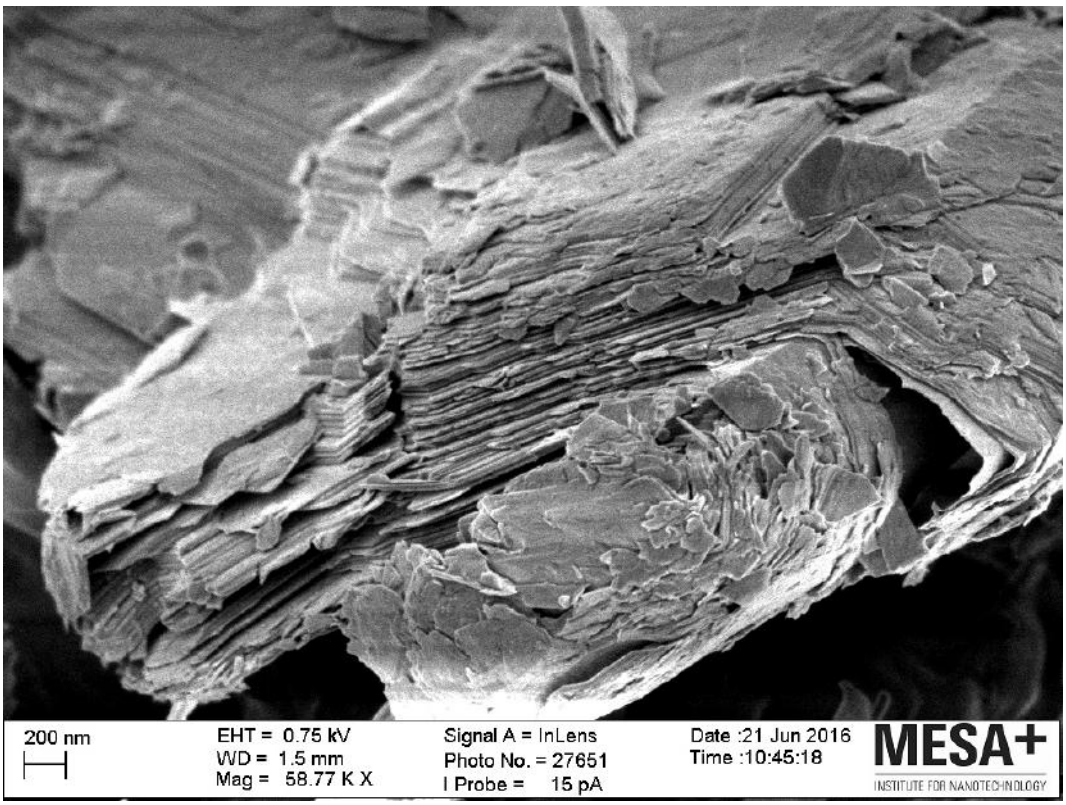

Figure A.72

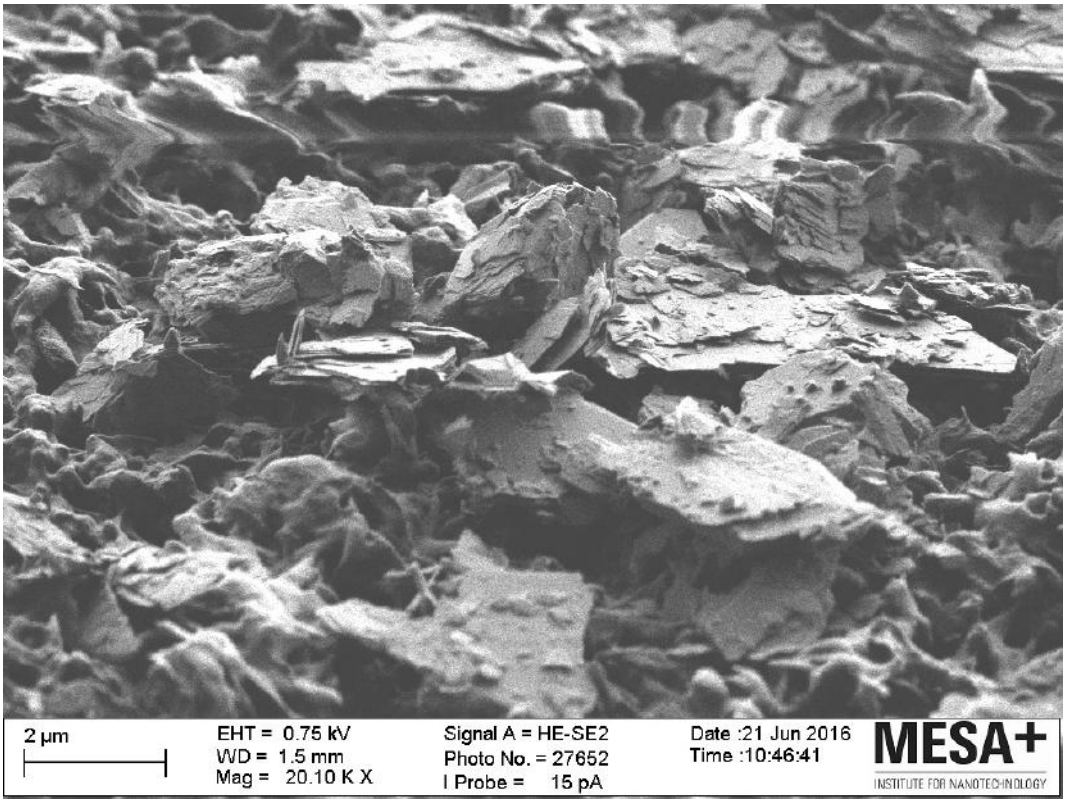

Figure A.73

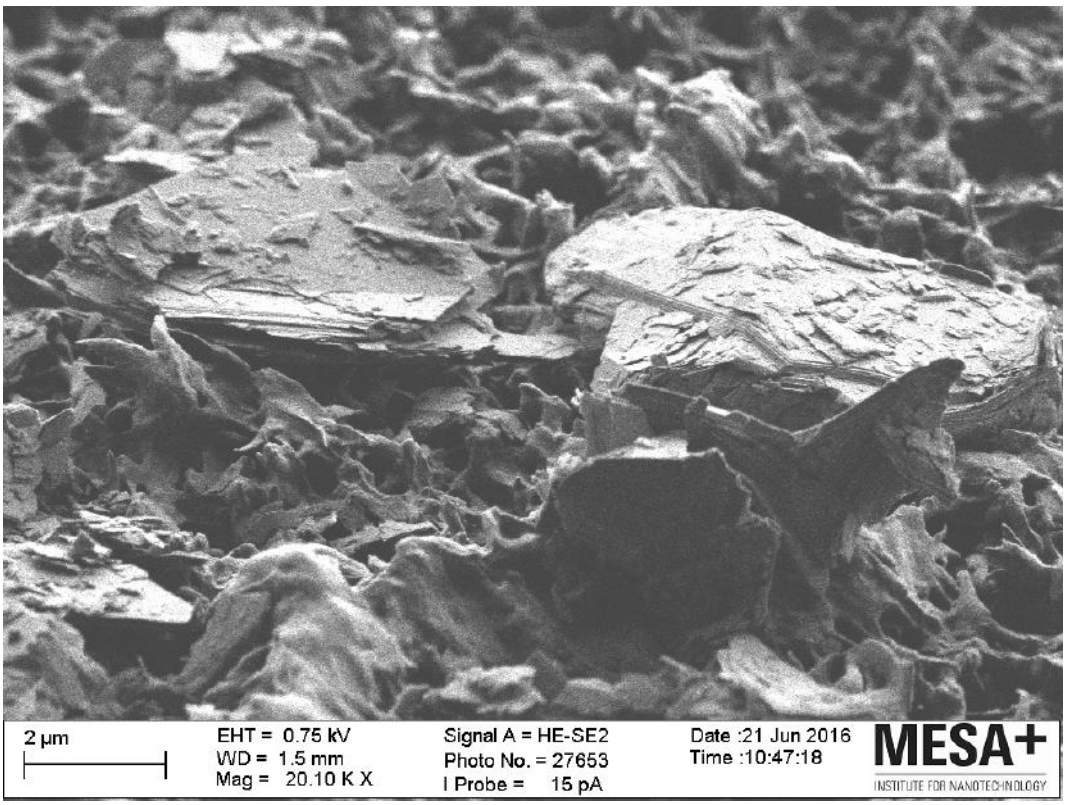

Figure A.74

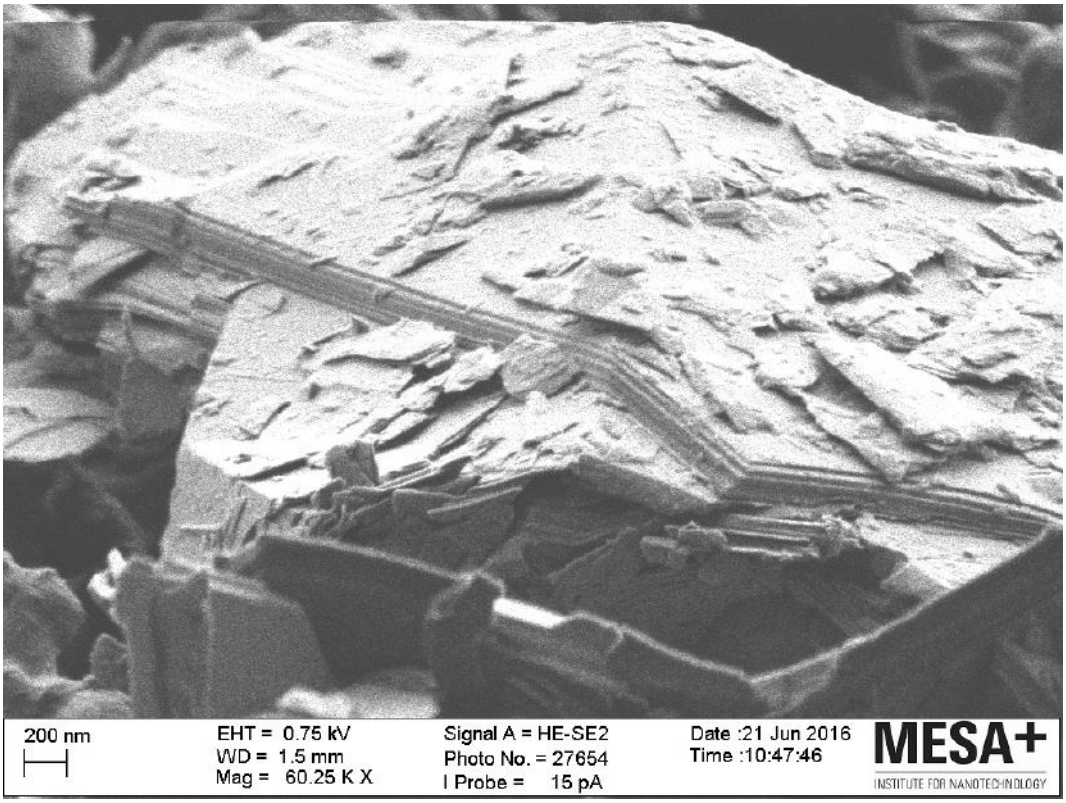

Figure A.75

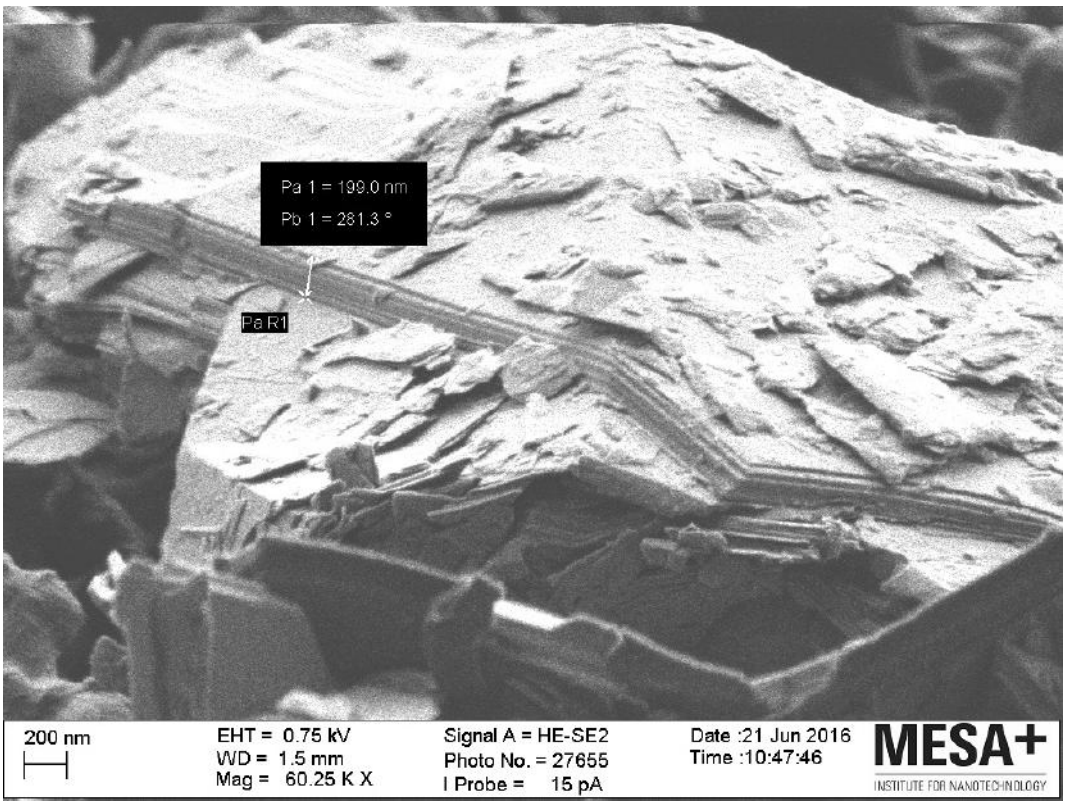

Figure A.76

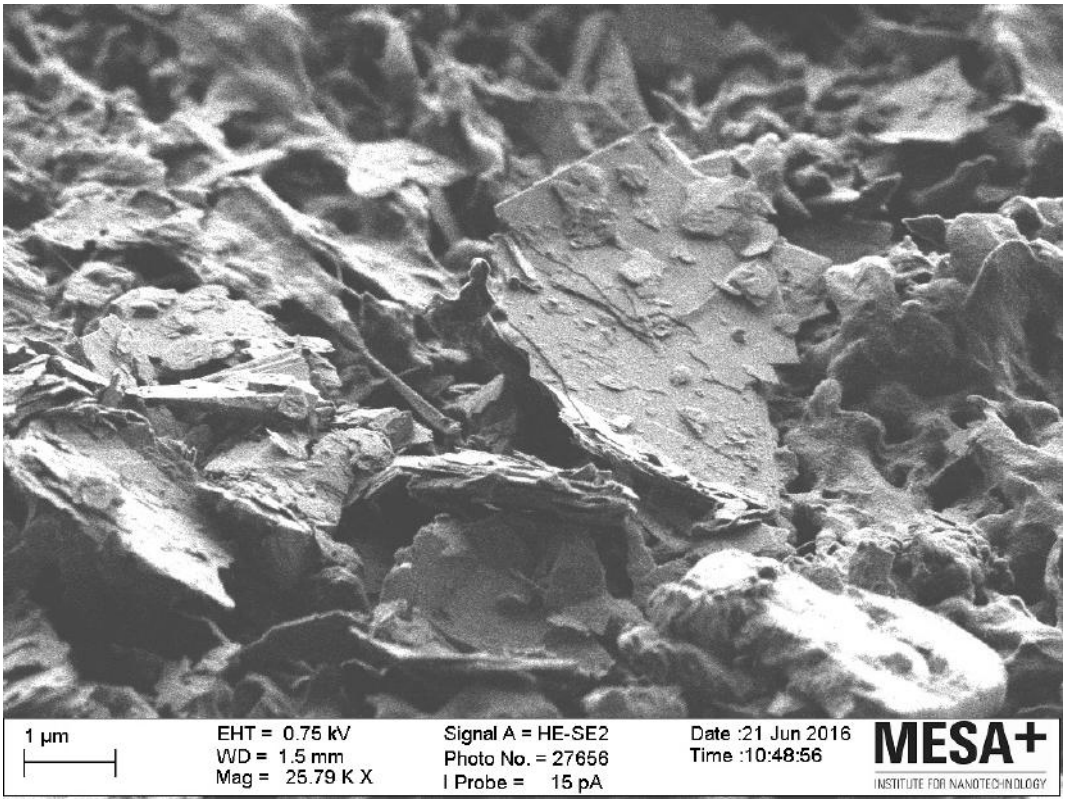

Figure A.77

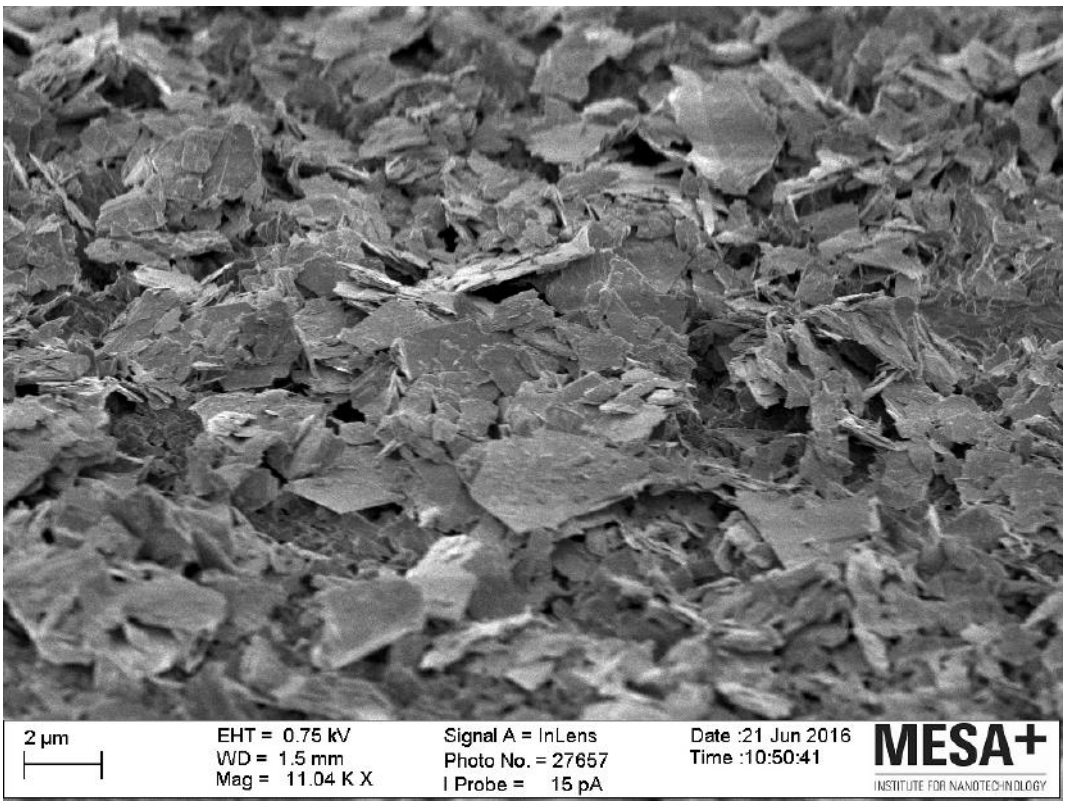

Figure A.78

A.1.6 C_NP

Absorption Spectra

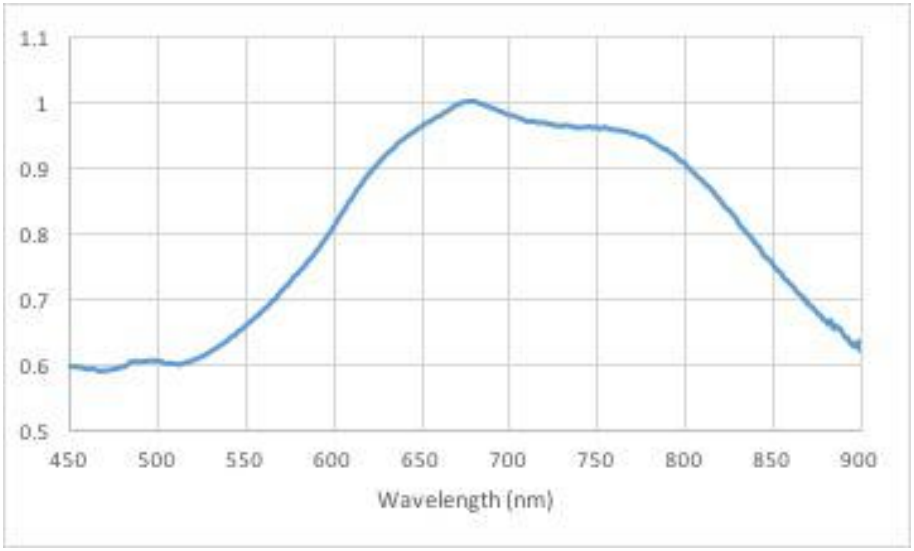

Figure A.79: Normalised absorption spectra for a maximum absorption intensity of 0,129 at the wavelength of 680 nm.

SEM

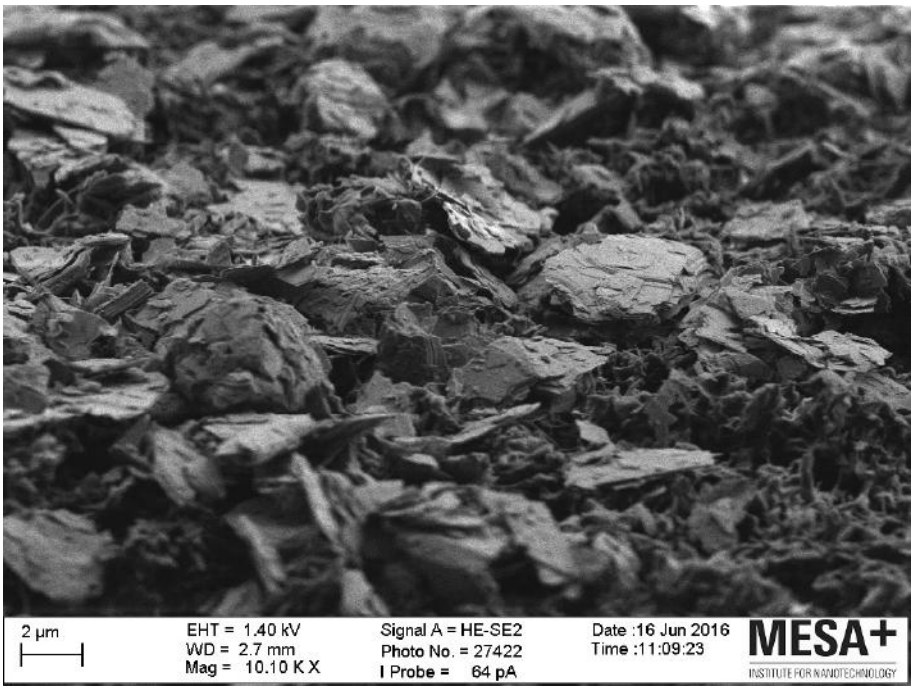

Figure A.80

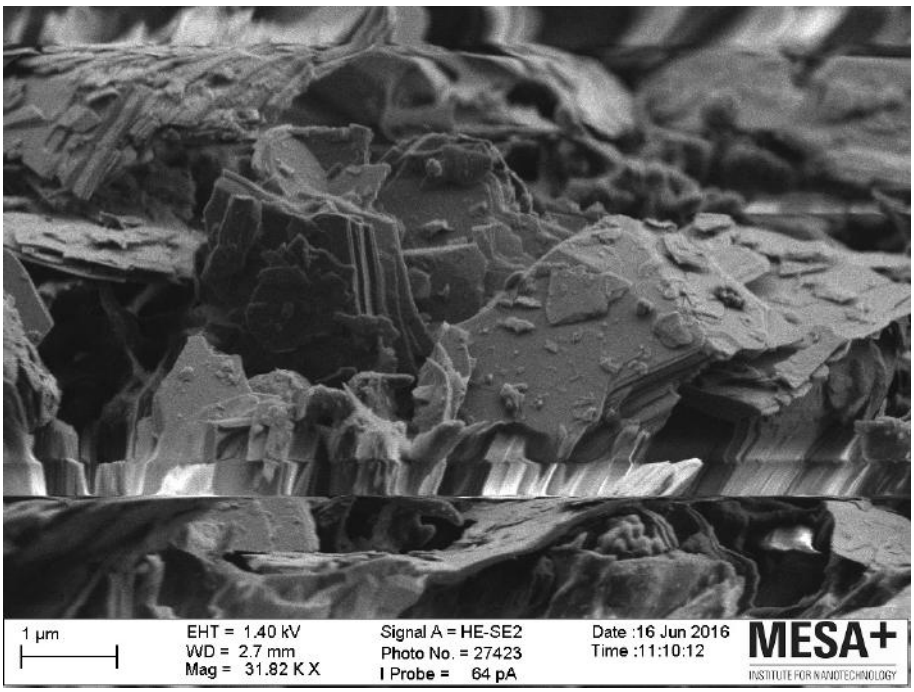

Figure A.81

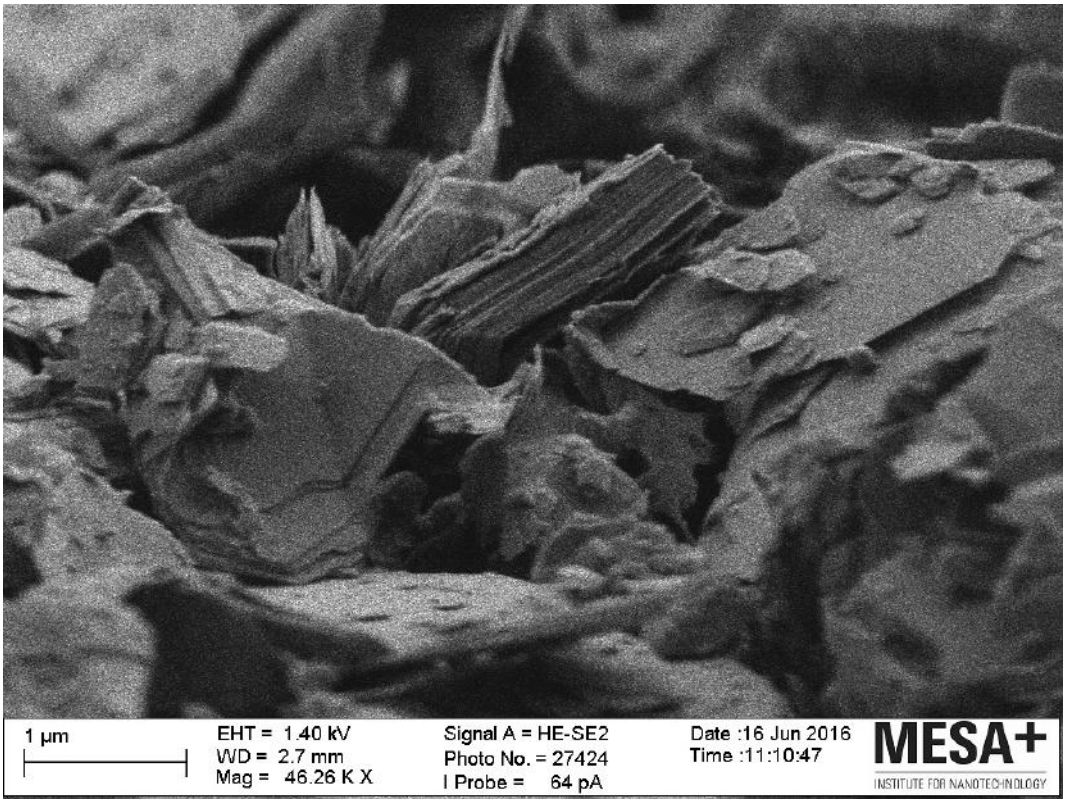

Figure A.82

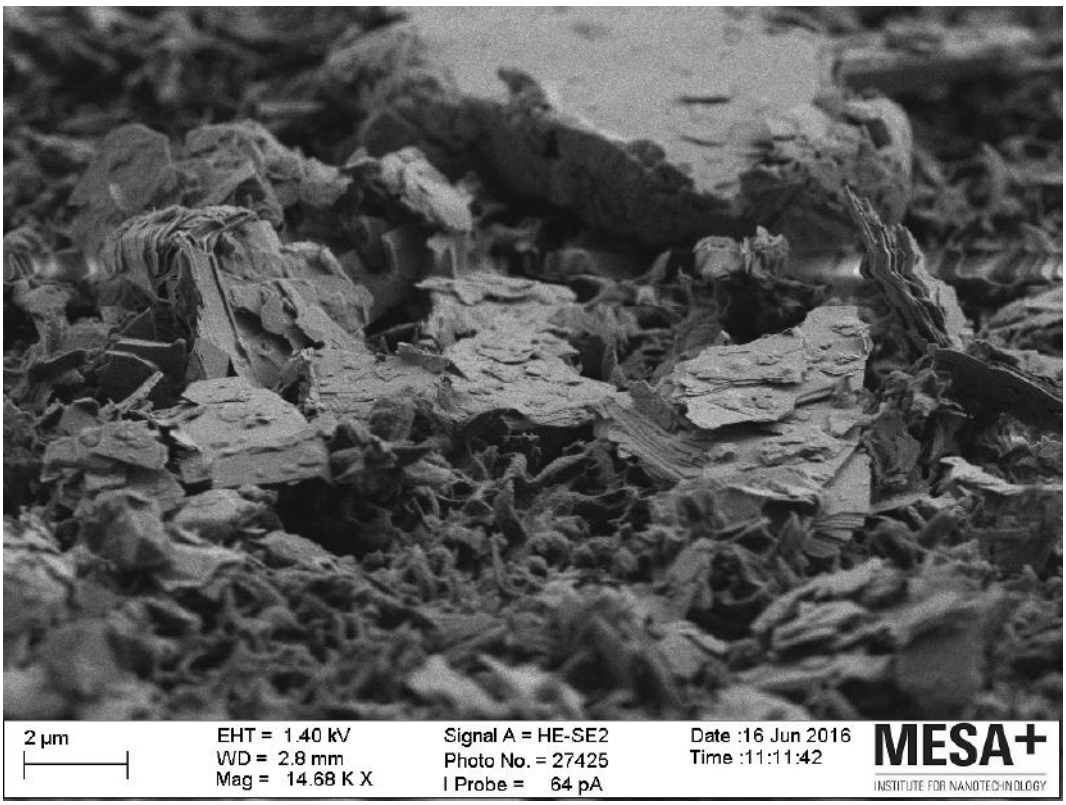

Figure A.83

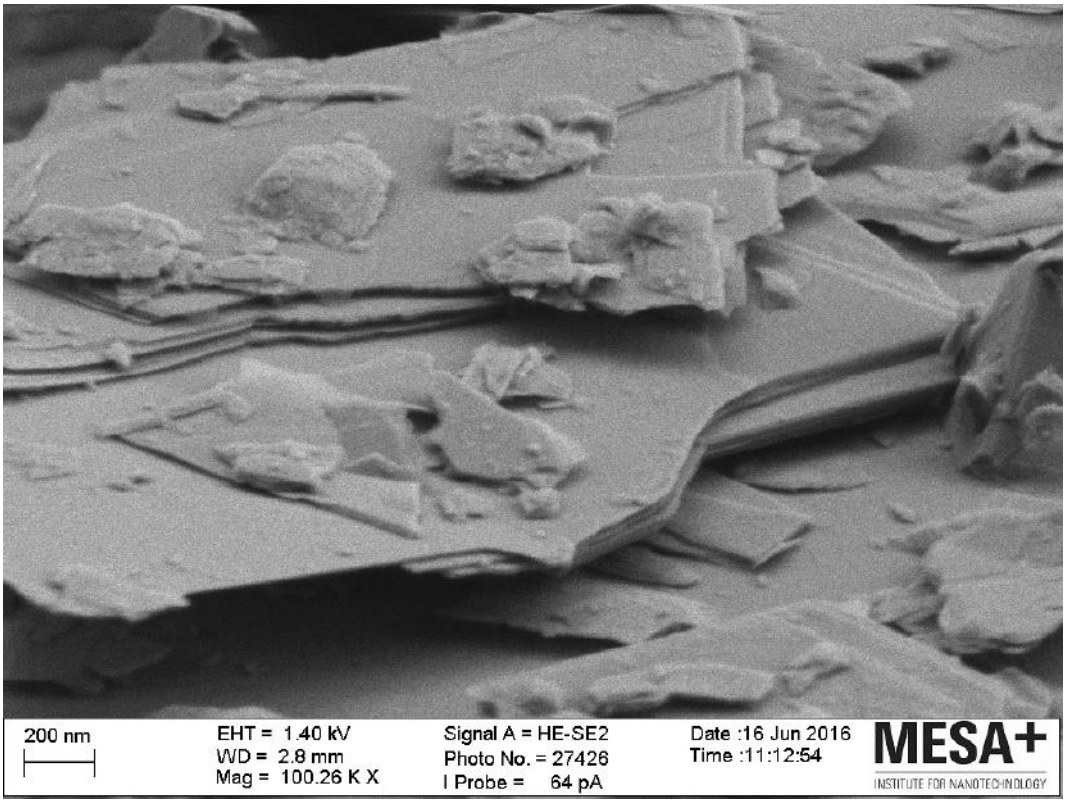

Figure A.84

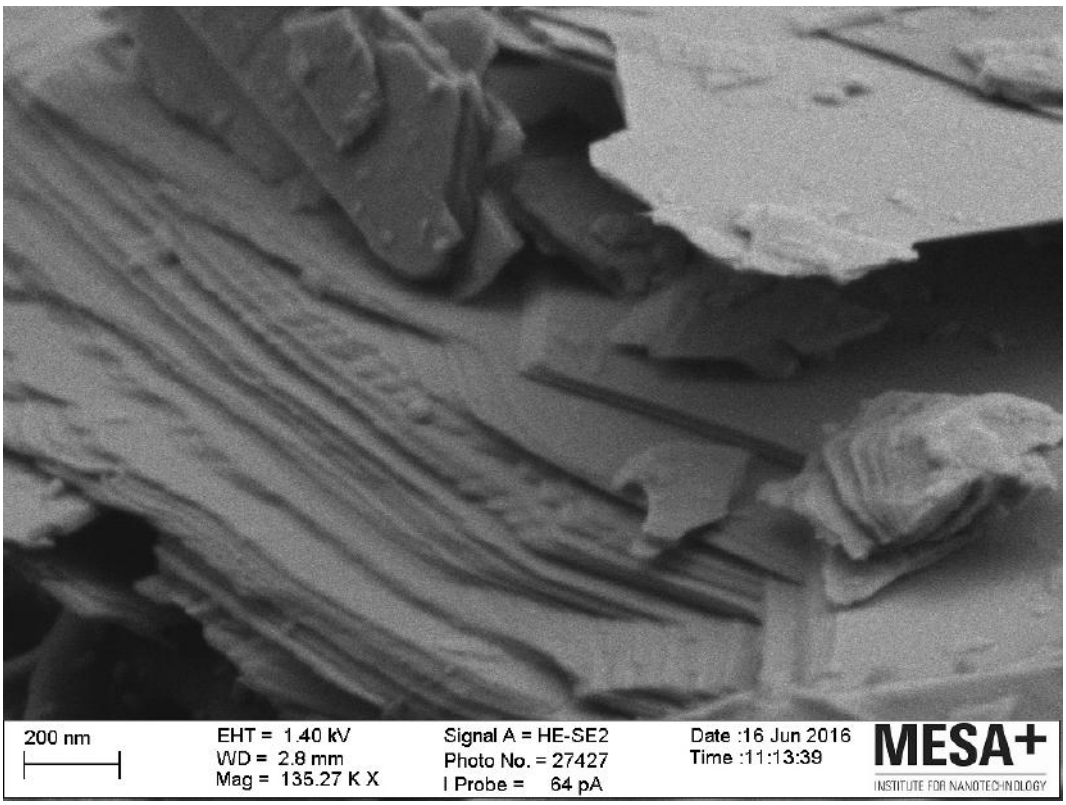

Figure A.85

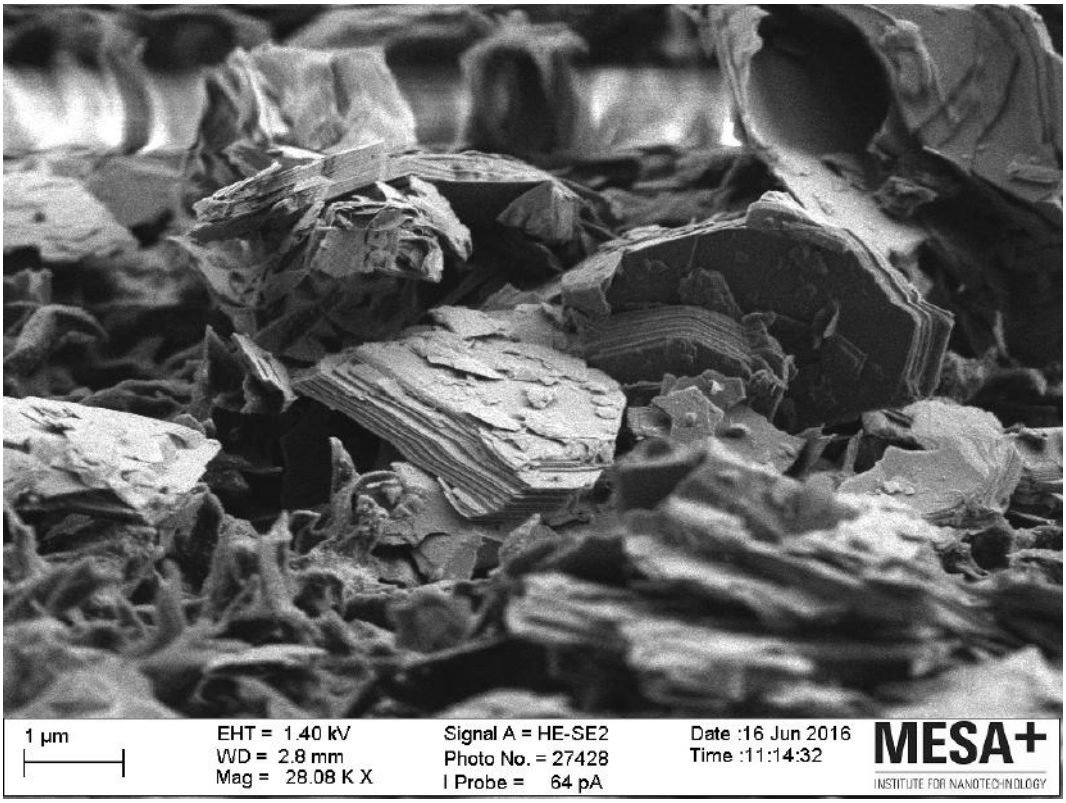

Figure A.86

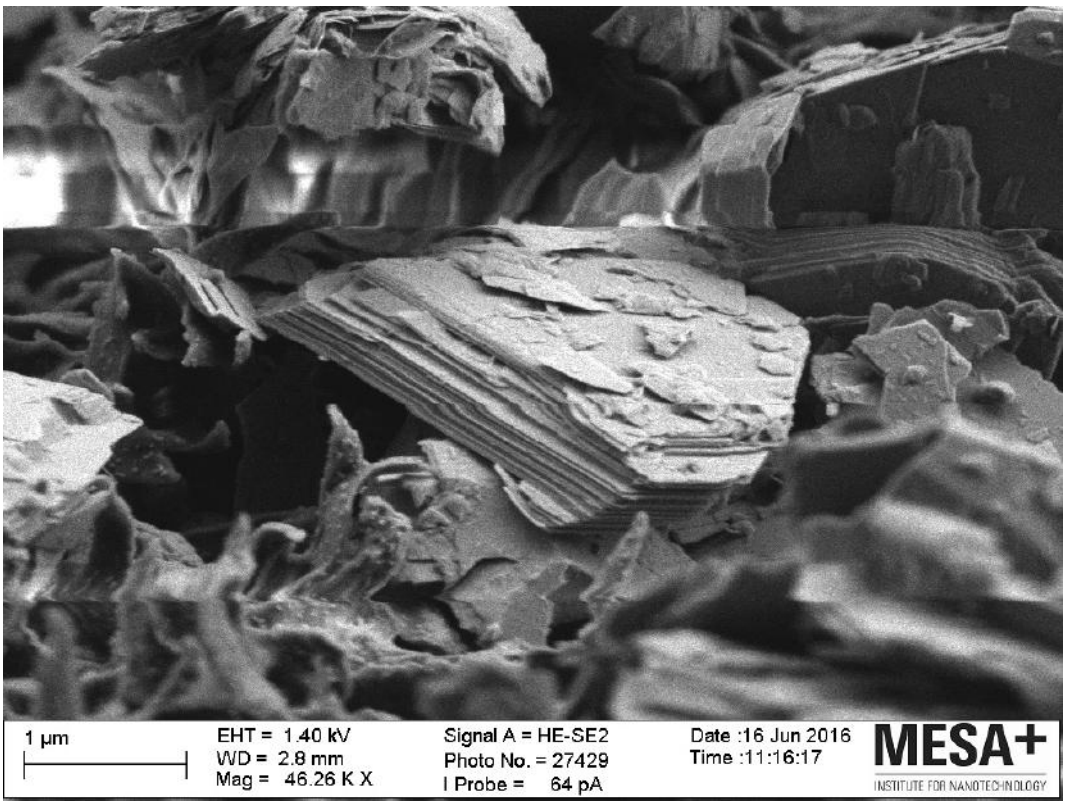

Figure A.87

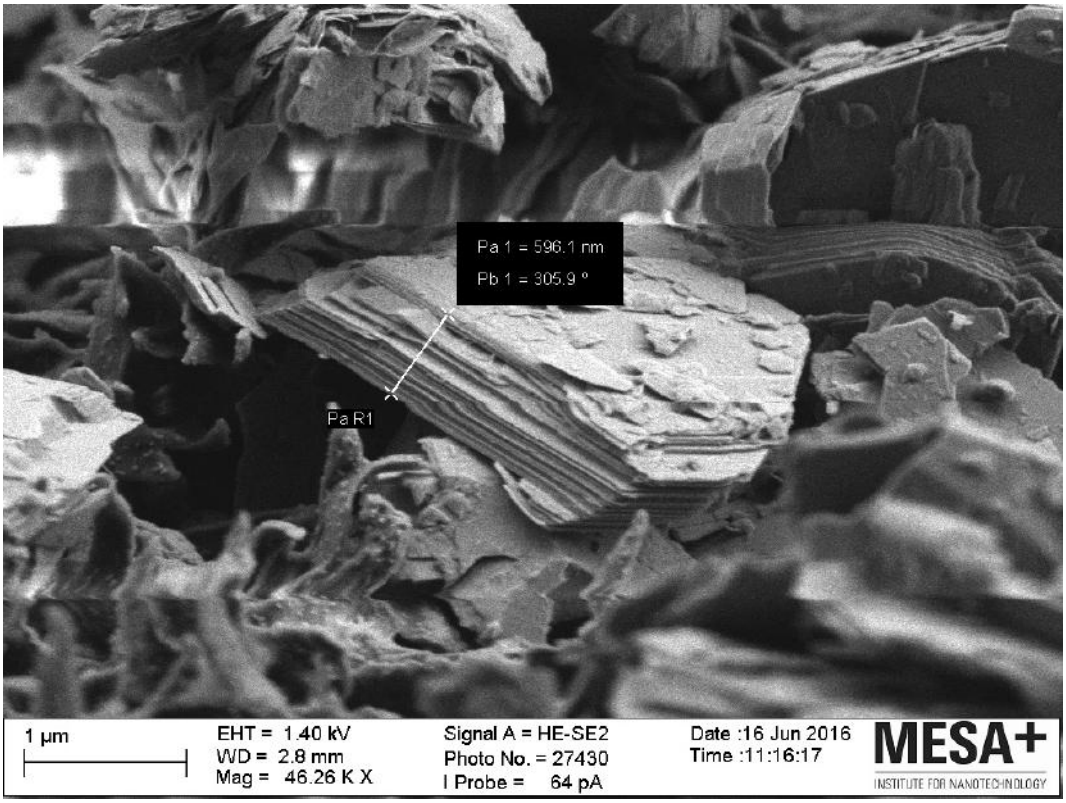

Figure A.88

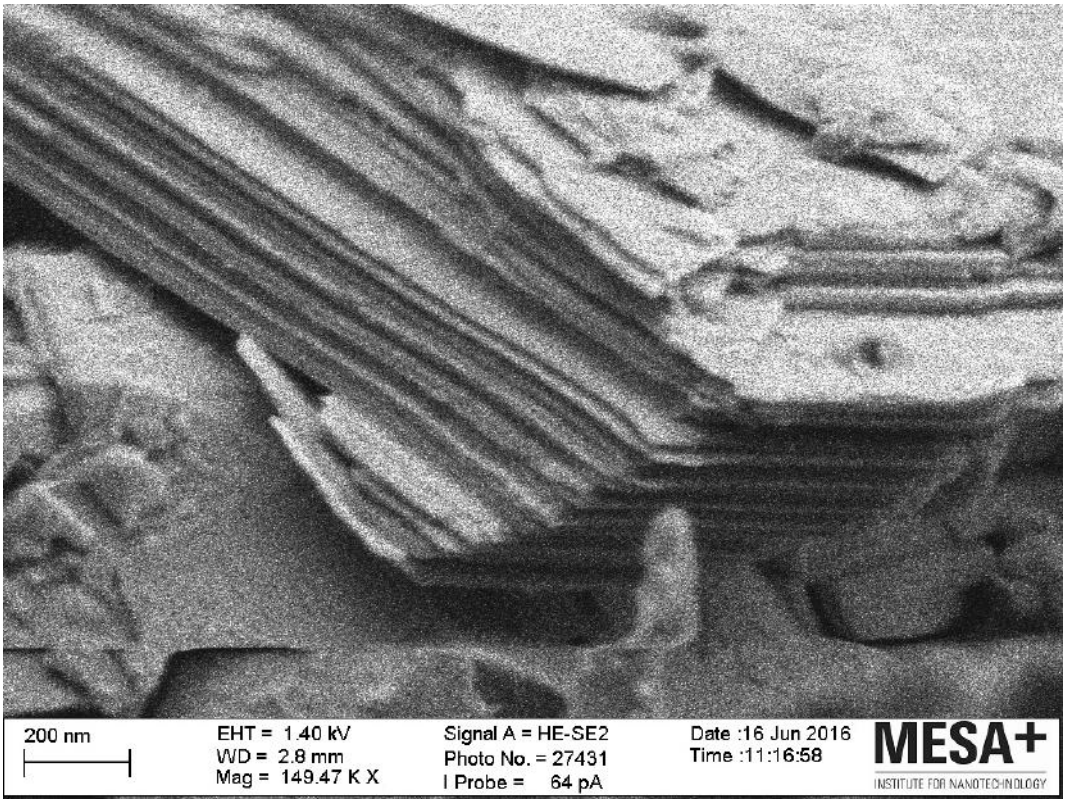

Figure A.89

A.1.7 MBP

Absorption Spectra

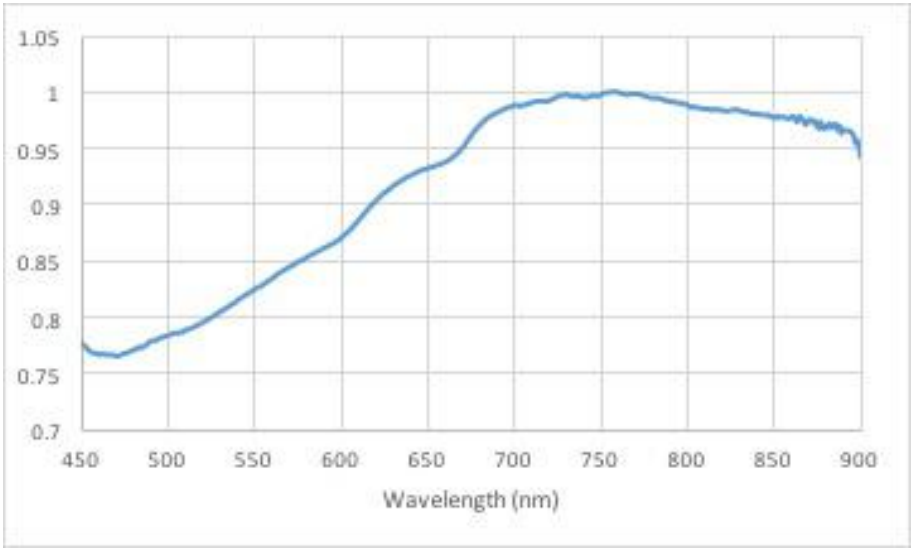

Figure A.90: Normalised absorption spectra for a maximum absorption intensity of 0,210 at the wavelength of 758 nm.

SEM

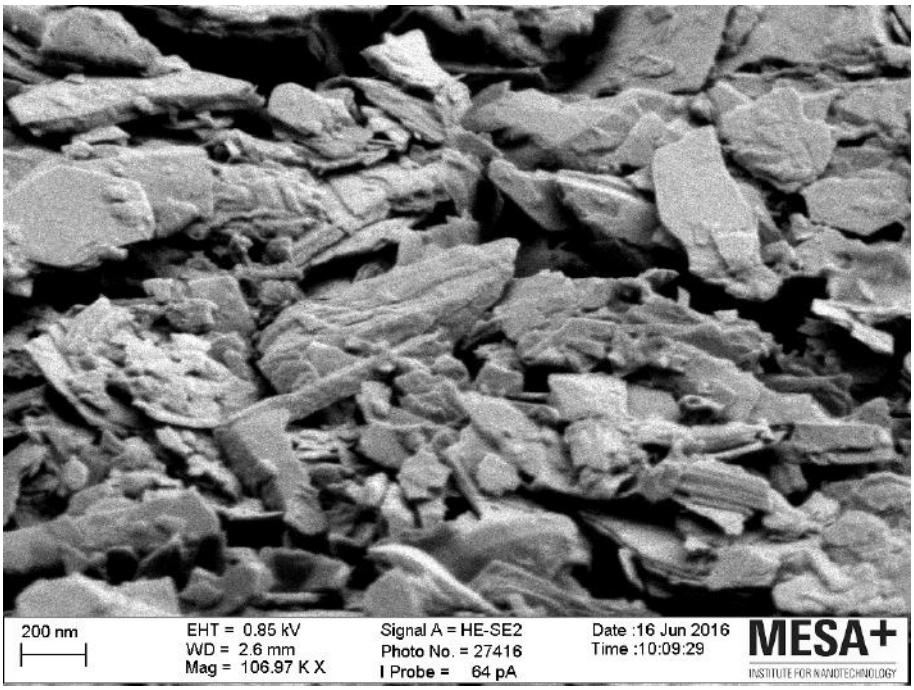

Figure A.91

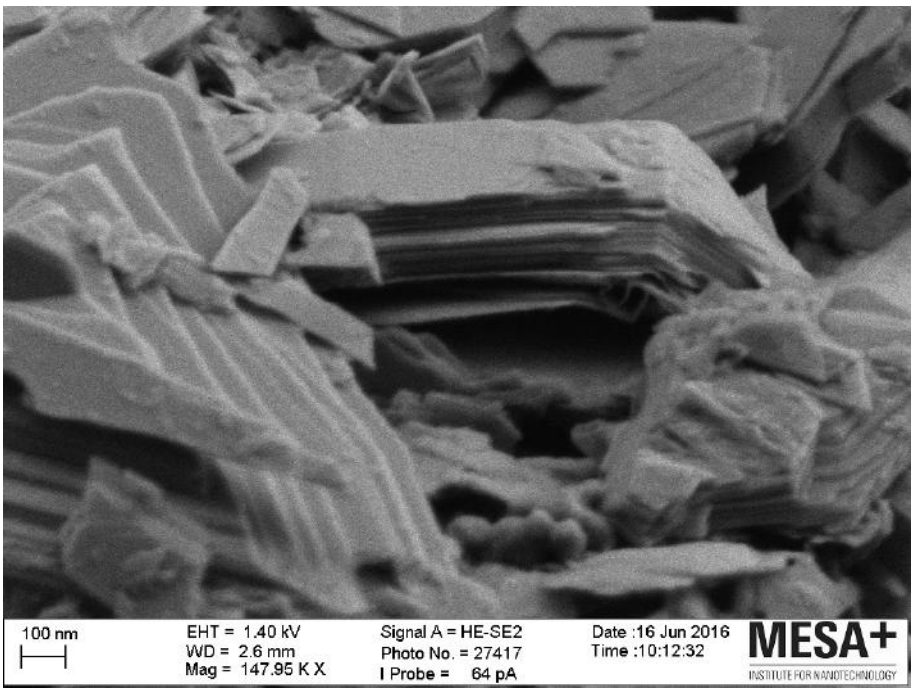

Figure A.92

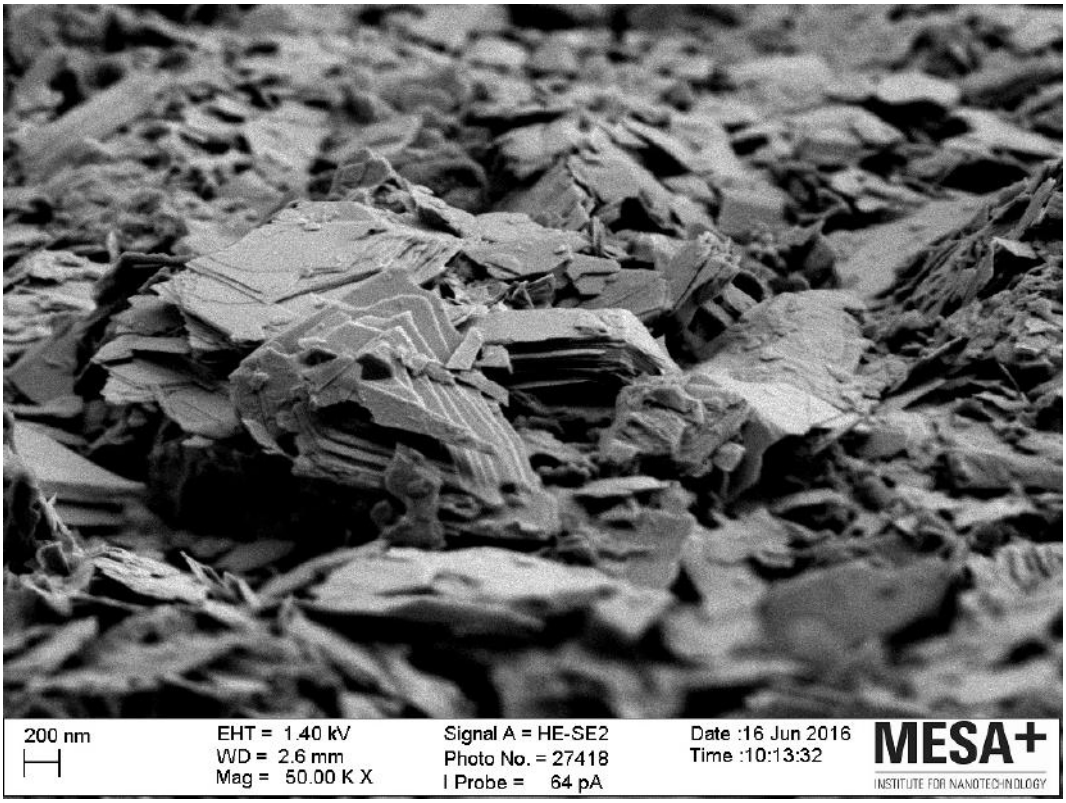

Figure A.93

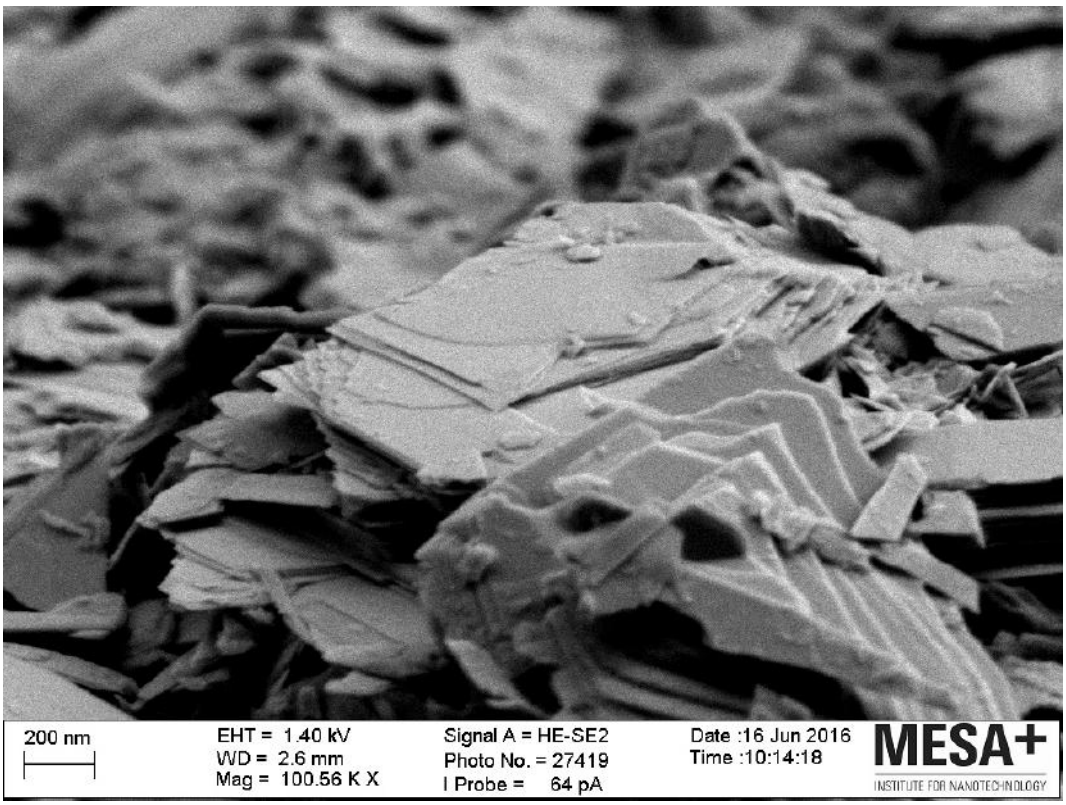

Figure A.94

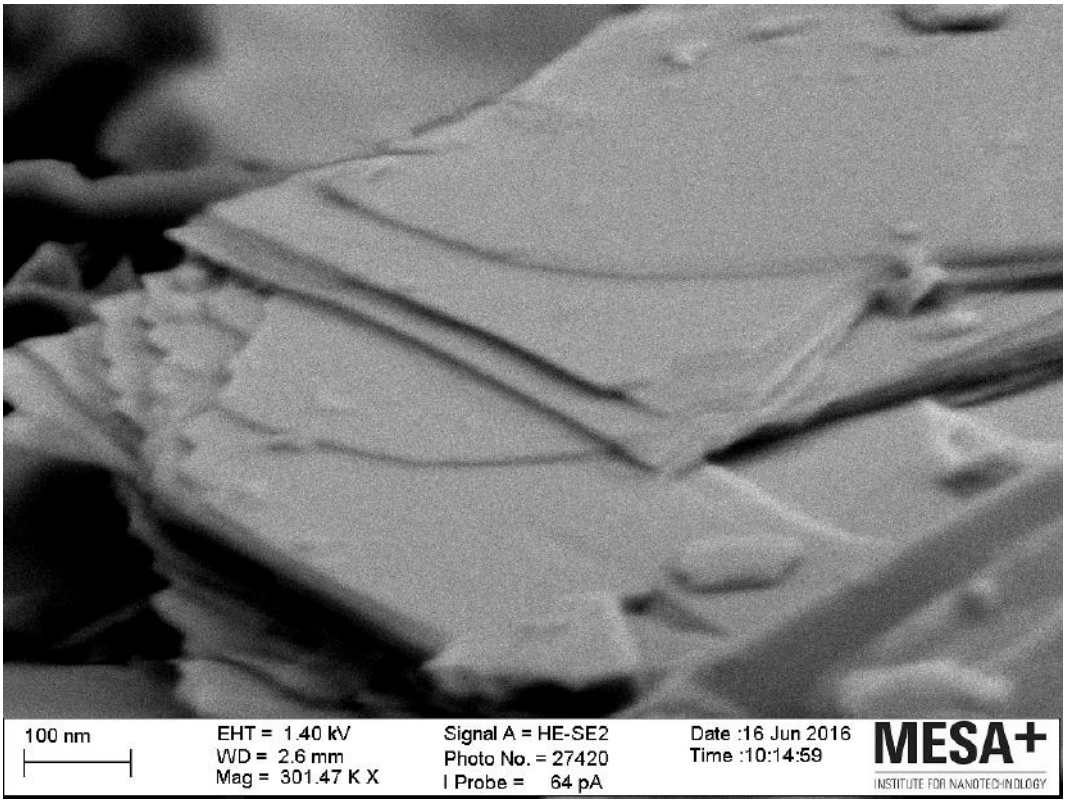

Figure A.95

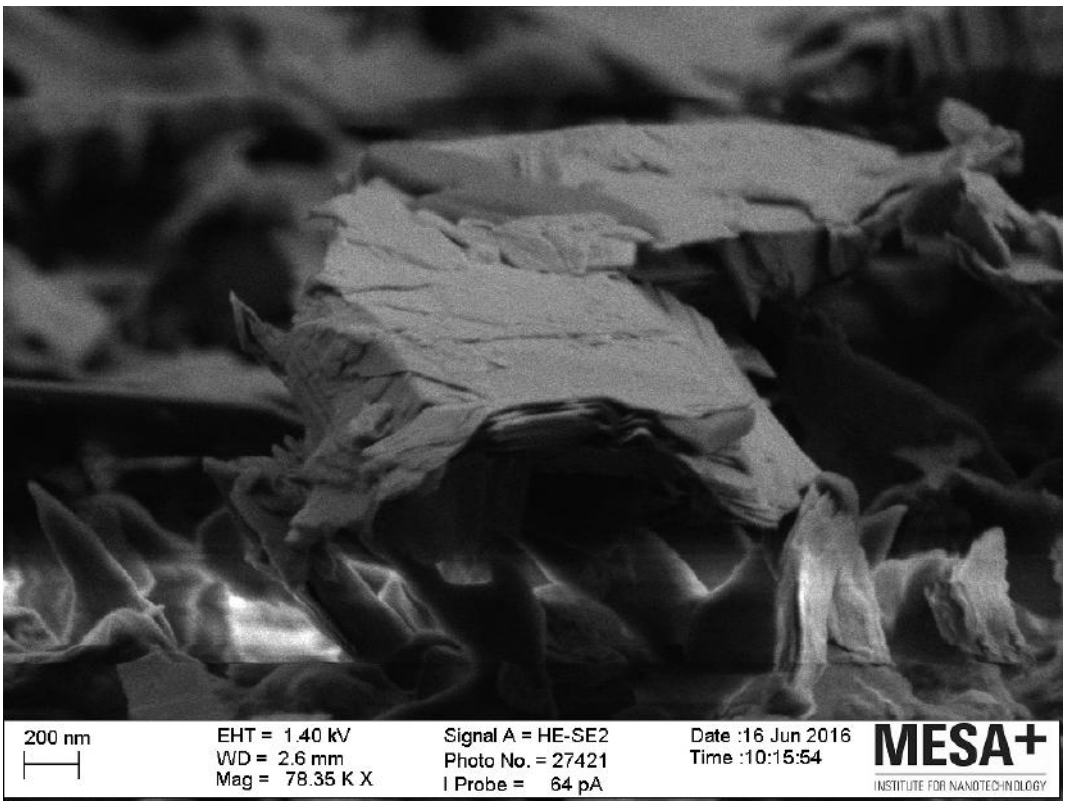

Figure A.96

A.1.8 BBNP 20min

Absorption Spectra

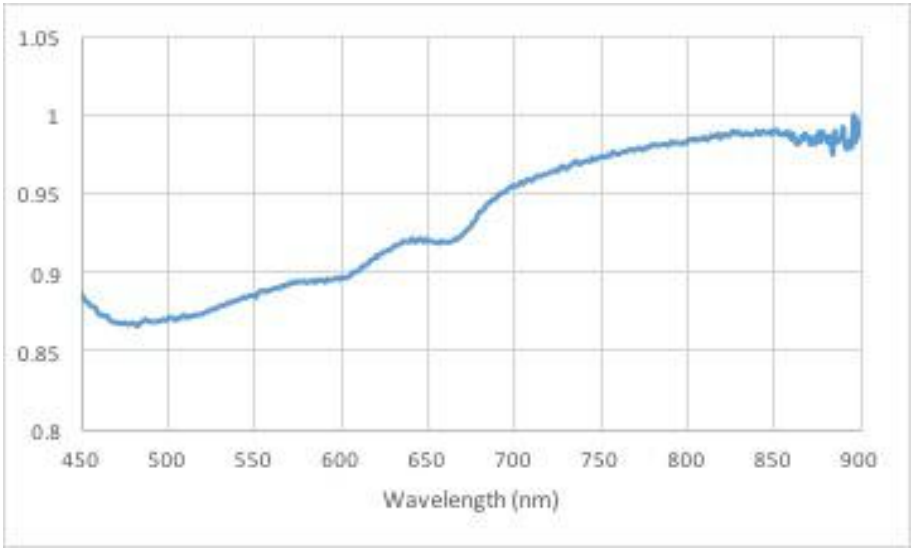

Figure A.97: Normalised absorption spectra for a maximum absorption intensity of 0,131 at the wavelength of 895 nm.

SEM

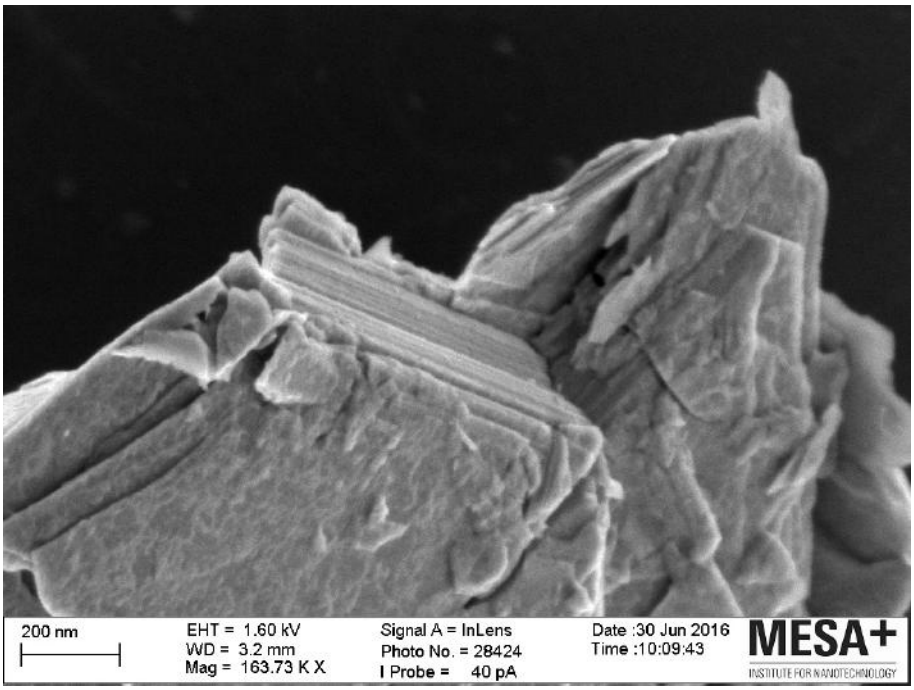

Figure A.98

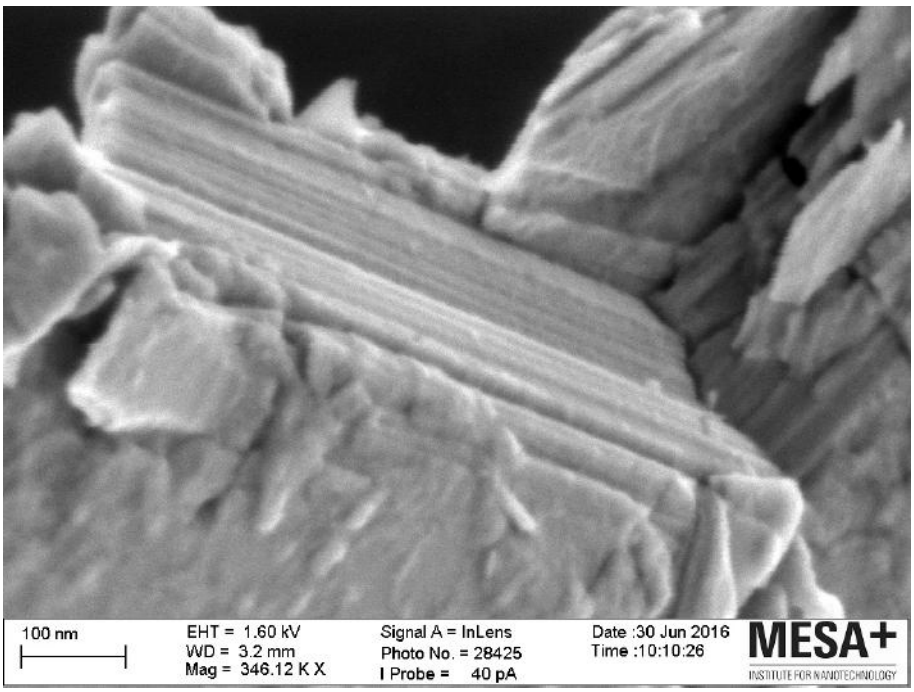

Figure A.99

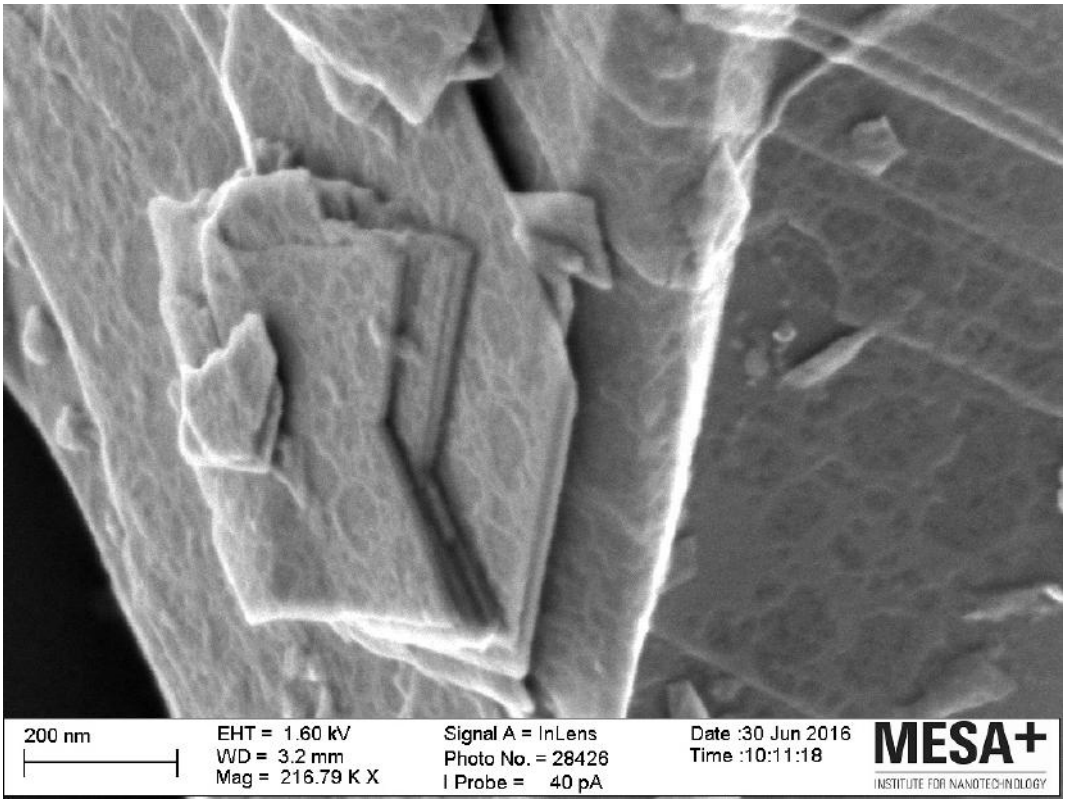

Figure A.100

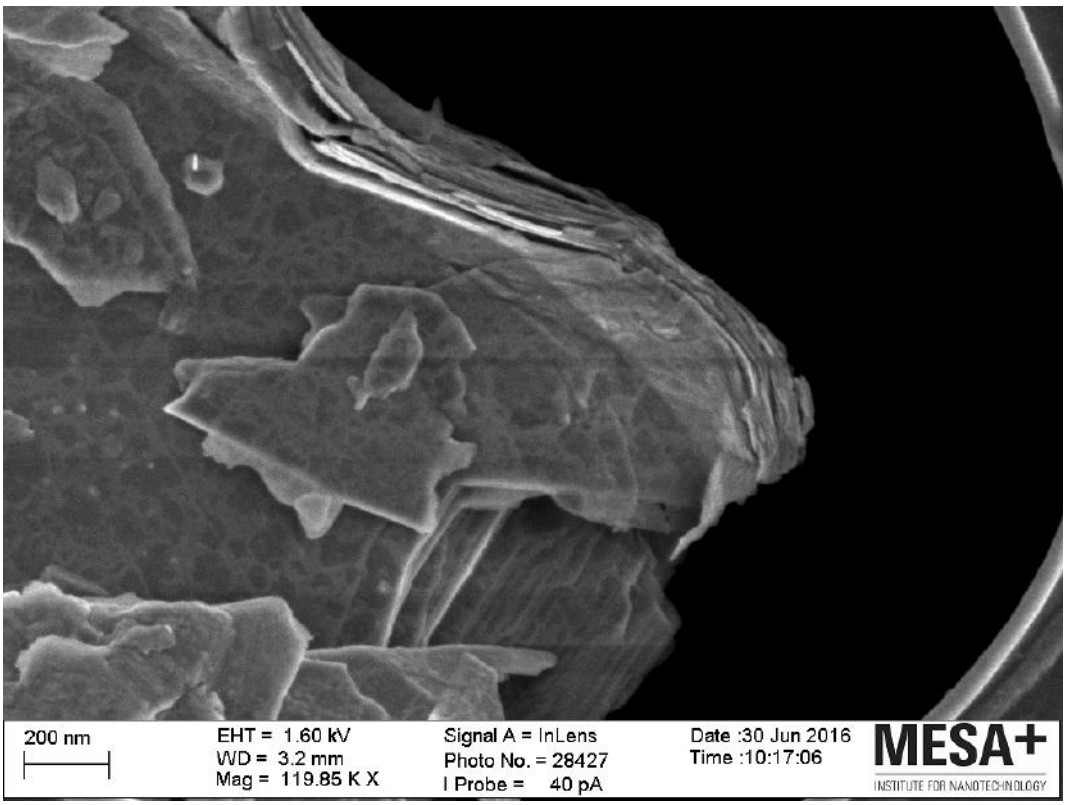

Figure A.101

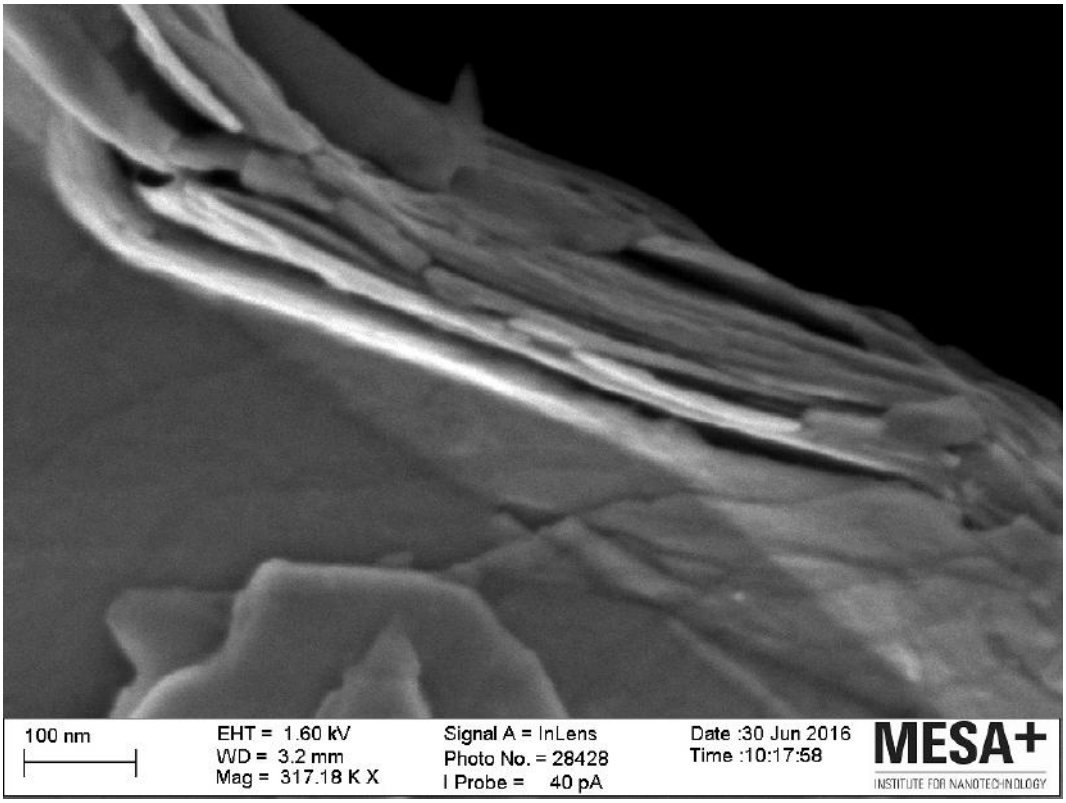

Figure A.102

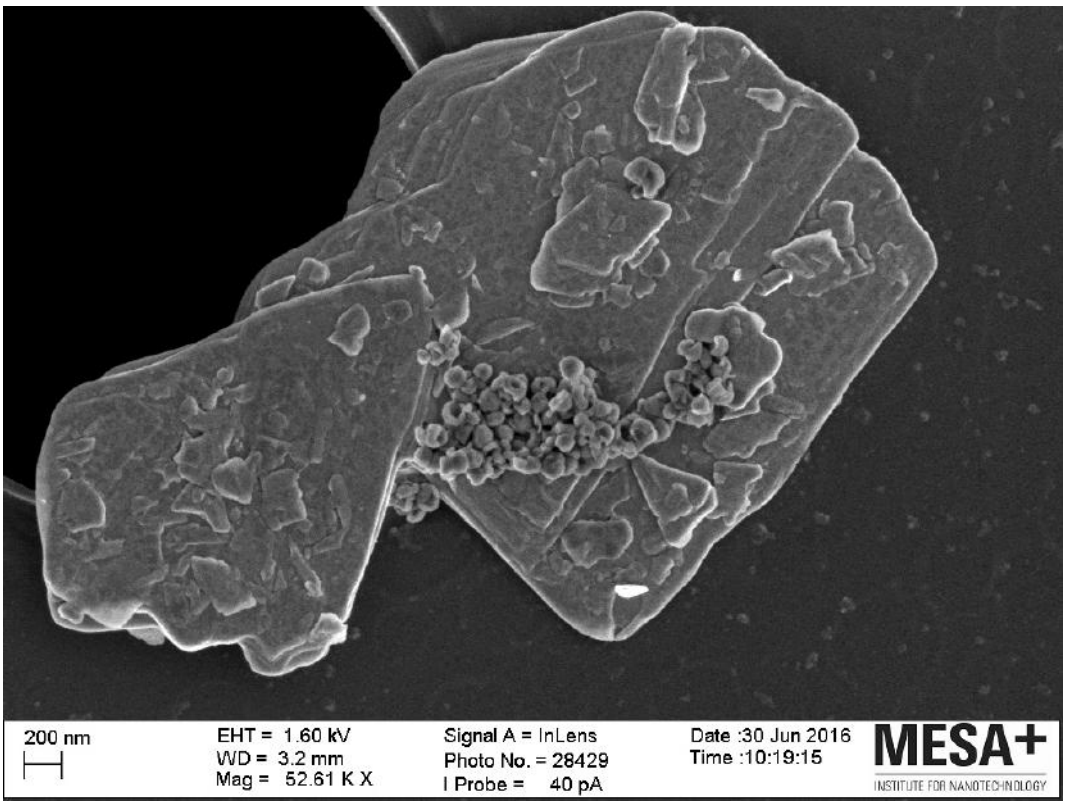

Figure A.103

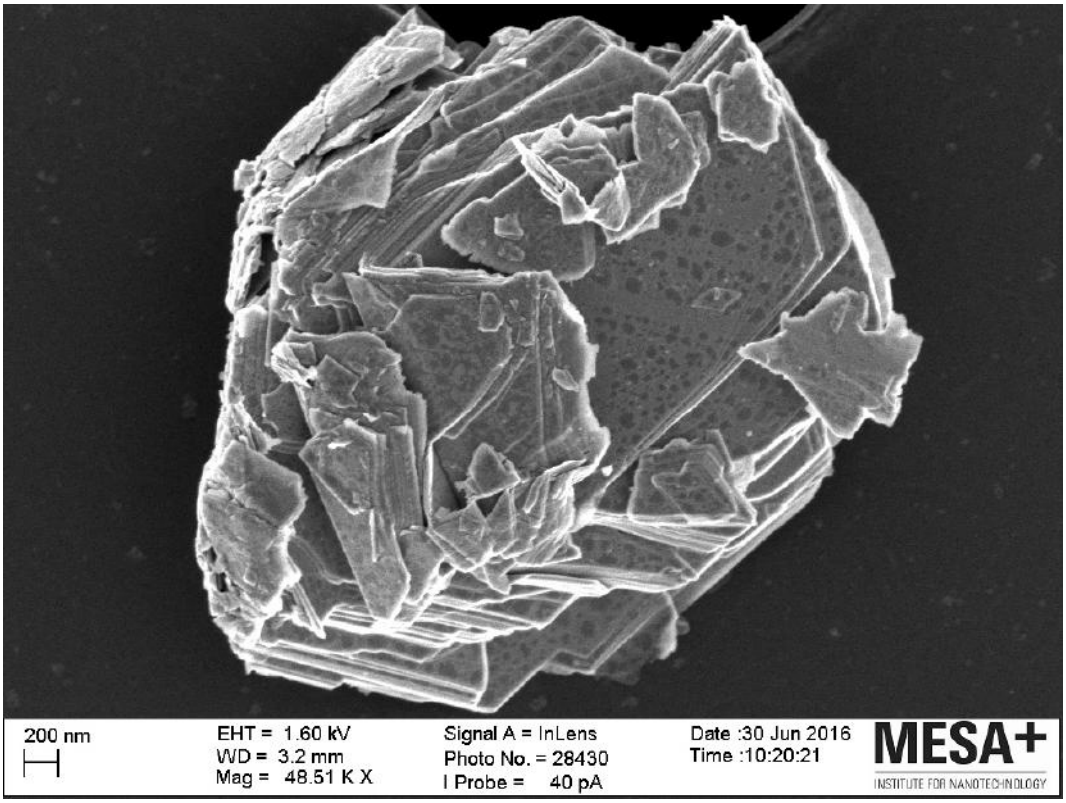

Figure A.104

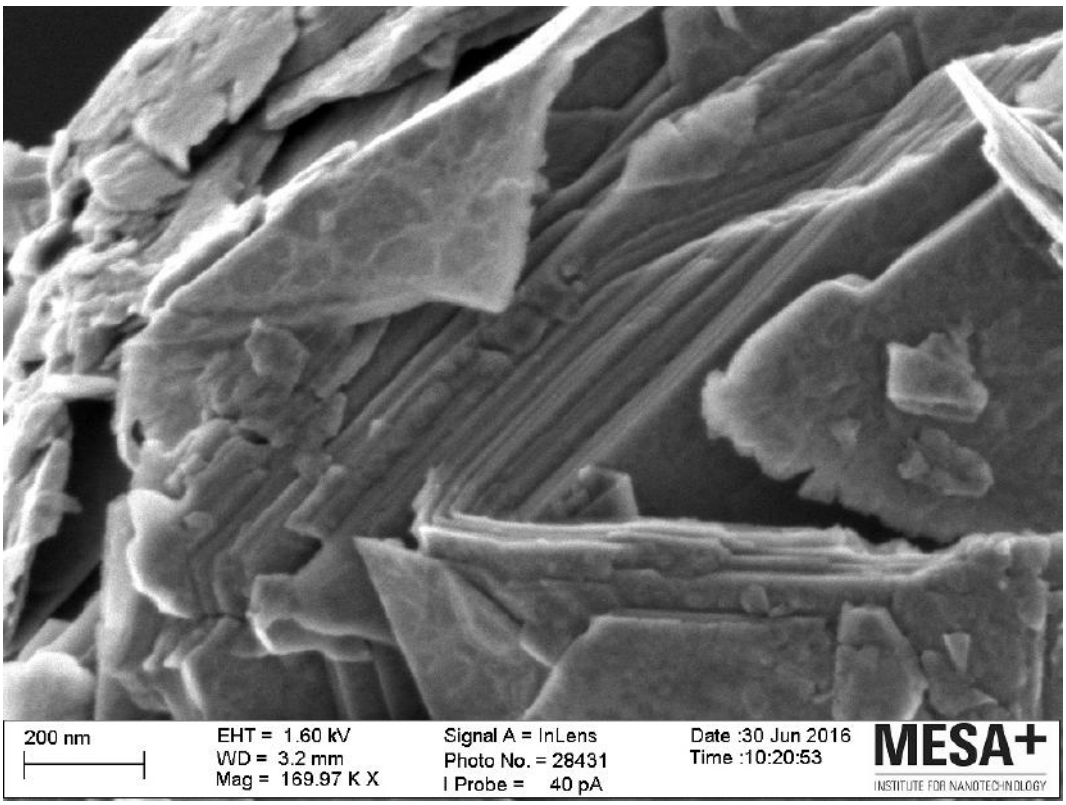

Figure A.105

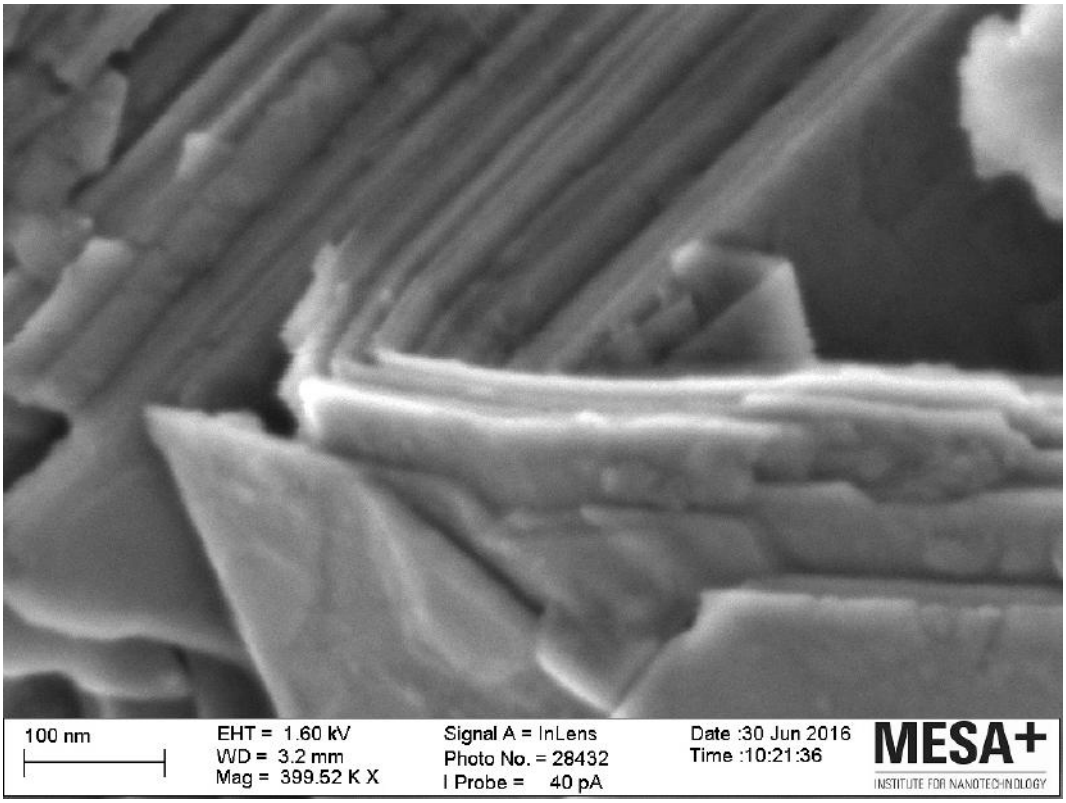

Figure A.106

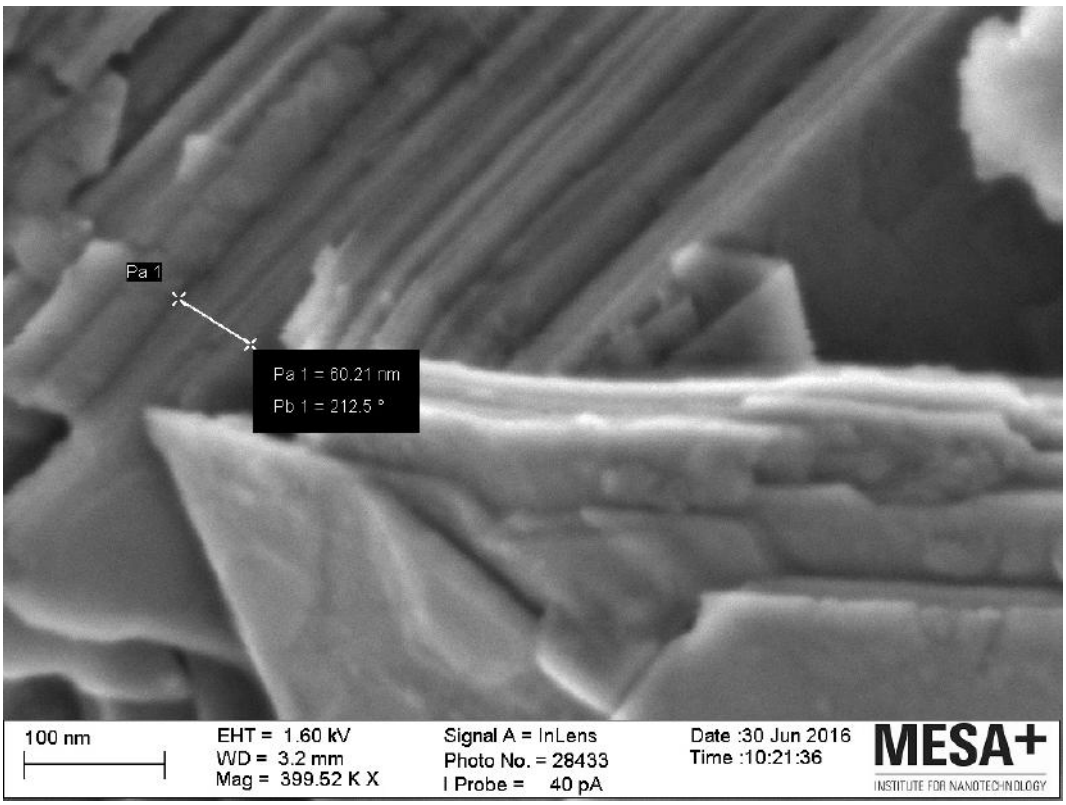

Figure A.107

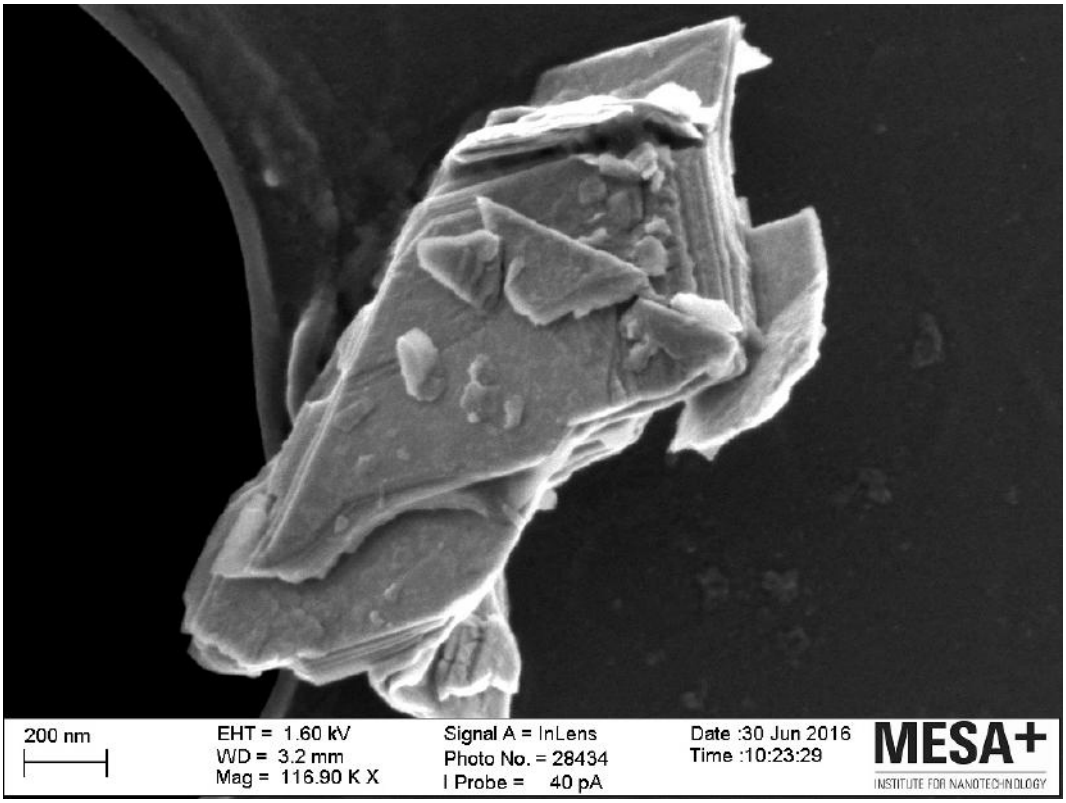

Figure A.108

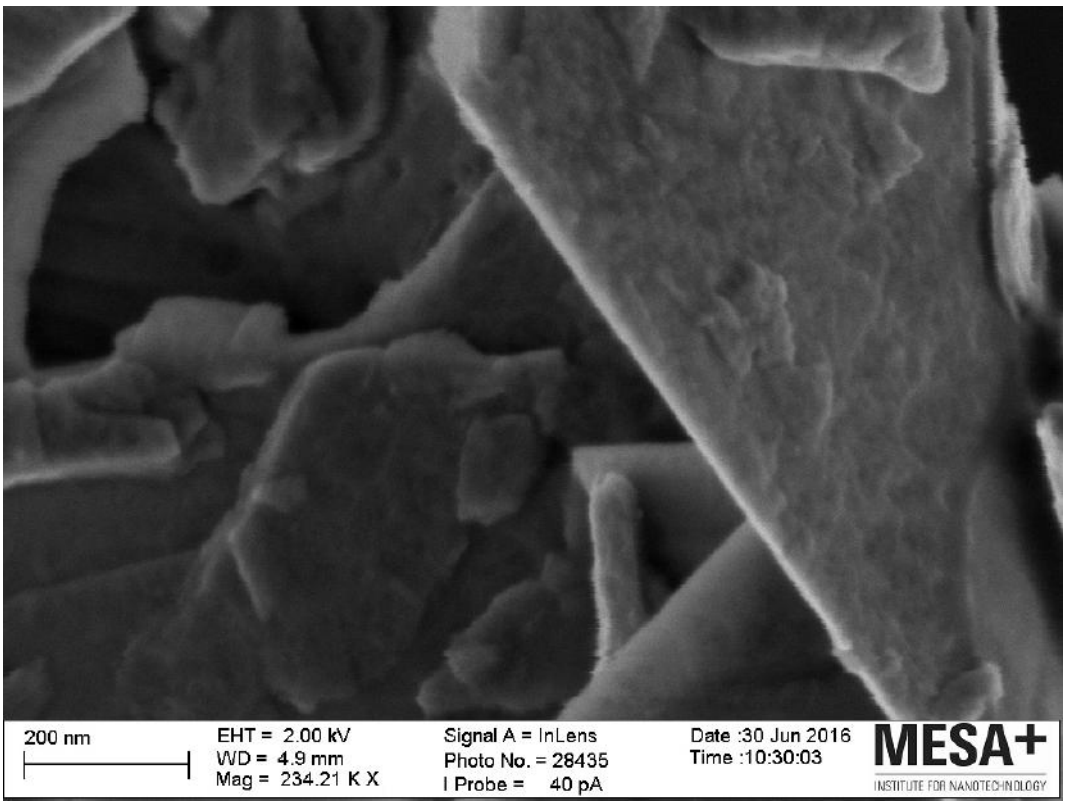

Figure A.109

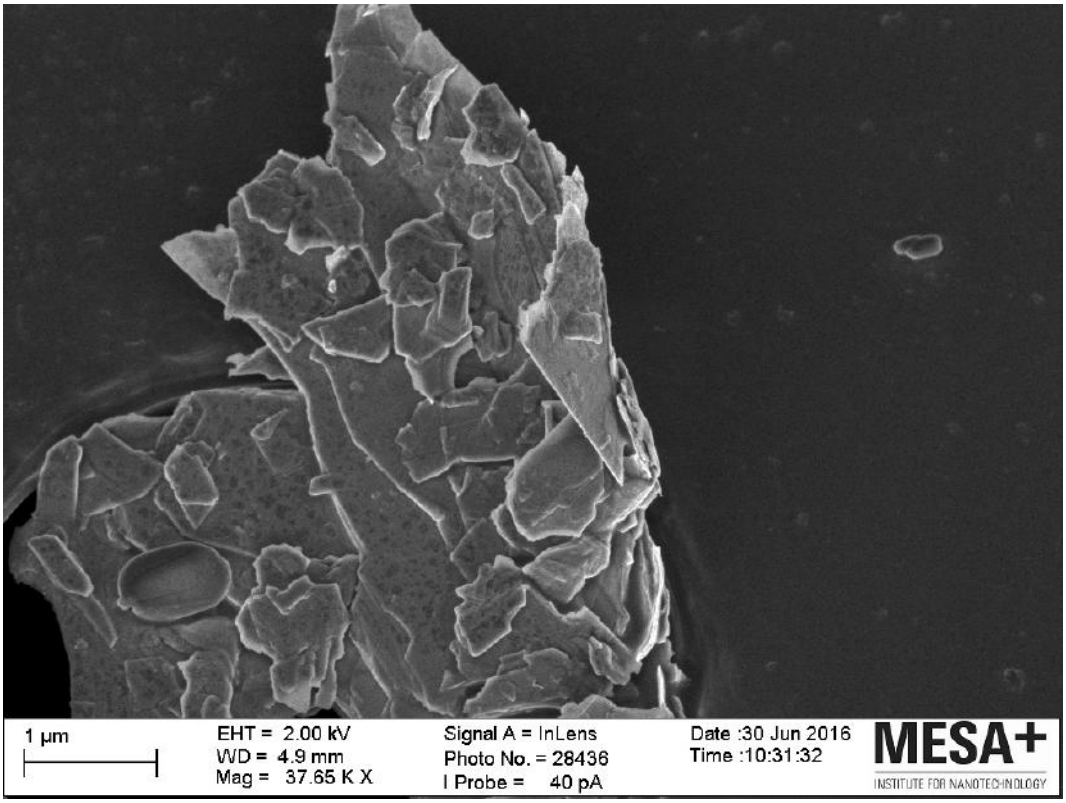

Figure A.110

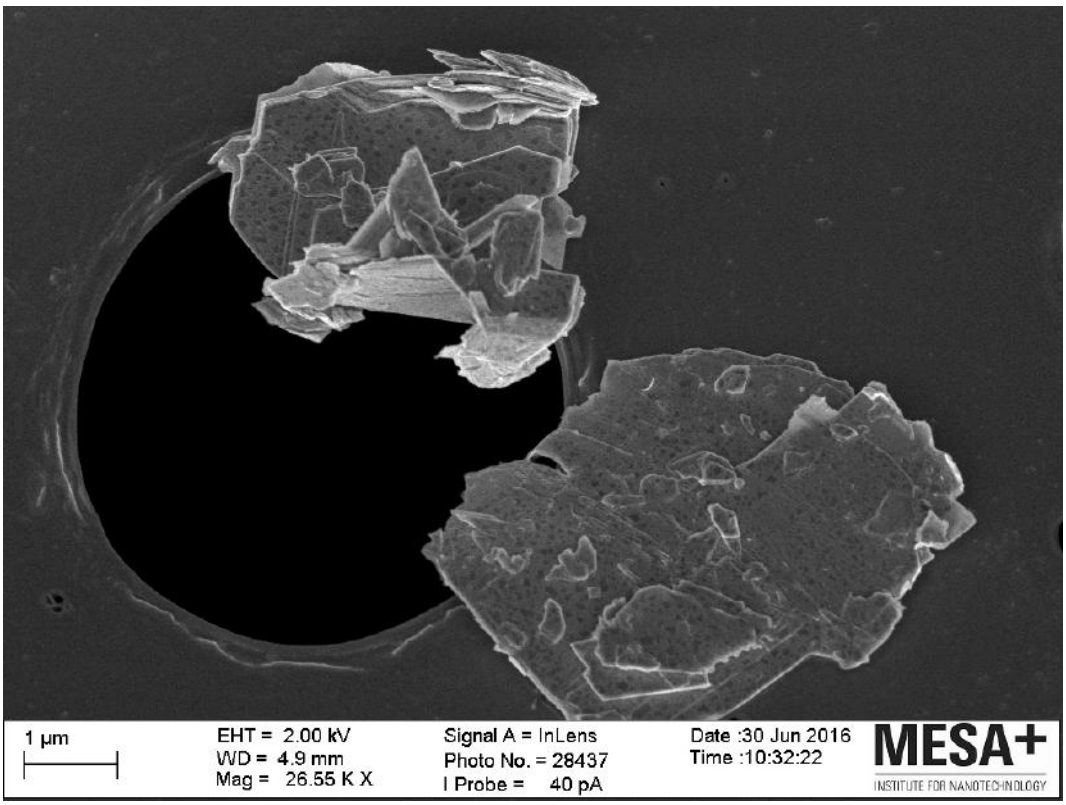

Figure A.111

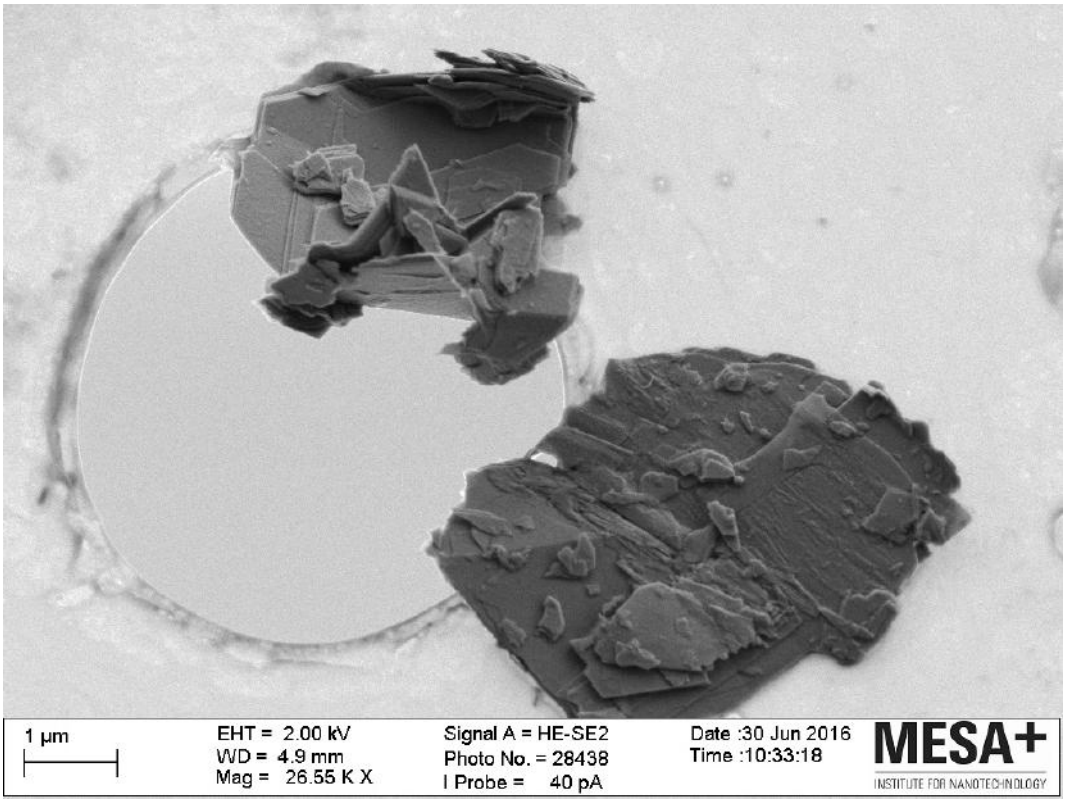

Figure A.112

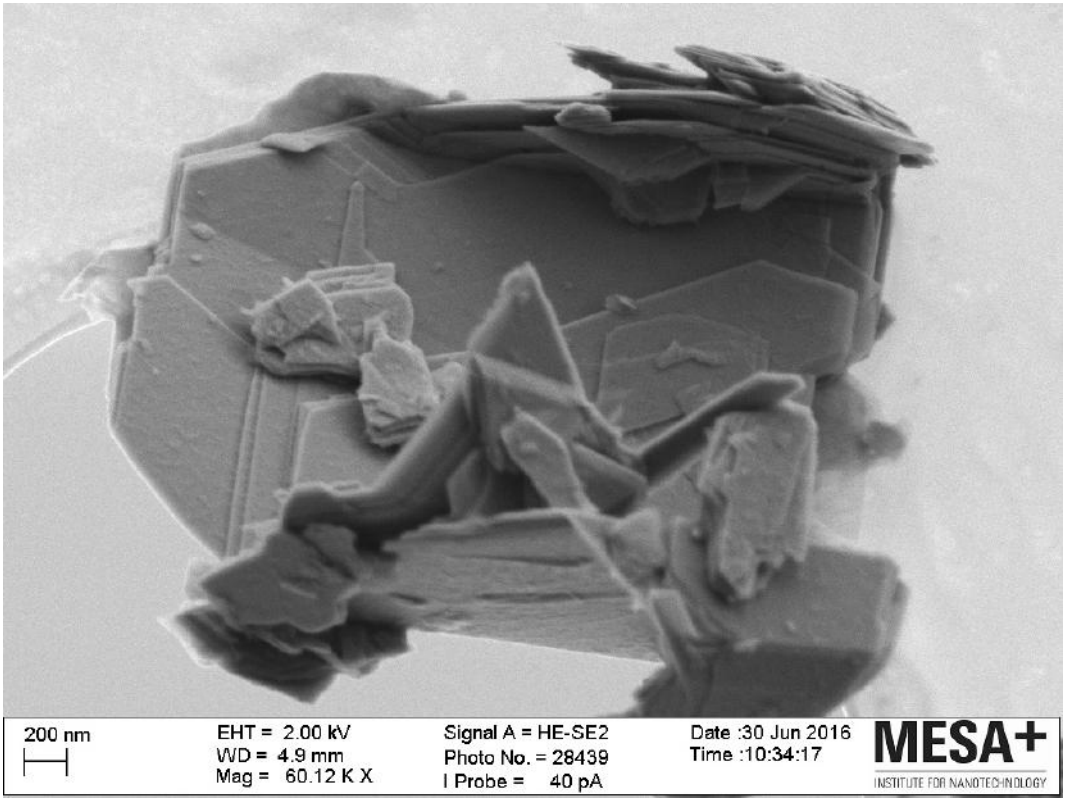

Figure A.113

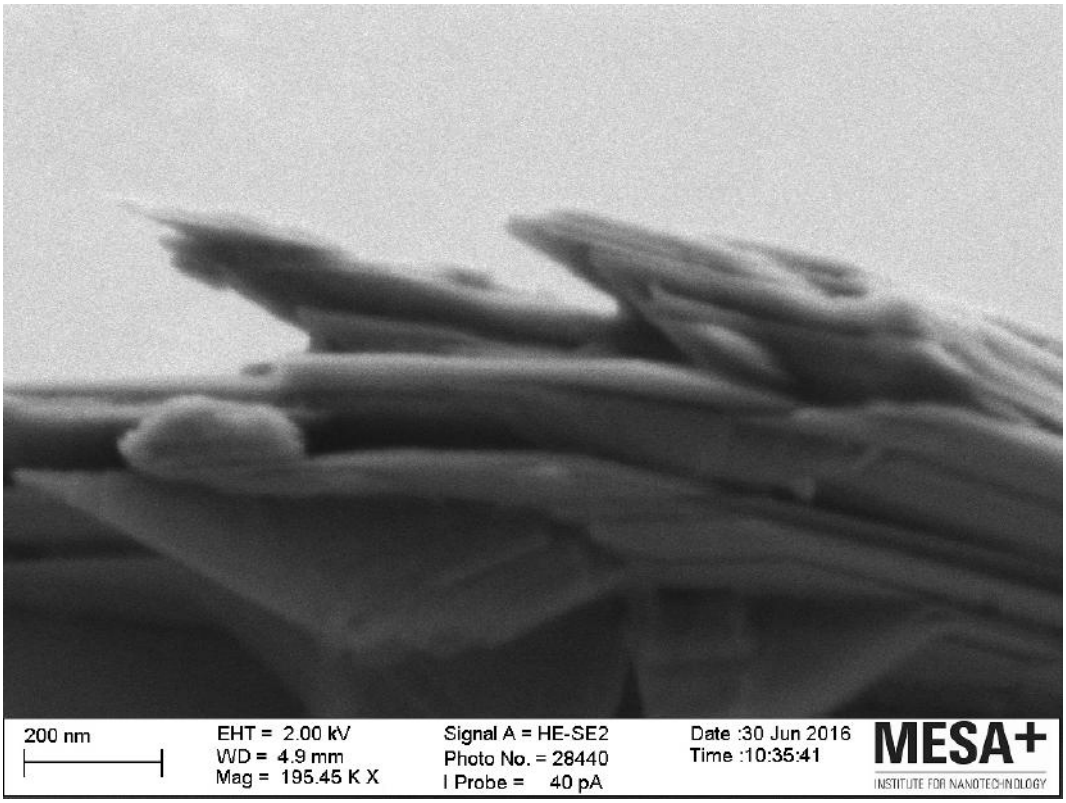

Figure A.114

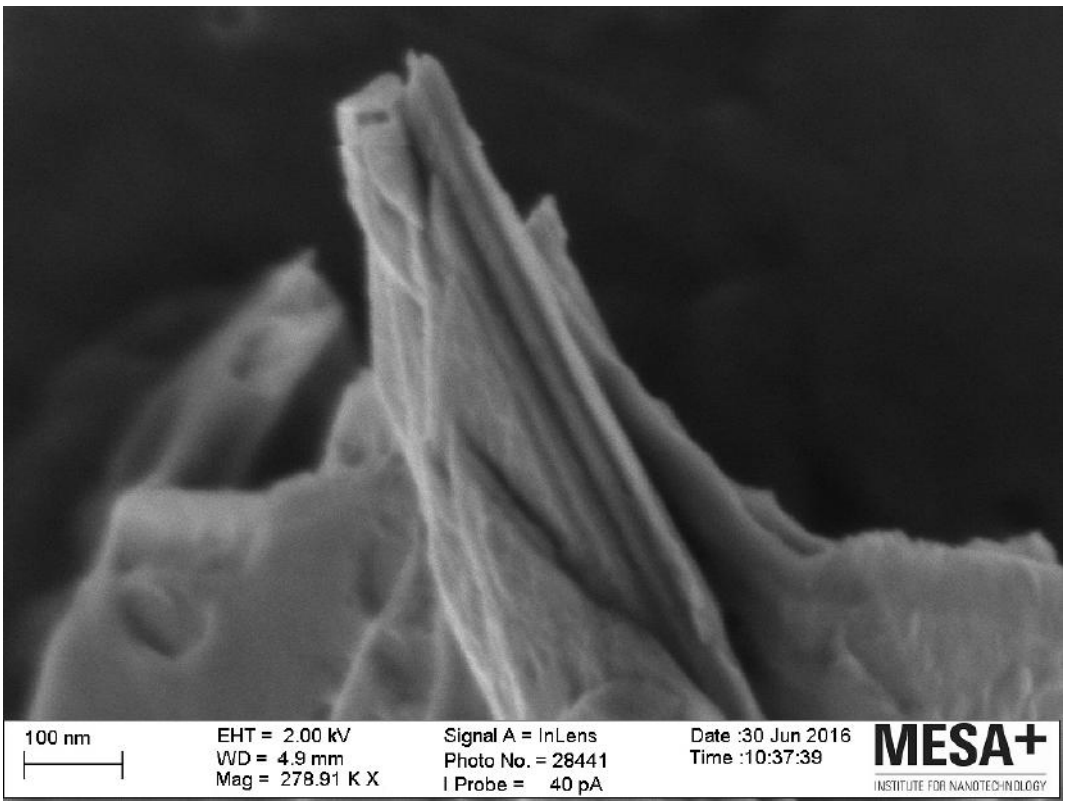

Figure A.115

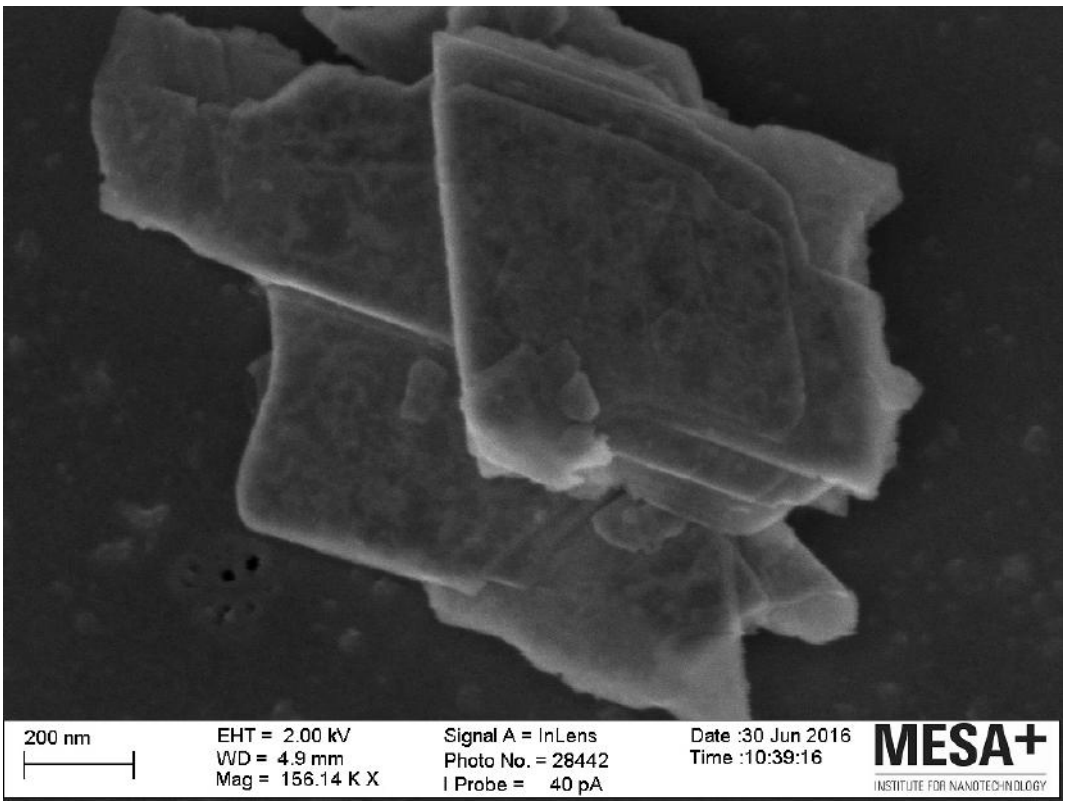
200 nm
EHT = 2.00 kV
WD = 4.9 mm
Mag = 156.14 K X
Signal A = InLens
Photo No. = 28442
I Probe = 40 pA
Date :30 Jun 2016
Time :10:39:16
MESA+
INSTITUTE FOR NANOTECHNOLOGY

Figure A.116

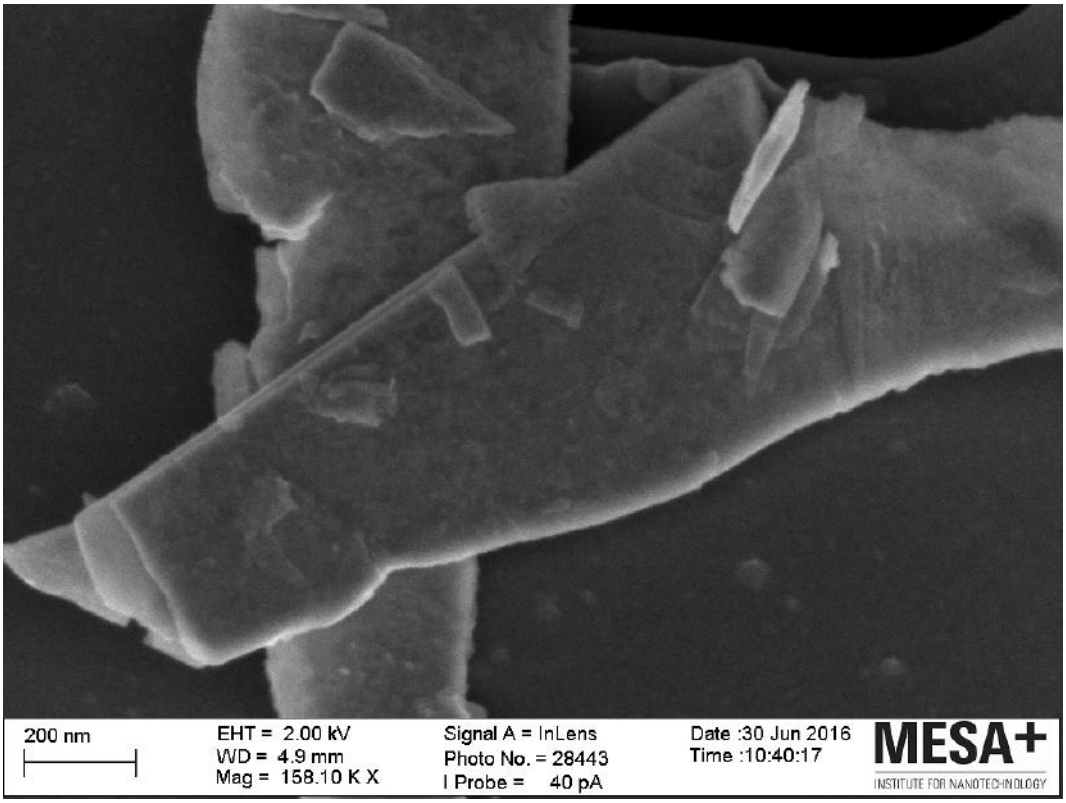

Figure A.117

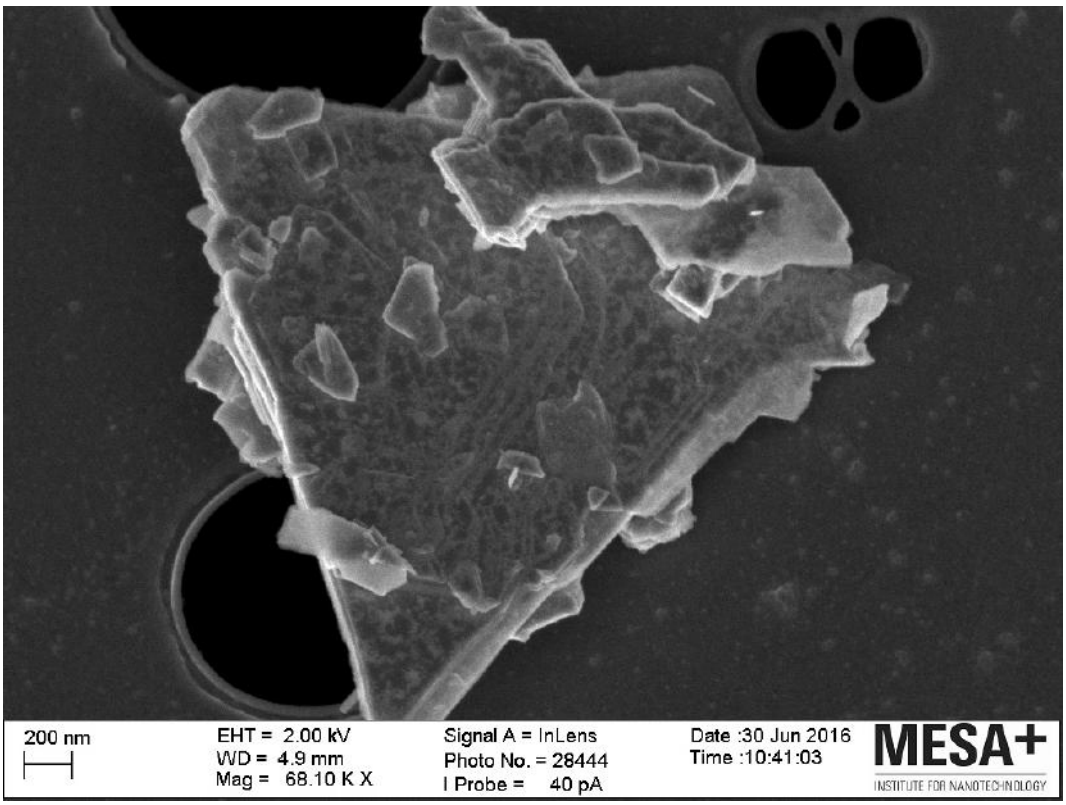

Figure A.118

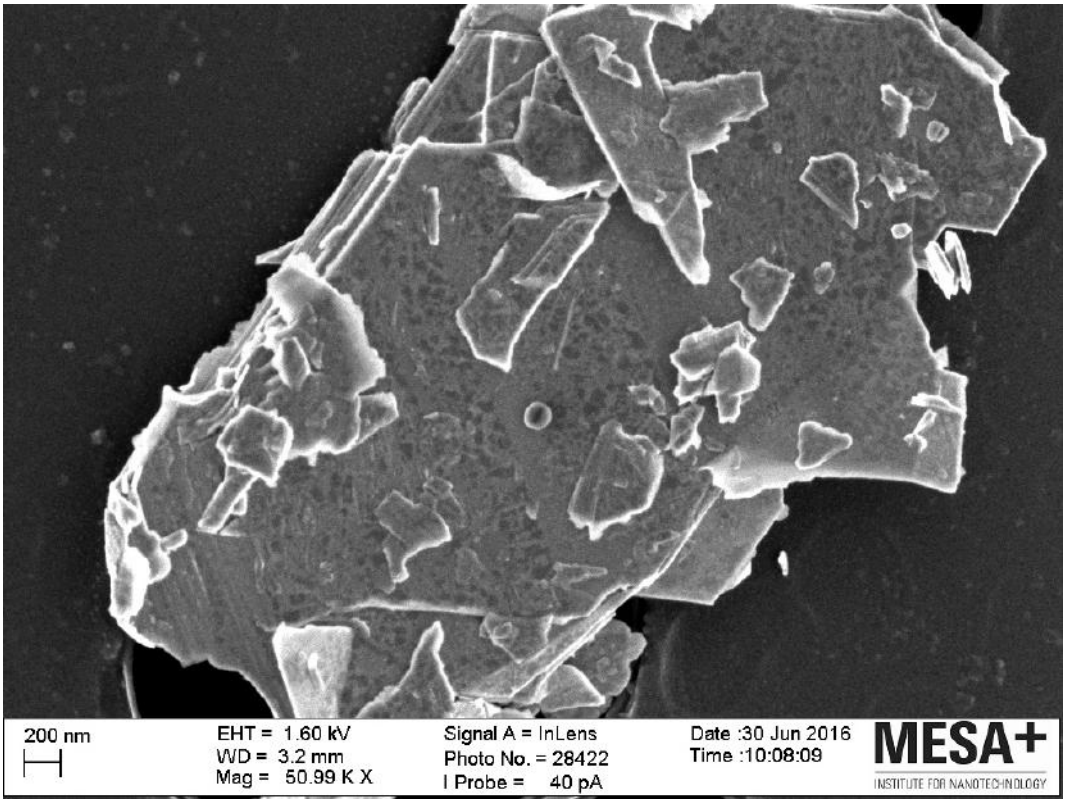

Figure A.119

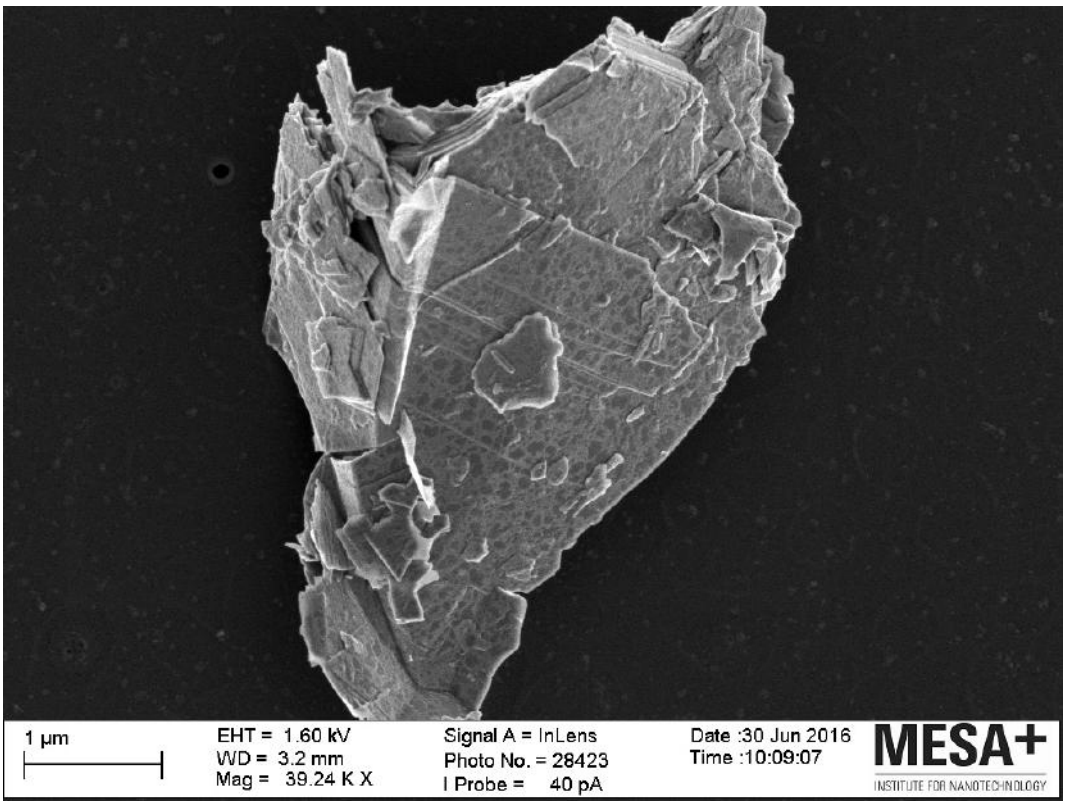

Figure A.120

A.1.9 BBP 20min

Absorption Spectra

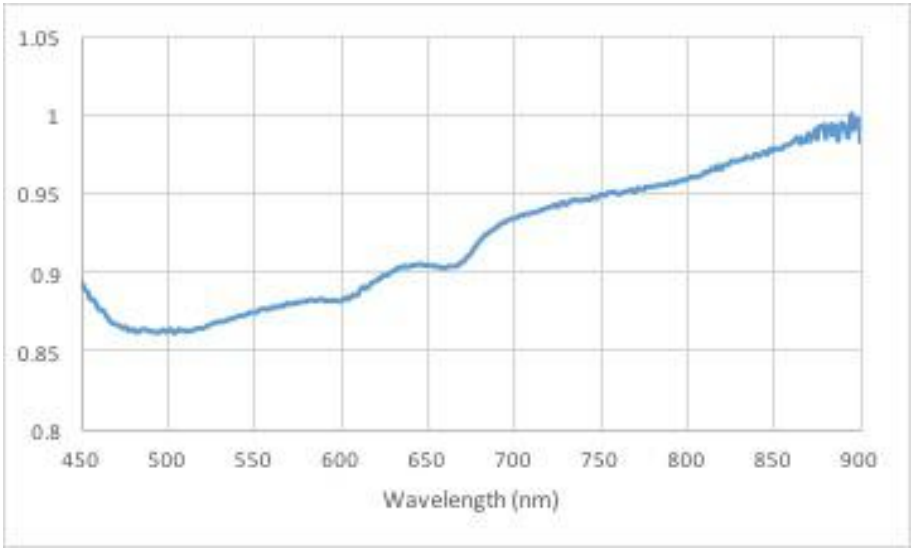

Figure A.121: Normalised absorption spectrum showing the maximum absorption intensity was not reached at the wavelengths close to the bands respective to the MoS_2 nano-sheets.

SEM

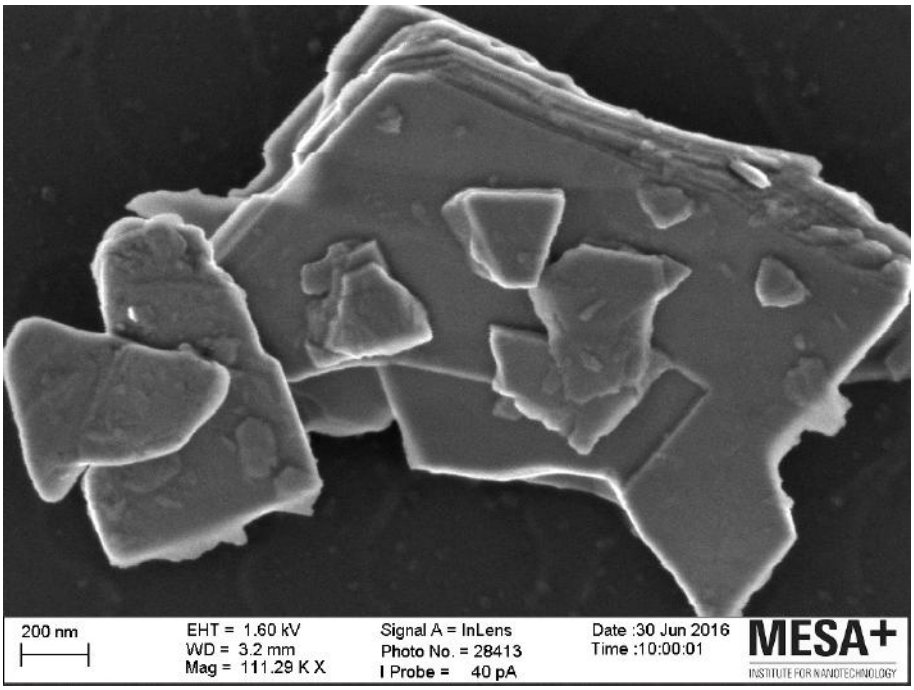

Figure A.122

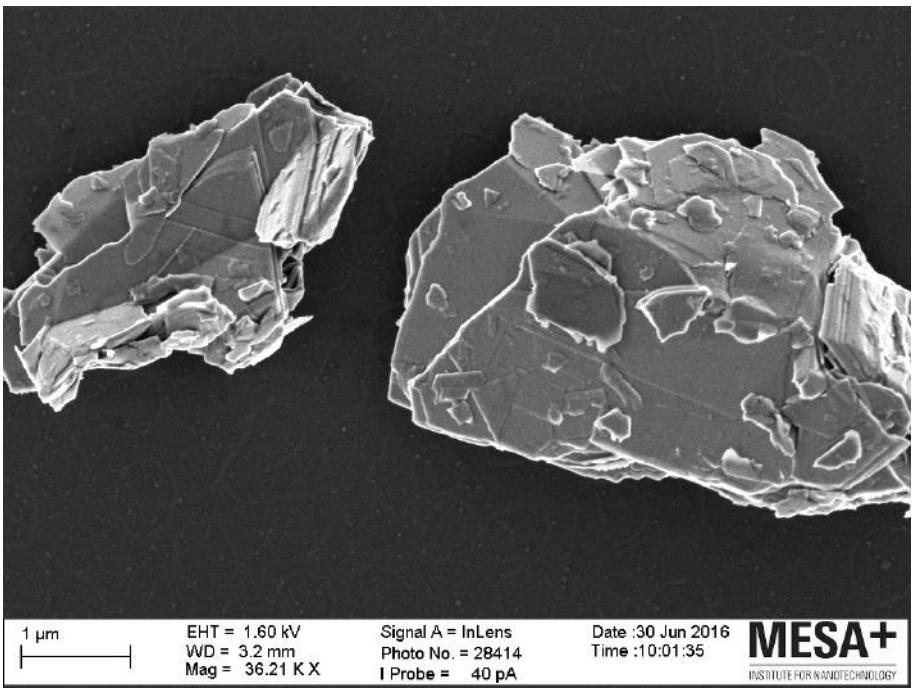

Figure A.123

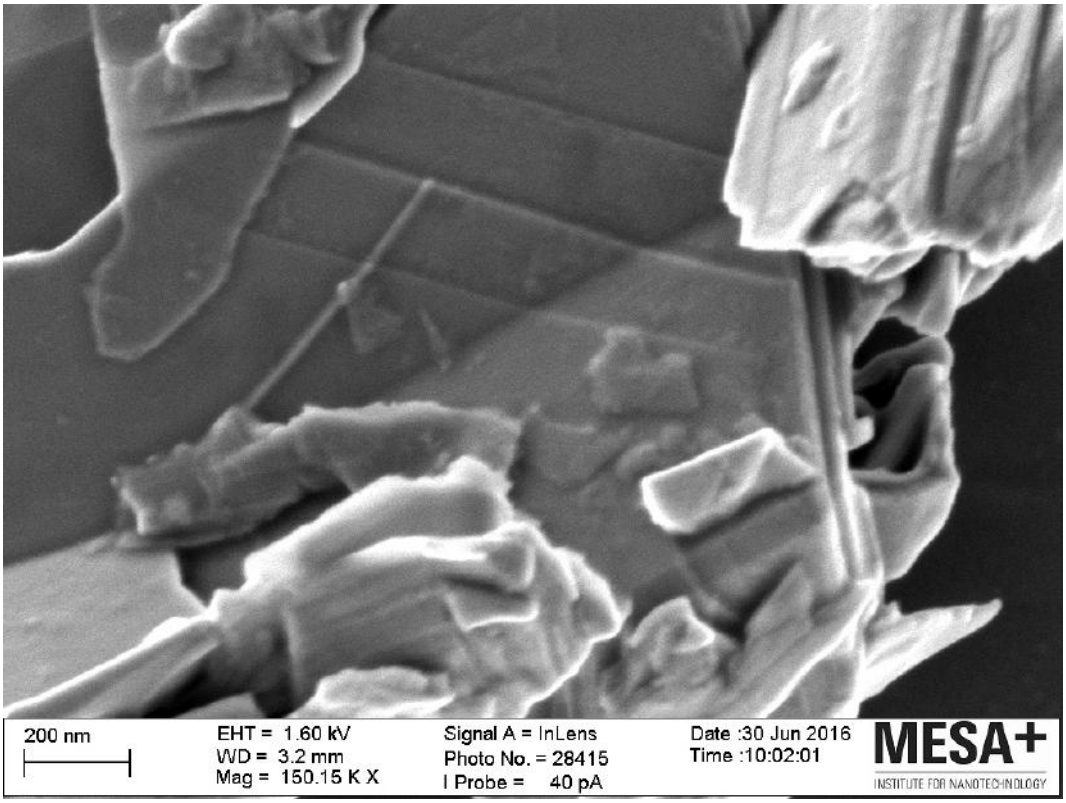

Figure A.124

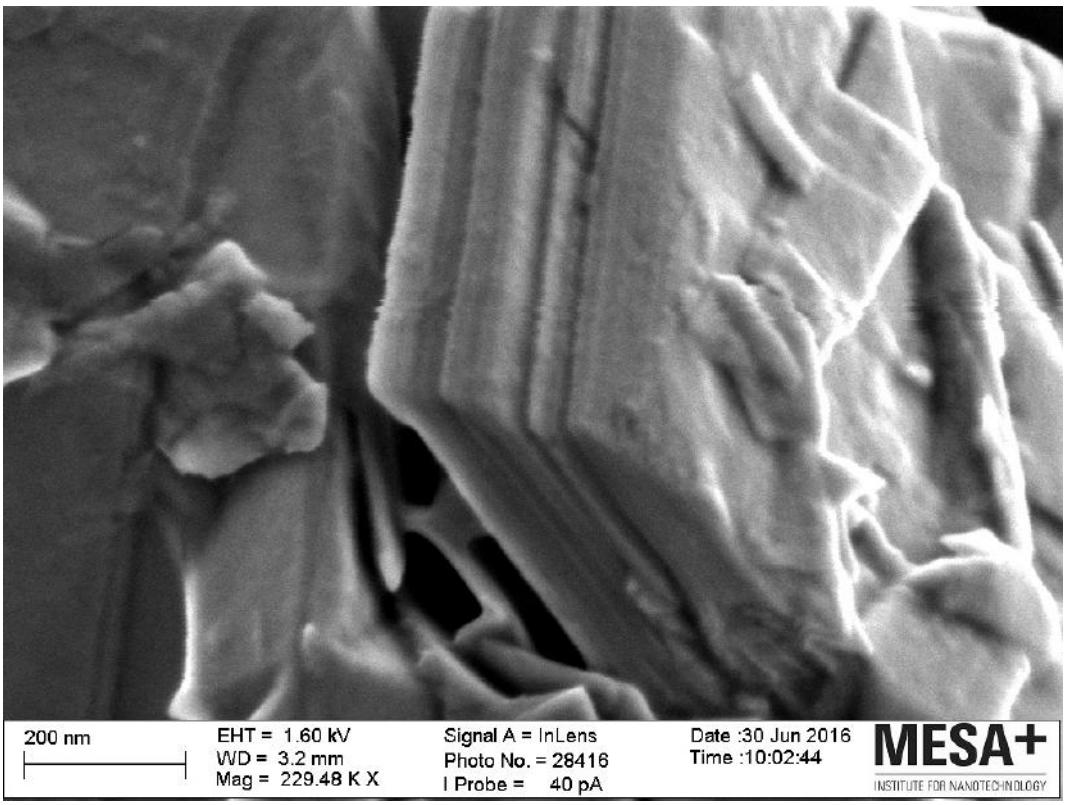

Figure A.125

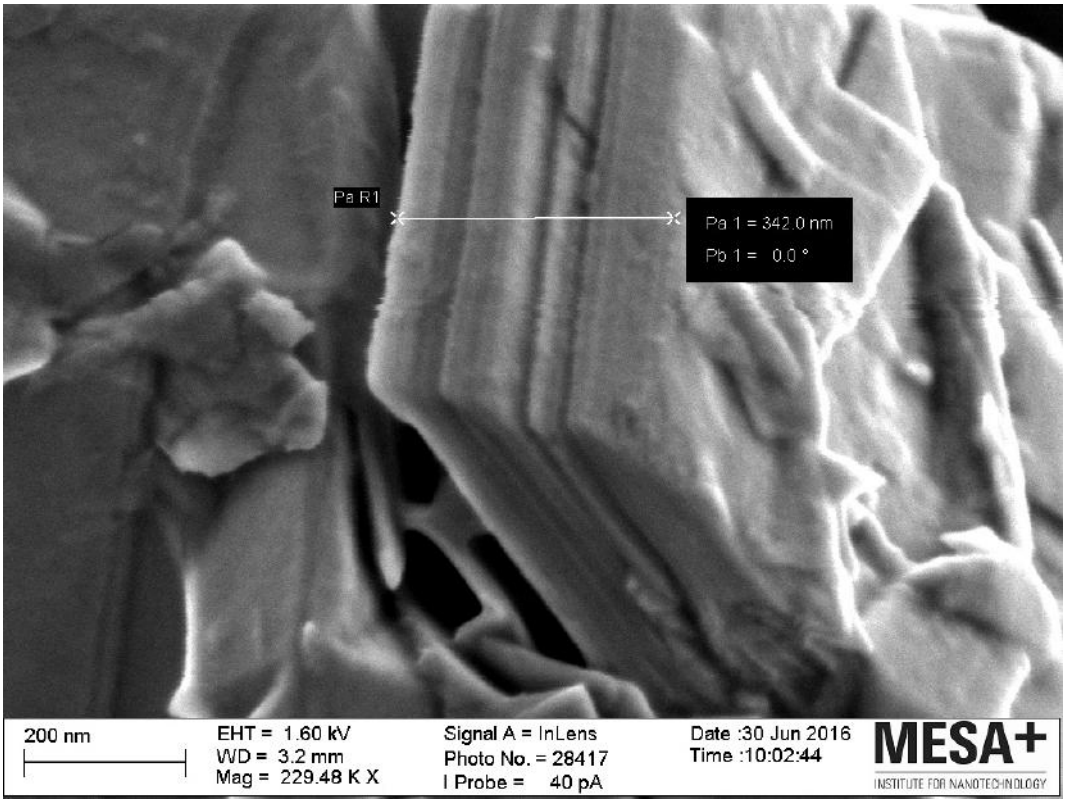

Figure A.126

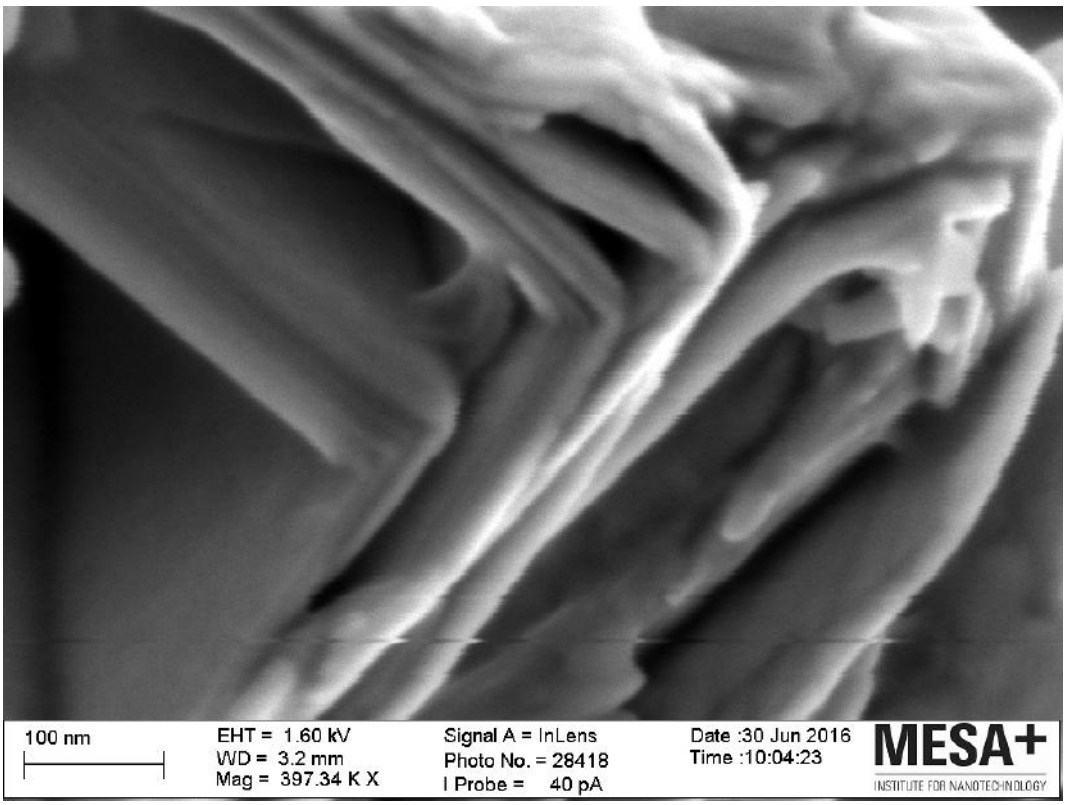

Figure A.127

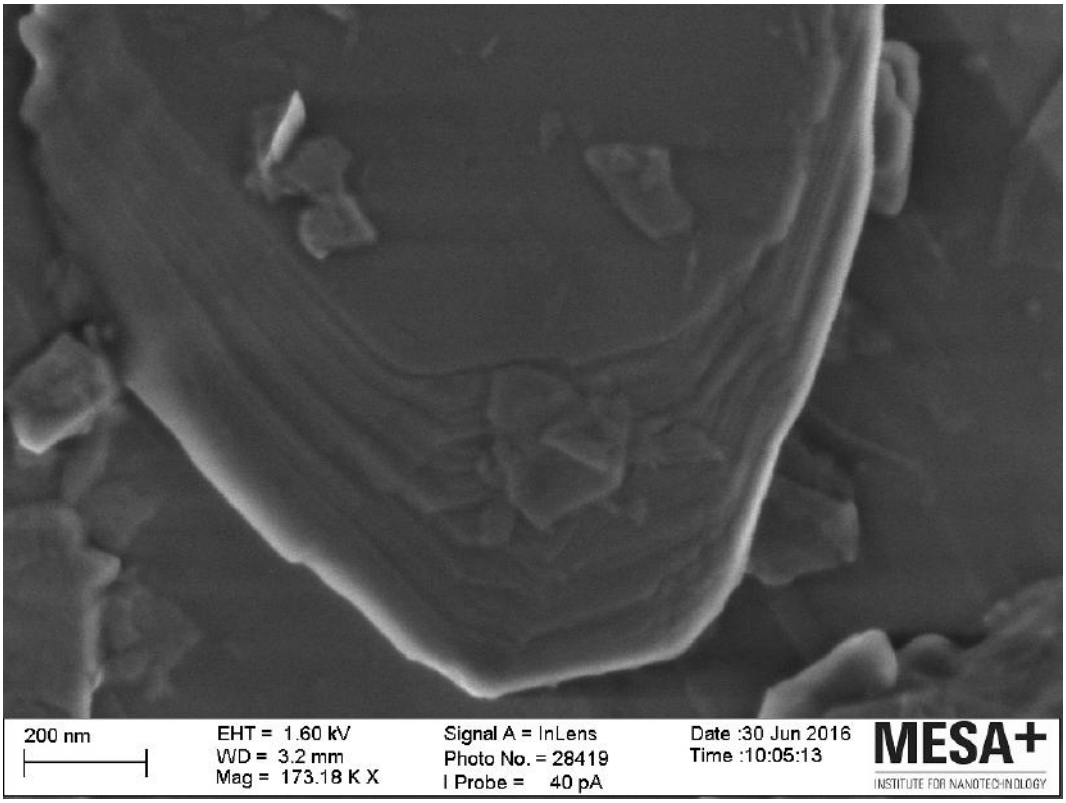
200 nm
EHT = 1.60 kV
WD = 3.2 mm
Mag = 173.18 K X
Signal A = InLens
Photo No. = 28419
I Probe = 40 pA
Date :30 Jun 2016
Time :10:05:13
MESA+
INSTITUTE FOR NANOTECHNOLOGY

Figure A.128